Fast track to renewables

Low emission electricity for south west Australia by 2030

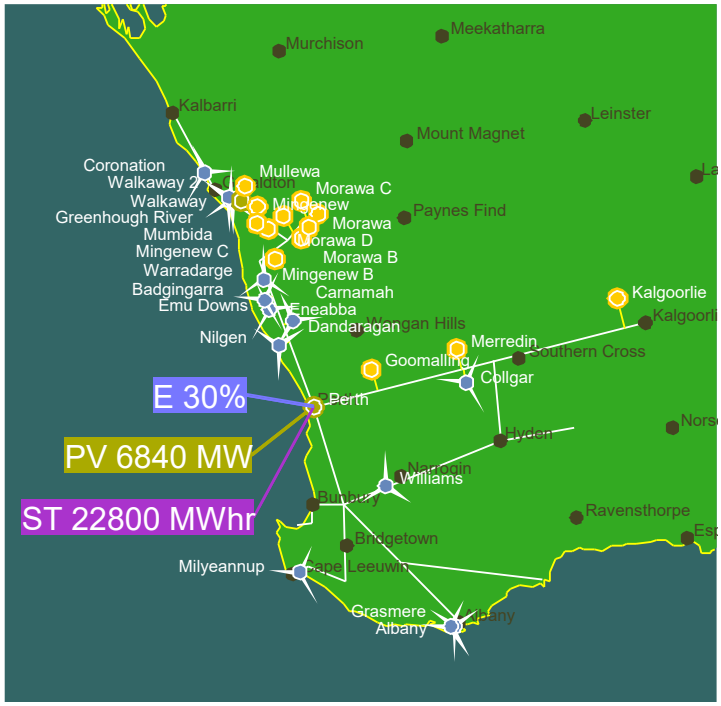

Dean Laslett

BSc, BEng

This thesis is presented for the degree of Doctor of Philosophy of Murdoch University

2017

Supervisors: Professor Philip Jennings and Doctor Chris Creagh

Produced in the open source LibreOffice word processor and Zotero bibliographic management software.

Declaration

I declare that this thesis is my own account of my research and contains as its main content work that has not been previously submitted for a degree at any tertiary education institution.

.....

(Dean Laslett 2017)

Publications

Four journal articles have been composed as part of this thesis:

1. Laslett, D., C. Creagh, and P. Jennings. 2014. "A Method for Generating Synthetic Hourly Solar Radiation Data for Any Location in the South West of Western Australia, in a World Wide Web Page." *Renewable Energy* 68 (August): 87–102. doi:10.1016/j.renene.2014.01.015.

2. Laslett, D., C. Creagh, and P. Jennings. 2016. "A Simple Hourly Wind Power Simulation for the South-West Region of Western Australia Using MERRA Data." *Renewable Energy* 96 (October): 1003–14. doi:10.1016/j.renene.2016.05.024.

3. Laslett, D., C. Carter, C. Creagh, and P. Jennings. 2017. "A Large-Scale Renewable Electricity Supply System by 2030: Solar, Wind, Energy Efficiency, Storage and Inertia for the South West Interconnected System (SWIS) in Western Australia." *Renewable Energy* (under review).

4. Laslett, D. 2017. "Greenhouse emissions and provisional costs for 100% renewable scenarios for the South West Interconnected System (SWIS) in Western Australia, based on solar, wind, energy efficiency, and battery storage." *Renewable Energy and Environmental Sustainability* (under review).

Abstract

Could renewable energy be implemented rapidly and on a large scale to supply the demand of stationary electrical grid systems?

This thesis takes a step towards answering this question by simulating 100% renewable energy scenarios for the South-West Interconnected System (SWIS), which supplies electricity to most of the population and industry in the south-west of Western Australia (SWWA). The SWIS is remarkable in that it is both isolated from other grids and currently has little available hydro-power.

Solar and wind energy were chosen as the energy sources to be simulated because they are commercially mature technologies, already have a presence in the SWIS, are widely available in many other parts of the world, yet they are geographically and temporally variable. To simulate the operation of rooftop solar PV and large scale solar and wind power plants, heuristic models were built to generate synthetic hourly values of solar and wind energy resources anywhere within the SWWA. An integrated simulation of the SWIS grid was built using simple models of population increase, energy efficiency, distributed battery storage and seasonal power to gas storage.

The construction schedules required to build a 100% renewable system for the SWIS by the year 2030 were found to be achievable for scenarios with a mix of solar PV, solar thermal and wind. If solar PV, wind and battery storage capacity could maintain exponential growth, then the required growth rates are less than current global growth rates. Energy efficiency would need to improve at a greater rate, though still moderate, than the current global improvement rate. However, the more that energy efficiency is improved, the lower the total demand, and the easier the task becomes for the other technologies.

The findings of this thesis have positive implications for world-wide rapid transformation to low emission electricity generation.

Acknowledgements

My gratitude, appreciation and thanks to my Supervisors Philip Jennings and Chris Creagh for making this PhD thesis possible, and to Murdoch University for supporting the candidature that allowed this thesis to be developed. Thanks to Craig Carter for much helpful advice and feedback; Martina Calais and Jonathan Whale for helpful comments; Ian Foster, Department of Agriculture and Food, Western Australia, Jatin Sala, and Tom Lyons in providing meteorological station data and for access to supercomputer climatic data. Thanks also to the National Aeronautics and Space Administration (NASA) for providing open access to the MERRA database. Thanks to Dan Churach for many funny or stimulating conversations which reaffirmed the reasons to stay motivated on this project; my writing space mates Graeme Thompson, Jane Genovese, Keegan Martens, and Jessie He, we kept our dreams alive together. The author Kim Stanley Robinson challenged global society to change. Justin Wood channelled much insightful analysis onto social media which also helped with motivation and writing inspiration. Thanks to Adzira Hussain, Siti Salmi Jamali, Maryam Shahabi, Asma Meda and Zakia Afroz for making me welcome in the IT PhD room with many good times and yummie food, and to all my friends, colleagues and bush walking companions who helped keep me sort of sane throughout this time.

Dean Laslett 2017

Table of Contents

1 Introduction.....1

1.1 Global warming.....1

1.1.1 Greenhouse emissions from stationary electrical generation, and the SWIS grid.....2

1.2 Pathways to emissions reduction.....3

1.3 Research questions.....4

1.4 Methodology.....5

1.5 Thesis structure.....6

2 Overview of low emissions technologies.....9

2.1 Nuclear power.....9

2.1.1 Current status.....10

2.1.2 Life-time of reserves.....11

2.1.3 Grid penetration.....13

2.1.4 Radioactive waste.....14

2.1.5 Safety.....15

2.1.6 New reactor designs.....17

2.1.7 Breeder and burner reactors.....18

2.1.8 Thorium cycle.....19

2.1.9 Nuclear fusion.....20

2.1 Carbon capture and storage (CCS).....20

2.1.1 Global potential.....22

2.1.2 Australian potential.....22

2.1.3 Current technological status.....23

2.1.4 Advantages and problems of CCS....24

2.1.5 Lifetime of world fossil fuel reserves....26

2.2 Renewable energy....27

2.2.1 Global potential of renewable energy....27

2.2.2 Solar energy....28

2.2.2.1 Solar PV....29

2.2.2.1.1 Technological status of PV....30

2.2.2.1.2 Material constraints....30

2.2.2.2 Solar thermal....31

2.2.2.2.1 Technological status....32

2.2.2.2.2 Thermal storage....32

2.2.2.3 Environmental impacts of solar energy technologies....33

2.2.3 Wind energy....35

2.2.3.1 Technological status....35

2.2.3.2 Material constraints....35

2.2.3.3 Environmental effects of wind turbines....36

2.2.3.4 Effect of climate change on the wind resource....39

2.2.4 Variability of supply and grid integration of solar and wind power....40

2.2.4.1 Wind variability....43

2.2.4.2 Integrating wind power into the grid....44

2.2.4.3 Wind backup generation....45

2.2.4.4 Wind weather forecasting....47

2.2.4.5 Solar PV variability and grid integration....48

2.2.4.6 Short term variability versus log term variability....50
2.2.4.7 Paradigm of flexibility....52
2.2.5 Bioenergy....53
2.2.5.1 Technological status....54
2.2.5.2 Australian and Western Australian potential....56
2.2.5.3 Environmental issues....59
2.3 Storage....61
2.3.1 Material, energy and environmental constraints....63
2.4 Energy efficiency....64
2.4.1 The "efficiency paradox"....65
3 Comparing nuclear, CCS and renewable energy....69
3.1 Greenhouse emissions comparison....69
3.2 Speed of emissions reductions....73
3.2.1 Energy payback time and limits to expansion of low emission generation....75
3.3 Cost....77
3.4 Water use....79
3.5 Conclusions....81
4 Towards a low emissions SWIS grid....85
4.1 Examples of renewable energy electricity systems....85
4.2 Simulations of renewable energy electricity systems....86
4.3 The use of energy storage and P2G technologies....90
4.4 Simulating a 100 percent renewable SWIS grid....92
5 Solar irradiance model....97

5.1 Background....97
5.1.1 Irradiance in clear sky conditions....105
5.2 Method....110
5.2.1 Defining cloudiness....110
5.2.2 Estimating cloudiness....113
5.2.3 Generation of daily cloudiness....114
5.2.4 Generation of hourly cloudiness....119
5.3 Results and discussion....123
5.3.1 Monthly average daily horizontal radiation....123
5.3.2 Daily average horizontal radiation....124
5.3.3 Hourly irradiance....125
5.4 Summary....129
6 Solar thermal model with storage....131
6.1 Method....131
6.2 Calibration results....141
7 Wind power model....145
7.1 Background....145
7.2 Method....154
7.3 Results....172
7.4 Summary....177
8 Integrated power system scenarios....181
8.1 The SWIS in more detail....182
8.2 Method....186

8.2.1 Transmission losses....189
8.2.2 Solar PV model....191
8.2.3 Existing and proposed wind farms....193
8.2.4 Distributed battery storage model....195
8.2.5 Power to gas (P2G) storage model....196
8.2.6 Energy efficiency model....196
8.3 Results....198
9 Discussion....213
10 Conclusions....219
10.1 Research questions revisited....219
10.2 Summary of key findings....220
10.2.1 Literature search....220
10.2.2 Model development....222
10.3 Limitations and further research....230
10.4 Final words....235
Glossary....237
Appendices....247
A Solar simulation model....247
B Wind simulation model....261
C Formulation of statistical measures....278
References....279

List of Tables

Table 2.1. Renewable energy resources in 2004.....28

Table 3.1. Average life cycle greenhouse gas emission intensity for different energy generation technologies.....72

Table 3.2. Energy Payback Time (EPBT) for low emission technologies.....76

Table 3.3. Levelised Cost of Energy (LCOE) comparison between several alternative technologies in the United States.....77

Table 3.4. Levelised Cost of Energy (LCOE) and capacity factor comparison between several alternative technologies for Australia.....79

Table 3.5. Water use for electrical power generation technologies.....80

Table 3.6. Advantages and disadvantages of alternative technologies for reducing emissions from electrical power generation.....82

Table 5.1. Sinusoid coefficient indices.....118

Table 5.2. Model comparison of monthly average daily horizontal radiation errors.....124

Table 5.3. Comparison of daily horizontal radiation.....125

Table 5.4. Hourly horizontal irradiance comparison of models that use a cloudiness coefficient.....127

Table 5.5. Comparison with other hourly irradiance models.....128

Table 6.1. Start up stages for the solar thermal power tower receiver.....140

Table 6.2. Stages for the solar thermal power tower power block.....141

Table 6.3. Solar thermal station operating constants.....142

Table 7.1. Example Root Mean Square Error (RMSE) for different orders of Autoregressive Moving Average (ARMA) models of the MERRA daily average wind speed square root residual at a single MERRA node.....161

Table 7.2. Example Bayesian Information Criterion (BIC) and ranking in ascending order for different orders of Autoregressive Moving Average (ARMA) models of the MERRA daily average wind speed square root residual at a single MERRA node.....162

Table 7.3. Example Root Mean Square Error (RMSE) between different Autoregressive Moving Average (ARMA) models and the MERRA hourly wind speed transformed residual at a single node.....166

Table 7.4. Example Bayesian Information Criterion (BIC) and ranking in ascending order for different orders of Autoregressive Moving Average (ARMA) models of the MERRA hourly wind speed transformed residual at a single node.....166

Table 7.5. SCADA and simulated overall average Capacity Factor (CF) for six wind farms within the SWWA using three simulation models: the Weibull model, the normal residual model, and the transformed residual model.....174

Table 7.6. Errors in the yearly and monthly average Capacity Factor (CF) estimation, daily average CF frequency distribution, diurnal peak hour distribution and hourly average CF frequency distribution of three simulation models compared to measured SCADA wind power data.....175

Table 8.1. Grid conversion and transmission loss parameters.....190

Table 8.2. Measured and simulated average yearly Capacity Factor (CF) for the six largest wind farms within the South West of Western Australia.....194

Table 8.3. Proposed wind farms in the SWWA region.....194

Table 8.4. Distributed storage simulation parameters.....195

Table 8.5. Installed capacity for each 100% renewable scenario for the SWIS electrical grid.....206

Table 8.6. Yearly constant installation rates required for each 100% scenario to be completed by the year 2030.....207

Table 8.7. Yearly exponential installation rates for each 100% scenario to be completed by the year 2030.....208

Table 8.8. Synthetic inertia from reserving the upper and lower 5% of storage capacity for each 100% renewable energy scenario.....209

Table 8.9. Potential peak power flow running through the three main transmission corridors to Perth for each 100% renewable energy scenario.....210

Table 10.1. Advantages and disadvantages of alternative technologies for reducing emissions from electrical power generation.....221

Table A.1. Coastal set points and distance parameters.....259

Table A.2. Model cloudiness generation coefficients.....260

Table B.1. Wind turbine power curve parameters.....268

List of Figures

Figure 1.1. Simple schematic of the SWIS grid backbone in the South West of Western Australia.....3

Figure 3.1. Emission intensity of nuclear power with respect to uranium ore grade.....71

Figure 4.1. Typical summer and winter daily load profile on the SWIS grid for the year 2009.....94

Figure 4.2. Daily average SWIS load demand over one year for 2009.....95

Figure 5.1. The three types of irradiance falling upon a surface perpendicular to the position of the sun in the sky.....107

Figure 5.2. k_{cloud} as a function of cloudiness for sinα = 0.1, M = 9, t_{bcs} = 0.3 and t_{dcs} = 0.182.....112

Figure 5.3. Simplified coastline of Western Australia and locations of meteorological stations.....117

Figure 5.4. Normalised frequency distribution of measured hourly cloudiness residual yh, compared to a normal distribution and a translated Weibull distribution.....121

Figure 5.5. Sample measured and synthetic hourly horizontal irradiance for a 3 day period, starting at midnight on the first day.....126

Figure 5.6. Normalised frequency distribution of clearness index k_t from measured horizontal radiation, synthetically generated using the Aguiar and Collares-Pereira TAG algorithm, and derived from model cloudiness values.....129

Figure 6.1. Approximation of solar to receiver efficiency drop off with low solar altitude angle.....137

Figure 6.2. Receiver to storage efficiency drop off with low receiver input power.....138

Figure 6.3. Storage to electrical efficiency drop off with low electrical output power.....140

Figure 6.4. Stored thermal energy over one week for 200 MW solar power tower with 15 hours storage.....143

Figure 7.1. Typical wind turbine and wind farm power curve.....153

Figure 7.2. MERRA nodes used to simulate wind speed in the South-West region of Western Australia.....156

Figure 7.3. Seasonal MERRA wind speeds near Walkaway and Albany wind farms.....157

Figure 7.4. Normalised frequency distribution of MERRA daily average 50m wind speed compared to a translated Weibull distribution.....158

Figure 7.5. Normalised frequency distribution of MERRA daily average 50m wind speed square-root residual compared to normal distribution.....158

Figure 7.6. Example auto-correlation of the MERRA daily average wind speed square-root residual at a single node.....160

Figure 7.7. Example partial auto-correlation of the MERRA daily average wind speed square-root residual at a single node.....161

Figure 7.8. Variation in summer sea-breeze peak hour with distance from the coast-line. 163

Figure 7.9. Normalised frequency distribution of MERRA 50m wind speed residual and transformed residual compared to normal distribution.....163

Figure 7.10. Example auto-correlation of the MERRA hourly wind speed transformed residual at a single node.....165

Figure 7.11. Example partial auto-correlation of the MERRA hourly wind speed transformed residual at a single node.....165

Figure 7.12. Normalised frequency distribution of MERRA and simulation hourly 50m wind-speed residual.....168

Figure 7.13. Change in average wind shear factor with time of day for a coastal site and an inland site.....169

Figure 7.14. Average correlation with inter wind farm distance for wind farm power output for the SWWA.....171

Figure 7.15. Normalised frequency distribution of average daily capacity factors.....176

Figure 7.16. Diurnal Capacity Factor (CF) peak hour distribution.....176

Figure 7.17. Normalised frequency distribution of average hourly capacity factors.....177

Figure 8.1. SWIS grid backbone links used by the model.....183

Figure 8.2. Typical summer and winter daily load profile on the SWIS grid for the year 2009.....187

Figure 8.3. Scenario S1, "Small is beautiful": 3.42 GW Rooftop PV, 11.4 GWh of storage, 30% EE improvements.....198

Figure 8.4. Scenario S2, "PV": 19 GW Rooftop PV, 90.25 GWh of storage, 30% EE improvements.....199

Figure 8.5. Scenario S3, "Solar thermal": 2.8 GW solar thermal (15h thermal storage), 6.84 GW Rooftop PV, 22.8 GWh of storage, 30% EE improvements.....201

Figure 8.6. Scenario S4, "Wind": 7.947 GW wind, 6.84 GW Rooftop PV, 166.25 GWh of storage, 30% EE improvements.....202

Figure 8.7. Scenario S5, "Mixed Solar thermal and wind": 2.5 GW solar thermal (15h thermal storage), 1.947 GW wind, 6.84 GW Rooftop PV, 22.8 GWh of storage, 30% EE improvements.....203

Figure 8.8. Scenario S1 example three day load profile of winter demand peak reduction using household 3.6 kW rooftop solar systems with 12 kWh storage and 30% energy efficiency improvements.....204

Figure 8.9. Scenario S2 example winter three day load profile of complete renewable energy generation using 19 GW of solar PV systems with 90.25 GWh of storage and 30% energy efficiency improvements.....204

Figure 8.10. Scenario S5 example winter three day load profile of complete renewable energy generation using 2.5 GW of solar thermal stations (with 15h thermal storage), 1947 MW wind power, 6.84 GW rooftop solar PV systems with 22.8 GWh of storage and 30% energy efficiency improvements.....205

Figure 8.11. Solar thermal power plant capacity required for different levels of distributed storage capacity for variations of scenario S5.....205

1 Introduction

1.1 Global warming

The world is warming. By the year 2012, the global mean surface temperature had risen by 0.85°C compared to 1880 (IPCC 2013). Since the mid 20th century, the main driver has been human activity. While there seems to be no broad international consensus on distinguishing dangerous climate change from acceptable climate change, a global average temperature rise of 2°C has become the de-facto international benchmark (Anderson and Bows 2008). Recent findings suggest that even a rise of 2°C may no longer result in a safe level of climate change, and that a rise of 1.5°C is safer (Steffen et al. 2015).

There are gases in the atmosphere which trap heat and raise the temperature and have various natural source and sink processes. Pollutants that are released into the atmosphere as a result of human activity and which contribute to enhanced warming are termed anthropogenic emissions, or more commonly greenhouse gas emissions. The primary anthropogenic emissions, in order of importance, are carbon dioxide gas (CO_2), soot particles, methane gas (CH_4), halocarbons, tropospheric ozone, and nitrous oxide gas (NO_2). The need to reduce these emissions is becoming more urgent. Recent estimates require a drop in emissions by 2050 to between 5 and 30% of 2010 levels and also keeping the atmospheric CO_2 concentration under 430 ppm to limit temperature rise to 1.5°C by 2100 (Pachauri et al. 2015). Greenhouse gases such as NO_2 or methane have well defined lifetimes and will reach stable concentrations in the atmosphere even if the rate of emission remains constant (Meehl et al. 2007). However the behaviour of CO_2 is different. One reason for this is that the

capacity of global carbon sinks is expected to fall as a consequence of human activity and temperature rise. Thus in order to prevent dangerous climate change, there must be a cap on the *cumulative* amount of carbon dioxide that will be released into the atmosphere (Meinshausen et al. 2009). If a position of global equity in per capita emissions is adopted, different countries will have different time-frames and trajectories for their carbon emission reductions. Countries with historical and current high annual emissions per capita (such as Australia) must reduce their emissions more quickly than low emissions per capita countries. Another reason that emissions must be reduced quickly is that about half of current global warming is being masked by aerosol particles (Jacobson 2009). So the Earth is not feeling the full impact of the warming yet. Reduction in aerosol particles in the atmosphere could result in sudden and dramatic changes in climate. There is also the possibility that the Earth's climate system could reach a "tipping point" where there are irreversible impacts (Lontzek et al. 2015). The likelihood of a tipping point occurring is uncertain but expected to increase with rising temperatures.

1.1.1 Greenhouse emissions from stationary electrical generation, and the SWIS grid

In 2005-2006, electricity generation accounted for 45.5%, the largest component, of Australia's primary energy consumption (Syed and ABARE 2007), and approximately the same fraction of Australia's greenhouse gas emissions. Rapid emissions reduction will therefore require rapid reduction in emissions from electricity generation. In the South West of Western Australia (SWWA), the principal electricity supply and distribution system is the South West Interconnected System, or SWIS (Figure 1.1). This grid presents an interesting case study for reducing emissions, because it is isolated from all other major grids, so there is no possibility of importing electricity to cover shortfalls, or

exporting excess generation. Also there is also currently little available hydro-power capacity that could be used for storage. Therefore the task of balancing generation with demand is more difficult. If the SWIS grid could be quickly converted to a low emissions system, while maintaining reliability, then many other places in a similar situation could too.

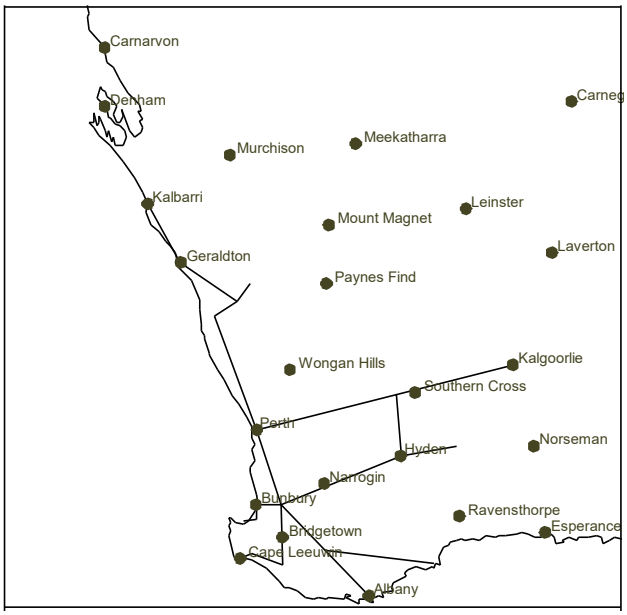

Figure 1.1. Simple schematic of the SWIS grid backbone in the South West of Western Australia.

1.2 Pathways to emissions reduction

What are the options for reducing greenhouse emissions from energy generation and the risk of dangerous anthropogenic climate change? Four technological options have widely been suggested: using nuclear energy, using fossil fuels with carbon capture and storage (CCS), using renewable forms of energy, and finally geo-engineering. The first three options aim to reduce emissions, while the fourth option, geo-engineering, refers to a number of proposed technologies designed to alter the Earth's climate if deployed on a broad scale (Pachauri et al. 2015). Some forms of geo-engineering aim to reduce emissions, but other forms aim to reduce the net energy falling upon the earth

from the sun. Currently there is not enough evidence or experience to properly assess the benefits, and possible side effects of geo-engineering, so it is not considered further here. This thesis will concentrate on two forms of renewable energy, sun and wind, and will demonstrate how the SWIS grid could be rapidly converted to a low emissions energy system.

With any of the technological options, improving energy efficiency so that energy demand is reduced will make the task easier. So from now on, any reference to renewable energy can be taken to also include energy efficiency measures.

1.3 Research questions

The principal objective of this research is to answer the following questions:

1. Do existing solar and wind renewable energy systems currently offer the best path for achieving a rapid transition to a sustainable, low emission, electricity system for the South West of Western Australia? The principal criterion is the ability to rapidly expand generation and reduce greenhouse gas emissions. There are also ancillary criteria that should be considered, such as reliability, water use, and environmental impact. Cost is also an important factor. However, given the urgency of the climate situation, rapid reduction in greenhouse emissions must outweigh near term cost, or the long term cost is likely to be much greater, and could be catastrophic (Stern 2013).

2. As a corollary to the first question, just how far can the renewable energy path be taken? Can solar and wind renewable energy systems, aided by storage and energy efficiency improvements, completely replace the

existing conventional generation systems? Is a 100% renewable energy system a technically feasible option for the SWIS?

1.4 Methodology

Even when considering a local level, the global context of any particular technology choice is important, as there are implications for the availability of infrastructure, skills-base, economies of scale, and possible materials shortages and manufacturing bottlenecks. Therefore the research methodology of this thesis will be divided into two parts:

1. The first part is partly qualitative and will review the characteristics of each of the low emission technology options of nuclear, CCS, and renewable energy on a global scale. The potential advantages and disadvantages of each will be considered and compared. This review aims to assess the viability of renewable energy as an option for rapidly reducing greenhouse emissions (perhaps the only viable option). A search will be conducted for examples of large scale electrical grids that already operate wholly or substantially on renewable energy. Since most large grids still rely on fossil-fuel generation, a search will also be conducted for simulations of hypothetical 100% renewable energy systems based on existing grids.

2. The second part of this thesis will concentrate on developing a numerical simulation of the SWIS grid powered by a combination of solar, wind, energy storage, and energy efficiency. Since solar and wind are the main resources that are available to be utilised in the SWWA, the aim will be to develop models for generating synthetic values of solar and wind power generation based on the spatial and temporal meteorological

characteristics of the SWWA region. Using these models, the energy generated by a hypothetical solar or wind power plant of arbitrary capacity, placed anywhere within the SWWA region, can be estimated. Models for the operation of battery storage and solar thermal storage will also be developed. These capabilities will be integrated into an overall simulation of power supply and demand on the SWIS grid. With load demand mediated by energy efficiency improvements and population increase, a number of hypothetical power system scenarios will be developed, with the aim of achieving 100% renewable generation of the load demand. All of these models will be kept as simple as possible to maximise the ability for interactive operation and the addition of more power stations or storage to the scenarios. The criteria for achieving 100% will be the ability to meet current SWIS grid reliability standards using renewable generation only. Additionally, the required capacity for each technology must be moderate enough to allow a rapid time schedule for installation. Additional information about the methodology can be found in section 4.4.

1.5 Thesis structure

Chapter 1 has laid out the current situation, and the urgent challenge to minimise the risk of dangerous climate change by rapidly reducing greenhouse emissions. Chapter 2 will give a brief overview of nuclear energy, CCS and renewable energy and examine their potential to quickly reduce greenhouse gas emissions from stationary electricity generation on a global scale. Chapter 3 will compare these options and argue that renewable energy and energy efficiency are viable and rapidly scalable options. Chapter 4 will cover current examples and simulations of renewable energy electricity systems, laying out

the framework for the simulation of solar and wind energy (both commercially mature and widely available forms of renewable energy), and an integrated 100 percent solar and wind system for the SWIS, using storage and energy efficiency. Chapter 5 will detail the methodology, calibration and validation for the meteorological simulation of solar irradiance in the SWIS region. This chapter is based on the journal article "A method for generating synthetic hourly solar radiation data for any location in the south west of Western Australia, in a world wide web page" (Laslett et al. 2014). Chapter 6 will detail the methodology and calibration of the solar thermal power model with storage. Chapter 7 will detail the methodology, calibration and validation for the meteorological simulation of wind power. This chapter is based on the journal article "A simple hourly wind power simulation for the South-West region of Western Australia using MERRA data" (Laslett et al. 2016). Chapter 8 will detail the integration of the wind and solar models into the simulation constructed for this thesis, which also allows for the balancing of supply and demand for the SWIS power system using storage, including solar thermal storage, and energy efficiency. Models for solar PV power generation, distributed battery storage and energy efficiency will be developed in this chapter. Chapter 9 will discuss the results of the simulation. Chapters 6, 8, and 9 are based on the journal article "A large-scale renewable electricity supply system by 2030: solar, wind, energy efficiency, storage and inertia for the South West Interconnected System (SWIS) in Western Australia." (Laslett et al. 2017). Finally, chapter 10 will draw conclusions.

2 Overview of low emissions technologies

This chapter provides an overview of the characteristics of commonly cited technological options for reducing greenhouse emissions from electricity generation. These are nuclear, CCS, solar and wind. Storage and energy efficiency measures are also included.

2.1 Nuclear power

Nuclear physics theory defines a stable nucleus as that with the least total energy. Experiments have found that the most stable nuclei are found in the middle of the periodic table. Both lighter and heavier elements are less stable. Therefore, some heavier isotopes have the potential to fission, producing lighter elements of lower total energy. The release of energy can be used for electricity generation. Some lighter elements also have the potential to fuse, producing heavier elements of lower total energy. The only nuclear technology in current wide-scale operation collects heat from the fission of the heavy unstable uranium 235 isotope (U-235), and converts the heat into electricity via steam turbines. Plutonium 239 (Pu-239), which is produced from neutron bombardment of U-238 in both standard and "fast-breeder" reactors, has also been used (Jacobson 2009), as has uranium 233 (U-233).

U-235 and Pu-239 by themselves decay slowly. However, fission of these isotopes can be triggered by bombardment with neutrons, and typically releases 2 to 3 neutrons for every neutron absorbed (Von Hippel and Bunn 2010). Hence, when bombarded with neutrons from previous fission events, the rate of fission can be greatly increased, which in turn produces more neutrons

and leads to more fissions. This amplification is referred to as a chain reaction. In a nuclear bomb the chain reaction is uncontrolled. In a nuclear reactor, the chain reaction is controlled to generate a steady source of heat energy which can be converted into electricity. Materials that are capable of sustaining a nuclear chain reaction are called fissile.

2.1.1 Current status

Over the past 15 years, nuclear power generation has exhibited little growth. Globally in 2014 there were 391 commercial reactors in operation (Schneider and Froggatt 2015), 44 less than in 2009, and 53 less than the peak in 2002. In 2014 the combined nuclear capacity was 337 GW, less than the 2008 capacity of 370 GW. Despite the drop in reactor numbers, capacity increased from 2002 until 2007, and remained steady until 2011. This was achieved through larger reactors replacing smaller ones, and through uprating the capacity of existing reactors (Schneider and Froggatt 2015). Actual energy generation peaked in 2006. In 2011 the Fukushima disaster caused a sharp decline in the number of operating reactors, combined capacity and energy generation. All of these have begun increasing again since 2012. However new construction starts have declined since 2013, and at least 75% of all existing construction sites have been delayed. The average construction time for reactors completed between 2005 and July 2015 was 9.4 years.

The global average age of nuclear plants has been increasing, and was 28.8 years at mid 2015. The overall average age at shut down is about 25 years, but many early reactors only operated for a few years, and the age range of reactors shut down since 2014 was from 36 to 42 years. Assuming an average reactor lifetime of 40 years before shut down, Schneider and Froggatt (2015) estimate that in addition to the 62 reactors listed as under construction, 19 extra reactors

would need to be ordered and built by 2020 to maintain the current number of operating reactors, and 188 reactors would be needed by 2030. This build rate is about four times the installation rate achieved between 2005 and 2014.

Another possible way to maintain reactor numbers is to increase operational lifetime beyond 40 years on average. Reactor lifetime can be extended up to 60 years in the US, however, both uprating capacity and lifetime extension of reactors could pose extra safety risks and complicate decommissioning. Also since the reactors involved in the Fukushima disaster were at least 37 years old, more questions have been raised about extending reactor lifetimes, and there has been a tendency toward accelerated shut down of older reactors rather than life time extension.

The overall picture of the current status of nuclear power raises doubts over the ability to increase or even maintain its current share of world electricity production.

2.1.2 Life-time of reserves

There are varying estimates of the life-time of recoverable uranium ore reserves. MIT (2003) estimated that a fleet of 1500 reactors, each generating 1000 MWe, operating for 50 years requires about 15 million tonnes of uranium. Using these figures, a single 1 GWe reactor requires 200 tonnes per year. Capacity factor is the ratio of actual electricity generated compared to the amount that would be generated if the plant ran continuously at rated power. Operational nuclear capacity in the year 2008 was about 370 GWe (Schneider et al. 2009) and generated about 2600 TWh, or on average 297 GWe operating continuously, giving an average capacity factor of ~0.8. Assuming that a 1 GWe reactor will consume 200 tonnes of uranium per year, operating at a capacity factor of 1, the current nuclear fleet requires about 59 kilotonnes per year. Known resources of

uranium were also estimated at about 3 to 4 million tonnes. Using the figure of 4 million, there is approximately 68 years of supply at current nuclear generation rates. Nuclear power supplies about 14% of world electricity demand (Schneider et al. 2009), so if nuclear power were scaled up to supply all of the current demand, current reserves would last about 9.5 years. This figure will be even less if there is growth in demand. Hohmeyer and Trittin (2008) estimated global reserves as between 6.7 and 23 years, at current usage rates. However, MIT (2003) estimated that a doubling in price of uranium would multiply the reserves by a factor of 10, giving 95 years of reserves at current global demand rates, or 680 years at current nuclear generation rates. Mudd (2014) concluded that uranium supply is mostly an economic and political issue, rather than a resource constraint issue.

Another source of nuclear fuel is the weapons grade uranium and plutonium presently held in global nuclear bomb stockpiles (Pearce 2008). This can be considered a favourable option, because there is no extra energy use or greenhouse emissions from the mining and processing of un-enriched ore. WNA (2009) estimated that there are about 2000 tonnes of highly enriched uranium and about 260 tonnes of weapons grade plutonium in Russian and United States (US) weapons stockpiles. These in total could displace enough uranium mine production to give an extra 13 years of fuel reserve at current nuclear generation rates. If nuclear generation was scaled up to meet all of the current global electricity demand, there would be an extra 1.8 years of fuel reserve.

There are large quantities of low grade uranium ore in the earth's surface and in sea water at low concentrations. For both, the energy needed to extract the uranium is likely to exceed the energy that can be produced (Diesendorf 2005). MacKay (2010) discussed a sea water extraction technique developed in Japan,

but noted that most of the water in the sea is inaccessible, and that ocean current systems cycle water around approximately once every 1000 years. The issue of net energy return was raised, and also the collector area required to scale up this technology to meet global energy demand.

Fast breeder technology produces plutonium from the spent fuel of conventional reactors. The plutonium can also be used to produce energy, effectively multiplying the fuel reserves by up to 60 times (Diesendorf 2005). However, MIT (2003) recommended against the use of breeder technology or one-pass spent fuel recycling. The reasons given were cost, short-term waste management issues, proliferation risk, and safety issues.

2.1.3 Grid penetration

High penetrations of nuclear power into an electricity system raise a number of technical issues. The mechanisms of radioactive decay chain kinetics are complex. Delayed neutron emission means that changing the heat output level of a nuclear reactor core by changing the neutron chain reaction kinetics is a complex process that must be performed gradually (Patterson 1983). Nuclear reactor start up and shut down can take many hours. Nuclear plants have long ramping times and a limited ability to reduce output (Denholm and Margolis 2006). They can be designed and configured for more rapid ramping, but have shown a higher unscheduled outage rate when operated at less than maximum output (Martinot 2016). The case of France might serve as an illustration. France has a large difference between summer lowest load and winter highest load. The large winter peaks are due to the wide-spread use of electric space and water heating. These peaks are not covered by nuclear, but by fossil fuel plants or imports (Schneider et al. 2009). This suggests that nuclear is not suitable for meeting peak load demand.

Another issue arises from the large unit size of reactors and unplanned shut downs. Such shut downs for whatever reason (e.g. earthquake, safety problem, terrorist incident, or even a problem elsewhere in the grid) can withdraw large amounts of power very suddenly, especially if more than one reactor must be shut down (Lovins 2009). As mentioned above, reactors can't restart quickly after a shut down. In one example, the August 2003 north east US blackout, 9 nuclear reactors were forced to shut down, even though the problem did not originate with them. For the first 3 days after shut down, their combined power output was less than 3% of normal, and their average power output over 12 days after shut down was less than 50% (Lovins 2009).

2.1.4 Radioactive waste

When fission occurs, U-235 and Pu-239 nuclei split unevenly into a range of fission by-products with atomic masses centred around 95 and 135 (Patterson 1983). The fission by-products tend to be beta radiation emitters, emitting fast moving electrons as excess neutrons change to protons. Some neutrons are captured by other nuclei rather than causing fission, so heavy trans-uranic isotopes are also produced, all of which are unstable and prone to alpha, beta, and gamma ray emission. Hence the operation of a nuclear reactor produces radioactive wastes that present health and environmental risks on a time scale of tens of thousands of years (MIT 2003). The many millions of tonnes of uranium mine tailings can also remain dangerously radioactive for tens of thousands of years (Patterson 1983). At the end of their operational lifetime, many parts of a nuclear reactor will be contaminated with radioactivity, and must remain isolated from the environment and public access for many years. There has been no successful demonstration of a disposal system for these nuclear wastes (MIT 2003). Although there have been proposals for 'fast-burner' reactors that would fission the problematic long-lived radioactive wastes and

reduce the long time periods required for isolation, two reviews have concluded that the process is not effective enough to avoid the need for long term repositories and the heightened operational and proliferation risk is not justified (Von Hippel and Bunn 2010).

2.1.5 Safety

The safety risk of current nuclear fission technology comes from three kinds of events: an accident that releases radiation or radioactive material anywhere in the fuel chain, an act of terrorism, or an exchange of nuclear weapons. The Chernobyl accident in 1986 demonstrated the disastrous consequences of a major nuclear reactor accident. The reactor at Chernobyl used a design with a positive void coefficient, meaning that loss of cooling causes reactor heat output to increase (Shlyakhter and Wilson 1992). There was also no outer containment shield. Therefore the nuclear industry hoped that bad design and poor operation could be blamed, and that such an accident would never happen in the west (Thomas 2012). MIT (2003) made two estimates of core damage frequency due to accident, based on US reactor designs. One is based on the historical record of reactor operation in the US from 1957 to 2002. The one incident of core damage at Three Mile Island in 1979 gave an estimate of 1 in 2679 reactor years, or just under $4x10^{-4}$ per year per reactor. The other estimate was based on identification of possible failures that could occur in a reactor, and their probabilities and consequences. This method produced an estimate of $1x10^{-4}$ incidents per year per reactor. Under a scenario of tripling of US nuclear generation capacity by 2050, and using the second more optimistic estimate, 4 core accidents would occur in 50 years. A core damage accident does not necessarily mean a release of radiation into the environment, or to reactor workers. However MIT (2003) considered that this accident rate was unacceptably high, because of the significant public health risk, and the loss of

public confidence in nuclear power even if containment was successful in all four cases. Additionally, little is known about the safety of the overall fuel cycle, other than reactor operation.

The earthquake and tsunami that hit Japan in 2011 demonstrated that Western designed reactors are vulnerable to unexpected events, such that the frequency of core damage accidents may be greater than estimated. At the Fukushima Dai-Ichi nuclear reactor complex, four operating reactors shut down successfully (with two already shut down), but grid power to the cooling systems was cut, and the emergency backup generators were crippled by the tsunami (Aoki and Rothwell 2013). The severity of the accident was magnified by high level management failures in the aftermath of the earthquake. Cooling systems were not restored, leading to hydrogen explosions, fuel core meltdowns, and release of radiation into the environment. Four years after the accident, high radiation levels remain inside each reactor building, hampering clean up efforts (Schneider and Froggatt 2015). Large quantities of radioactive water, used to cool the fuel cores, are accumulating on site. Storage and leakage into the environment are a constant problem. Both the Chernobyl and Fukushima disasters have led to long term population displacement, widespread health effects, and enormous economic costs.

Accidents are not the only hazard posed by current nuclear fission technology. Jacobson (2009) linked the presence of a civilian nuclear power program with the ability to build a nuclear weapon. A precise probability of nuclear weapon exchange was not calculated, but a scenario involving the detonation of weapons onto cities totalling 1.5 mega tonnes Trinitrotoluene (TNT) equivalent was defined, and a rough estimate of 1 event in 30 years due to war or terrorism was calculated. This scenario was estimated as only about 0.1% of the yield range of a full-scale nuclear war. The author also noted that globally there is

enough nuclear material to produce more than 3 times the current number of 30 000 nuclear warheads. However, these estimates must be set against the fact that there has been no hostile nuclear weapon exchange in over 65 years. The increased proliferation risk associated with the use of breeder technology or one-pass spent fuel recycling was one of the reasons why MIT (2003) recommended against the deployment of these technologies. Spent fuel recycling was used by India as a cover for their covert nuclear weapon program (Von Hippel and Bunn 2010). Martin (2015) raises concern over the threat to civil liberties and Patterson (1983) raises the spectre of a totalitarian social structure becoming necessary to ensure the safety of nuclear reactors and materials.

2.1.6 New reactor designs

Nuclear fission reactors have been categorised into 4 classes, or "generations" (from I to IV), with most currently operating reactors in generations II or III (Schneider et al. 2009). Generation IV is not expected to become available for the next 20 years. Since 2000, a "generation III+" class has been defined. These are distinguished from generation III by the greater use of "passive safety" systems, where safety relies more on inherent design features, rather than on active engineered systems. Four units were in operation in Japan as of 2009, with several more under construction.

MIT (2003) considered that a core damage accident frequency of 1 in 100,000 reactor years (a 10 fold reduction on their estimate of current risk), or less than 1 accident in 50 years, was an acceptable level for a three fold expansion of US nuclear capacity by 2050. The authors also cited claims by advanced light water reactor designers that they can meet this standard. However, no new reactor design has completed an operational lifetime, and hence their safety record

remains uncertain. Doubts have been raised about the overall safety of reactors with passive safety features, for two reasons. Firstly, the pressure generated by gravity-fed passive emergency cooling systems is less than pump-driven active systems, and hence performance is less certain in situations where hot fuel may produce high back pressures. Secondly, the reliability requirements for the active safety systems have been loosened, and less robust containment has been allowed (Von Hippel and Bunn 2010).

US nuclear generation in 2008 was 800 TWh (Schneider et al. 2009), or about 31% of the world total of 2600 TWh. Hence on a global scale, to achieve a risk probability of less than 1 accident in 50 years, the core damage frequency would need to be less than 1 in 325,000 reactor years, or $3x10^{-6}$ per reactor per year.

2.1.7 Breeder and burner reactors

Breeder reactors use an existing neutron source (most probably a fissile fuel) to transform other non-fissile materials (such as the much more common U-238) into fissile isotopes, producing more fissile fuel than they consume and thus extending the lifetime of the original fuel (Cochran 2010). Fast breeder technology can produce plutonium from the spent fuel of conventional reactors, which can be used to produce energy, effectively multiplying fuel reserves by up to 60 times (Diesendorf 2005). Breeder reactors were originally proposed as far back as World War II, but initial development programs tailed off as uranium reserves for conventional reactors were found to be more abundant than expected, and growth in nuclear generation less than expected (Cochran 2010). MIT (2003) also recommended against the use of breeder technology or one-pass spent fuel recycling. The reasons given were cost, short-term waste management issues, proliferation risk, and safety issues. Research interest has persisted, as breeder reactors can also be used to convert heavy transuranic

elements present in existing nuclear waste into lighter fission products ("burning"), reducing the volume of waste and the level of radioactivity (Cochran 2010). However, as mentioned in section 2.1.4 above, this process is not considered effective enough to avoid the need for long term repositories and leads to heightened operational and proliferation risk.

Generally, breeder reactor operation has not been successful, with multiple and lengthy shut downs, and many sodium coolant fires. Russia has achieved respectable operational levels in the BN-600 breeder reactor by using multiple redundant steam generators. The system can tolerate frequent sodium fires by switching from one damaged generator to another while the first is repaired. A further breeder reactor, the BN-800, has begun operation, although still operating at much reduced capacity.

2.1.8 Thorium cycle

Thorium fission is thought to offer potential advantages over uranium fission. Thorium is estimated to be three times more abundant in the Earth's crust (Kazimi 2003). In general there is less long-lived, hazardous radioactive waste produced by the thorium cycle than the uranium or plutonium cycles. The thorium cycle is also considered to offer better proliferation resistance. Thorium could be used to develop nuclear weapons, but is more difficult than using plutonium. Concerns have been raised that U-233 could easily be diverted from a thorium reactor to make a nuclear or dirty bomb (Ashley et al. 2012).

There are also disadvantages to the thorium cycle when compared to the conventional uranium cycle. Naturally occurring thorium ore has a predominant isotope, Th-232, that is not in itself fissile, and unlike uranium ore, does not have significant quantities of fissile isotopes that can be used to generate neutrons to sustain a continuous nuclear reaction. Instead an external

source of neutrons must be supplemented with the fuel, such as U-233, U-235 or Pu-239. However, thorium is harder to use in existing light-water reactors, because of the build up of neutron absorbing intermediate products. Another option is to insert Th-232 into the surrounding blankets of breeder reactors, which supply the neutrons, as proposed in the Indian nuclear program (Von Hippel and Bunn 2010). India has limited local supplies of uranium but a much greater thorium resource. Th-232 has already been used to blanket balls of U-235 in high temperature gas cooled reactors, thus acting as an extender to the U-235 fuel (Schaffer 2013). These and other thorium reactor technologies, such as molten salt reactors (D. G. Green 2015), are in the research and development stage, but are not expected to make any significant contribution to world energy production for at least another 20 years (Schneider and Froggatt 2015).

2.1.9 Nuclear fusion

Another kind of nuclear reaction might have potential for electricity generation. Hydrogen fusion involves the fusing of deuterium-2 or tritium-3, which are heavier isotopes of hydrogen, to form helium. Deuterium can be obtained from sea water. The more unstable tritium-3 (half-life 12 days) isn't found abundantly in nature, but can be manufactured from lithium. Hydrogen fusion technology is in the experimental stage. Even with steady technological progress, fusion power is not expected to be available in significant quantities before the second half of the 21st century (Turnbull et al. 2015).

2.1 Carbon capture and storage (CCS)

Geosequestration, or Carbon Capture and Storage (CCS) is a technology that attempts to capture the carbon dioxide produced in the fossil fuel combustion process and store it for long periods of time, thus preventing the carbon dioxide

from entering the atmosphere (Diesendorf 2006a). CCS can be divided into three phases: capture, transportation, and storage.

Currently there are three main methods of capture: "pre-combustion", or before the fuel is burnt to provide energy; "post-combustion", or after the fuel is burnt; and "oxy-fuel combustion", which involves injection of oxygen during combustion resulting in easier post-combustion separation (IPCC 2005). In many cases, a post-combustion system can be 'bolted on' to an existing power station. Also under development are fuel cell systems that convert fossil fuel to electricity in an electro-chemical reaction without combustion (Damen et al. 2006). CO_2 can be captured from the fuel cell after the reaction has taken place, or the fuel can be reformed to separate CO_2 beforehand, creating hydrogen as the fuel. Fuel cell systems have shown the potential to operate at higher conversion efficiencies (sometimes more than 50%) than combustion processes. Natural gas is considered to have lower emissions than coal, but in some gas fields, CO_2 emissions may offset this advantage, so capture at the point of extraction (rather than the point of combustion) may be required as well (Diesendorf 2006a). There may also be significant fugitive methane emissions.

The two main methods of CO_2 transport are via pipeline and via ship. Possible storage methods include geological storage (in formations such as oil and gas fields, unminable coal beds and deep saline formations), ocean storage (direct release into the ocean water column or onto the deep sea floor), storage in mineral carbonates, and industrial consumption of CO_2 (IPCC 2005). Geological storage can be divided into the use of depleted oil and gas reservoirs, use of deep saline aquifers, using CO_2 in enhanced oil and gas recovery (EOR), and using CO_2 in enhanced coal bed methane recovery (ECBM).

2.1.1 Global potential

The global storage potential in geological formations is uncertain but is estimated to be at least about 2000 Gt CO_2 (IPCC 2005). There could be much more storage potential in saline formations. Ocean CO_2 storage capacity could be in the range of thousands of gigatonnes, but depends on what level of atmospheric stabilisation is achieved, and on environmental constraints. Industrial consumption is not expected to contribute much to emissions reductions. In 2009, the fossil fuel emission rate was about 30 Gt CO_2 per year (Jacobson 2009).

The proximity between emissions sources and potential carbon storage sites is an important factor in determining the technical and economic feasibility of CCS. IPCC (2005) used a criterion of 300 km proximity for assessing the geographical match between point sources of carbon emissions and possible geological storage sites, concluding that many point sources are in proximity to storage sites, but in general there is a lack of information regarding the proximity of sources to potential storage sites. Globally, only a small proportion of large point sources of carbon emissions are within proximity to potential ocean storage sites. By 2050, around 30 to 60% of CO_2 emissions from electricity generation will be technically suitable for capture. There is also potential for capture from biomass plants, but the proximity of storage sites to future large biomass plants has not been studied.

2.1.2 Australian potential

The storage potential for CCS in Australia has been estimated as 740 Gt CO_2 (Bradshaw et al. 2002). In 2005-2006, electricity generation accounted about 45% of Australia's greenhouse gas emissions (Syed and ABARE 2007), or very roughly around 250 Mt CO_2 per year. So there is enough storage capacity for

many hundreds of years of emissions. However, technical factors such as multiple well site interference, and the need to keep the reservoir pressure below the fracture pressure, place limitations on maximum storage rates (Allinson et al. 2009). A maximum storage rate of 100 to 115 Mt CO_2 per year was estimated (Bradshaw et al. 2002), implying that CO_2 can't be stored at a high enough rate to capture total emissions. Only just under half of annual electricity emissions could be stored.

2.1.3 Current technological status

CCS can be applied to large point sources of CO_2 emissions (IPCC 2005), but not small point sources (e.g. vehicles with internal combustion engines). However, CCS could still contribute to emissions reductions in transport if there is a large-scale switch towards using electric or hydrogen based power trains in the vehicle fleet, and the electricity or hydrogen is produced from fossil fuels. Direct conversion of fossil fuel to electricity or hydrogen using fuel cells is in the demonstration phase (Damen et al. 2006). Pre-combustion and post-combustion capture are considered to be technologically and economically feasible under certain circumstances (IPCC 2005), while oxyfuel combustion is in the demonstration phase (Leung et al. 2014). There already exists a mature market for transport by pipeline, and transport by ship is considered to be economical under certain circumstances.

Storing carbon using EOR is an economically mature storage technology and could be used for storage in old gas and oil fields. There have been several small scale pilot and commercial deep saline aquifer storage projects, but there is a need for more post-injection monitoring. ECBM is in the demonstration phase but reduction in permeability of the coal seam is a technical issue needing to be solved. All forms of ocean storage are still in the research phase. Ocean

storage does not include storage in oil or gas fields that happen to be underneath the ocean. Storage in mineral carbonates is in the research and demonstration phase, but there remain a number of uncertainties (Leung et al. 2014). Industrial consumption is commercially mature, but is not expected to contribute much to emissions reductions (IPCC 2005). Another possibility is storing carbon by reaction of CO_2 with metal oxides to form stable carbonates. However the natural reaction rate is slow and must be enhanced by pre-treatment of the minerals, which is presently energy intensive. This technique is generally in the research phase, although some projects using metal oxides from waste streams are in the demonstration phase.

Extending the findings of Viebahn et al. (2007) globally, some countries may face the need for large-scale replacements or substitutions of fossil-fuel plants in the next 10-15 years, either to meet emissions targets or to replace plants at the end of their lifetimes. This is before many CCS technologies may be economically mature. In this case retrofitting is the only feasible way for CCS to make a significant contribution to reducing emissions. Scott et al. (2015) suggest that the current storage creation rate of CCS systems is insufficient to match the rate of reductions in greenhouse gas emissions required to prevent dangerous climate change.

2.1.4 Advantages and problems of CCS

A potential advantage of CCS is that it offers the possibility of deep cuts to CO_2 emissions without disrupting existing energy supply systems and the global economy. However Diesendorf (2006a) highlights a number of problems, including increased water use and pollution, land degradation, worker health problems, and high danger levels. The main reason for these problems is that extra energy must be diverted to the geosequestration operation, reducing

overall efficiency and increasing the amount of fossil fuel that must be combusted per unit output of energy. This also means extra cost. Both industrial fixation and production of carbonates will require mining of the raw materials and disposal of the carbon products in land-fill. Each will require additional transport and land clearing (IPCC 2005), which may detract from the net carbon storage.

A major concern is the risk of leakage from the storage sites. In addition to releasing CO_2 back into the atmosphere, negating the benefit of CCS, there are potential risks to human health. High leakage rates combined with stable atmospheric conditions could cause local CO_2 concentrations in the air that are high enough to harm animals or people (IPCC 2005). In addition to human health concerns, elevated CO_2 concentrations in the shallow sub-surface include harmful or lethal effects on plants and subsoil animals and groundwater contamination. The potential effects of large scale leakages include higher greenhouse emissions, suffocation of humans and animals, acidification of waterways, damage to ecosystems, and if brine from saline aquifers is pushed to the surface, contamination of drinking water and soil salinity (Diesendorf 2006a).

IPCC (2005) found that the risk of leakage of CO_2 from pipelines is low (perhaps lower than existing hydrocarbon pipelines), but a sudden and large leakage of CO_2 could be quite dangerous to human health. Geological storage leakage can be categorised as either abrupt (maybe through an injection well failure or through an abandoned well), and gradual (through undetected faults, fractures or wells). Based on existing experience and modelling, IPCC (2005) claim that well selected and managed geological formations are very likely to retain 99% of stored CO_2 over 100 years, and likely over 1,000 years. Trapping mechanisms could make the stored CO_2 more secure over time, such that it might be

retained for up to 1,000,000 years. The authors also claim there is no known mechanism for sudden CO_2 leakage from ocean storage. However, Jacobson (2009) claims that leakage rates over such time scales are impossible to predict. Liquified CO_2 injected into the ground will be under high pressure and take any opportunity to escape. The low pH value of CO_2 will tend to weather rock over time, and if a leak does occur, there is uncertainty over whether it would be detected, or if the leak could be plugged, especially if it is happening over a wide area. Where CO_2 is bound in limestone or other non-volatile minerals, then the risk of leakage will be presumably much less, but these sites may be hard to find (Diesendorf 2006a). Jacobson (2009) highlights the risk of leakage through existing rock fractures and porous soil, or new fractures resulting from earthquakes. Another potential problem is that CCS itself may cause small earthquakes. Pressure build-up caused by CO_2 injection could trigger small seismic events (IPCC 2005). Ocean storage has the potential to increase water acidity and the carbon will return to the global carbon cycle eventually. Viebahn et al. (2007) notes the extra emissions from mining and transport (due to the higher energy requirement of CCS), as well as extra emissions of methane.

2.1.5 Lifetime of world fossil fuel reserves

Shafiee and Topal (2009) estimated that coal reserves in 2005 equate to about 65% of world fossil fuel reserves with oil and gas split approximately evenly for the remaining 35%. Using a model that accounts for increases in consumption, the authors estimated that reserves for coal, oil, and gas will last for 106, 34, and 36 years respectively. Using 2005 as a base year, reserves for coal, oil, and gas would last until 2111, 2039, and 2041 respectively. If coal is substituted for oil and gas after 2041, coal reserves will be exhausted sooner. Gadonneix et al. (2010) was slightly more optimistic, estimating the ratio of reserves to annual

consumption in 2008 for coal, oil, and gas to be 128, 41, and 54 respectively. Using 2008 as a base year, reserves for coal, oil, and gas would last until 2136, 2049, and 2062 respectively. If the use of CCS technologies decreases the efficiency of energy conversion, then these estimates must be reduced further. The conclusion that must be drawn is clear: using CCS can only be a temporary solution, as fossil fuels are likely to run out over the next century. There must eventually be a global transition to other energy sources.

2.2 Renewable energy

Renewable energy systems are those that harvest natural energy fluxes and convert the captured energy into a form usable by human civilisation. The energy fluxes can be divided into three categories according to their origin (Hohmeyer and Trittin 2008). Energy from the sun striking the earth is the first source, providing a solar radiation resource over large areas of the Earth's surface. This source in turn drives global wind and wave systems and the hydrological cycle which provides water at high potential energy, and biomass through photosynthesis. The second source is radioactive decay within the Earth's crust which provides heat for geothermal energy. The third source is the gravitational energy of the moon (and to a lesser extent the sun), which powers the ocean's tides.

2.2.1 Global potential of renewable energy

Many of these natural energy fluxes are essentially inexhaustible over the time-frame of the life of the Earth and contain many times the current global energy use of human society (Hohmeyer and Trittin 2008). Table 2.1 gives estimates of the available energy fluxes. These fluxes provide a free 'fuel', but are often diffuse, variable, and distributed over the Earth's surface in a pattern different

to the current distribution of energy demand. This thesis will concentrate on solar and wind as the two forms of renewable energy that have the most commercially mature systems for harvesting and conversion into electricity, are widely available in the SWWA region, and already have a presence on the SWIS grid. Bioenergy is also discussed, as it provides one means for long term energy storage across seasons, and the South West region of Western Australia has potential bioenergy resources. Wave energy is also under active development and modelling the potential contribution to the SWIS grid is worthwhile for a future study.

Table 2.1. Renewable energy resources in 2004.

Renewable source	**Annual energy flux (EJ/y)**	**Ratio of annual flux to annual demand**
Solar	omitted	omitted
Wind	omitted	omitted
Hydro	omitted	omitted
Bioenergy	omitted	omitted
Ocean (wave and tidal)	omitted	omitted
Geothermal	omitted	omitted
Current annual energy demand (2004)	omitted	omitted

Source: Hohmeyer and Trittin (2008).

2.2.2 Solar energy

Solar radiation is diurnal and most intense at lower latitudes (Hohmeyer and Trittin 2008). There are two currently commercially available methods for generating electricity from solar energy: Photovoltaic (PV) cells, which convert photons directly into electricity; and solar thermal, which converts the photons into heat as an intermediate step. The heat is then converted into electricity.

2.2.2.1 Solar PV

In PV cells the energy of incident photons causes electrons to jump to a higher energy quantum state, providing a source of electrical potential (voltage). Electricity flows when there is a pathway for the electrons to flow back into the lower energy state. Only photons within a certain energy range can be utilised, and the efficiency of conversion is low, less than 20% for most current commercially available PV cells. However efficiencies are on a continuous improvement pathway (Hohmeyer and Trittin 2008), with the best laboratory cells reaching 40% at highly concentrated solar intensities, and cells with efficiencies greater than 20% about to enter high volume production (Owano 2015). Conversion efficiency falls at low values of solar irradiance and if the cell temperature increases (Huld et al. 2010). Direct current (DC) to alternating current (AC) conversion losses also reduce overall efficiency. Despite these limitations, the use of solar PV has grown strongly, doubling about every two years on average (Jean et al. 2015). Global installed capacity reached 177 GW in 2014, compared to 3.7 GW in 2004, giving an average annual growth rate of 47% (REN21 2015).

Although higher efficiency cells are more expensive, collector systems can focus and concentrate sunlight, reducing the required PV cell area. Because these systems can only focus direct sunlight, their suitability for more cloudy climates has been questioned (Barnham et al. 2006). If there are more clouds, the proportion of diffuse to direct sunlight tends to be greater. However, tests have shown that in many Japanese cities which have cloudy maritime climates, a concentrator system could generate around twice as much electricity per unit area as a conventional flat plate system.

2.2.2.1.1 Technological status of PV

Barnham et al. (2006) plotted the future trends in PV using three "generations". The first generation of crystalline cells have efficiencies of around 20%. The second generation, comprising of thin film or other technologies, when fully developed will have similar efficiencies but lower cost per kW, and the third generation, using novel approaches, aim to have efficiencies higher than 30% or much lower costs per kW, or both. Although the distinctions are becoming blurred, these different generations roughly correspond to the classification of PV cells into commercial wafer, commercial thin film, and emerging thin film by Jean et al. (2015). The first generation is in wide-scale commercial production and costs have fallen dramatically (Meneguzzo et al. 2015). There is active research to achieve higher efficiencies and use less silicon, but theoretical efficiency is limited to around 31% (Barnham et al. 2006). Second generation solar cells are commercially available with cadmium telluride cells reaching efficiencies of around 16% (Meneguzzo et al. 2015). Third generation cells include organic materials and nanocrystalline solar cells. They are mostly in the research stage, with efficiencies just above 10% (M. A. Green et al. 2015). However perovskite cells have achieved efficiencies of around 20% in the laboratory. Concentrating solar PV cells have attained efficiencies of more than 40% in the laboratory. The trends for this technology are clear: increasing efficiencies, falling costs, and rapidly rising installed capacity. The growing production volumes of solar PV cells mean that costs are also falling due to economies of scale (Köberle et al. 2015).

2.2.2.1.2 Material constraints

Solar PV currently only provides a small fraction of global energy demand (Jean et al. 2015). The question arises as to whether there will be any material constraints if capacity is scaled up to meet a significant part of this demand.

Although there have been shortages of PV grade silicon, this has been due to manufacturing capacity bottlenecks rather than a shortage of silicon. For large scale deployment of first generation polycrystalline silicon solar PV cells, there may be, however, shortages of silver, which is used as an electrode, and flat glass, which is used as a substrate and encapsulation layer. For second generation thin-film PV cells, substituting indium oxide electrodes with zinc oxide electrodes may avoid limitations to large-scale deployment due to limited indium reserves. However copper indium gallium selenide (CIGS) cells may still face supply limitations. For high efficiency cells used in concentrator systems, reserves of germanium (Ge) might limit large scale deployment, unless more abundant gallium (Ga) is substituted for Ge. With the pace of research and progress in solar PV technology, it is very difficult to predict where future bottlenecks may lie. Many of the newer PV technologies currently in the research phase require less material and use materials that are widely abundant.

2.2.2.2 Solar thermal

Solar thermal power systems differ from PV systems in that photons are not directly converted into electrons. There is an intermediate stage of conversion into heat energy (phonons). Because of this intermediate stage, solar thermal systems have the potential to store energy and provide electrical capacity on demand, even through the night. As with concentrated PV, a collector system focuses and concentrates direct sunlight onto a heat absorber medium. This absorber medium then transfers the heat into steam to drive a turbine, or to a heat storage medium. In some designs, the heat absorber medium is the same as the heat storage medium. Four types of collector systems have been commonly used. They are parabolic trough, linear fresnel collector, stirling dish, and power tower (Baharoon et al. 2015). The first two are categorised as "line focus"

technologies, while the last two are known as "point focus" technologies. Line focus collectors are cheaper and technically easier to produce, but point focus technologies can achieve higher light concentration and higher temperatures. Higher temperatures allow higher thermal to electrical conversion efficiencies and lower cost per unit of energy generated. Line focus technologies have single vertical axis sun tracking, while point focus technologies have dual axis sun tracking. Solar thermal plants are considered to have a high ramping capability (Denholm and Mehos 2011).

2.2.2.2.1 Technological status

Solar thermal plants without storage have been operating for two decades (Hohmeyer and Trittin 2008), and since 2005, there has been increasing commercial production, with global capacity growing from 354 to about 3425 MW in 2013 (Bilgili et al. 2015). Parabolic trough technology can be considered commercially mature because it has been operating commercially for more than 28 years (Baharoon et al. 2015), and most of the currently operating solar thermal plants use parabolic trough receivers. There are also a number of solar power tower projects in operation or under development (Tian and Zhao 2013). They are considered more suitable for achieving very high temperatures and hence greater efficiencies (Vignarooban et al. 2015). Very few linear fresnel collector or stirling dish systems are in operation, although research is ongoing. Recently a 125 MW_e linear fresnel collector system was commissioned in India.

2.2.2.2.2 Thermal storage

Heat storage systems can be classified into three types in order of ascending storage capacity: sensible heat storage, latent heat storage, and chemical heat storage (Tian and Zhao 2013). Sensible heat storage stores and releases energy by raising and lowering the temperature of the storage medium. Currently molten salts are favoured for the heat storage material because of their high

temperature thermal stability, low vapour pressure, low viscosity, high thermal conductivity, non-flammability and low toxicity. The use of molten salt heat storage has been commercially proven, but corrosion can become a problem, mainly because of the higher temperatures achievable with molten salt than with other possible materials (Vignarooban et al. 2015). There are several parabolic trough solar thermal power stations currently in operation from 50 to 150 MW in capacity and with 7 to 8 hours of molten salt thermal storage (Tian and Zhao 2013). A 110 MW solar power tower station with 10 hours of molten salt thermal storage is operating in California (NREL 2016). Latent heat storage stores energy by injecting heat into a material and causing a phase change (either from solid to liquid or liquid to gas) rather than increasing the temperature. Energy is released by reversing the phase change. With thermochemical storage, heat is absorbed by an endothermic chemical reaction, and released when the reaction is reversed. Latent and chemical heat storage have the potential for much higher storage capacity, but must overcome current limitations in heat transfer ability, durability, and chemical stability. They are still in the research phase.

2.2.2.3 Environmental impacts of solar energy technologies

Tsoutsos et al. (2005) list the possible adverse environmental impacts of solar energy technologies, including visual impact, land use requirements for large-scale stand-alone power stations, water use requirements in arid areas, accidental release of toxic materials during construction, manufacturing and operation, thermal pollution, and possible fauna deaths from flying into the focused light of solar thermal and concentrating solar PV systems. These impacts must be balanced against the positive environmental consequences of avoided CO_2 emissions, avoided climate change, and associated habitat retention; and compared with the environmental impacts, including continuous

emissions of toxic chemicals during operations, and water use of the displaced fossil-fueled or nuclear generators. In the case of roof-top and distributed PV generators, habitat destruction during operation maybe negligible, although the land use requirements of large-scale PV manufacturing centres must be taken into account. Avoidance of the necessity of grid upgrades and/or extensions may be of great benefit to habitat and aesthetic appeal retention. Large utility scale PV generators may have significant land clearing requirements however (Hernandez et al. 2014), with the potential for habitat destruction and biodiversity loss. Currently, the total land use requirement for large scale PV generators is about 3.4 ha/MW (Ong et al. 2013). This value would decrease with improving solar PV cell efficiencies, but the land use of large-scale PV manufacturing centres must also be taken into account. Large scale concentrating solar energy technologies also have significant land use requirements, currently estimated at about 4.0 ha/MW (Ong et al. 2013). Hertwitch et al. (2015) found that the land use requirements for both these solar technologies were generally less than for coal fired power generation (with or without CCS). Nevertheless, careful siting would be required to minimise habitat and biodiversity loss. Hence some sites with a high solar resource may be unsuitable.

Hosenuzzaman et al. (2015) points out that low emission solar PV systems have positive environmental and human health effects as they replace fossil fuel generation. Emissions of CO_2, NO_x and SO_2 gases are reduced, noise is reduced, and incidence of respiratory and cardiovascular diseases are lowered. However, in the case of some types of PV cells, small quantities of toxic material may be released in the event of fire.

2.2.3 Wind energy

Approximately one percent of the solar energy absorbed by the Earth is converted to kinetic energy in the form of atmospheric wind, which is eventually dissipated by friction with the Earth's surface (Peixoto and Oort 1992). Wind turbines convert part of the kinetic energy of wind into the rotational energy of the turbine, which is in turn converted into electrical energy via an electromagnetic generator.

2.2.3.1 Technological status

Wind energy is currently the most widely used (in terms of energy generated) form of renewable energy (other than existing large-scale hydro and traditional biomass). Global wind power capacity reached around 370 GW in 2014, compared to 48 GW in 2004 (REN21 2015), an average annual growth rate of 22% per year. The vast majority of large scale wind farms have used horizontal axis turbines (Islam et al. 2013). The capacity of the largest individual turbines has increased from under 100 kW in the 1980s to over 1 MW by 2010, with a corresponding increase in size. Most large wind turbines are located on land but there is a trend to locate large turbines offshore. Recently, interest in vertical axis wind turbines has increased, as these are thought to hold several potential technical and environmental advantages.

2.2.3.2 Material constraints

In the case of a large-scale global deployment of wind power in order to achieve completely renewable energy supply, Smith Stegen (2015) raises the possibility of shortages of rare earth materials needed for generator permanent magnets, noting that one country, China, dominates processing of rare earth materials, and urges a concerted diversification effort for the scale up of wind energy. Possible strategies to mitigate shortages include reducing or eliminating the use

of rare earth materials in permanent magnets, substituting permanent magnets for other technologies, recycling, and opening new mines. One possibility is to use switched reluctance generator wind turbines, which do not require permanent magnets (Mendez et al. 2014). Some wind turbine manufacturers already avoid the use of neodymium in their turbine generators.

2.2.3.3 Environmental effects of wind turbines

Habitat displacement and tree removal are two environmental concerns regarding the building of wind turbines. Threats to bird life are often cited as an objection to wind turbines. However, compared to other threats, the present impact of wind turbines is quite small. The mortality rate in the US is only 0.014% of the biggest cause of death: buildings and windows (DOE 2008). If wind power generation in the US grew to 20% of the total electrical energy generated, a factor of approximately 26 to 1, then this figure would rise to 0.37%, and for 100% of electrical energy, 1.83%, assuming there were no other synergistic effects on bird mortality that would cause the mortality rate to rise faster than in linear proportion to wind power generation. Jacobson (2009) also compared bird deaths due to wind turbines with other causes of death in the US, with similar findings. The number of bird deaths due to turbines was extrapolated to a global scenario of large scale deployment of wind power, with 1.4 to 2.3 million 5 MW turbines installed. The number of bird deaths was estimated to be from 1.4 to 14 million per year, which is less than 1% of the deaths due to other anthropogenic causes. From the figures given for US bird deaths due to other causes, the minimum number of deaths in the US alone is 200 million per year, which is much more than the maximum global death estimate due to wind turbines. However Tabassum-Abbasi et al. (2014) claims that bird population decline due to large scale deployment of wind power may be greater than predicted by linear extrapolation of present bird death rate

statistics. There are several reasons. Many previous studies have not taken into account scavenger removal before deaths are recorded. As wind power scales up, more sites with higher potential fatality rates need to be used. The effect of wind farms on birth rates must also be considered as habitat displacement reduces the number of available nesting sites.

Conversely, estimations of fatality rates often do not take into account the bird lives that would be saved if wind power enabled conventional generators to be retired, reducing greenhouse emissions and other pollution. The Royal Society for the Protection of Birds concluded that climate change is the most serious threat to wildlife (Macintosh and Downie 2006), which implies that well sited wind turbines are likely to have a net beneficial effect on birds and other wild-life. Islam et al. (2013) suggest that using vertical axis wind turbines may reduce bird fatalities as birds will perceive the turbine outline as a solid object and avoid the space that the blades move through altogether. Tabassum-Abbasi et al. (2014) propose a number of planning and management practices to minimise bird deaths, including providing corridors along bird flight paths within large wind farms.

Some studies in the US and Canada have raised concerns about the number of bat deaths caused by wind turbines (DOE 2008). Bats are relatively long lived mammals with low re-productive rates and so populations may be particularly susceptible to long-term decline due to wind-turbine fatalities. Macintosh and Downie (2006) found that the mortality rate for birds and bats from wind turbine collisions is typically less than five birds and five bats per turbine per year. However, some sites may pose higher localised risks so care must be taken with siting of individual wind turbines and wind farms. The same planning and management practices proposed by Tabassum-Abbasi et al. (2014) for birds can also be applied to bats.

Potential impacts on humans living near wind turbines include noise, shadow flicker, and electromagnetic interference (Tabassum-Abbasi et al. 2014). DOE (2008) rates the sound generated by a modern wind turbine at a distance of 350 m as between the sound level of a quiet bedroom and a car travelling at 64 kph. Macintosh and Downie (2006) rate the noise level of a 10 turbine wind farm at 350 m very similarly, slightly more than a quiet bedroom and less than a car travelling at 64 kph at 100 m, indicating that at the turbine spacing of most modern wind farms, the closest turbine will dominate the noise generation and that this is a low level provided an adequate buffer zone surrounds the wind farm. Tabassum-Abbasi et al. (2014) found that the annoyance from wind farm noise may be greater than expected because it is generated in otherwise quiet areas, and that the noise often varies with wind speed and direction, making it more difficult to ignore. However the authors also noted that annoyance tends to be greater if the turbine is visible, and that those who receive an economic benefit from the turbine are less likely to be annoyed. No direct links have been found between turbine noise and health effects, such as sleep disturbance or psychological distress, so any perceived health effect is probably mediated by annoyance. On large modern turbines, shadow flicker may be seen up to almost 5 km away near dawn or dusk, but the region of visibility moves with the position of the sun. Modern turbines with non-metal blades have reduced electromagnetic interference, however there are many more of them and many more people with portable electronic devices. Both effects can be minimised by siting wind farms away from areas of human activity.

Macintosh and Downie (2006) report that the incidence of turbine fires in Australia has been very low, with only 2 fires reported in 20 years of operation, neither of which spread beyond the turbine. The fact that wind turbines are

likely to be placed in previously cleared land lowers the risk of a turbine fire spreading.

Lu et al. (2009) report that world-wide, large-scale implementation of wind power could result in significant alteration to global atmospheric circulation, that may affect the wind resource even in locations far from existing wind farms, although no significant change to temperatures are foreseen.

2.2.3.4 Effect of climate change on the wind resource

Because the energy density in the wind is proportional to the cube of the wind speed, changes in the average wind speed and wind speed distribution could have significant impacts on wind power generation at a particular site (Pryor and Barthelmie 2010). A warmer global climate means there is more heat energy in the climate system, which might be expected to cause generally higher wind speeds. However, there may be significant changes to the geographic distribution of wind speeds, the variability at a particular site, turbulence intensity, and the frequency distribution of extreme wind speeds, extreme direction changes, and gusts. Energy density is also proportional to air density, and air density is inversely proportional to temperature, so a warming trend will lead to a slight decline in energy density at the same wind-speed. An increase in the frequency of temperature extremes may affect turbine operation, with more icing in some locations and more high temperatures in others. Since many wind turbines lie in coastal regions, and increasingly off-shore, sea level rise may have an impact on foundations, towers, and road access. All of these may impact on energy generation, and stress loadings, which will impact on maintenance costs, design cost, financial returns, and safety, but the overall effect of climate change on the wind resource is uncertain so far.

2.2.4 Variability of supply and grid integration of solar and wind power

Bayless (2010) summarised the traditional objections to large-scale deployment of variable generators onto an electrical grid. A number of criteria were provided that must be met for the stability of the system to be maintained. They are capacity, the ability to remain running under varied conditions, and frequency control. Base load generation plants were defined as plants of large capacity that generate energy at a virtually constant rate at low cost. It was claimed that these plants currently provide the elements of stability on typical grids, and that on a global scale, most base load plants are coal based or nuclear, with some combined cycle natural gas and large hydro. Wind, solar, and small hydro were dismissed as variable sources that usually generate far from load centres, and require more transmission infrastructure. Geothermal and biomass, although not as variable, were also claimed to have geographical and capacity limitations. Solar thermal plants with storage, which can generate at night, were neglected.

Bayless (2010) claimed that to provide capacity, renewables require extra reserves or added storage, something that conventional (fossil and nuclear) plants provide for themselves. Indeed the "capacity credit" for a generator, defined as the capability to generate power on demand, has traditionally been regarded as zero for a variable renewable energy generator, unless some kind of storage or backup is added (Perez et al. 2009). Another of the requirements, frequency control, is aided by electo-mechanical inertia in the system, which is currently provided by the large turbines of conventional fossil and nuclear power stations (Bayless 2010). Large scale wind power (with lots of small turbines) could also provide significant inertia, but because their distance from the load is likely to be much further than conventional plants, response time and transients may be a problem. Ramping rate is the speed at which a

generator can change output. The more inertia there is in the system, the less ramping rate capacity is needed by backup generation. Bayless (2010) identified coal as a technology with generally high inertia but low ramping rate capacity, nuclear with even lower ramping rate capacity, and gas-turbines as a technology with high ramping rate capacity. The author claimed that with lots of smaller generating units online (as may be with renewables) transmission flows will be more unpredictable, with more rapid ramping rates, and maintaining stability will be more complex and difficult. Bayless (2010) also claimed that while conventional plants are mostly independent of one another (except for hurricanes), renewables such as hydro, wind and solar are not, because they are dependent on the weather, although the author did allow that widely dispersed wind and solar farms have low correlation and this reduces overall variability.

These objections can be contested. Although batteries and photovoltaic systems have no intrinsic rotational inertia, there are ways in which they could provide faster responding active voltage and frequency stability control to compensate for the reduced system inertia. Battery storage systems have a very rapid response rate and can provide voltage and frequency stability capability if they are maintained in a partially charged state (Cha et al. 2012). They can also provide 'synthetic rotational inertia' or 'inertia mimicking' (Ulbig et al. 2013). Solar PV systems can also be configured to provide synthetic inertia (Rahmann and Castillo 2014). The fuels for coal, gas, and nuclear are often only found far from load centres. In the case of nuclear, this is often in a different country (though not in the Australian case). Hence there is a real possibility of supply disruptions. In reality it is highly unlikely that large capacity new conventional power plants of any kind will be able to be sited near urban centres. Coal has significant pollution problems, coal and nuclear have water requirements, and

nuclear in particular will suffer from the "Not In My Back Yard" (NIMBY) syndrome. The transportation of fuel and perhaps water may also require new infrastructure and extra surface area. While the transport fleet runs on fossil fuels, any fuel transport requirements, whether fossil or nuclear, will decrease net energy generated, increase emissions and thus reduce the mitigation effectiveness. In the case of coal generation on the SWIS, energy is generated at the point of coal extraction (Collie) rather than the main load centre (Perth). Gas is however piped to Perth from the north-west of Western Australia.

Hence contrary to the claim that renewable power will need more grid infrastructure, new conventional plants may need as many new transmission lines as utility scale renewable plants. Generation systems distributed within the existing grid, whether renewable or conventional, may avoid the need to reserve more land area and large capital outlays for additional transmission lines. Although the best biomass resource may be far from load centres, it can also be transported to plants close by. According to Hohmeyer and Trittin (2008), the majority of the capital cost of electrical power systems is in the transmission and distribution systems, and not the power plants themselves.

The claim that conventional plants are mostly independent of one another ignores the evidence. Several nuclear plants at once can be affected by an earthquake or tsunami (Japan), large scale grid failure (US 2003 blackout), or weather (France). An August 2003 blackout shut down 20 US and Canadian reactors instantly and without warning (Sovacool 2009). In Japan, a data falsification scandal in 2002 caused the shut down of 17 nuclear reactors (Schneider and Froggatt 2015). Seven nuclear reactors produced no electricity after an earthquake in July 2007, and the Fukishima disaster of 2011 resulted in the total shut down of Japan's entire nuclear fleet.

It is worth examining the variability of the two most mature forms of renewable energy, wind and solar PV, in more detail.

2.2.4.1 Wind variability

DOE (2008) found that wind generation variability for 14 turbines to be small (average 0.4%) for short time periods (in the order of one second) but increasing to 7% for time periods in the order of one hour. As the number of turbines is increased, the variability decreases. The same report also presented the results of a study that shows decreasing hourly capacity factor variability as more wind farms from a wider geographic area over Minnesota and North Dakota are included in the analysis. There is also a decrease in the frequency of very high or very low hourly capacity factors. Giebel (2000) found that the combined wind power output data estimated from 60 meteorological stations in Europe was much smoother than the output data from any single station. Sinden (2007) showed that correlation between the wind power output of two sites decreases with distance, being on average less than 0.2 for distances greater than 800 km. 2080 pairs of sites throughout the UK were compared.

All of these studies suggest that as the amount of wind generation in a power supply system is increased, then the variability does not increase as much as expected or may actually decrease. Widén et al. (2015) reviewed a wide range of studies and concluded that there was clear evidence that installing wind generators with a wide geographic dispersion reduces variability in aggregate power output.

Archer and Jacobson (2003) found that the frequency of low wind events over a network of 8 sites in the central US was less than 2%, which is greater than the reliability of conventional generation. DOE (2008) claimed that actual data and mesoscale numerical modelling show that a sudden loss of all wind power on a

system as a result of loss of wind is not a likely event. However, there may still be occasions when there is little wind across a large geographical area, for example when a large anticyclone crosses the region. Sinden (2007) showed that low wind speed events (less than 4 ms^{-1}) affecting more than half of the United Kingdom (UK) did occur, although in less than 10% of all hours in a year of measurements. There were no hours in which a low speed event affected the whole UK.

2.2.4.2 Integrating wind power into the grid

Several studies have examined the feasibility of introducing large amounts of wind energy into power supply grids. Sovacool (2009) found nine studies that showed variability becoming easier to manage, not more difficult, as more variable renewable energy sources were deployed. Smith et al. (2007) claimed that the primary considerations for wind power penetration up to 20-30% are economic rather than physical. DOE (2008) pointed out that wind is an energy resource rather than a capacity resource but Sinden (2007) cited a number of studies that conclude that wind power does reduce the need for conventional fossil fuel capacity.

The amount of conventional capacity which can be reliably foregone is termed "capacity credit". DOE (2008) cited a number of methods of estimating capacity credit (here termed Effective Load Carrying Capacity or ELCC) that give results ranging from 5 to 40% of rated wind plant capacity, the variability depending primarily on the timing of wind energy production compared to the times of high system load. Holttinen et al. (2007) found that the capacity credit of wind power in the German power system varies with season and is quite low (5.1-8.6%), but this has been calculated with a very high reliability requirement (99%). The same study also found that as wind capacity increased in the Irish

power system, capacity credit (in MW) increased at a less than linear rate. Capacity credit had a high of about 35% at 500 MW capacity, reducing to about 14% at 3500 MW capacity. There was a similar trend in Norway (30% at low wind penetration down to 14% at 15% penetration), but the decrease was reduced by geographic dispersion of wind farms. The same trend was found in England, where capacity credit was similar to capacity factor at low wind penetration levels, but decreased as wind penetration increased. Despite this noted decrease, Archer and Jacobson (2007) found that there was no saturation in benefits as the number of interconnected wind farms increased. Holttinen et al. (2007) summarised these results by stating that wind capacity credit will be higher in cases of low wind penetration, larger geographic dispersion, and/or high capacity factor at times of peak load (or more generally, if there is a positive correlation between wind output profile and system load profile). Zhang et al. (2013) confirmed these findings.

2.2.4.3 Wind backup generation

Diesendorf (2006b) claimed that at low penetrations of wind energy, no further backup is required because the grid already has peak load capability to handle fluctuations in demand. However this will change as penetration increases. Additional peak-load backup is required in the event of a lull (purchasing power from another grid is not an option for the SWIS), but this does not have to be operated continuously. The author also claims that when conventional power stations break down, they are generally off line for longer than wind-lulls or sunless days. Diesendorf (2006b) estimated that at 20% wind penetration from geographically dispersed wind-farms, to maintain the same level of supply reliability, extra peak-load capacity equivalent to around 25% of the wind-power capacity needs to be added to the system.

This may be too stringent. In one example reported by DOE (2008), extra reserve capacity equivalent to 7% of the wind generation capacity was needed to reach 25% wind energy penetration. This study also found that managing large output variations and steep ramping rates over short time periods (less than 1 hour) may pose challenges in areas with smaller regulation and load-following capacity, but for wind capacity penetrations (rated wind capacity divided by maximum load capacity) of between 20 and 35% these variations were within the capabilities of the expected extra needed reserve capacity. Holttinen et al. (2007) reported estimates of increased reserve requirement for many areas in Europe (and Minnesota in the US), ranging from 1 to 5% of wind capacity at lower penetration levels (5-15%) to 4 to 9% of wind capacity at higher penetration levels (15 to 25%). In a recent wide ranging study, Holttinen et al. (2013) found an emerging trend toward allocating reserves dynamically based on the state of the power system, wind generation and load.

The two results, that wind power can provide a capacity credit at a set reliability rating, enabling other generation units to be retired; and that wind power also requires extra reserve generation capacity to be added, appear to contradict each other, but in fact the two types of generation capacity are different. Diesendorf (2006b) sums this up by stating that at high penetrations, wind power changes the optimum economic mix of base-load generators to peak load generators in favour of more peak-load and less base load. Base-load generators are characterised by high capital cost, low operating cost at peak efficiency, inability to respond quickly without significantly reducing efficiency if forced to operate at other than rated power, and they can't be switched on or off quickly. In contrast, peak-load generators are characterised by low capital cost, high running cost, can respond rapidly to changes in demand, and can be switched on and off quickly.

This does not necessarily mean that wind power's effectiveness in reducing greenhouse gas emissions is significantly compromised as penetration increases. Macintosh and Downie (2006) concluded that at 20% wind energy penetration in the UK, emission savings are reduced by a little over 1% by the need to provide extra services. Note that although in most cases the extra reserve generators are assumed to be fossil based, there is no requirement that they be so. Holttinen et al. (2007) points out that the wide-scale uptake of solar generation may aid in the smoothing out of the variability of individual technologies.

There are several small electricity systems in Australia with a high penetration of wind power, including King Island in Tasmania, Denham in Western Australia, and Mawson in the Australian Antarctic Territory (Outhred 2003). Denham has flywheel backup as does Coral Bay, which also has over 70% penetration of wind power.

An alternative that may reduce reserve requirements is the concept of deliberately over-rating wind-farm capacity and curtailing excess generation (Cavallo 1995). Overall capacity factor will be higher than expected from a typical wind farm. The cost of the extra wind turbines is compensated by the lower cost per kWh of the lower capacity transmission line, leading to little or no increase in the overall cost of the combined system. Instead of curtailment, excess generation could be used for on-site hydrogen or methane production (Jentsch et al. 2014).

2.2.4.4 Wind weather forecasting

Wind weather forecasting is one potential way to reduce the costs of uncertainty in wind power production. Physics based models tend to show better long term (up to 48 hours ahead) and wide-scale prediction, while

statistics based models show better short term prediction, up to 6 hours ahead (Lei et al. 2009). Often the two approaches are combined to improve accuracy, and over the last decade the incorporation of artificial intelligence based methods such as artificial neural networks, and fuzzy logic has resulted in further improvements. Foley et al. (2012) reported errors of 10% for one hour forecasts, rising to 20% for 48 hour ahead forecasts. Because wind farms are often placed at sites that amplify the effects of local topographical features, it has also been shown to be worthwhile to incorporate fine-scale localised wind flow models (Georgilakis 2008). Georgilakis (2008) also claims that geographic dispersion and weather forecasting can be synergistic, such that the aggregate wind forecasting error for multiple geographically dispersed wind-plants can be reduced by 30 to 50% compared to the total of the individual wind-plant forecasting errors.

According to Ahlstrom et al. (2005), wind forecasting already has become valuable for scheduling other power sources in advance. However, as the installed wind power capacity increases, a small error in the wind forecast results in larger errors in power output prediction (Chen and Blaabjerg 2009). The exact timing of passage of weather fronts can be difficult to predict, which can lead to large errors in the exact timing prediction of changes in wind power production (Georgilakis 2008).

2.2.4.5 Solar PV variability and grid integration

The technical potential of solar PV is many times greater than global electricity consumption but the variability of the supply presents challenges for large scale implementation into existing electrical grids. On a daily time scale, solar PV power variability is more predictable than wind. After dawn there will be a large up ramp, before dusk there will be a large down ramp, no solar

availability during the night, and peak availability around the middle of the day (Milligan et al. 2015). There can be large variability at a single location during the day from cloud transients, but this is moderated by having many geographically dispersed generators. So just how much PV can be realistically integrated into existing electrical grids? Denholm and Margolis (2006) point out that the large conventional generators that supply most grids have a minimum output level below which the plant must be shut down, leading to costly and potentially lengthy start up procedures. So, if there are times when PV output is high enough and load demand is low enough to meet this threshold, then the PV output will most likely be rejected to avoid shut down. The authors found that if the minimum conventional generator output level is 35% of peak load, then the maximum economically realistic energy contribution for PV is about 17% of system energy demand. However if the flexibility of the conventional generators is increased, then the amount of PV can be increased. If the minimum conventional output level is 20%, then the maximum PV level rises to 25%, and if the minimum conventional output level is 0% (meaning generators can be switched off and on without economic penalty), then up to 50% PV energy contribution may be economically feasible. To increase PV penetration beyond this point, load shifting and/or energy storage will be required. Eltawil and Zhao (2010) conducted a literature survey of studies into the impact of high penetration of distributed PV generators into typically existing electricity grid configurations. Penetration was defined as the ratio of nameplate PV capacity to maximum load. Several studies suggested that the maximum practical penetration limit was quite low. An upper limit of 5% was suggested if all of the PV comes from one geographically concentrated power station, the limit being imposed by ramp-rate limitations of the conventional generators in the event of cloud transients causing rapid swings in PV power output. This limit might be

increased to 15% if the PV distributed generation was geographically dispersed. However, the authors found other studies suggesting that the upper limit is significantly greater, possibly up to 50%.

Contrary to this view of PV generators as undermining grid stability, PV systems can contribute to system stability during peak load demand times by operating at less than maximum possible power output (Rahmann and Castillo 2014). This enables them to provide synthetic inertia by altering generated power in response to changes in system frequency.

To achieve very high penetration levels, the issue of how well PV supply can match the load demand becomes important. Mitchell et al. (2009) found that in the last 5 to 10 years the hot weather peak load (a time when the benefit to the grid of PV generation is high due to its ability to reduce peak load required from conventional generators) for a site near Sydney, Australia, has extended from 3pm to 6pm, and is high as late as 8pm (daylight saving time when the sun sets). Aligning at least some of the panels in a north-westerly direction rather than directly north would shift the peak generation point of the PV generators to a later time which more closely matched the peak load profile, although the overall yearly average generation would be reduced.

2.2.4.6 Short term variability versus log term variability

These studies provide evidence of the feasibility of large scale deployment of variable solar and wind energy generation into electrical grids, at least up to a certain penetration, without loss of reliability. Sovacool (2009) found evidence that the variability of renewables became easier to manage the more they were deployed. Despite this evidence, the traditional view of increased difficulty with more deployment has been entrenched in many places. Sovacool (2009) conducted a survey of 45 different institutions connected with electricity

generation in the US, and found that many system operators and utilities considered renewable energy resources to be inadequate providers of base load and peaking power due to factors such as forecasting complexity, the need for supplemental generation, and grid interaction. Since then however, views have been changing, with system operators becoming more comfortable with variable energy generators as experience increases, and the realisation that in some respects, for example recovery after a disturbance, they offer superior performance to conventional generators (Milligan et al. 2015).

In reality, fossil and nuclear plants were also found to have shortcomings, including outages, cost variance, and variance in demand forecasts (Sovacool 2009). Outages were found to vary between 5 and 20% of the time. Even though it can be anticipated, nuclear power plant refuelling in the US shuts down a reactor for an average of 37 days every 17 months (Lovins 2007). Thus the maximum reliability of nuclear power plants is on average 93 percent. If a large unit size fossil or nuclear generator trips, the system must deal with the loss of large blocks of power (maybe even 1000 MW or greater) instantly. Because of their large unit size and long construction lead times, conventional and nuclear plants were found to suffer from completion delays, cost over-runs, and variance in demand forecasts (Sovacool 2009). These add uncertainty to the system. It is much harder to forecast demand several years in advance than it is to forecast the weather a day or two in advance, which necessitates a deliberate over-estimation of demand forecasts and increases costs. The large up-front capital cost, payable years before any electricity is generated, also increases financial risk and complicates financing. Perhaps this is why construction 'boom and bust' cycles for fossil and nuclear plants have occurred since 1980 in the US.

Thus it could be said that while wind and solar introduce short time-scale uncertainties into the system, nuclear and coal-CCS and other large scale forms of energy generation introduce long-time scale uncertainties into the system. It has been argued that responsiveness to short time scale uncertainties have already been built into the system: load demand is also highly dependent on the weather, so regardless of supply variability, reserve and rapid response capacity must be built into the system anyway. Sovacool (2009) notes: "the entire electric utility system is already built to address variability, just of a different type". Sovacool (2009) found that the higher technical reliability and small unit size, combined with accurate weather forecasting actually gives variable renewable systems an advantage: changes in supply can be predicted and prepared for in advance. It could be said that the single failure criterion is a lot easier to meet for a generation system based on renewables, since the capacity of a single wind turbine or solar array is much smaller.

On longer time-scales, Sovacool (2009) concluded that the shorter lead times and smaller unit sizes for solar and wind projects enable a more accurate response to load growth, and reduce the financial risks associated with financing plant construction for several years before they start producing any electricity.

2.2.4.7 Paradigm of flexibility

Rather than base-load or peak-load generators, Peter et al. (2007) divided different energy sources into the categories of "fluctuating" and "adjustable". Denholm and Hand (2011) examined the overall flexibility of power systems and concluded that both conventional and renewable technologies contain a mix of 'flexible' and 'inflexible' generation systems. The challenge is to match

these two types on a continuous basis. The paradigm of 'base-load' and 'peak-load' generation could be considered to be outdated. Another paradigm shift could also be added to the list: that of demand side management. Even Bayless (2010) suggested demand response as another level of control to bolster system stability. During the 2008 Texas wind drop (Ela and Kirby 2008), selective shedding of industrial loads meant that households and critical services such as hospitals were not affected. This raises the possibility of using the raw materials of flexible industrial processes as another way to store energy and help balance supply with demand. Demand management coupled with the transformation of electric power systems towards lots of smaller generators distributed over the grid increases the potential to reduce the frequency of massive blackouts and means that the 'hard failure' paradigm of current systems can become a 'soft failure' paradigm.

2.2.5 Bioenergy

Bioenergy is the conversion of biological material into energy. Residues and wastes from agricultural, forestry and municipal operations are presently the main sources of biological material, or biomass (Gadonneix et al. 2010). Hence bioenergy can be thought of as an indirect form of solar energy, as most biological species either collect and store energy from the sun, or consume other species that do so. The period of time between initial collection of the solar energy and final use by human civilisation could be decades for some forestry operations. This time period is greater than solar and wind energy systems, but much less than fossil fuels, which are solar energy stored on geological time-scales. Because most forms of bioenergy feedstock, commonly called biomass, can be stored, electricity generation is subject to less variability than solar or wind resources.

2.2.5.1 Technological status

Bioenergy technologies can be divided into three generations (Ho et al. 2014). First generation bioenergy technologies convert sugar and starch crops (e.g. sugar cane, corn, and maize) or oil bearing crops into a form that can be used for energy production or transportation fuels. Concerns have been raised that increases in bioenergy production may lead to competition for land currently used for food production (Gadonneix et al. 2010). Second generation technologies aim to convert the non-edible portions of plants (called lignocellulosic material) into a form usable for energy generation. These have the potential to avoid displacement of crops grown for food. Third generation technologies, such as the utilisation of algae, aim for integrated production of energy, transportation fuels, and bio products. Algae has an added advantage in that it can use saline or waste water resources (Ho et al. 2014).

Biomass is available in solid, liquid and gaseous forms, and "upgrading technologies" that convert bulky raw biomass into denser and more effective energy carriers are currently under development (Gadonneix et al. 2010). Pelletisation is in commercial operation, while pyrolysis is in the demonstration phase and both torrefaction and hydrothermal upgrading are in the research or early demonstration phase (Gadonneix et al. 2010).

Currently there are three technological streams for electrical power generation: combustion, co-firing, and anaerobic digestion (Gadonneix et al. 2010). There are also three major types of combustion technology currently under consideration: direct combustion, gasification, and pyrolysis (Evans et al. 2010). Direct combustion, also called incineration, combusts the biomass with high levels of oxygen present, into carbon dioxide and water. The resulting hot gases are used to heat water into steam which drives a turbine. Gasification combusts the biomass with low levels of oxygen present, to produce gases that are fed to

a gas turbine. Pyrolysis combusts the biomass with no oxygen present, to produce gases, or combustible liquids, that are fed to a gas turbine. If the liquid or gas is transportable, pyrolysis has the potential to spatially separate the biomass combustion stage from the electricity generation stage.

Steam cycle direct combustion is in commercial operation (Gadonneix et al. 2010). Gas turbines fuelled by biomass gasification (BIG-GT), with promise of higher electrical conversion efficiency, are not yet in the large scale commercial phase (Asadullah 2014), although integrated gas combined cycle systems using residue from pulp and paper production are (IEA 2007). Some systems combining gasification with a steam cycle are in the early commercial phase (Gadonneix et al. 2010). Pyrolysis is in the research and development stage (Digman et al. 2009). Two other technologies, Stirling engine and organic Rankine cycle combustion, are both in the demonstration phase (Gadonneix et al. 2010).

Combustion is the most common form of generation, generally in the form of Combined Heat and Power (CHP) systems (REN21 2010), leading to an increase in the overall efficiency of energy production. Direct co-firing with coal power plants is also in commercial operation, parallel co-firing is in the pre-commercial stage, and indirect co-firing is in the demonstration phase. One stage anaerobic digestion is in commercial operation, while 2-stage anaerobic digestion and biogas upgrading is in the early-commercial stage. Microbial fuel cells are in the research phase (Gadonneix et al. 2010).

In 2013, bioenergy electricity generation reached 396 TWh (IEA 2014), or about 1.8% of total world electricity generation.

2.2.5.2 Australian and Western Australian potential

Currently, bioenergy in Australia comes mainly from sugar cane residue, wood waste, and gas capture from waste landfill and sewage (Geoscience Australia and ABARE 2010). Landfill gas is generated by the decomposition of organic wastes in anaerobic conditions, and has been found to contain around 50% methane by volume (WMAA 2007). Methane has a greenhouse gas potential over 20 times that of carbon dioxide. Therefore energy generation by conversion of landfill methane to carbon dioxide reduces emissions in two ways. Emissions of methane to the atmosphere are replaced by emissions of the less potent carbon dioxide, and the energy generated also avoids emissions from fossil energy generation. If the organic waste came from a biological source, then the carbon dioxide was originally removed from the atmosphere, and thus the carbon cycle becomes emissions neutral. Potential future resources of bioenergy are crop and food residues from harvesting and processing of agricultural and silvicultural crops, energy crops, and urban solid wastes (Geoscience Australia and ABARE 2010). Since most municipalities are aiming to reduce the material flow to landfill, any expansion of landfill gas capacity is uncertain.

The wheatbelt is a series of land areas stretching across the southern portion of Australia that is characterised by generally flat terrain and rainfall in the range of 300 to 600 mm per year, falling mainly in the winter season (Bartle and Abadi 2010). The wheatbelt lies between the higher rainfall southern coastal regions and the arid interior, and has an area of approximately 100 million hectares (Bartle et al. 2007). It was estimated that around 20 million hectares was cropped for grains and oil seeds in 2004-2005. Investigation of the potential for bioenergy crops in the wheatbelt was originally motivated by salinity control. Development of second generation lignocellulosic technologies has the potential to complement existing agriculture rather than replacing it, and

concurrently rehabilitate salt-damaged land or at least help to prevent further damage (Bartle and Abadi 2010). One particular candidate technology, the use of oil-mallee crops, has been extensively studied. These species have the ability to re-sprout from the root system after harvesting (called coppicing). Thus there can be several harvests without the need to regrow from a sapling.

Wu et al. (2008) found that the ratio of biomass energy content to non-renewable energy input (called the energy ratio) exceeded 40 to 1 for oil mallees grown in the Western Australian wheatbelt. Most of the non-renewable energy inputs came from harvesting and transport, so there is potential for improvement. In contrast, canola grown for biodiesel in the same region achieved an energy ratio of less than 7. The energy productivity in the context of biomass is defined as the energy contained in the biomass per unit area planted per unit time. Wu et al. (2008) estimated an average energy productivity for oil mallee in the Western Australian wheatbelt of around 206.3 GJ per ha per year (57.31 MWh per ha per year). Bartle et al. (2007) estimated the land area usable for cropping and pasture in the wheatbelt of Western Australia as 16.6 million hectares. The authors also considered that only about 50% of this area had a soil type that was suitable for growth of woody crops for biomass, establishing an upper limit to capacity. IEA (2007) estimated the electrical conversion efficiency of a dry biomass combustion power plant at between 30% and 34%. So if an area equal to 2.5% of the usable Western Australian wheat belt was devoted to oil mallee crop rotation for example, and a biomass plant with a conversion efficiency of 30% was used to generate power, then the potential average output capacity would be around 814 MW. This does not mean that 2.5% of usable land has been withdrawn from food production. It might be considered necessary to use this land for salinity control in any case.

Municipal Solid Waste (MSW) represents another potential source of bioenergy. Residual MSW is left after the recyclable and organic contents have been removed. Murphy and McKeogh (2004) found that the energy content in residual MSW is dependent on the plastics content. Residual MSW with no plastic has an energy content of 4 GJ/tonne, while Residual MSW that is all plastic has an energy content of around 13.5 GJ/tonne. In Ireland the energy content of MSW was found to be 13.26 GJ/tonne, similar to the Netherlands (13.5 GJ/tonne), Denmark (11.3 GJ/tonne), and Japan 12.6 (GJ/tonne). Two combustion technologies that have been used to recover energy from MSW are incineration and gasification. Murphy and McKeogh (2004) estimated that incineration could generate 0.564 MWh of electricity for every tonne of MSW combusted, and gasification 1.083 MWh. Thus the conversion efficiencies for incineration and gasification in Ireland would be 15.3% and 29.4% respectively. Psomopoulos et al. (2009) found that from actual operating data for the US, one tonne of MSW could generate 0.6 MWh of electricity on average, but did not specify an average energy content. At an electrical conversion efficiency of 15.3%, the energy content would be about 14.1 GJ/tonne, similar to the other countries mentioned above.

However, recycling is considered a more favourable use of waste than energy recovery as there is less embodied energy required to recycle many materials than to extract them from raw materials or ores (WMAA 2007). There is the risk that energy recovery could divert materials that would otherwise be recycled, especially if there is competition for high energy content materials such as plastics. However, contrary to this expectation, Psomopoulos et al. (2009) found that communities in the US with waste to energy generation facilities had a higher rate of recycling than those without. Globally, many jurisdictions have implemented a policy of maintaining a waste 'hierarchy', with recycling given a

higher priority. The aim is to recycle all that is feasible before energy recovery is performed.

WAWA (2012) reported that almost 5.4 million tonnes of material were disposed to landfill in Western Australia in 2009. Almost 1.3 million tonnes came from municipal sources, 3.135 million tonnes from construction and demolition, and 0.967 million tonnes from the commercial and industrial sector. If 1 million tonnes of landfill were used to generate electricity per year (approximately 18.5% of the 2012 estimate), then 600 GWh of electricity could be produced per year, based on the findings by Psomopoulos et al. (2009) above. This is an average generation capacity of about 68.5 MW. If the average conversion efficiency were increased by using more gasification plants, from 15.3% to 22% for example, then the average generation capacity would rise to about 98.5 MW. However, if all plastics were recycled and thus removed from the residual MSW then the energy content would decrease. If the energy content dropped to around 4 GJ/tonne, then incineration at 22% efficiency of 1 million tonnes per year would generate 241 GWh of electricity per year, or an average capacity of 27.5 MW. Gasification at 30% efficiency would generate 329 GWh of electricity per year, or an average capacity of 37.6 MW.

2.2.5.3 Environmental issues

For bioenergy generation from agricultural and forestry operations, the aim is for low overall greenhouse emissions, as there is a cycle of storage of carbon from the atmosphere in the biological growth phase, and release of the same amount of carbon in the harvesting and energy conversion phase (Hohmeyer and Trittin 2008). The growth phase is then repeated. Psomopoulos et al. (2009) concluded that about 64% of the combustible biomass found in MSW in the US could be considered renewable, implying that the materials were originally

derived from plant or animal organic matter grown in a similar carbon storage cycle. However, there have been concerns that bioenergy greenhouse emissions are higher than expected (Hohmeyer and Trittin 2008). Two proposed mechanisms are the release of nitrous oxide (N_2O), and land clearing. N_2O has a greenhouse potential approximately 300 times greater than CO_2 (Gutierrez 2005). Land clearing by burning stimulates N_2O emissions. If the land is then used for agricultural purposes, the available nitrogen in the soil is increased by the use of fertilisers and atmospheric deposition, among other processes. The rate of N_2O emissions is increased. However, in Western Australia, the use of oil-mallee crops is designed to combat salinisation and generate electricity and other bio-products using existing cleared land, rather than by clearing new land.

The emission intensity of a waste combustion process is inversely dependent on the combustion temperature, but also dependent on the nitrogen content of the waste (Gutierrez 2005). Hence combustion processes with higher temperatures, such as gasification should be favoured. Also with gasification, the nitrogen content of the fuel is mostly converted to ammonia which can be easily removed. Psomopoulos et al. (2009) rated nitrogen oxide emissions from MSW power plants as less than coal-fired power plants, but more than natural gas fired power plants. However, if residual MSW is not converted to energy or some other product, then the alternative is landfill. Decomposing trash emits carbon dioxide and methane, some of which will escape into the atmosphere even in landfill sites with a gas collection system. Methane is a potent greenhouse gas. Also combustion of MSW can reduce the volume of residual waste. Therefore the need to clear land for new landfills is reduced.

Emissions of odours and toxins from MSW energy recovery operations is also a significant concern. However Psomopoulos et al. (2009) found that toxic

emissions from waste to energy operations in the US, particularly dioxins and mercury, has significantly decreased in recent years, due to tighter standards and introduction of emissions control technology, to the point where other sources such as fossil power stations and backyard burning have much higher toxin emissions. Landfill gas and sewage gas often need to be scrubbed to remove sulphur compounds and other trace elements that cause air pollution (Rasi et al. 2011), including sewage gas utilised for power generation at Woodman point in Western Australia (Charles et al. 2006).

Coarse Woody Debris (CWD) in native forests plays a significant environmental and ecological role. Because of slow decomposition rates, CWD provides a component of wildlife habitat in many Australian forest types, and carbon can remain stored for long periods of time (Woldendorp et al. 2002). In forests around the world, it has been found that downed logs can provide sites for seedling establishment, and CWD is important for nutrient cycling, stream quality and aquatic habitat. However, there have been few Australian studies into the role of CWD. Therefore, CWD should not be considered as a potential fuel source for bioenergy production.

2.3 Storage

Energy storage is considered one of the methods for balancing supply and demand on electric grids with increasing amounts of variable power sources such as solar and wind (Zakeri and Syri 2015). In this context storage can be defined as a system that is able to accept excess electrical power from the grid, store it in some form, and then deliver it back to the grid in the form of electrical power when needed. Storage technologies can be classified according to the physical form in which the energy is stored, such as gravitational, kinetic, chemical, electrochemical, magnetic, or electrical. Commonly cited storage

technologies include pumped hydro, Compressed Air Energy Storage (CAES), flywheels, fuel cells, batteries, superconducting magnetic energy storage, and ultra-capacitors. Thermal storage associated with concentrating solar thermal power stations, although considered to be potentially highly useful for balancing supply and demand, does not strictly conform to this definition, as the input energy is in the form of photons rather than electrons, and is considered in section 2.2.2.2.2 above.

The cycle efficiency of a grid storage technology can be defined as the ratio of energy delivered back to the grid to the energy accepted from the grid. Zakeri and Syri (2015) considered flywheels and batteries to be the most efficient storage mechanisms for short-term energy storage. However storage loss rates from flywheels can be high, reducing suitability for storage at hourly or longer time scales. The self discharge rate for ultra-capacitors is lower, but higher than batteries. Pickard et al. (2009) implied that to achieve balance for a large electricity grid running entirely on variable sources, storage capacities in the order of GW days will be needed. There are several battery technologies in large scale commercial production, such as Li-ion, that may be suitable for short term storage at the GW day scale.

For long term storage, Zakeri and Syri (2015) consider pumped hydro and CAES to be the most efficient options. However for the SWIS, there seems to be a shortage of these options at the GW day scale. There is currently no large scale topographic pumped hydro capacity in the SWIS region, although SEN (2013) proposed using ponds on cliffs above the ocean near Geraldton and Albany, as well as existing dams in the hills east of Perth. Also, while conventional CAES is a developed technology, it requires the use of fossil fuel for operation. Adiabatic CAES needs no fossil fuel input, but it is still in the research and development phase (Barbour et al. 2015). One potential long duration storage

option is a cycle of using excess generation to electrolyse water into a hydrogen or methane fuel (Jentsch et al. 2014). The fuel can then be stored, used for transport, or converted back into electricity at a later time when generation is insufficient, using either gas fired power stations, internal combustion engines or fuel cells. However the use of hydrogen as a storage medium might be less efficient than using batteries. Kaldellis et al. (2009) estimated the overall efficiency rate of hydrogen storage at 30 to 40%. Hadjipaschalis et al. (2009) also noted that the currently mature technologies for storing hydrogen have drawbacks. Pressurised hydrogen gas storage has a low volumetric energy density. Metal hydride storage has a higher energy density, but requires a thermal management system and typically uses rare earth materials, so resource availability may be an issue. Hydrogen can be further converted to methane, resulting in improved stability, storage density, and allowing the use of existing gas transportation and electricity generation infrastructure (Zakeri and Syri 2015). The estimate of overall efficiency is still low, at 33 to 40%. However, reasons for keeping this option under consideration are the potential for seasonal energy storage and high battery manufacturing energy requirements.

2.3.1 Material, energy and environmental constraints

Barnhart and Benson (2013) found that although the production of bulk materials required for large scale storage battery deployment will need to increase substantially, the main limitation may be the manufacturing energy requirements for several prominent battery technologies, including lithium-ion and sodium sulphur batteries. Also, with current fossil fuel dominated energy generation, the emissions required to manufacture battery storage capacity are substantial (Ahmadi et al. 2015), meaning that several hundred cycles of operation are required for a net reduction in emissions. This may inhibit large-scale deployment unless cycle lives are improved significantly. The reuse of

batteries produced for EV's as stationary energy storage may improve net emission reductions (Ahmadi et al. 2015). There are also significant environmental issues with battery production which will become more prominent as manufacturing is scaled up. The electrodes of Li-ion batteries do not need to use toxic heavy metals such as cadmium and lead. However, nickel and cobalt are often used, and the electrolyte may also pose toxicity problems (Larcher and Tarascon 2014). The extraction and disposal of nickel and cobalt pose toxicity impacts (Peters et al. 2017). Substitution of nickel and cobalt with manganese is possible (Larcher and Tarascon 2014), and lithium iron phosphate batteries do not use nickel or cobalt (Peters et al. 2017). A high level of recycling may also decrease net manufacturing energy requirements.

2.4 Energy efficiency

Energy efficiency improvements can be defined as a reduction in the energy used for a given service (heating, lighting, etc.) or level of activity (WEC 2008). It does not refer to reduction in energy used by reducing services or level of activity (unless the same service can be achieved with a reduction in activity) - this is more accurately called energy conservation (Herring 2006). Hohmeyer and Trittin (2008) concluded that there is great synergy between the capacity of some renewable technologies of even relatively modest power density and efficient energy service demand.

Estimates of the potential for savings through energy efficiency measures vary widely. The potential can also be divided into two different categories: technical potential, and economic potential (Saddler et al. 2004). Technical potential refers to what is technically possible with no cost limitations. Economic potential refers to implementation of all measures that are cost effective, that is, at least break even in terms of cost savings through reduced energy demand versus the

cost of implementing the measures. NFEE (2003) makes estimates of the technical potential for energy savings through efficiency measures in the Australian economy. The residential sector could achieve savings of between 34% and 73%; the commercial sector, between 27% and 70%; and the industrial sector, between 22% and 46%. These are overall energy savings, rather than electricity savings.

However, depending on the technologies used, energy efficiency measures may encounter resource bottlenecks, similar to other renewable energy technologies. For example, many high efficiency Light Emitting Diode (LED) lights use rare earth elements (Smith Stegen 2015), so further upscaling may depend on finding substitute materials or technologies.

2.4.1 The "efficiency paradox"

There is a postulate that improvements in energy efficiency at the level of individual services might paradoxically lead to an increase in energy use. This is known as the energy efficiency paradox, and is also known as the Khazzoom-Brookes postulate (Rubin 2007). Other common names are 'the Jevons Paradox" and the "rebound effect" (Sorrell 2009). The same critique has also come from parts of the environmental movement, who argue that improvements in materials and energy efficiency alone will not be effective. Changes in lifestyle, consumption, and outlook are required to reduce overall energy consumption and emissions (Herring 2006).

The efficiency paradox may be divided into three categories: direct rebound, indirect rebound, and system-wide rebound (Herring 2006). According to standard economic theory, the cost reduction of the service enabled by decreased energy use leads to increased market accessibility and hence increased demand for that service. This is direct rebound. Even if a particular

energy service user does not increase their demand for that service, the savings from cost reduction may be spent on another service that requires energy. This is indirect rebound. The third category, system-wide rebound, represents the sum effect of direct and indirect rebound on the whole energy system (i.e. economy), plus any other effects that emerge at the macro-level. For example, a technological change resulting in increased energy efficiency may change the consumption of a fuel or material, which changes the price and hence demand for that resource in other sectors of the economy, leading to a change in overall energy use.

If the total rebound effect is greater than zero, then energy savings from an energy efficiency measure will be less than expected from summing the individual unit efficiency gains. If the rebound effect is greater than 1 (or 100%), then the energy efficiency measure has in effect backfired, causing greater energy use. Herring (2006) cited as evidence for the efficiency paradox that in Western Europe for the past 25 years (until 2006), overall energy use has increased, despite improvements in energy efficiency. Rubin (2007) described the same trend in the US. However, neither study quantifies the effect of population increase, and they do not present their evidence in terms of per capita energy use. Sorrell (2009) concluded that the evidence for actual backfire (rebound > 1) is inconclusive, and suggested that the amount of rebound may be dependent on the kind of energy efficiency improvement. Improvements in general purpose technologies such as steam engines (historically), electric motors, and computers may have a high rebound. Dedicated efficiency improvements, for example thermal insulation, may have lower rebound, because of smaller effects on economy wide productivity and economic growth. These economy wide effects imply that rebound may be smaller in developed economies than in developing economies. Rebound may also be lower in high

income households than in low income households, who are saving money by energy conservation measures (i.e. forgoing energy services). For example, a high income household which already is completely air conditioned will not use more air conditioning if energy efficiency has improved, but a lower income household may now be able to afford the more energy efficient air conditioning.

3 Comparing nuclear, CCS and renewable energy

Each of the technological options examined in the previous chapter has its unique characteristics, however there are many factors that can be directly compared to assess the practicality of large scale deployment of each technology, and its effectiveness in helping to avoid dangerous climate change.

3.1 Greenhouse emissions comparison

In this section the estimated life cycle greenhouse gas emission intensities of solar, wind, bioenergy, storage, nuclear and CCS are compared. There is a wide variation in emission estimations for nuclear power. While the nuclear power generation process is, in itself, almost totally emission free, the whole nuclear fuel life cycle is not (Diesendorf 2005). Most of the stages in the life-cycle use energy that currently comes from fossil fuels, such as the mining and milling of uranium ore to produce yellow-cake (U_3O_8), the conversion of yellow cake into uranium hexafluoride (UF_6), enrichment to increase the concentration of U-235, fabrication of uranium oxide (UO_2) fuel rods, power station construction, operation and maintenance, storage, optional reprocessing, waste management of spent fuel, and power station de-commissioning. Sovacool (2008) surveyed a number of studies that produced estimates of emissions for the whole nuclear life cycle ranging from 1.4 g of carbon dioxide equivalent per kWh (g CO_2e/kWh) to 288 g CO_2e/kWh, with a mean value of 66 g CO_2e/kWh. The author pointed to errors in methodology for both the low-end and high-end estimates. Pearce (2008) noted that life-cycle emissions for nuclear energy

would change if deployed on a large scale. For the currently mined high grade ores, the emissions per unit of energy generated for a nuclear plant are more likely to be in the range of the mean estimate given above, but for low grade ores, the emissions will be higher (Sovacool 2008), not only because more ore must be processed to obtain the same amount of yellow-cake, but also because the area of mine that must be reclaimed is greater. According to Pearce (2008), the extraction energy is inversely proportional to the ore concentration. Mudd and Diesendorf (2008) also found a dependence on ore grade if the grade dropped below 0.1% yellow-cake. Wallner and Wenisch (2011) predicted that emissions would increase to within a range of 82 to 210 g CO_2e/kWh if the ore grade declined to the range of 0.01% to 0.02%. Norgate et al. (2014) estimated a life cycle emissions value of 33.9 g CO_2e/kWh based on an extracted ore grade of 0.15%. The authors also reported a current world mean production ore grade in the order of 0.12%, and a world average ore grade in reserves of 0.042% based on 2009 data. These disparate results can be collated into a general equation relating emissions to ore grade:

$$e = 30.46 + \frac{0.52}{og} \tag{3.1}$$

where e is the greenhouse emission intensity in g CO_2e/kWh, and og is the uranium ore grade in %.

Nugent and Sovacool (2014) surveyed a number of studies estimating the life cycle greenhouse gas emissions of solar PV and wind energy. A mean value of 34.1 g CO_2e/kWh was found for wind energy, and 49.9 g CO_2e/kWh was found for solar PV. The emissions of nuclear power can be compared (Figure 3.1).

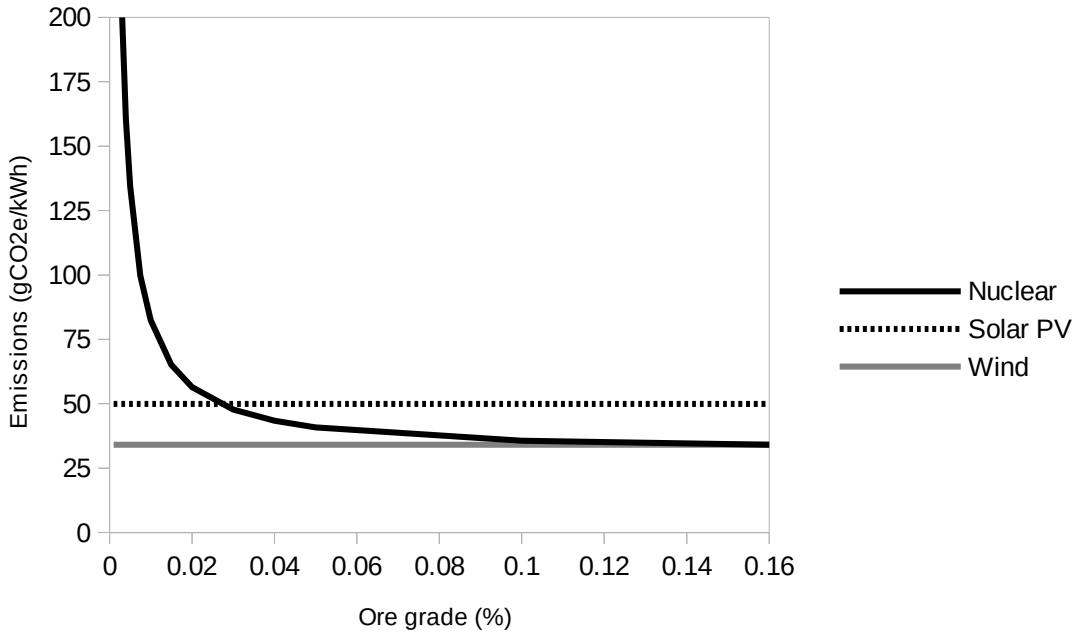

Figure 3.1. Emission intensity of nuclear power with respect to uranium ore grade. Average emissions for solar PV of 49.9 g CO_2e/kWh and wind of 34.1 g CO_2e/kWh (Nugent and Sovacool 2014) are provided for comparison.

Norgate et al. (2014) predicted that production ore grades would decline to around 0.01% by 2065 if nuclear power generation grows at a rate of 1.9% per year. However if nuclear power were to play a major part in meeting world electricity demand, then it must grow more quickly, and production ore grades would decline much more rapidly. Therefore although presently the emissions for nuclear power may be around 34 g CO_2e/kWh, the value will rise with time and greater use, and it is reasonable to compare the mean value of 66 g CO_2e/kWh found by Sovacool (2008) with the other technologies (Table 3.1).

The infrastructure emissions for storage systems refers to the greenhouse gases emitted during manufacture, installation and decommissioning of the storage. The total emission intensity of power output from storage will depend on the source of the input power and the round trip storage efficiency (Oliveira et al. 2015). For renewable energy generation systems with no or low emissions

during operation, such as wind or solar PV, the total emissions intensity of power output from storage will be similar to the sum of the power source value and the storage infrastructure value. However in a power system containing both a renewable source and storage, not all the generated energy will be stored, so the overall emissions intensity of the system will be less than the sum of the power source technology value and the storage technology infrastructure value.

Table 3.1. Average life cycle greenhouse gas emission intensity for different energy generation technologies.

Technology	**Mean greenhouse gas emissions (g CO_2e/kWh)**	**Reference**
Hydrogen storage infrastructure	3	Oliveira et al. (2015)
Battery storage infrastructure	50.6	Oliveira et al. (2015)
Wind	34.1	Nugent and Sovacool (2014)
Solar PV	49.9	Nugent and Sovacool (2014)
Solar thermal	37	Whitaker et al. (2013)
	60-73 with molten salt thermal storage	Klein and Ruben (2013)
Bioenergy	81	Cherubini et al. (2009)
Nuclear	34 at ore grade 0.15%	Norgate et al. (2014)
	66 average	Sovacool (2008)
Gas (CCS)	247	Hertwich et al. (2015)
Oil (CCS)	190	Kleijn et al. (2011)
Coal (CCS)	201-263	Hertwich et al. (2015)
Gas (without CCS)	527	Hertwich et al. (2015)
Oil (without CCS)	850	Kleijn et al. (2011)
Coal (without CCS)	791-933	Hertwich et al. (2015)

Infrastructure for storage systems refers to manufacture, installation and decommissioning. During operation, emissions from stored power depend on the source power technology and round trip efficiency.

Emissions from the manufacture of renewable energy and storage technologies should decrease as the system wide emissions of the power supply grid falls (Pearce 2008). Similarly for nuclear power, reduction in ore grade and increase in required extraction energy may become less significant to life cycle emissions

as mine site power supplies and ore transportation are sourced more and more from low emission energy sources. However Wallner and Wenisch (2011) found that below an ore grade of 0.0086%, the required energy input for nuclear power exceeded the energy generated.

There is considerable uncertainty over the level of fugitive emissions of greenhouse gases from the supply chain of coal and gas generation, both with or without CCS, such that the advantage of gas compared to coal may be significantly reduced (Bouman et al. 2015).

3.2 Speed of emissions reductions

Because of the effect that higher atmospheric CO_2 concentrations and temperatures might have on carbon sinks, and other mechanisms detailed in section 1.1 above, emissions avoided sooner are more important than emissions avoided later, and therefore, the speed at which each technology can begin to reduce emissions, and the amount that can be reduced per unit time, is important.

In the present day, manufacturing infrastructure for nuclear plants has greatly contracted from that experienced during the last peak nuclear building cycle around 1980 (Schneider et al. 2009), leading to significant construction schedule and project cost risk. Large scale investment in manufacturing infrastructure requires order certainty, which so far hasn't happened. Shortages of skilled labour have also been identified, with a large proportion of existing employees nearing retirement age. Both of these trends must be addressed before any increase in nuclear construction can take place. Given the currently aging nuclear reactor fleet, projections of nuclear power generation 40 years into the future have raised doubt that overall global nuclear capacity could expand

significantly before 2050, unless life-time extension beyond 40 years becomes standard (Schneider et al. 2009). However, since 2012, world nuclear power generation has begun to grow again (Schneider and Froggatt 2015), rising by around 50 TWh to 2410 TWh in 2014. This is still 9% lower than its 2006 peak of 2660 TWh. In contrast, between 2006 and 2014, wind power generation grew by 573 TWh (a greater than 5 times expansion), and solar generation grew by 181 TWh (a greater than 40 times expansion) (Schneider and Froggatt 2015). Since Australia has little nuclear power plant manufacturing infrastructure or expertise, it is dependent on the global industry for any nuclear reactor program, unless it first builds its own infrastructure and expertise.

Between 2006 and 2013, world bioenergy electricity generation rose steadily from about 200 TWh to about 400 TWh, an average growth rate of just over 10% per year (IEA 2014). There has yet to be any significant impact on global electricity generation by CCS (Scott et al. 2015). In Australia, Saddler et al. (2004) concluded that a mix of extensive (but well within technical feasibility) energy efficiency improvements, renewable energy generation, and gas-fired generation could reduce emissions by more than five times as much as CCS alone in the year 2030, and cumulative emissions to 2030 by ten times as much.

Out of these alternatives, the technologies that have demonstrated the greatest potential for growth in generation are solar, wind, and biomass. While nuclear has historically been established much earlier than solar and wind, generation had been declining until the last three years. Many questions remain over its future growth capability.

3.2.1 Energy payback time and limits to expansion of low emission generation

To build an entire energy or electricity supply system based on low emission sources will require a huge transition that involves both the expansion of alternative capacity, the retirement of conventional power plants, and the training or re-training of large numbers of personnel. This effort to re-align energy systems on a large scale will require a large energy input in itself, and presently energy is sourced mainly from greenhouse intensive sources. The resultant pulse in greenhouse emissions may push the Earth's climate system over a tipping point (Steffen 2007). Hence it is important to use as little energy as possible for this transition. An important metric for making choices about which low emission technologies to use is the Energy Pay Back Time (EPBT). The EPBT in years can be defined in general terms as:

$$EPBT = \frac{Embodied\ energy}{Annual\ energy\ generation} \tag{3.2}$$

where embodied energy is the energy required to manufacture and deploy the technology. The EPBT can be said to represent how long a generator takes to pay back its "energy debt", and start generating low emissions energy for the system, and provides a quantitative comparison between technologies (Table 3.2). If an energy generation technology has a long EPBT, then the rate at which it can be scaled up, without significantly increasing the risk of encountering a tipping point, is restricted.

The EPBT estimate for energy efficiency is based on building insulation measures, and can be considered illustrative. Nevertheless, this result reinforces the idea that energy efficiency measures would be a favourable initial option for transformation to a low emissions energy system. However, it could be

expected that as the level of energy efficiency improvements increases, it will become progressively more difficult to apply further improvements. The required embodied energy and the EPBT will increase. The EPBT estimate for bioenergy is based on the Mongolian Salix plant (Wang et al. 2015). The EPBT for oil mallee may be similar, since both plants live in arid zones. No information could be found on the EPBT for CCS, perhaps because there are so few operational CCS plants. The long construction times and EPBT for nuclear power must call into question whether this technology can reduce emissions quickly enough and minimise the risk of reaching a tipping point.

Table 3.2. Energy Payback Time (EPBT) for low emission technologies.

Technology	EPBT (years)	Reference
Energy efficiency	0.1-1.5[a]	Itard (2007)
Wind	0.2-0.67	Asdrubali et al. (2015)
Solar thermal	0.63-1.33	Asdrubali et al. (2015)
Solar PV	0.75-3.67	Asdrubali et al. (2015)
Bioenergy	3.2[b]	Wang et al. (2015)
Nuclear	5.9-14.1 (2.5% to 0.01% ore grade)	Lenzen (2008)

[a]Energy efficiency EPBT based on building insulation measures. [b]Bioenergy EPBT is based on using Mongolian Salix plant. PV stands for photovoltaic.

In contrast, the modularity and scalability of many renewable energy technologies opens the possibility for them to self-supply the expansion in their generation capacity, in effect to becoming energy breeders and avoiding a large initial greenhouse emissions pulse. Fthenakis et al. (2008) examined hypothetical solar PV breeding systems for two different PV technologies and found that life cycle emissions could be significantly reduced. Boudghene Stambouli et al. (2014) proposed a Sahara desert solar PV breeder to take advantage of the abundant sun, space and sand. The aim is to establish up to 100 GW of generation capacity by 2050.

3.3 Cost

Comparing the cost of alternate low emission power generation technologies is complex, because of the different assumptions made over which parts of the life cycle should be included. Also because of the dependence on climate of many renewable energy technologies, cost estimates will differ for different regions. A common measure that is used to assess costs is the Levelised Cost of Energy (LCOE) (Darling et al. 2011). A recent comparison of US LCOE (Lazard 2015) gave the ranking shown in Table 3.3, with a lower rank meaning a lower cost. Even though costs will be different in the SWWA, this comparison is useful because of the presence of operating nuclear power in the US. Also, energy efficiency and biomass were included in the comparison.

Table 3.3. Levelised Cost of Energy (LCOE) comparison between several alternative technologies in the United States.

Technology	LCOE range (US$/MWh)	Rank
Energy efficiency	omitted	1
Wind	omitted	2
Solar PV utility scale	omitted	3
Gas (without CCS)	omitted	4
Biomass	omitted	5
Coal (without CCS)	omitted	6
Nuclear	omitted	7
Solar PV rooftop commercial and industrial	omitted	8
Solar thermal tower with storage	omitted	9
Gas (peaking, without CCS)	omitted	10
Solar PV rooftop residential	omitted	11

The cost of nuclear power does not include decommissioning costs, and the cost of the wind and solar technologies does not include the cost of integration, estimated at between $2-10 per MWh. Source: Lazard (2015).

Energy efficiency measures were awarded the lowest costs of all, and as such should be given the highest priority for implementation. Although they have a

higher cost, the solar rooftop technologies can supply electricity at the point of demand, without having to travel through transmission and distribution grids.

Doubts have been raised over cost estimates of nuclear power. For example, even during a time of high construction rates in the 1970s, many reactors in the US were completed late and often over budget (Schneider et al. 2009). In recent times much fewer new reactors have been built, so calculating the actual costs is more uncertain. Because of the long construction times, and small number of new reactors under construction, it is difficult to ascertain if economies of scale will lead to significant cost reductions. It is possible that shortage of skills and manufacturing capacity might mean that reactors built later will cost more. Insufficient standardisation of the newer "generation III+" reactor design may also prevent cost reductions. By 2015, 16 out of 18 of these reactors under construction were behind schedule (Schneider and Froggatt 2015), which is bound to put upward pressure on costs. Schneider and Froggatt (2015) estimated the cost of the Fukushima disaster as at least US$100 billion and rising. However, this disaster may also have an effect on the cost of reactors yet to be built, as safety standards are tightened.

A recent estimate of LCOE for Australia (EPRI 2015) did not include energy efficiency or bioenergy, but did include CCS (Table 3.4). The need for extra storage and reserve generation under scenarios with very high penetration of variable renewable sources will also add to the cost. However, Delucchi and Jacobson (2011) concluded that the world could be completely supplied from renewable sources and storage at a similar cost to current energy prices. Mathiesen et al. (2011) found that 100 percent renewable energy systems may be economically beneficial compared to fossil fuel systems. The costs of solar thermal stations are currently higher, as they are not as far along the development curve. However, solar thermal stations with storage have value

because they can continue to generate power for longer periods than PV alone (reflected in the higher capacity factors in Table 3.4), including during the winter night time peak demand period. Elliston et al. (2014) found that the cost of a 100% renewable energy system for the national grid in Eastern Australia, including solar thermal stations, was competitive with fossil fuel based low carbon alternative systems, so a similar finding is plausible for the SWIS in Western Australia. Riesz et al. (2016) found that the lowest cost renewable energy system scenarios for Australia had very high levels of wind power generation. In contrast, the economic damage due to climate change could be at least several percent of global Gross Domestic Product (GDP) if greenhouse emissions are not mitigated (Revesz et al. 2014)

Table 3.4. Levelised Cost of Energy (LCOE) and capacity factor comparison between several alternative technologies for Australia.

Technology	LCOE range (A$/MWh)	Capacity factor range	Rank
Wind	omitted	omitted	1
Solar PV utility scale	omitted	omitted	2
Solar PV rooftop commercial	omitted	omitted	3
Gas (CCS)	omitted	omitted	4
Solar PV rooftop residential	omitted	omitted	5
Nuclear	omitted	omitted	6
Coal (CCS)	omitted	omitted	7
Solar thermal with 6h storage	omitted	omitted	8

The cost of nuclear power assumes a mature nuclear industry in Australia. The capacity factor is the ratio of the actual amount of electricity generated by the plant compared to the maximum amount that could be generated. CCS retrofit of existing plants reduces power output by 32.5%. Source: EPRI (2015).

3.4 Water use

The SWWA is a semi arid region where fresh water supply can be restricted, so the water use of a power generation technology is of significant importance. Similarly to conventional power plants, most solar thermal stations use a steam turbine to generate electricity from heat, and the conversion efficiency depends

on the temperature difference between steam entering and leaving the turbine. A continuous supply of water will be needed if it is used to cool the steam. If air cooling is used then much less water is needed (mainly to clean mirrors), but the temperature of the steam leaving the turbine is higher, and thermal to electrical conversion efficiency is lowered. However, because of the higher operating temperatures achievable by solar power towers, the steam entering the turbine is hotter and efficiency loss is less pronounced. Air cooling will be used on a number of solar power tower systems (Gesthuizen 2011). Jacobson (2009) estimates water use as 0.14 to 2.94 L/kWh, depending on whether water cooling is used. Baharoon et al. (2015) rates water use at 3 to 4 L/kWh if water cooling is used, and 0.2 L/kWh if air cooling is used. The water use is similar for each type of collector except for Stirling dish systems which have air cooling only. Jacobson (2009) rates the water use of nuclear at 1.5-2.73 L/kWh, comparable to the majority of parabolic trough solar thermal power stations that use water cooling, but more than the air cooled power towers (Table 3.5).

Table 3.5. Water use for electrical power generation technologies.

Technology	Water use (L/kWh)	Reference
Wind	0.00379	Jacobson (2009)
Solar PV	0.15	Jacobson (2009)
Solar thermal air cooled	0.14-0.2	Jacobson (2009), Baharoon et al. (2015)
Bioenergy (Oil Mallee)	0.75	RIRDC (2001)
Gas (CCS)	1.13-1.18	Ou et al. (2016)
Nuclear	1.5-2.73	Jacobson (2009)
Coal (CCS)	2.94-3.52	Ou et al. (2016)
Solar thermal water cooled	2.94-4	Jacobson (2009), Baharoon et al. (2015)

Nuclear power plants require more water than fossil fuel plants (Jacobson 2009). Most is returned to the source at a higher temperature, but some is lost to evaporation. This raises potential issues of damage to water habitats. Because

nuclear plants must be sited near water sources, they are vulnerable to flooding and storm surges, which might have a greater frequency and severity due to climate change. They will also be vulnerable to drought. Power generation relies on the temperature difference between steam and river or lake water, so nuclear plants may not be able to generate electricity if the water source becomes too hot (Jacobson 2009), as occurred during the European heat wave of 2004, when several nuclear reactors in France were shut down.

3.5 Conclusions

The advantages and disadvantages of each low emission power generation alternative are summarised in Table 3.6. Jacobson (2009) reviewed different energy options for mitigating global warming on a global scale. Air-pollution, mortality and energy security were also used as criteria. The technical ability of each technology to supply the stationary electrical generation and transport sectors was considered. For stationary generation, the use of wind power was found to be the most favourable, followed by other renewable energy technologies (except for large scale hydro). Even if safety, health and other environmental concerns are disregarded, both fossil CCS and nuclear are ultimately constrained by resource limitations unless there are significant new reserve discoveries or low energy use extraction techniques are developed. Hence further investment in deploying these technologies is a dead end unless alternatives such as renewables cannot be deployed quickly enough to avoid dangerous climate change, or cheaply enough to avoid the economic attractiveness of interim measures. However the growth rates of solar and wind energy systems are currently much greater than either nuclear or CCS systems. The ability to expand nuclear and CCS systems fast enough to avoid dangerous climate change has been shown to be questionable (section 3.2).

Table 3.6. Advantages and disadvantages of alternative technologies for reducing emissions from electrical power generation.

Technology	Advantages	Disadvantages
Nuclear power	Current large installed base	Can't provide peaking power efficiently, safety concerns, weapons proliferation, waste disposal, cost, poor scalability, slow pace of emission reductions, resource limitations, high water use, threat to civil liberties
Renewable energy	Modularity, good scalability, rapid pace of emissions reductions, wide distribution of resources	Variability, diffuse resource, need for storage or reserve generation, possible material constraints, possible constraint on battery deployment, high water use for solar thermal with water cooled systems
Carbon Capture and Storage (CCS)	Can be applied to existing power plants	Poor scalability, unknown pace of emission reductions, leakage concerns, cost, health concerns, resource limitations, high water use

The use of renewable energy and energy efficiency seems to be the most viable option. On a global scale, there are more than enough renewable energy sources to meet world energy demand, though some countries have more resources available than others. Embodied energy and life-cycle emissions of any of the technological choices, coupled with the risk of reaching a climate tipping point, mean there is an upper bound to their growth rate if they are to play an effective role in reducing greenhouse emissions. The goal of raising global living standards through wide scale provision of energy services must be met without excessive growth in high emission energy demand. Renewable energy breeding and improvements in energy efficiency are potential ways to achieve this. Some efficiency rebound is inevitable and perhaps desirable to widen

accessibility of energy services. To restrain net manufacturing energy requirements, recycling of batteries and improving their cycle lives will be high priorities if this technology is to be used for grid electrical energy storage on a large scale.

The short-term spatial and temporal variability of solar and wind energy systems is a challenge that must be met for these technologies to have a significant impact. Storage and the use of sustainable bioenergy as reserve generation are ways to balance the supply and demand variability. Conversely, the modularity, scalability, and short lead times of solar and wind technologies mean there is lower long-term demand and financial uncertainty than in large fossil or nuclear plants. Small fossil fuel cell or gas turbine technologies may also reduce long-term financial uncertainty. The distributed nature of many renewable energy forms and their localised sources of energy confers energy security advantages compared to fossil and nuclear power in many countries (though not in the case of Australia which has its own coal and uranium reserves). The lower levels of air pollution and waste disposal problems are also advantages.

4 Towards a low emissions SWIS grid

The global context of any particular technology choice used within the SWIS is important, as there are implications for the availability of infrastructure, skills-base, economies of scale, and possible materials shortages and manufacturing bottlenecks. The previous chapters demonstrated that although concerns have been raised about the practicality of the renewable solution to low emission electricity generation, other studies have highlighted advantages, and indicated that it might be the only viable option to reduce emissions fast enough. This chapter will look at examples and simulations of renewable energy electricity systems, and outline the ground work for developing a renewable energy simulation for the SWIS grid.

4.1 Examples of renewable energy electricity systems

Some places have already achieved, or plan to achieve, electricity systems based almost completely on renewable energy sources. The island of El Hierro in the Canary group plans to generate all electricity from a combination of wind and solar, with a pumped hydro system balancing supply and demand. Energy efficiency is also expected to play a big part (Droege 2012). The Danish island of Samso at times generates almost all of its energy demand from renewable sources, mainly wind. Supply and demand are matched on an hour by hour basis, by using bioenergy or transferring power to and from other grids. Some countries supply a large part of their electricity demand from hydroelectric resources, for example Uruguay, Bhutan, Albania (Gardiner 2013) and New Zealand (Sims et al. 2016). The Australian state of Tasmania also supplies

around 80% of electricity demand using hydroelectricity (ESIEP 2011), and the Australian Capital Territory has set a target for 100% renewable energy by 2020 (ACT Government 2016). The electricity system of Iceland is 99% supplied from renewable sources, based on hydro and geothermal energy (Droege 2012). The Icelandic economy contains heavy industries, but this example is atypical in that large scale geothermal and hydroelectric resources are not available to many other countries or regions. Instead, they must rely on locally available renewable energy resources that are likely to be spatially and temporally variable in nature, such as sunshine and wind. So far, not a single large scale electrical grid has transitioned to a 100% renewable system without the help of large scale hydro or interconnection with another grid.

4.2 Simulations of renewable energy electricity systems

There have been a number of scholarly articles published that use measured renewable energy resource data at specific locations to simulate how the large-scale stationary energy needs of a country, state, or region might be supplied with renewable energy generation systems on an hour by hour basis.

Lehmann (2003) provided several scenarios for a 100% renewable energy system for Japan based on a combination of energy efficiency, solar, wind, geothermal, and hydro. Daily supply and load profiles were provided for a typical winter day, but only for a scenario which assumes a high level of energy imports.

Barrett (2006) demonstrated the technical feasibility of a 95% renewable electricity system for the United Kingdom based on a combination of energy efficiency, wind, solar, wave, tidal, biomass, pumped hydro storage and

demand management, and provided sample annual supply and load profiles, and hourly profiles for typical winter and summer days.

Mills and Morgan (2007) showed simulations of the California and Texas electricity grids being supplied on an hour by hour basis over the whole of year 2006 by solar thermal plants. The plants have a peak capacity equal to the peak recorded load in that year, 16 hours of thermal storage, and large excess collector area to supply the storage with energy. It was found in both cases that 4 times the base collector area was necessary to completely supply the grids in all seasons, meaning that at low load times, excess capacity must be shed by turning part of the collector array away from the sun. The base collector area was defined as the collector area necessary to generate power at the peak capacity when solar insolation is at a maximum (solar noon at mid-summer on a clear day). The results were extrapolated to the entire US. It was noted that 16 hours of storage would not be enough to guarantee supply in the event of prolonged poor weather events, but geographic diversity in siting of many smaller plants would tend to average this out. At 3 times the base collector area, there was little need to shed excess capacity with 16 hours of storage, and it was estimated that a total collector area of 177 km by 177 km could supply most of the US, with wind, hydro, solar PV and efficiency improvements supplying the rest.

Peter et al. (2007) simulated a renewable energy system supplying the Spanish province of Catalonia. The simulation was run over 4 typical weeks, one each during Spring, Summer, Autumn and Winter, for the year 2006. The 'adjustable' sources of hydro, geothermal, and biomass were used to balance supply with demand on an hour by hour basis, with a greater reliance on sun and wind during the Spring and Summer months, and a greater reliance on hydro-power, geothermal, and biomass during Autumn and Winter when there was less sun

and lower wind speeds. A synergy between resource availability and generation was noted, with higher precipitation in winter increasing the hydro-resource. The greater demand for heat in winter also suggested a potential for co-generation from geothermal and biomass plants.

Herbergs et al. (2009) simulated renewable energy supply and demand profiles for a "typical" country belonging to the Organisation for Economic Cooperation and Development (OECD) for one week in winter. Demand reduction from energy efficiency measures was included. The results indicated the possibility of supplying the energy demand completely from renewable sources.

Hoste et al. (2009) provided scenarios that match 100% renewable electricity supply with demand for California in 2020 with a combination of wind, solar, geothermal, and hydro. Hourly supply and demand profiles are provided for typical days in Spring and Summer.

Blackburn (2010) matched solar power generation at three sites and wind power generation at a further three sites to load demand for the US State of North Carolina on an hourly, daily, and seasonal basis. Hypothetical wind and solar generation were scaled to produce approximately 80% of the average daily load, and balance between supply and demand was achieved using a combination of pumped hydro storage, biomass generation, gas turbine backup, purchase of power from other grids and demand management.

Connolly et al. (2011) developed scenarios for 100% renewable energy supply for Ireland, with different mixes of biomass, hydrogen, and renewable energy. The hydrogen energy system scenario had an electrolysis capacity of up to 10 GW for conversion of excess electricity to hydrogen.

Budischak et al. (2013) developed a 99.9% renewable energy supply simulation for a large regional grid in the eastern United States using solar, wind and storage, while Jacobson et al. (2015) developed a 100% renewable energy simulation for the whole of the United States based on solar PV, solar thermal, wind, wave power, geothermal, energy efficiency and hydropower.

Wright and Hearps (2010) developed a plan for 100% renewable energy electricity generation across the west, south, and east of Australia by 2020, based on concentrating solar thermal and wind power systems. Crop waste biomass and hydroelectricity were used as backup. This plan also covers transportation, heating and cooling energy, which is assumed to switch to electricity as a source rather than using fossil fuels. Balancing of the isolated SWIS grid is achieved by linkage to the eastern states National Electricity Market (NEM) grid via a long distance High Voltage Direct Current (HVDC) transmission line. The NEM grid extends from Tasmania to Queensland. The plan also aims to achieve a 20% improvement in energy efficiency. Modelling was carried out at half hourly intervals for the years 2008 and 2009. Solar irradiance data were obtained from satellite observations, and hourly wind power generation data were obtained from existing wind farms. Total generation was compared to historical load demand data.

Elliston et al. (2012) developed 100% renewable electricity scenarios for the east coast of Australia throughout the whole year of 2010 on an hour by hour basis. Solar PV, concentrating solar thermal and wind power systems were used for generation. Pumped hydro and biomass gas turbine plants were used to balance supply with demand. Similarly to Wright and Hearps (2010), solar irradiance data were obtained from satellite observations, and wind power generation data were obtained from existing wind farms. Total generation was

compared to historical load demand data. However the time scale was hourly rather than half hourly.

4.3 The use of energy storage and P2G technologies

Along with biomass, most of the above simulations relied on hydro-power as a backup to balance supply with demand on an hour by hour basis. Exceptions are Mills and Morgan (2007), which relied on solar thermal storage, and Budischak et al. (2013) who relied on different forms of large scale electrochemical storage, including batteries (which can consist of many small distributed systems). The hydro-power option is not currently available to the SWIS, but the use of energy storage technologies has been identified as having great potential to complement variable renewable energy systems (Luo et al. 2015). Budischak et al. (2013) found that with very high deployment of variable renewable energy systems and varying load conditions, the storage not only must have enough energy, but also enough power generation capacity to meet a portion of the instantaneous demand. As the share of renewable energy increased from 30% to over 90%, wider geographic distribution and more diverse forms of energy generation were required. The portion of instantaneous demand required to be met by storage might even be reduced, such that there was a trade off between excess generation capacity (up to 3x load) and storage. The more capacity, the less storage. The balance between these two, to obtain the least cost scenario, will depend on the relative costs of each. Load curtailment and fossil backup are also options for meeting infrequent shortfalls. Fossil generators increase emissions and cannot absorb excess generation to be used later, but existing plants can be used. Some loads may have the capability to increase with excess generation and curtail during times of shortfall. Weitemeyer et al. (2015) found that for Germany, storage was needed above

50% generation by wind and solar, and seasonal storage was needed at generation levels above 80%. The use of an integrated energy supply approach, where heating, cooling and transport energy demand are included along with electrical demand, and energy can be switched between all three forms and stored, is also considered to enhance the potential for utilisation of variable renewable energy sources (Lund et al. 2012), (B.V. Mathiesen et al. 2015). Although this thesis concentrated on the electrical demand only, the integrated energy approach can be utilised through what is commonly termed Power to Gas (P2G). Electricity is converted to a fuel, such as hydrogen or methane, for long term storage, and then reconverted back to electricity by burning the fuel in gas turbines, or by some other process (Cheng et al. 2009). Although the round trip efficiency is very low compared to other storage systems, the storage capacity is very high, so this approach may also have the potential to provide a seasonal storage system (Weitemeyer et al. 2015), and thus reduce the power generation capacity required to be built in order to generate enough electricity during seasons of low wind and solar availability (Guandalini et al. 2015). However, although a few pilot plants are in operation, this technology has yet to be used on a large scale and requires further technical and economic development (Götz et al. 2016). In arid and semi arid regions, water consumed by the power to gas process could be a significant constraint, although seawater has been used as a source (Götz et al. 2016). A portion of the water used in the P2G process can also be recycled (Davis and Martín 2014), and if the P2G plant is close to a gas turbine power plant, then the CO_2 emitted can be fed back into the methane conversion process. However, steps must be taken to minimise leakage of stored methane, itself a potent greenhouse gas, to the atmosphere.

Flywheels can also provide energy storage, but are not suitable for seasonal storage because of the high energy leakage rates and short storage times (Ferreira et al. 2013).

4.4 Simulating a 100 percent renewable SWIS grid

The findings from chapter 3 indicated that solar and wind systems could rapidly expand generation and reduce greenhouse gas emissions from the SWIS. Reiterating the second research question from section 1.3, just how far can the renewable energy path be taken? Can solar and wind renewable energy systems, aided by storage and energy efficiency improvements, completely replace the existing conventional generation systems? Is a 100% renewable energy system a technically feasible option for the SWIS?

Although no large industrial economy is currently supplied completely by variable renewable energy sources such as sun or wind, section 4.2 above described a number of simulations that demonstrate the feasibility of such a system. Hence this study aims to use numerical simulation to examine the feasibility of achieving a 100% renewable SWIS grid, using a combination of solar, wind, energy storage, and energy efficiency. Solar PV and wind energy were chosen because they are commercially mature with falling costs, widely available in other places of the world, already have a presence in the SWIS, yet are geographically and temporally variable. Solar thermal energy was also chosen because it is considered to be a low emission technology with rapid response rates and storage capability, and is entering commercial operation, although on a smaller scale than PV or wind. Bioenergy is another option worthy of consideration, especially as a reserve source of energy, as it can be stored and used on demand.

Both Wright and Hearps (2010) and Elliston et al. (2012) have used satellite solar irradiance data and historical wind power generation data to estimate total power generation. This was then compared to historical demand data. This study will take a similar though slightly different approach. Hourly measurements of solar irradiance reaching the ground have been recorded at a number of weather stations throughout the SWWA. This data will be used to develop a regional solar irradiance model such that a solar thermal power station or solar PV station can be simulated no matter where it is sited within the SWWA. Measured hourly wind speed data at typical hub heights is not widely available within the SWWA, but satellite derived hourly wind speed estimates at 50 metres above ground level are available from the Modern-Era Retrospective Analysis for Research and Applications (MERRA) database (Rienecker et al. 2011). Using this data, a regional wind power generation model will be developed such that a wind farm can be modelled no matter where it is sited within the SWWA. This frees the overall simulation from having to use existing wind farm sites, a restriction of the above two studies.

Both Wright and Hearps (2010) and Elliston et al. (2012) have also emphasised the use of solar thermal storage and pumped hydro to balance supply and demand. This study will instead emphasise the use of solar thermal and battery storage. This is because of the current lack of pumped hydro capacity available to the SWIS grid. The potential of P2G storage will be investigated as a way to store energy seasonally. Energy efficiency measures will also be modelled, as they have been shown to be among the most effective, rapid, and least cost ways of reducing emissions.

This study will compare the total generation to historical SWIS grid demand data on an hour by hour basis. This demand data is the sum of all residential, commercial and industrial loads. Why an hourly time scale? Typical summer

and winter daily demand curves for the year 2009 are shown in Figure 4.1. Peak demand occurs in the afternoon during summer and evening during winter. Comparison at a coarser time scale, such as daily, will not capture this diurnal variation in demand. While the summer demand peak is well matched to solar PV output, in winter the demand peak lies after daylight hours. The difference between winter daily minimum demand and peak demand will likely be accentuated in the coming years as more and more solar PV is installed on home and commercial rooftops.

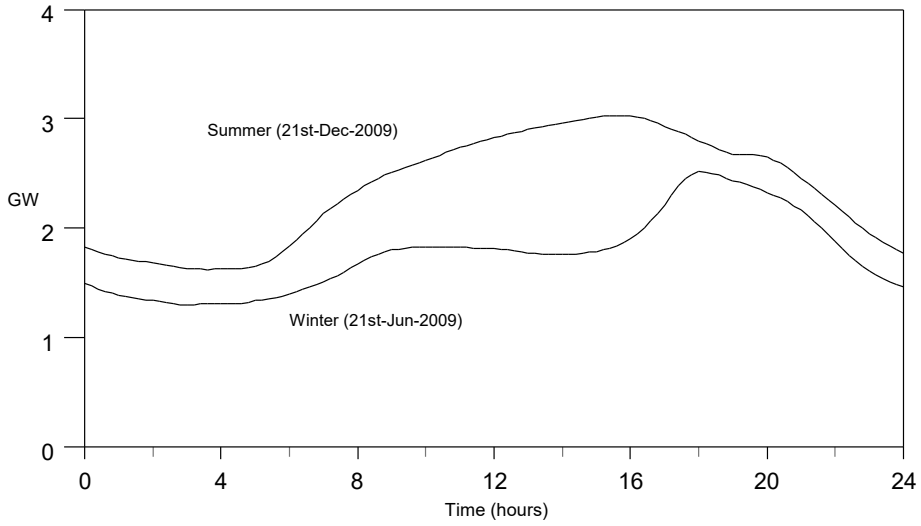

Figure 4.1. Typical summer and winter daily load profile on the SWIS grid for the year 2009.

An hourly time scale allows comparison between the bulk quantities of energy generated and required. However the hourly simulation must also be extended to a yearly duration, as there are daily, weekly and seasonal variations in grid demand (Figure 4.2), and seasonal variations in renewable energy resources. On shorter time scales, there already exist systems for balancing supply and demand, such as rotational inertia and primary and secondary frequency regulation. Because these systems operate at time scales much shorter than one

hour, they are not modelled here, except that any energy they require will be accounted for in the load profile. However, the characteristics and configuration of the large scale power stations on the grid may affect their operation, which must be taken into account.

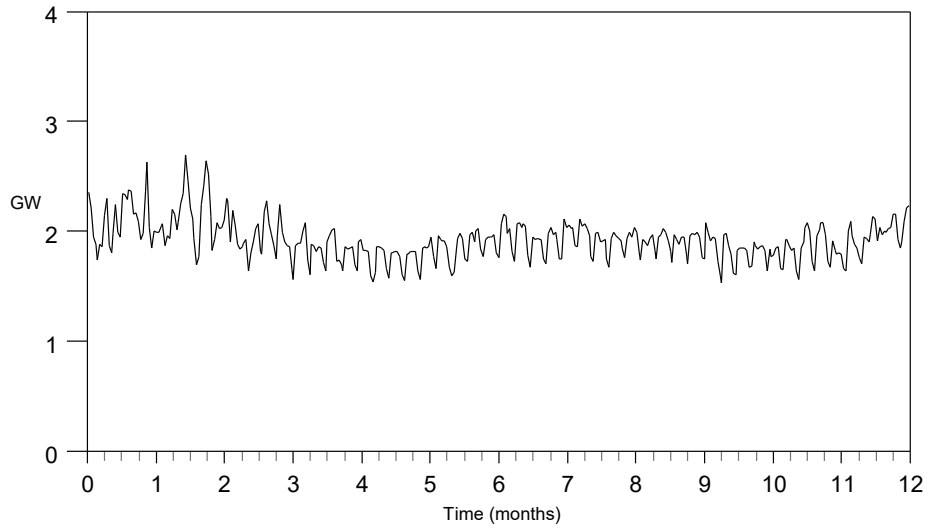

Figure 4.2. Daily average SWIS load demand over one year for 2009. The starting date is 21st December.

The simulation developed in this study will be designed to maximise flexibility, and enable the creation of different scenarios with different mixtures of solar PV, solar thermal, wind power and storage capacity. Currently the SWIS grid aims to achieve two reliability targets. The first reliability target is a less than 0.05% Loss of Load Probability (LOLP), estimated as the fraction of time that energy generation fell short of the load demand (MR 2012). The second target is a 0.002% shortfall in generated energy over one year. When it is clear if it is possible for a renewable energy system to meet these standards, and just how much solar PV, solar thermal, wind power and storage capacity is required, an implementation schedule will be constructed and the feasibility of transitioning to a 100% renewable SWIS grid will be examined.

Recent estimates require a drop in global emissions by 2050 to between 5 and 30% of 2010 levels to limit temperature rise to 1.5ºC by 2100 (Pachauri et al. 2015), and many global emission reduction studies set a target year of 2050 (Loftus et al. 2015). However, Australia as a historical and current high per capita emission country has an obligation to reduce emissions more quickly. Therefore 2030 was set as the target year for completing the renewables transition, less than 15 years from the present. The demand data will be upwardly adjusted for projected increase in population to the year 2030, and energy efficiency improvements will be deducted.

The output from rooftop PV will also be deducted from the total grid demand data. Therefore demand data from the year 2009 was chosen as the baseline, because after this time, rooftop solar PV began to make significant inroads into demand profiles. Since most rooftop PV is 'behind the meter', only net grid demand is recorded, and so after 2009 it is not possible to separate the amount of intrinsic energy demand from the amount of PV generation.

5 Solar irradiance model

This chapter will detail the development of a regional hourly solar irradiance model, which is needed to simulate power generation from solar PV and solar thermal power stations. First of all some background information about the components of solar radiation and the statistical modelling of solar power generation will be presented. Then the model development methodology and results will be detailed in the following sections. This chapter is based on the journal article "A method for generating synthetic hourly solar radiation data for any location in the south west of Western Australia, in a world wide web page" (Laslett et al. 2014).

5.1 Background

Systems that utilise solar energy are now a globally significant method to generate low emission energy. It is insufficient to use an average daily value of solar radiation to simulate these systems because solar radiation reaching the ground can vary significantly within a single day. Energy demand can also vary widely over the course of a day. To investigate the balancing requirements of systems that use significant amounts of solar energy, there is a need to develop algorithms to simulate radiation on finer time-scales. For the purposes of developing an interactive simulation of solar energy systems in the South West Region of Western Australia, an algorithm to generate synthetic hourly solar radiation data over a range of locations, with diurnal and seasonal variations that are a reasonable representation of actual local conditions, is needed.

Previously, for many locations solar radiation has only been measured on a horizontal surface. Hence much theoretical work and synthetic data algorithm development has concentrated on horizontal surfaces (e.g. Mora-Lopez and Sidrach-de-Cardona (1998) and Hontoria (2002)). In this chapter, all references to the word 'horizontal' refer to radiation falling on a horizontal surface rather than the component of radiation travelling in a horizontal direction. These horizontal surface algorithms are generally inadequate for the simulation of most solar power generating devices, because the collecting surfaces are usually not horizontal. Radiation incident on the earth's surface can be divided into three components, and the degree of tilt from the horizontal affects each component differently. The three components are the beam (also called direct) component that has come from the sun; the diffuse component, resulting from radiation that has been scattered in the atmosphere; and the reflected component, resulting from radiation reflected off other surfaces. The diffuse and reflected components are indirect, although there is a dependence on the beam radiation they originate from. Radiation falling on a horizontal surface includes both beam and diffuse components lumped together (in theory, the reflected component is zero for horizontal surfaces in isotropic surroundings). Solar power systems that use mirrors to focus and concentrate radiation utilise only the beam component. Photovoltaic (PV) surfaces utilise all three components.

Under clear skies, each component of radiation can be theoretically estimated from the position of the sun in the sky and variations in Earth's orbit. If clouds, haze, smoke, fumes, or atmospheric pollutants are present, then the beam component will be reduced in a spectrum dependent way, and since the diffuse and reflected components are dependent on the beam component, they will also be affected. The characterisation of these effects over varying time and spatial

scales is one of the biggest challenges facing any synthetic data generation algorithm.

Full scale physics-based meteorological or global circulation models are very computationally intensive and usually require a super computer. However, if measured irradiance data is available, then there is the possibility of using simpler empirical techniques to predict future irradiance. Graham et al. (1988) posited that any data set, real or synthetic, that captures underlying climatological behaviour and has similar probability characteristics to a long term historical data set, if it existed, should be sufficient to simulate the performance of a solar power generation system. Gazela and Mathioulakis (2001) detailed methods for constructing a "Typical Meteorological Year" (TMY) database from long term weather data. The database would typically contain values for several variables, including solar irradiation, over an entire year, and ideally, represent the gamut of typical weather patterns for a particular location. However Muneer et al. (2007) pointed to a common problem with existing solar radiation data sets: the beam and indirect components are seldom measured independently. Graham et al. (1988) pointed to another common problem. To accurately assess the performance of many systems that use solar radiation, radiation data on a time scale that captures transient changes are required. For example, hourly data is necessary to capture changes in the position of the sun throughout the day. Measurements on these fine time scales are not available in many places in the world. It may be possible to get reasonably accurate estimates for missing data by using alternate synoptic information such as pressure, temperature, and cloud cover. Models that can do this are called Meteorological Radiation Models (MRMs).

Generation of fine time scale variation using common statistical distributions has been investigated. Semenov et al. (1998) found that using a normal

distribution to generate synthetic solar radiation values did not match well with the distribution of measured solar radiation in general and at a site in the UK in particular. Punyawardena and Kulasiri (1996) compared 17 years of measured daily bright sunshine duration at a meteorological station in Sri Lanka with different statistical distributions and concluded that the best statistical fit was the Weibull distribution. Boland (1995) performed a Fourier spectrum analysis of solar radiation data for several sites in Australia (including two in Western Australia), and found that solar radiation followed seasonal and diurnal cycles.

Several algorithms attempt to generate finer time scale radiation data using data from longer time scales. Perhaps the simplest approach was taken by Celik (2002), who generated clear sky radiation curves and then modified the amplitude such that the average daily radiation was similar to one of several typical daily values within a particular month. Hence atmospheric conditions such as cloudiness are taken into account in an overall fashion. This approach could be used to generate data on any time scale but does not capture any of the transient variation that may be present on that time scale. Gordon and Reddy (1988) used data from widely varying climatic conditions to develop a simple functional form for the probability density function of daily radiation but found that there is location dependence. More sophisticated Autoregressive Moving Average (ARMA) and Fourier analysis techniques have been developed to synthesise radiation data (Hontoria et al. 2002), but these have also been found to be location dependent.

In contrast, Liu and Jordan (1960) found much earlier that if the clearness index was used as the variable to be analysed, instead of radiation, then the probability features were quasi-universal. The clearness index (k_t) is defined as the ratio of global (i.e. total) radiation falling on a horizontal plane at the surface

of the Earth (I_h) to the total extraterrestrial radiation falling on a plane horizontal to the surface but at the top of the atmosphere (I_{hex}):

$$k_t = \frac{I_h}{I_{hex}} \tag{5.1}$$

The symbol K_t is commonly used to represent daily clearness index, the ratio of total daily radiation (H) falling on a horizontal plane at the surface to the total daily extraterrestrial radiation (H_{ex}) falling on a plane horizontal to the surface but at the top of the atmosphere:

$$K_t = \frac{H}{H_{ex}} \tag{5.2}$$

Graham et al. (1988) claimed that most of the seasonal variation in daily radiation is due to variation in the extraterrestrial radiation, which can be accounted for by using the clearness index. This finding has been prominent in the development of a number of empirical algorithms to synthesise data when measurements are only available on a longer time scale. These algorithms operate over different time scales, such that it is conceivable to use them in cascade, ultimately synthesising data on an hourly or finer time scale, when measurements are only available on a monthly or yearly time scale. Mora-Lopez and Sidrach-De-Cardona (1998) proposed a method to generate synthetic hourly values of the clearness index directly from monthly average values of the daily average clearness index. The method involved incorporating a seasonal component as well as a component related to the diurnal sun cycle. However, the authors found the algorithm was not universal.

Both Graham and Hollands (1990) and Aguiar and Collares-Pereira (1992) developed well known algorithms to synthesise hourly data from daily average clearness index values, with time of day dependent probability distributions. The Aguiar and Collares-Pereira (1992) algorithm, called the TAG algorithm, claimed better statistical consistency between the synthetic data and measured data for clearer months. Also, since a wider range of locations were used to develop the TAG algorithm, it may perhaps be more widely applicable. Remund et al. (1998) provided modifications to the TAG algorithm for locations where the sun might be occluded by the skyline, such as in mountainous regions.

There have been several models using Artificial Neural Networks (ANNs) developed to generate synthetic hourly data from average daily solar radiation. Hontoria et al. (2002) developed an ANN model based on data from several locations in Spain, and found that their model matched the measured data more closely than either the Graham and Hollands (1990) or Aguiar and Collares-Pereira (1992) models. However Reikard (2009) reported mixed results, with ANN models significantly outperforming autoregressive models only at higher temporal resolutions, in the order of a few minutes. ANN models can also be much more numerically intensive. More recently, satellite remote sensing data has been used to provide estimates of surface radiation. The quantity of data required to comprehensively represent solar radiation behaviour over all seasons and cover an entire region would be large.

A number of shortcomings with the clearness index approach have become apparent. The beam and diffuse components of radiation falling on a horizontal surface are bundled together into measurements of the clearness index. Generation of synthetic radiation values for surfaces oriented at an angle other than horizontal will require individual quantification of these components and

also the reflected component. Since both clearness index and the diffuse component are affected by atmospheric processes such as clouds, it was hoped that there might be a close relationship between the two (Hollands and Huget 1983). However, it has been found that the diffuse component can vary widely for very similar values of clearness index. Skartveit et al. (1998) found that clouds have a complex effect on the diffuse component. For example, in the case of broken or scattered cloudiness conditions, the diffuse component can be so high that the measured clearness index exceeds the theoretical clear sky value. Perez et al. (1990) identified two limitations of using the clearness index: firstly, there is a dependency not only on atmospheric processes, but also on solar elevation. Secondly, the complexity of the diffuse component relationship means that in some situations it might be impossible to differentiate two different cloud conditions with the same clearness index. The authors proposed the use of a normalised clearness index that is solar elevation independent as a possible solution to the first limitation.

Approaches that use cloudiness metrics rather than clearness index have also been taken. Yang and Koike (2002) developed a Sky Clearness Indicator (SCI) coefficient that accounts specifically for cloud effects, modifying the surface global horizontal radiation from its clear sky value. Butt et al. (2010) developed a method of estimating cloudiness using high frequency (2 minute interval) measurements of global horizontal surface irradiance. Although this method of defining cloudiness was somewhat imprecise, the authors found a straight-line relationship between the diffuse fraction (ratio of diffuse horizontal irradiance to global horizontal irradiance) and their cloudiness metric for two locations in the Amazon.

Clearness index usually has lower values earlier and later in the day because of the increased air mass sunlight travels through when the sun is low in the sky.

In contrast, cloudiness metrics are not expected to exhibit such a strong trend because they modify the clear sky transmissivities rather than directly modifying the solar radiation. As such, they perhaps can be claimed to be a "purer" measure of the local cloud condition at the time. There is a hierarchy here. Direct measurements of radiation contain effects due to variations in Earth's orbit, the position of the sun in the sky, air mass, and cloud condition. Measurements of clearness index contain effects due to the latter two, and cloudiness metrics aspire to capture only the cloud condition.

In this chapter, the aim was to develop a numerically simple algorithm that can generate synthetic values of radiation data for any location within the South West region of Western Australia, with hourly, diurnal and seasonal variations in solar radiation that give a reasonable representation of actual local conditions. Australia lies in the Southern hemisphere, so simply using models developed for Northern hemisphere locations may not achieve this aim. Lanini (2010) pointed out that stratospheric sulphate aerosol content is higher in the Northern hemisphere, increasing the diffuse fraction. Hence a new model was developed that is a combination of the approaches of Yang and Koike (2002) and Aguiar and Collares-Pereira (1992). Firstly, equations to estimate the theoretical clear sky values for beam, diffuse, and reflected radiation were obtained from previous studies. Then, to represent the effects of cloud, a coefficient of cloudiness was defined that modifies all three components of clear sky radiation individually, and so can be used to model the performance of both concentrating solar power systems and tilted PV systems on cloudy days. An autoregressive algorithm was developed to generate synthetic hourly values of this cloudiness coefficient, with parameters that are themselves seasonally and locationally dependent and able to be calibrated with locally measured data from Western Australia.

It was considered that using latitude and longitude as the location coordinates would not lead to the numerically simplest operation of the model. Latitude provides information about the position of the sun in the sky, but there is little more direct information about climatic conditions in latitude and longitude values. For example, they do not say whether the location is over land or sea. In Western Australia, the climate is usually drier further inland. There are two areas of higher annual rainfall, one in the South West corner, and one in the tropical North. Since clouds are needed to generate rain, a correlation between cloudiness patterns and rainfall patterns can be expected. So if location coordinates are represented by a distance along the coast from a set starting position, and then a distance inland from this point on the coast, the relationship between seasonal solar radiation and location might take a simpler form. The model was developed to mimic this geographic pattern of annual rainfall.

The development of this new model indicates that the approach of using a pure cloudiness metric and alternate positional coordinates can provide an algorithm that is simple enough to use interactively and provide a viable alternative to using satellite data. There is scope for adaptation to other parts of the world with a similar pattern of declining inland rainfall, such as the West coast of North America, the West coast of South Africa, and the West coast of South America.

5.1.1 Irradiance in clear sky conditions

The first stage in developing a model for irradiance in cloudy conditions is to estimate irradiances for clear sky conditions. This has already been done in previously developed theory (e.g. Kumar et al. (1997), Gates (2003) or Liu and

Jordan (1960)). Later, in the methods section, new equations for modifying the clear sky irradiances due to the effects of cloud are developed.

The solar altitude angle, α, the vertical angle of the sun to the surface of the Earth, affects the amount of solar energy reaching the Earth not only because of geometrical effects but also because of the amount of air the light has to travel through. The sine of the solar altitude angle, $\sin\alpha$, can be calculated directly from the day of the year, time of day, and estimates of variation in Earth's orbit (see Appendix A). The air mass ratio, M, is the ratio of the atmospheric path length a beam of light must travel through, compared to the path length if the sun was at the zenith (i.e. the shortest path length). One of the most numerically simple approximation formulas for M as a function of $\sin\alpha$ comes from Young (1994):

$$M = \frac{1.002432\sin^2\alpha + 0.148386\sin\alpha + 0.0096467}{\sin^3\alpha + 0.149864\sin^2\alpha + 0.0102963\sin\alpha + 0.000303978} \tag{5.3}$$

This approximation has the advantage that the solar altitude angle does not have to be explicitly calculated.

The total (or global) irradiance falling on the Earth's surface at the ground can be divided into three types: the beam irradiance, I_b, the diffuse irradiance, I_d, and the reflected irradiance, I_r (Figure 5.1). Beam irradiance comes directly from the sun, and is also called direct irradiance. The extraterrestrial beam irradiance, I_o (W/m^2), is the irradiance arriving at the top of the atmosphere on a plane perpendicular to the direction of the sun. The fraction of of incident light that travels through a medium is called a transmittance. The beam irradiance arriving at the Earth's surface, I_b (W/m^2), also on a plane perpendicular to the

direction of the sun, can be related to I_o by defining a beam radiation atmospheric transmittance, t_b, such that:

$$I_b = t_b I_o \tag{5.4}$$

t_{bcs} is the beam atmospheric transmittance under clear sky conditions. At very high elevations with extremely clear air, t_{bcs} may be as high as 0.8, while for a clear sky with high turbidity it may be as low as 0.4 (Gates 2003).

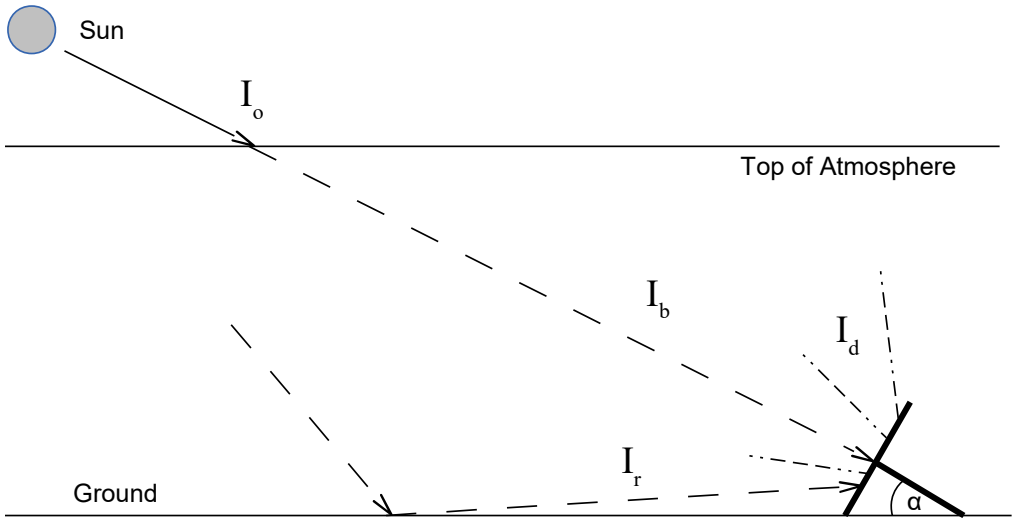

Figure 5.1. The three types of irradiance falling upon a surface perpendicular to the position of the sun in the sky. I_o is the extraterrestrial beam irradiance. I_b is the beam irradiance falling on the surface. I_d is the diffuse irradiance falling on the surface. I_r is the reflected irradiance falling on the surface. α is the solar altitude angle.

A simple formula based on Bourghers law (Kreith and Kreider 1978) can be used to estimate t_{bcs} from M:

$$t_{bcs} = K_{b1} e^{K_{b2} M} \tag{5.5}$$

where K_{b1} and K_{b2} are constants. K_{b2} is an absorption constant and is negative. If a surface is oriented in a direction other than perpendicular to the sun's position in the sky, then the incident beam irradiance will be reduced. Many data sets and many studies deal only with measurements of solar radiation falling on a horizontal surface. Therefore expressions for horizontal surface radiation must be developed if comparison with these models is to be made. The beam irradiance falling on a horizontal surface, I_{hb} (W/m^2), will be:

$$I_{hb} = I_o t_b \sin\alpha \tag{5.6}$$

Diffuse radiation arises from beam radiation that has been scattered by the atmosphere. The diffuse irradiance I_d (W/m^2) on a plane at the Earth's surface can be related to the extraterrestrial beam irradiance I_o (W/m^2) by defining a diffuse atmospheric transmittance, t_d such that:

$$I_d = 0.5\, I_o t_d \sin\alpha\left(1+\cos\left(tilt\right)\right) \tag{5.7}$$

where tilt is the vertical angle of the plane compared to the horizontal. This equation implies that for surfaces tilted at angles other than horizontal, the diffuse irradiance will be less because the surface will not "see" the full sky hemisphere (Rudy 1997). If the surface is vertical, then the diffuse radiation falling on it will be halved, as it only "sees" half of the full sky hemisphere. Liu and Jordan (1960) formulated the following relationship between clear sky diffuse transmittance t_{dcs} and the beam atmospheric transmittance under clear sky conditions t_{bcs}:

$$t_{dcs} = 0.271 - 0.294\, t_{bcs} \tag{5.8}$$

This equation implies that a higher beam transmittance means less diffuse radiation, as would be expected. Beam transmittance t_{bcs} for a dust free clear sky typically ranges from 0.4 to 0.8, and the corresponding diffuse transmission coefficient t_{dcs} ranges from 0.153 to 0.037 (Gates 2003). The diffuse irradiance falling on a horizontal surface, I_{hd} (W/m^2), will therefore be:

$$I_{hd} = I_o\left(0.271 - 0.294\, t_{bcs}\right)\sin\alpha \tag{5.9}$$

For a surface under consideration, a part of both the beam and diffuse components of clear sky radiation may be reflected by the surroundings. Based on a formula given by Gates (2003), the reflected radiation falling on a surface, I_r (W/m^2), in isotropic surroundings can be related to I_o by:

$$I_r = 0.5 r_g\, I_o\, t_r \sin\alpha\left(1 - \cos\left(tilt\right)\right) \tag{5.10}$$

where t_r is the reflectance transmittance, and r_g is the ground reflectance coefficient averaged over the solar wavelength spectrum (see Monteith and Unsworth (1990)). Gates (2003) gives a reflectance coefficient for vegetation of 0.2, and also a formula that relates the clear sky reflectance transmittance t_{rcs} to the clear sky beam transmittance t_{bcs}:

$$t_{rcs} = 0.271 + 0.706\, t_{bcs} \tag{5.11}$$

such that if clear sky beam transmittance increases, then so does clear sky reflectance transmittance. If the surroundings are not isotropic, then in principle it is still possible to explicitly model reflected radiation, but the equations will be complex and site specific. For a horizontal surface, tilt is zero, and the estimate for reflected radiation from equation 5.10 is zero. In this case:

$$I_{hcs} = I_o \left(t_{bcs} + t_{dcs} \right) \sin \alpha \tag{5.12}$$

where I_{hcs} is the clear sky irradiance falling on a horizontal surface (W/m^2). Note that multiple reflection effects between the Earth's surface and the atmosphere are present even if the tilt is zero. These effects can be modelled or made implicit in the diffuse transmittance estimation. For an example see Suckling and Hay (1977). Some authors have included an explicit term for these effects (Davies et al. 1985). It may be more important to have an explicit term if multiple cloud layers are modelled, as for example in Yang and Koike (2002), and there is a need to differentiate between intrinsic cloud behaviour and ground-atmosphere reflection effects.

5.2 Method

So far, theoretical equations for the transmittances t_b, t_d, and t_r have been formulated for clear skies, based on results from previous studies. To effectively model radiation under all weather conditions, there is a need to quantify the behaviour of these transmittances under cloudy conditions. In this chapter, a new metric of cloudiness was defined, its effects on t_b, t_d, and t_r were quantified, and an algorithm for generating synthetic cloudiness values at any location in the South West region of Western Australia was developed. The algorithm was calibrated and verified using cloudiness values obtained from hourly horizontal surface radiation data measured at a set of meteorological stations. Use of the word 'horizontal' refers to radiation falling on a horizontal surface.

5.2.1 Defining cloudiness

Previous studies have attempted to quantify cloudiness from observation (e.g. Muneer et al. (2007)). However, it is not simply the amount of cloud that

matters. Cloud type, height, distribution, and layering will also affect irradiance in an ever-changing manner. To maintain simplicity, no distinction was made between these different aspects of cloudiness. Instead the level of cloudiness was quantified by how much beam transmittance is affected. A cloudiness transmission factor, t_c, was defined as a fractional modifier to the clear sky beam transmittance, t_{bcs}, due to cloudy conditions:

$$t_b = t_c t_{bcs} \tag{5.13}$$

The "cloudiness"(c) was defined such that the cloudiness transmission factor t_c is reduced by increasing cloudiness until t_c is zero when c is one:

$$t_c = 1 - c \tag{5.14}$$

How much will cloudiness affect the diffuse transmittance, t_d? A diffuse cloudiness function, $k_{cloud}(c)$, was defined that modifies the clear sky diffuse transmittance t_{dcs}:

$$t_{gh} = t_b + t_d = (1 - c) t_{bcs} + k_{cloud}(c) t_{dcs} \tag{5.15}$$

where t_{gh} is the global irradiance transmittance for radiation falling on a horizontal surface. The observation by Butt et al. (2010) that the diffuse fraction, k_d, increases in a straight-line fashion with cloudiness was represented using:

$$k_d = \frac{t_d}{t_{gh}} = k_{dcs}(1 + K_{dr} c) \tag{5.16}$$

where k_{dcs} is the clear sky diffuse fraction, and K_{dr} is a slope constant. Combining equations 5.15 and 5.16 gives

$$k_{cloud}(c)=\frac{(1-c)(1+K_{dr}c)}{1-K_{dr}c\dfrac{t_{dcs}}{t_{bcs}}} \tag{5.17}$$

If the value of K_{dr} is high enough, then for some values of t_{bcs}, the k_{cloud} function increases with increasing cloudiness before reaching a maximum and then decreasing (Figure 5.2), and there are two possible values of cloudiness for the same value of k_{cloud}.

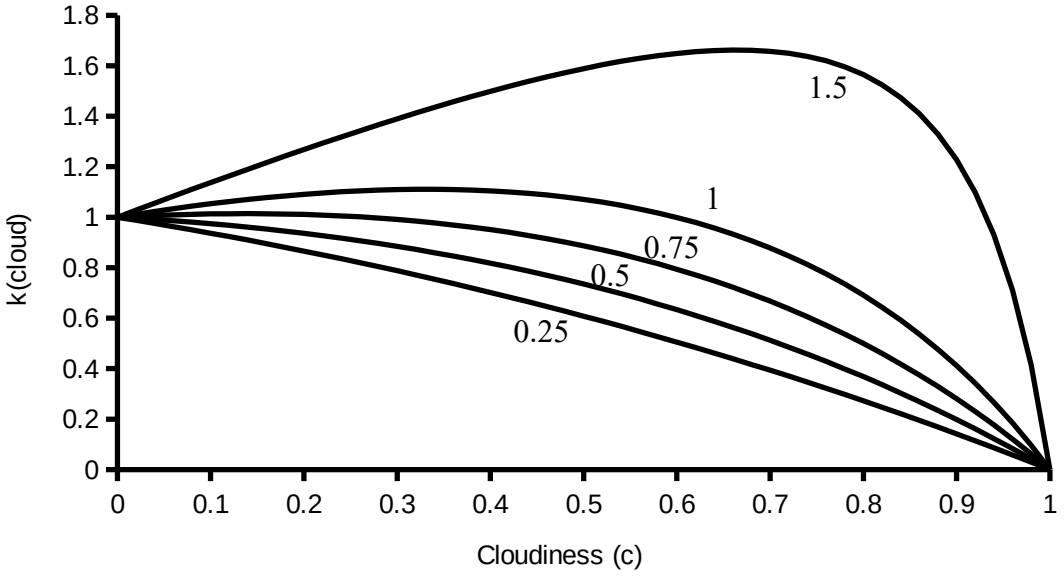

Figure 5.2. k_{cloud} as a function of cloudiness for $\sin\alpha = 0.1$, $M = 9$, $t_{bcs} = 0.3$ and $t_{dcs} = 0.182$. The 4 curves are for 4 different values of K_{dr}: 0.25, 0.5, 0.75, 1 and 1.5.

How much will cloudiness affect the reflectance transmittance, t_r? Hay (1979) implied that the reflected irradiance under cloudy conditions remains proportional to the global horizontal irradiance, and hence the reflectance transmittance will remain equal to the global horizontal transmittance:

$$t_r = t_{gh} = t_b + t_d = (1-c)\,t_{bcs} + k_{cloud}(c)\,t_{dcs} \tag{5.18}$$

5.2.2 Estimating cloudiness

To quantify the range and distribution of cloudiness over the South West of Western Australia, a way to estimate cloudiness from measured data was developed. Hourly horizontal solar radiation data from a network of 31 Western Australian Department of Agriculture weather stations for the years 2007 and 2008 were obtained. The data were originally stored in units of kJ/m^2 for 1 hour of radiation, so each value was divided by 3.6 to obtain a value for average hourly irradiance in units of W/m^2. Instrumentation error has the greatest relative effect when the sun is near the horizon and measured values of radiation are low. To minimise this error, only the data collected when the sine of the solar altitude angle, sinα, was greater than 0.1 were used.

Values for global horizontal transmittance, t_{ghm}, were obtained from these measurements using

$$t_{ghm} = \frac{I_{hm}}{I_{hex}} \tag{5.19}$$

where I_{hm} is the measured hourly horizontal solar irradiance (W/m^2), and I_{hex} is the extraterrestrial horizontal irradiance (W/m^2). I_{hex} was calculated using:

$$I_{hex} = S_o OF \sin\alpha \tag{5.20}$$

where S_o is the solar constant and OF is the orbital correction factor. These can be calculated or estimated from the day of the year, time of day, and location (see Appendix A). The solar constant S_o has been the subject of some debate. A value of 1367 W/m^2 has been widely used and was adopted here, but is subject to small variations due to solar activity (Gueymard 2004).

The cloudiness was estimated by combining equations 5.15 and 5.17 to give:

$$c = \frac{t_{gcs} - t_{ghm}}{t_{gcs} + K_{dr}\left(1 - \frac{t_{gcs}}{t_{bcs}}\right) t_{ghm}} \tag{5.21}$$

The value of K_{dr} was set to 0.8 so that the denominator of equation 5.21 was always positive for all values of global horizontal transmittance t_{ghm} obtained from measurements.

The daily average cloudiness c_d was calculated as the average of the hourly cloudiness values for those hours when the sun was above the horizon. If c_d was less than 0.05 and no hourly value of cloudiness was greater than 0.1, then the day was categorised as a clear sky day. A total of 4141 days (out of 21422 days of measured data across the 31 stations) were clear sky days.

A downhill simplex error minimisation algorithm (Press et al. 1992) was used to find the optimum values for K_{b1} and K_{b2} (see equation 5.5) that gave the best fit between the theoretical clear sky irradiance and the measured irradiance on the chosen clear sky days. To prevent negative cloudiness transmission factors, an additional weighting term was introduced within the error function calculation of the simplex algorithm so that if on any hour of any day (not just the clear sky days) the measured cloudiness using equation 5.21 exceeded 1 ($t_c < 0$), then the error value was dramatically increased.

5.2.3 Generation of daily cloudiness

The measurements for each day from each station were divided into two data sets, a training set and a test set (also called the calibration set and the validation set). The training set was used to establish the parameters of the algorithm. The synthetic data generated by the algorithm were then compared to the test data points. Because of the different ways that models from other

studies have separated data for calibration and validation, two different methods of separating data were used. In the first configuration, the measured data from each station were split almost equally into calibration data and validation data by assigning each day of data to one of the two groups using a pseudorandom number generator. In the second configuration, all the data from 7 stations (or about one quarter of the total) were reserved for validation data to test the algorithm. All the data from other 24 stations were used as training data to calibrate the algorithm.

Following the lead of Boland (1995) concerning seasonal variation in radiation, the monthly average of the mean daily cloudiness, and the monthly standard deviation in mean daily cloudiness were represented as varying sinusoidally with month:

$$c_{davmon} \approx K_{cd1} + K_{cd2} \sin\left(\frac{\pi}{6}\left(month + K_{cd3}\right)\right) \tag{5.22}$$

$$c_{dsdmon} \approx K_{cd4} + K_{cd5} \sin\left(\frac{\pi}{6}\left(month + K_{cd6}\right)\right) \tag{5.23}$$

where *month* is the month of the year (from 1 to 12). The sinusoid coefficients K_{cdi} (i = 1 to 6) were estimated for each station in the training data set by using the downhill simplex method to minimise the sum of the absolute errors between measured and estimated values of c_{davmon} and c_{dsdmon}.

In order to estimate the value of c_{davmon} and c_{dsdmon} for any location in Western Australia, a geographic relationship for the K_{cdi} coefficients was established. A shape map of the Western Australian Coastline was constructed from the GEODATA COAST 100K 2004 data package published by Geoscience Australia

(2004). This data set is based on a 1:100,000 scale map sheet. The shape map consists of a vector map of the coastline and state border in longitude and latitude coordinates. It does not include any of the islands off the coast of Western Australia that are included in the data package. Note that the distance along a coastline will depend on the precision of the coastline representation, with higher precisions generating longer distances. There were 74032 vertices in the constructed shape map, so a global simplification algorithm (Visvalingam and Whyatt 1993) was used to simplify the map down to a 500 vertex coastline map (Figure 5.3). The coastline is represented by a straight line segment drawn between each pair of vertices.

The intersection between the coastline and the state border with the Northern Territory in the north east corner was used as the starting point for calculating coastal distance. The position of each meteorological station in (*cpos*,*cdist*) coordinates, where *cpos* is the distance along the coastline and *cdist* is the shortest distance to the coast, was calculated from the latitude and longitude coordinates using Euclidean geometry.

To establish the geographic relationship, the value of each coefficient K_{cdi} (i = 1,6) was assumed to vary in a way roughly mimicking the rainfall pattern in Western Australia. That is, in a piecewise straight-line fashion along the coastline, and with a combination of initial increase and then exponential decay as distance inland from the coast increases. The value of each coefficient was estimated by interpolation using a number of setpoints positioned along the coast. See Appendix A for the detailed algorithm. The downhill simplex algorithm was used to optimise the number, position, and value of the set points such that the overall sum of the absolute errors between estimated and measurement derived values of the K_{cdi} coefficients at each of the meteorological stations in the training data set was minimised.

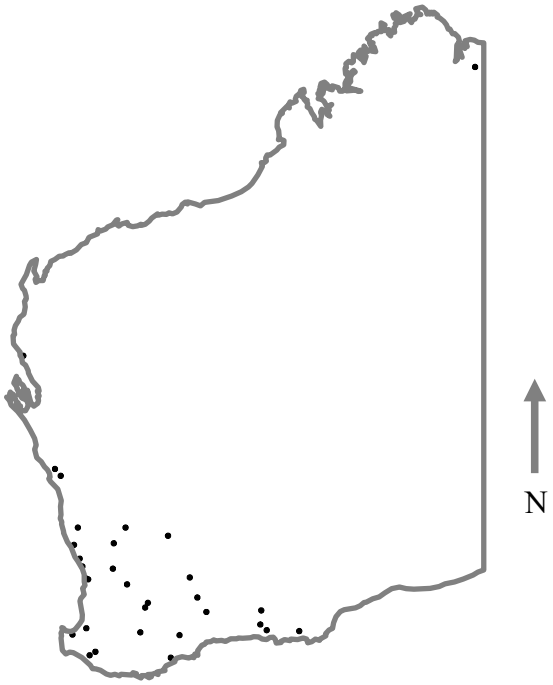

Figure 5.3. Simplified coastline of Western Australia and locations of meteorological stations.

To establish the frequency distribution of the daily cloudiness, the residual variable y_d was calculated for each day in each month of the training data set using the measured values for c_{davmon} and c_{dsdmon}:

$$y_d = \frac{c_d(measured) - c_{davmon}(mon)}{c_{dsdmon}(mon)} \tag{5.24}$$

The inverse cumulative frequency distribution, Cf^{-1}, of these values of y_d was approximated for each station in the training data set using:

$$Cf^{-1}(r) \approx K_{cf1} + K_{cf2}\, r + K_{cf3}\, r^2 + K_{cf4}\, r^8 \tag{5.25}$$

where r is the cumulative frequency. One purpose of using the residual variable y_d was to remove seasonal effects. However, because of the high number of clear sky days at many stations, the residual variables for each month were not

normally distributed and had predominantly positive skews. The coefficients K_{cfj} j = 1 to 4 were found to retain a seasonal dependence as well as the expected locational dependence, so they were estimated using the same technique as for c_{dmonav} and c_{dmonsd}:

$$K_{cfj} \approx K_{cd(4+3j)} + K_{cd(5+3j)} \sin\left(\frac{\pi}{6}\left(month + K_{cd(6+3j)}\right)\right) \quad for\ j = 1,4 \tag{5.26}$$

The sinusoid K_{cdi} coefficients, i = 7 to 18, were also adjusted for location using piecewise straight-line interpolation between coastal setpoints and a combination of linear and exponential functions for distance from the coast. As before, for each K_{cdi} the downhill simplex algorithm was used to optimise the number, position, and value of the coastal setpoints, such that the overall sum of the absolute errors between estimated and measurement derived values of the K_{cdi} coefficients at each of the stations in the training set was minimised. In total, 18 K_{cdi} coefficients are generated for each location using this technique (Table 5.1).

Table 5.1. Sinusoid coefficient indices.

Variable estimated	Index for mean	Index for amplitude	Index for season shift
c_{davmon}	1	2	3
c_{dsdmon}	4	5	6
K_{cf1}	7	8	9
K_{cf2}	10	11	12
K_{cf3}	13	14	15
K_{cf4}	16	17	18

Synthetic values of the residual variable y_d were obtained by generating pseudorandom values of r with a uniform frequency distribution between 0 and 1 and then transforming backwards:

$$y_d \approx Cf^{-1}(r) \tag{5.27}$$

Synthetic values of mean daily cloudiness, c_d, were calculated from y_d using:

$$c_d = c_{davmon} + c_{dcsdmon}\, y_d \tag{5.28}$$

5.2.4 Generation of hourly cloudiness

The measured hourly cloudiness values from every station were lumped together and categorised according to the sine of the solar altitude angle $\sin\alpha$ and the average daily cloudiness c_d. This assumes that for a given c_d, the statistical characteristics of cloudiness are the same for any location in Western Australia. The following function was used to estimate the average hourly cloudiness, c_{hm}, as a function of $\sin\alpha$ and c_d:

$$c_{hm}(c_d, \sin\alpha) = c_d\left(1 + K_{h0}\frac{(1-c_d)}{\left(1+K_{h1}c_d^2\right)}\left(\sin\alpha + K_{h2}\sin^2\alpha + K_{h3}\sin^3\alpha\right)\right) \tag{5.29}$$

The coefficients K_{h0} to K_{h3} were determined from the training data. Each measured cloudiness value was placed into one of 200 bins arranged in a 2 dimensional grid according to variations in steps of 0.05 for average daily cloudiness c_d and 0.1 for the sine of the solar altitude angle $\sin\alpha$. The mean cloudiness for each bin was calculated. The values of K_{h0} to K_{h3} were optimised using a downhill simplex algorithm to minimise the sum of the absolute differences between the mean of the measured hourly cloudiness values in each bin and c_{hm}. See Table A.2 in Appendix A for their values. With this function, when c_d is zero (a clear sky day), then c_{hm} is zero regardless of the value of $\sin\alpha$ or K_{h0} to K_{h3}. Similarly, if c_d is 1, then c_{hm} is 1.

For each bin, the standard deviation of the measured cloudiness values from the mean hourly cloudiness in each bin was calculated and the following function was used to estimate the standard deviation:

$$\sigma\left(c_d, \sin\alpha\right) = c_d\left(1-c_d\right)\left(\frac{K_{dv0}}{\left(1+K_{dv1}c_d\right)} + \frac{K_{dv2}}{\left(1+K_{dv3}c_d\right)}\sin\alpha + \frac{K_{dv4}}{\left(1+K_{dv5}c_d\right)}\sin^2\alpha\right) \tag{5.30}$$

The coefficients K_{dv0} to K_{dv5} were determined by using a downhill simplex algorithm to minimise the sum of the absolute differences between the measured standard deviations in each bin and $\sigma(c_d,\sin\alpha)$. See Table A.2 in Appendix A for their values. With this function, when c_d is zero (a clear sky day), then σ is zero regardless of the value of $\sin\alpha$ or K_{dv0} to K_{dv5}. Similarly, if c_d is 1, then σ is zero.

The hourly cloudiness residual function, y_h, was calculated for every measured hourly cloudiness value using:

$$y_h = \frac{c - c_{hm}\left(c_d, \sin\alpha\right)}{\sigma\left(c_d, \sin\alpha\right)} \tag{5.31}$$

It was found that a translated Weibull distribution gave a better fit to the frequency distribution curve for y_h than a normal frequency distribution (Figure 5.4), although a zero significance value for the Kuiper statistical test (Press et al. 1992) indicated that the distribution of y_h could not be considered to be identical to the Weibull distribution. Therefore a translated Weibull cumulative frequency distribution function was used to generate synthetic values of y_h from the output of a pseudorandom number generator:

$$r_w = \theta_w + \lambda_w\left(-\ln\left(1-r\right)\right)^{\left(\frac{1}{\kappa_w}\right)} \tag{5.32}$$

where r is a psuedorandom number between 0 and 1 with a uniform frequency distribution. r_w has a Weibull frequency distribution with mean of 0 and standard deviation of 1. θ_w is the translation parameter, λ_w is the scale parameter, and κ_w is the shape parameter. See Table A.2 in Appendix A for the values of these coefficients.

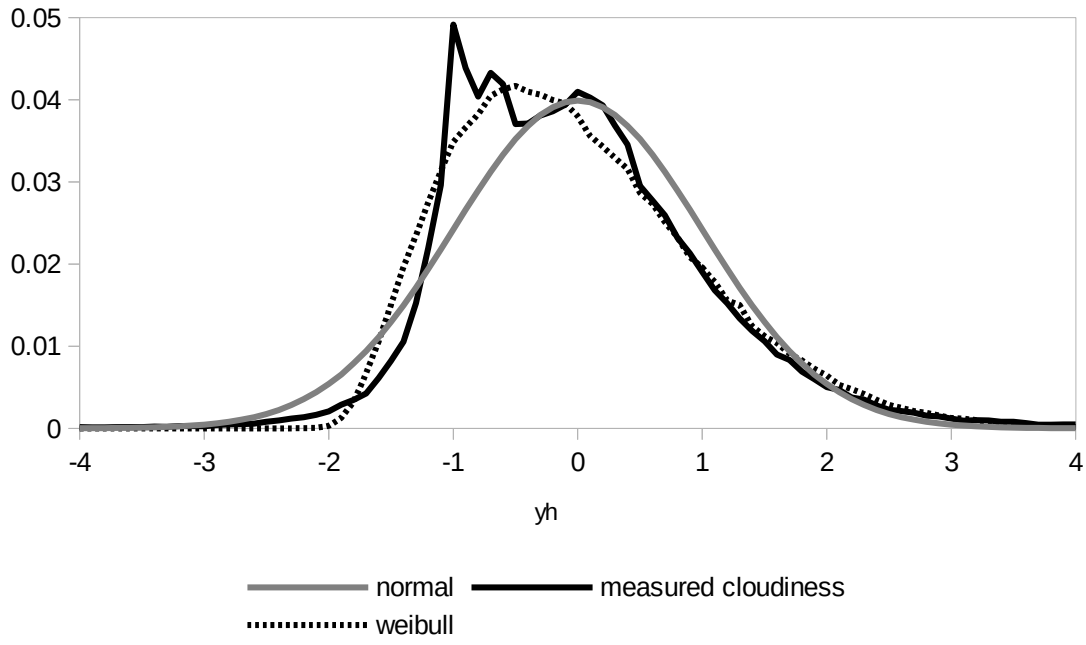

Figure 5.4. Normalised frequency distribution of measured hourly cloudiness residual y_h, compared to a normal distribution and a translated Weibull distribution.

Although time series analysis of hourly cloudiness values is limited by the short continuous sequences available during daylight hours, calculation of partial autocorrelation coefficients of the residual y_h showed a clear dependence on the cloudiness for the previous hour. Therefore, at each station and for each day, the relative first order autocorrelation between successive y_h values was calculated. These values were placed into 1 of 10 bins according to daily average cloudiness, such that each bin has an average cloudiness range of 0.1.

The following function was used to estimate the average first order autocorrelation:

$$\varphi(c_d) = K_{yac}\left(1 - 8\left(c_d - 0.5\right)^3\right) \tag{5.33}$$

where K_{yac} is the autocorrelation coefficient. K_{yac} was determined by minimising the sum of the absolute errors between the measured average autocorrelation values in each bin and $\phi(c_d)$. See Table A.2 in Appendix A for the value of K_{yac}. Synthetic hourly cloudiness values were generated with a first order regression component and a random component using the following three equations:

$$\sigma_d = \sqrt{\left(1 - \varphi(c_d)^2\right)} \tag{5.34}$$

$$y_h = \varphi(c_d)\, y_{h-1} + \sigma_d r_w \tag{5.35}$$

and

$$c = c_{hm}\left(c_d, \sin\alpha\right) + \sigma\left(c_d, \sin\alpha\right) y_h \tag{5.36}$$

where σ_d is the standard deviation of the random component, and c is the synthetic hourly cloudiness at hour h. For comparison with other models, synthetic values of horizontal irradiance I_h were calculated from the cloudiness using:

$$t_{gh} = \left(1 - c\right) t_{bcs} + k_{cloud}\left(c\right) t_{dcs} \tag{5.37}$$

$$I_{hex} = 1367\, OF\, \sin\alpha \tag{5.38}$$

and

$$I_h = t_{gh} I_{hex} \tag{5.39}$$

See Appendix A for the complete implementation of the algorithm. The values of the coefficients in Appendix A were calculated using all of the measured data as training data.

5.3 Results and discussion

In order to assess the performance of the model, model generated synthetic data and data derived from measurements were compared, and the overall differences quantified in a statistical manner. To capture seasonal and diurnal, as well as hourly, effects, the model was assessed on monthly, daily, and hourly time scales. These results were compared with other models that estimate solar radiation over a region or several locations (see below). The following statistical measures were used for comparison, depending on the study: Root Mean Square Error (RMSE), Mean Bias Error (MBE), Mean Absolute Percentage Error (MAPE), Standard Error (SE), and Mean Relative Variance (MRV). Definitions are given in appendix C. These measures were calculated for each station and then the average taken over all stations in the test data set. Because the results for the other studies were derived in different ways, two configurations of training and test data sets were assessed here (see Section 5.2.3). To avoid an artificially better ranking due to data set configuration, the results with the highest error were used for comparison.

5.3.1 Monthly average daily horizontal radiation

For each day of validation data, the daily average horizontal radiation, for both measured and synthetically generated data sets, was obtained from the hourly

horizontal radiation measurements. These daily values were in turn averaged over each month. The average RMSE between the measured and synthetic monthly values was 9.9% and the average magnitude of the MBE was 3.9%. The average error according to three measures was within the upper end of the range of several other models (Table 5.2).

Synthetically generated values of monthly average daily radiation were also compared with satellite derived monthly averaged data (BOM 2012) for 392 locations in the South West of Western Australia, compiled over the period 1990 to 2011. The RMSE was 19.2% (3.9 MJ/m^2/day), and the MBE was -3.7% (-0.75 MJ/m^2/day), indicating that the model generated radiation is conservative.

Table 5.2. Model comparison of monthly average daily horizontal radiation errors.

Study	Model type	Region modelled	MAPE (%)	RMSE (%)	SE (MJ/m^2/month)
Mohandes (2000)	Neural net	Saudi Arabia	10.1		
This model	Autoregressive	Southern Western Australia	8.3	9.7	55.15
Coops et al. (2000)	Meteorological	Locations in US, Glasgow, Canberra			54.75
Hutchinson et al. (1984)	Angstrom, Meteorological	Australia		5.35	
Sozen et al. (2005)	Neural net	Turkey	5.7		
Reddy and Ranjan (2003)	Neural net	India	3.0		
Mellit et al. (2005)	Neural net	Algeria	1.2		

5.3.2 Daily average horizontal radiation

For the daily horizontal radiation values obtained in Section 5.3.1 above, the average RMSE of the model developed here was 33.7% and the average magnitude of the MBE was 3.9%. In a straightforward comparison of daily horizontal radiation values, this model has a higher error than several other models (Table 5.3). However, it must be remembered that these other models

use measured daily meteorological information, so their errors are expected to be less.

Table 5.3. Comparison of daily horizontal radiation.

Study	Model type	Region modelled	RMSE ($MJ/m^2/day$)	Magnitude of MBE ($MJ/m^2/day$)
This model	Autoregressive	Southern Western Australia	6.3	0.68
Liu et al. (2009)	Meteorological	China	3.95	0.04
Fortin et al. (2008)	Meteorological and Neural net	Eastern Canada	3.74 – 5.45	
Liu and Scott (2001)	Meteorological	Australia	2.89 – 3.24	
Lyons and Edwards (1982)	Meteorological, measured 3 layer cloud amount	Western Australia	2.16 – 3.28	

5.3.3 Hourly irradiance

The average RMSE for hourly horizontal irradiance for each day of validation data was 43.1% and the average magnitude of the MBE was 3.9%. An example of the model generated hourly horizontal irradiance data is given in Figure 5.5. The models developed by Yang and Koike (2002) and Yang et al. (2006) use measured hourly meteorological data to derive a Sky Clearness Indicator coefficient (SCI) which is a measure of cloudiness. The SCI is used to estimate horizontal irradiance. To allow for more direct comparison with the Yang models, synthetic hourly cloudiness values were generated by the model developed here using measured daily average cloudiness (that is, the average calculated from the measured hourly cloudiness values), not the model generated daily average cloudiness. This will remove the errors present on diurnal and monthly time scales. Horizontal irradiance values were calculated from these hourly cloudiness values. The average RMSE and MBE magnitudes across all test data stations were 112.8 W/m^2 and 6.7 W/m^2 respectively. The

RMSE is still higher than the results obtained by Yang and Koike (2002) and Yang et al. (2006), which is expected as these models use hourly measured meteorological data (Table 5.4).

Reikard (2009) compared 6 models designed to forecast the hourly horizontal irradiance at sites in the USA at time periods from 1 to 4 hours ahead of the measured value. Some of the measured data were actually modelled data derived from measured meteorological variables, including cloud cover. Hence the results are also included here. The average Reikard model MAPE ranged from 35.18% for the most accurate model to 51.64% for the reference model. In contrast, this model achieved a lower MAPE of 29.1%, which is surprising given that only the measured average daily cloudiness was used, not measured previous hourly values. This result supports the validity of using an autoregressive approach to modelling hourly cloudiness using the value of average daily cloudiness.

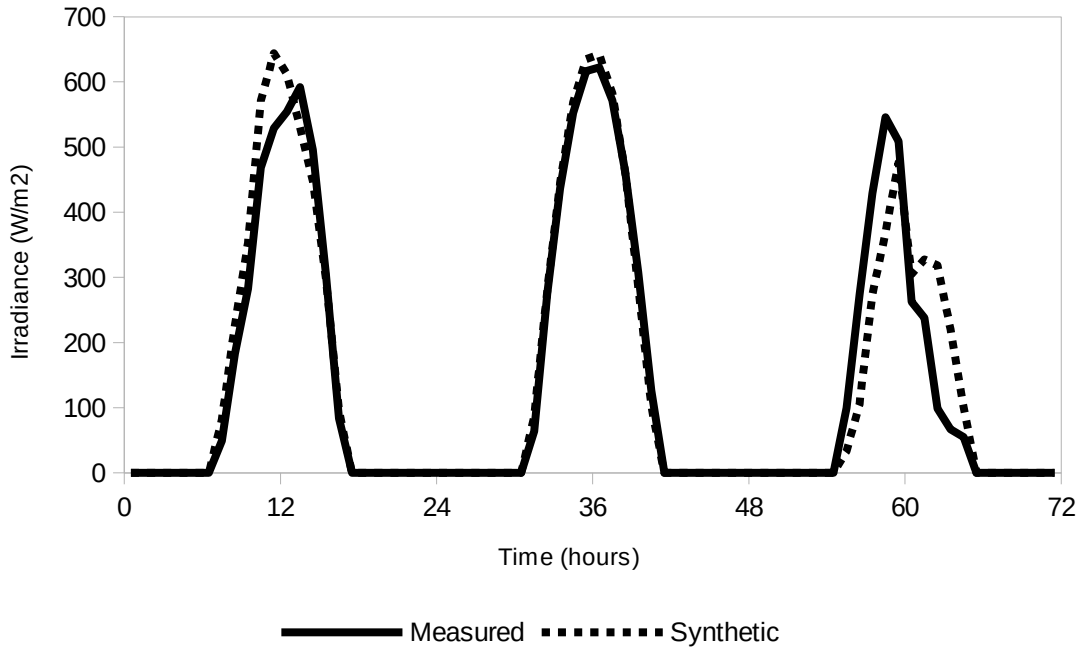

Figure 5.5. Sample measured and synthetic hourly horizontal irradiance for a 3 day period, starting at midnight on the first day.

Table 5.4. Hourly horizontal irradiance comparison of models that use a cloudiness coefficient.

Study	Model type(s)	Region modelled	MAPE %	RMSE (W/m^2)	MBE magnitude (W/m^2)
Reikard (2009)	Regression, ARIMA, Meteorological, Neural net	USA	35.18 – 51.64		
This model	Autoregressive	South West Western Australia	29.1	112.8	6.7
Yang and Koike (2002)	Meteorological	Japan and Islands		96	11
Yang et al. (2006)	Meteorological	USA and Saudi Arabia		52	14.2

Results for the model developed in this chapter were obtained using daily average of measured hourly irradiance.

The model developed in this chapter has errors that are within the middle of the range of several other models that do not use a measure of cloudiness (Table 5.5). Kambezidis et al. (1998) reported a high RMSE, but a very low MBE for the model they developed. Hence their model may warrant further development for use in the estimation of mean hourly irradiance. Many of the neural net models achieved very low errors. However, the concerns about neural net models expressed by Reikard (2009) of over fitting to noisy data must be kept in mind. The purpose of model building is not to mimic the measured data exactly, but to produce a comprehensive representation of typical measured data behaviour. These results indicate that the model developed in this chapter is at least comparable to other models in this task.

Model generated values for the hourly clearness index k_t (using measured daily average cloudiness) were calculated using equation 5.37. Values of k_t were also generated using the Aguiar and Collares-Pereira (1992) TAG algorithm. The distributions of both these synthetic datasets were compared to measurement

derived values of k_t (Figure 5.6). The RMSE between the synthetic values of the standard deviation of the hourly k_t values, calculated for each day of measurement data, was 0.061 for the TAG algorithm and 0.043 for the model developed here. These two results indicate that the model did not match the distribution of the measurement values precisely, but performed slightly better than the TAG algorithm on the same Western Australian dataset.

Table 5.5. Comparison with other hourly irradiance models.

Study	**Model type**	**Region modelled**	**RMSE (W/m^2)**	**Magnitude MBE(W/m^2)**	**Monthly average hourly irradiance RMSE%**	**Magnitude Monthly average hourly irradiance MBE%**	**Hourly Clearness Index kt MRV**
Kambezidis et al. (1998)	Meteorological, Sunshine duration	Athens, Lisbon	164.4-256.4	1.39-5.56			
Ahmad and Tiwari (2008)	Mean hourly irradiance profile	India			13.94	3.36	
Muneer and Younes (2006)	Meteorological, Sunshine duration	Several locations in Europe, India, Japan and Middle-East	127.7	32.8			
Seo et al. (2008)	Meteorological	Several world locations	120.3	10.5			
This study	Autoregressive	South west Western Australia	112.8	6.7	10.5	7.7	0.6671
Spokas and Forecella (2009)	Meteorological	USA and several world locations	111				
Hontoria et al. (2005)	Neural net	Jaen and Andalucia provinces in Spain					0.1153

Results for the model developed this study are obtained using daily average of measured hourly irradiance.

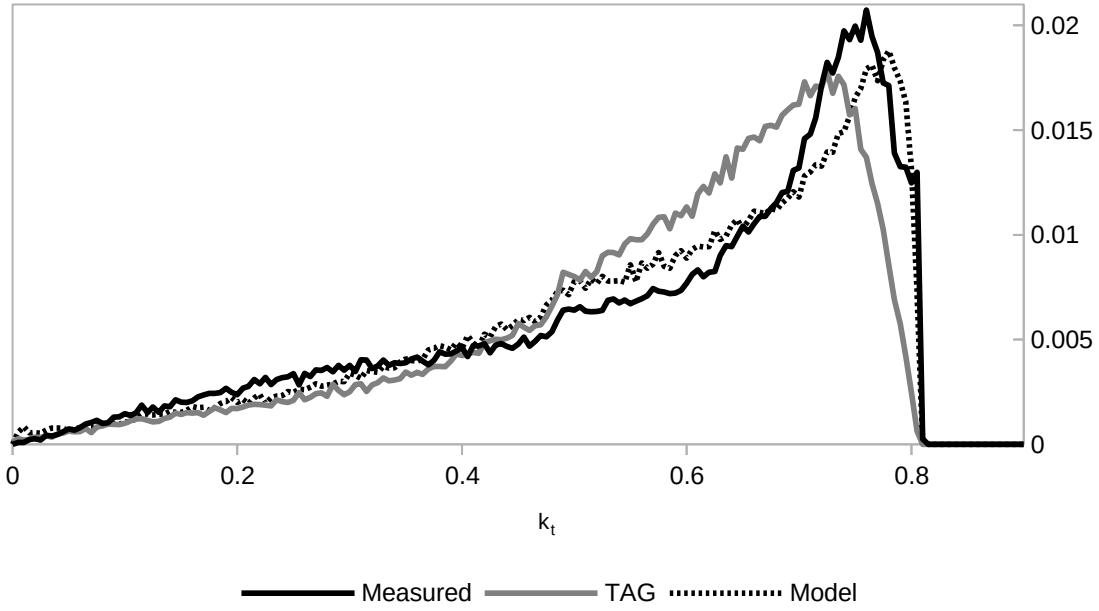

Figure 5.6. Normalised frequency distribution of clearness index k_t from measured horizontal radiation, synthetically generated using the Aguiar and Collares-Pereira TAG algorithm, and derived from model cloudiness values.

5.4 Summary

This model was developed to simulate solar irradiance on an hourly time scale for any location in the South West region of Western Australia. Because values of cloudiness are generated rather than global horizontal irradiance, the beam, diffuse and reflected components of irradiance can be obtained from the clear sky values. Therefore this model can be used in simulations of different kinds of solar power devices and different tilt angles to the horizontal, with direct applicability to both thermal and PV concentrating solar power systems.

The results indicated that the model generated synthetic hourly horizontal radiation data with accuracies within the range of other models developed for wide areas or several locations, and hourly cloudiness data with reasonably similar statistical characteristics to the measured data. However there are likely to be areas where local climatic conditions will produce measurements with

significantly different cloudiness characteristics. Detailed measurement and analysis would be required to obtain better accuracy in these areas. Data from weather stations concentrated in the Southern and Western region of Western Australia have been used to test the simulation, because this area is more significant for the simulation of broad scale power generation due to the proximity of grid infrastructure and major load centres. The representation of more remote regions in Western Australia is likely to be poorer, but would be improved by incorporating measurement data from these regions.

The approach of using alternative position metrics to latitude and longitude to simplify the required calculations resulted in a model that uses 337 coefficients, or 837 including the 500 vertex coastline. This is equivalent to the direct representation of just over 2.2 months of hourly data at one location. As such this approach provides a viable alternative to using satellite data and has scope for adaptation to other parts of the world with a similar pattern of declining inland rainfall, such as the West coast of North America, and the West coast of South Africa. The model coefficients are listed in Appendix A.

6 Solar thermal model with storage

The solar irradiance model developed in chapter 5 provides hourly values of solar irradiance, but this must be translated into output power for each type of solar generating plant. This chapter deals with solar thermal power stations, which have the capability to store energy for generation at a later time, and are also considered to be capable of fast ramping in response to changes in demand or generation from other types of renewable energy power plants. Therefore they may be an important component for any renewable energy generation system for the SWIS.

The solar thermal stations modelled here were based on power tower systems that use dual tracking heliostat mirror fields to focus sunlight onto a central tower receiver. Thus the thermal medium temperature can be higher, allowing efficiency to be greater, or to offset the drop in efficiency from using air cooling instead of water cooling. Unlike PV systems, they can only utilise the direct beam component of solar irradiance. Because diffuse and reflected radiation are coming from many different directions, it cannot be focused on the receiver by the mirrors.

6.1 Method

A generic energy balance model was used to estimate the energy flow through the system. Thermal storage was modelled on a two tank molten salt system. Lower temperature molten salt is stored in the 'cold' tank, before being passed through the central tower receiver where it is heated and then stored in the 'hot' tank. Some of this higher temperature molten salt is passed through a power

block where a steam turbine system uses the heat to generate electricity. This cools the molten salt and it is passed back to the cold tank. The cycle can be repeated as long as there is enough sunlight hitting the receiver to reheat the salt.

Rated power output is maintained for as long as the combination of incoming solar radiation and heat storage allows. If the fraction of molten salt in the hot tank drops below a set operational minimum, then the thermal storage is considered to have been exhausted, and there will be no more electrical power output available from storage until the hot tank is replenished from solar radiation.

For each solar thermal station in a scenario, the following algorithm was used to calculate the power output and energy stored. At a particular hour of the day, the available solar radiation power input, P_{in} (MW), to be converted into heat and then electrical output power was calculated using:

$$P_{\text{in}} = 10^{-6} I_{bn} ca \tag{6.1}$$

where I_{bn} is the beam irradiance falling normal to the collector array (W/m^2), and ca is the collector surface area (m^2). I_{bn} is obtained from the solar radiation model (chapter 5). The required collector area is dependent on the rated power. Firstly, a reference, or 'design point', base collector area, car (m^2), was calculated by assuming that the rated output power, P_{rated} (MW), would be achieved if the sun was at the solar zenith position (directly overhead), and a reference beam normal solar irradiance I_{bnref} (often around 1000 W/m^2) was falling on the whole collector array:

$$car = 10^{6} \frac{P_{rated}}{I_{bnref} e_{st} e_{te}} \tag{6.2}$$

where e_{st} is the design point solar-to-thermal conversion efficiency, and e_{te} is the design point thermal-to-electrical conversion efficiency. e_{te} includes parasitic electrical power required to keep the plant operating. It can be expected that some of the collectors in the array are off line at any one time for troubleshooting or routine maintenance. In the simulation, this is assumed to be a constant percentage of the total collector area. The online fraction *olf* can be defined as:

$$olf = 1 - \frac{capcdown}{100} \tag{6.3}$$

where *capcdown* is the average percentage of the collector array that is off line at any one time. If the solar thermal station has no storage, then the collector area required to deliver the rated power to the load at the reference beam solar irradiance was calculated as:

$$can = \frac{car}{olf} \tag{6.4}$$

where *can* is the no-storage collector area (m^2). For solar thermal stations with thermal storage, the collectors must provide for the energy to be stored as well as that immediately transformed into electricity, thus the collector surface area will be greater and is dependent on the rated design storage time, t_s (hours). For the storage medium, the maximum energy stored per unit volume E_{sv} (J/m^3) over the rated storage time t_s hours was calculated using:

$$E_{sv} = C_v\left(temp_{hot} - temp_{cold}\right)\left(1 - 0.01 r_{leak}\, t_s\right) \tag{6.5}$$

where C_v is the storage medium volumetric heat capacity ($J\ m^{-3}°C^{-1}$), $temp_{hot}$ is the operating temperature of the storage medium (°C) after heating, $temp_{cold}$(°C)

is the operating temperature of the storage medium after cooling to produce electricity, and r_{leak} is a heat leakage loss term (% per h). The storage energy E_{ts} (J) required to maintain the rated output power over the rated design storage time was calculated using:

$$E_{ts} = 3.6\,x\,10^{9} P_{rated} \frac{t_s}{e_{te}} \tag{6.6}$$

Therefore the effective required storage medium volume *svi* (m^3) can be calculated as the ratio of E_{ts} and E_{sv}:

$$svi = \frac{3.6\,x\,10^{9} P_{rated}\, t_s}{e_{te} C_v (temp_{hot} - temp_{cold})(1 - 0.01\, r_{leak}\, t_s)} \tag{6.7}$$

The final storage volume *sv* (m^3) was calculated assuming *svi* must be overrated to compensate for troubleshooting and maintenance downtime:

$$sv = \frac{svi}{olf} \tag{6.8}$$

Since not all of the storage medium will always be at the heated temperature $temp_{hot}$, the leakage loss rate will be less than $loss_{max}$. Hence the storage medium volume has also been overrated to compensate for any foreseeable thermal losses.

The total required collector area for operation and storage was calculated using the effective operational storage volume *svi*. To be able to load the storage medium with enough energy to provide the rated power for the rated storage time:

$$10^{6}\, cas\, TDR\, e_{st}\, olf = 3.6\,x\,10^{9} \frac{P_{rated}\, t_s}{e_{te}} + 0.01\, r_{leak}\, t_s C_v (temp_{hot} - temp_{cold})\, svi \tag{6.9}$$

where *cas* is the extra collector area required for storage (m^2), and *TDR* is the total daily radiation ($MJ/m^2/d$), which will depend on the location, season, and the local weather. Combining with equation 6.7 and rearranging gives:

$$cas = \frac{3600 t_s P_{rated}}{TDR\ e_{st} e_{te} olf}\left(1 + \frac{0.01 r_{leak} t_s}{1 - 0.01 r_{leak} t_s}\right) \tag{6.10}$$

The solar multiple, *sm*, can be defined as the ratio of total required collector area to collector area without storage:

$$sm = \frac{can + cas}{can} \tag{6.11}$$

or

$$sm = 1 + \frac{3.6 I_{bnref} t_s}{1000\, TDR}\left\{1 + \frac{0.01 r_{leak} t_s}{1 - 0.01 r_{leak} t_s}\right\} \tag{6.12}$$

At high values of solar multiple, large single unit power towers can run into limitations on tower height, receiver size and heliostat distance from the central receiver (Turchi et al. 2010), hence *sm* was limited to a maximum value of 3.5. The total collector area *ca* (m^2) was calculated using:

$$ca = can \times sm \tag{6.13}$$

The total effective collector area cae (m^2) is:

$$cae = olf \times ca \tag{6.14}$$

Choice of the value of *TDR* depends on how the solar thermal plant will be used. If a lower *TDR* from a typical winter day is chosen, then the solar multiple

will be higher and the plant is more likely to be able to maintain output during the winter months. However the required heliostat field area and construction costs will be greater, and there will more likely be excess irradiance during the summer months, forcing some of the heliostats to move focus away from the receiver. Conversely a higher *TDR* will decrease the solar multiple but increase the likelihood of the plant not being able to heat all of the storage medium on a day of low *TDR*.

The design point solar to storage conversion efficiency e_{st} was divided into two components, the design point heliostat solar field efficiency e_{sr} (or the solar-to-receiver efficiency) and the design point receiver-to-storage efficiency e_{rt}:

$$e_{st} = e_{sr} e_{rt} \tag{6.15}$$

Singer et al. (2010) and Gauche et al. (2012) found that the heliostat solar field efficiency drops off from its design-point value at low solar altitude angles. The solar altitude angle α measures the vertical angular distance between the sun and the horizon. A heuristic equation was developed to approximate this effect (see also Figure 6.1):

$$P_{recin} = P_{\text{in}}\, e_{sr} \left\{ 0.2 + sin\alpha \left(0.2 + \frac{7.8}{1 + 12\, sin\alpha} \right) \right\} \tag{6.16}$$

where P_{recin} is the input power from the solar field to the central receiver (MW).

There is also an efficiency drop when the solar power incident on the central receiver, P_{recin}(MW), is much less than the design-point receiver input power P_{recr} (MW), or more than P_{recr}. A heuristic equation was developed to approximate this effect (see also Figure 6.2):

$$P_{storein} = P_{recin}\, e_{rt} \left\{ 0.775 + 0.45 \frac{\left(P_{recin} / P_{\text{recr}} \right)}{1 + \left(P_{recin} / P_{\text{recr}} \right)^3} \right\} \tag{6.17}$$

where $P_{storein}$ is the power input to the thermal storage medium (MW). The receiver was designed so that P_{recr} is a multiple of the thermal power needed by the power block to generate P_{rated} MW of electrical power:

$$P_{recr} = \frac{P_{rated}\, sm}{e_{te}} \tag{6.18}$$

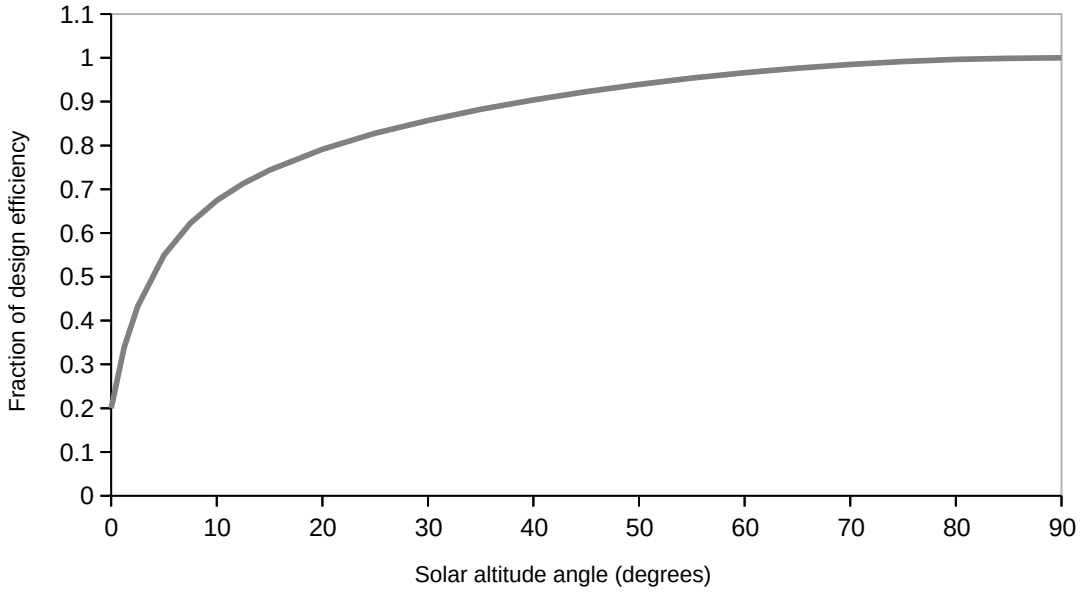

Figure 6.1. Approximation of solar to receiver efficiency drop off with low solar altitude angle.

If there is thermal storage, *sm* should be greater than 1 so that the receiver has enough capacity to transfer energy to the storage medium as well as the power block. The model also assumed that P_{recin} did not exceed a maximum limit P_{recmax}, which is slightly larger than P_{recr}. Some heliostats would be focused away from the receiver if there was excess solar power input.

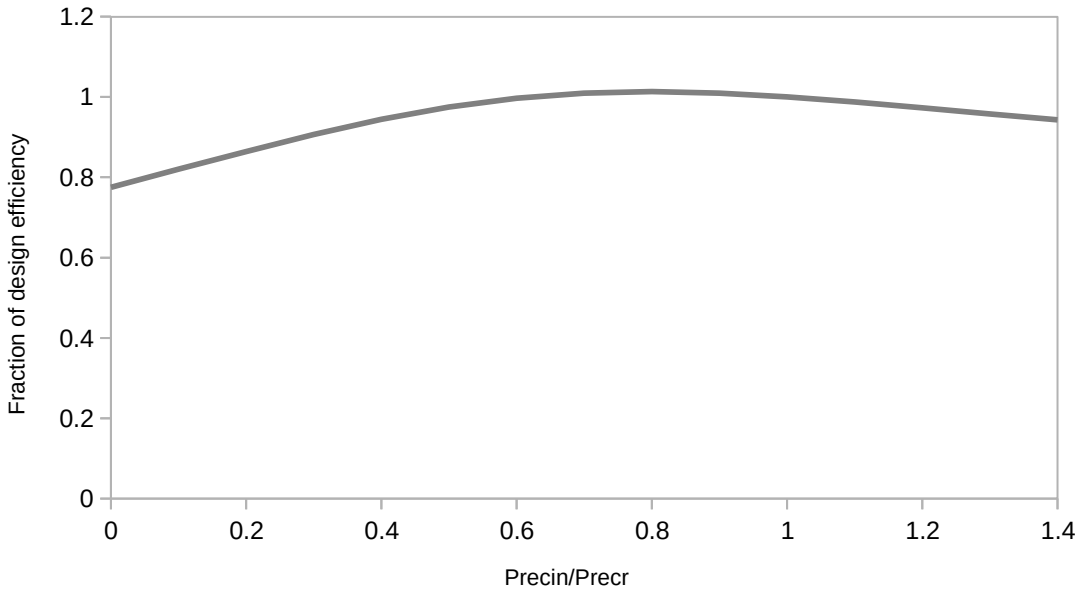

Figure 6.2. Receiver to storage efficiency drop off with low receiver input power.

Let P_{req} be the power output requested by the grid (MW). P_{req} can range from zero to P_{rated}. Let P_{out} be the actual power output of the power plant (MW). P_{out} can range from zero to P_{req}. The design point storage-to-electrical efficiency was divided into design point storage to thermal efficiency e_{tpb}, power block thermal-to-electrical efficiency e_{pb} and parasitic losses:

$$e_{te} = e_{tpb} e_{pb} \left(1 - 0.01 r_{parasitic}\right) \tag{6.19}$$

where $r_{parasitic}$ is the plant electrical parasitic loss factor (%). Wagner and Zhu (2011) approximated power block efficiency decreases under partial load conditions (Figure 6.3) with:

$$P_{out} = e_{te} P_{storeout} \left(0.5628 + 0.8685 f_{out} - 0.5164 f_{out}^2 + 0.0844 f_{out}^3\right) \tag{6.20}$$

where $P_{storeout}$ is the power output from the thermal storage medium (MW) and $f_{out} = P_{out}/P_{rated}$.

If $P_{storein} > P_{storeout}$, then energy is transferred to storage. Conversely, if $P_{storein} < P_{storeout}$, then energy is transferred from storage. As long as there is enough energy stored in the heated thermal storage medium, output power P_{out} is P_{req}. The change in heated fraction of the storage medium, Δf_{hot}, for one time step of the simulation was estimated using:

$$\Delta f_{hot} = \frac{3.6 x 10^9 t_{step}(P_{storein} - P_{storeout})}{C_v \, svi(temp_{hot} - temp_{cold})} - 0.01 r_{leak} t_{step} \quad (6.21)$$

where t_{step} is the time step (h). If f_{hot} reaches 1, then it was assumed that the power plant control system would allow no further increase by defocusing some or all of the heliostat collectors. If f_{hot} falls below a threshold $f_{hot,shutdown}$, the power plant goes to stand by, then shuts down if there is no more incident solar power from the heliostats hitting the receiver. Output from the power plant is reduced to zero. If this occurs during night time, then I_{bn} will remain at zero until the next dawn and the power station will produce no power until then.

For the power station to restart, first the heliostats must focus, then the receiver must restart, and then the power block must restart. The heliostats were set to focus on the receiver after dawn when the solar altitude angle rose above the deploy angle α_{deploy}. They were also set to defocus and stow before dusk when the solar altitude angle dropped below α_{deploy}. The receiver was set to restart once incident solar power from the heliostats reached a minimum fraction $f_{rstartup}$ of receiver rated power P_{recr}. The power block was set to restart once the receiver was fully operational. Both receiver and power block start ups were modelled as two stage processes (Tables 6.1 and 6.2). The receiver was shut down if the incident solar power dropped below $f_{rstartup}$, which happens immediately after the heliostats stow, before dusk.

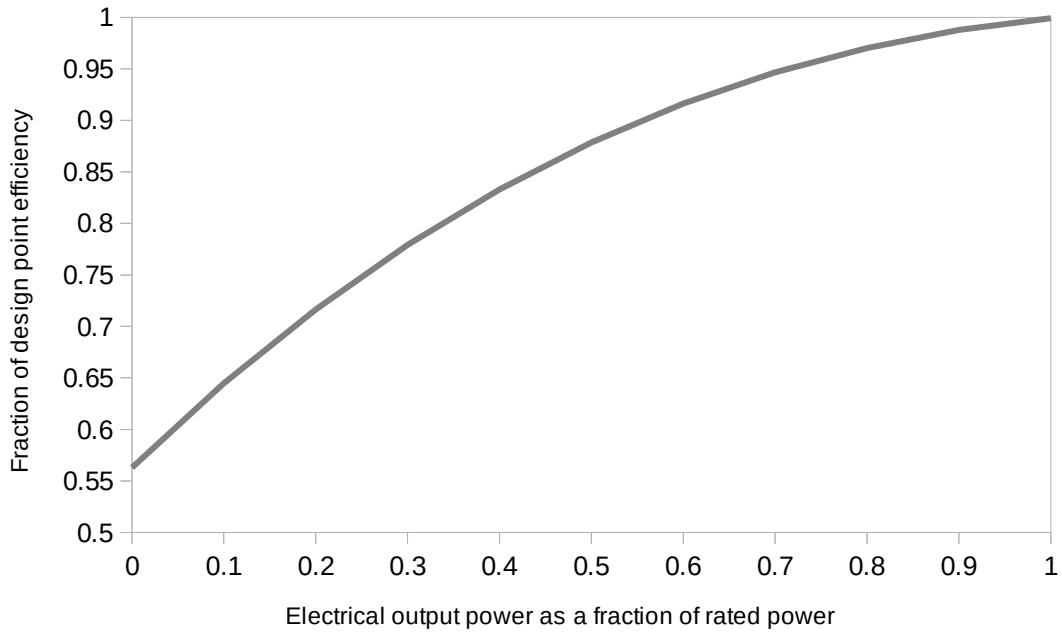

Figure 6.3. Storage to electrical efficiency drop off with low electrical output power.

Table 6.1. Start up stages for the solar thermal power tower receiver.

Stage	Name	Time period (h)	Description
0	Shut down	-	The receiver is shut down. No thermal energy is transferred to storage.
1	Start up	0.2	The receiver is warming up. No thermal energy is transferred to storage.
2	Operating	-	Normal operation. Thermal energy transferred to storage

A maximum ramp rate condition and minimum operational power level was also placed on the output power P_{out}:

$$-maxramp < \frac{P_{out}(t) - P_{out}(t - t_{step})}{60\, t_{step}} < maxramp \tag{6.22}$$

$$P_{out} \geq f_{outmin} P_{rated} \tag{6.23}$$

where *maxramp* is the maximum allowable ramping rate of the electrical output power (MW/min), and f_{outmin} is the minimum operating level as a fraction of rated output power P_{rated}. If the requested power P_{req} is lower than the minimum operating level, then P_{out} can be lowered, but the thermal power required by the power block will remain at the same level as if $P_{out} = f_{outmin}P_{rated}$.

Table 6.2. Stages for the solar thermal power tower power block.

Stage	Name	Time period (h)	Description
0	Shut down	-	Plant generates no electrical power
1	Start up	0.5	Heat transferred from storage to power block. No power generated. After time period is up, go to stage 3
2	Stand by	0.5	Heat transferred from storage medium to power block. No power generated. If more solar power is being transferred to receiver, then go back to stage 3 (operating). Otherwise, after time period is up, go to stage 0 (shut down).
3	Operating	-	Normal operation.

The design-point operating temperature ranges and physical quantities used for the simulation are given in Table 6.3 below.

6.2 Calibration results

There are no currently operating solar thermal power tower plants in the SWWA to compare the model with. Instead the model was calibrated to the power tower model used in the System Advisor Model (SAM) energy simulation system (Wagner 2008). The SAM model is based on the performance of a demonstration solar power tower plant. An example energy storage level comparison over one week between the two models is given in Figure 6.4.

Table 6.3. Solar thermal station operating constants.

Constant	Description	Value
I_{bnref}	Reference beam normal solar irradiance	986 W/m^{2}[a]
TDR	Total daily radiation used to calculate solar multiple	18 MJ/m^{2}/d[b]
e_{sr}	Solar field efficiency at design point	57.5%[c]
e_{rs}	Receiver-to-storage efficiency at design point	92.7%[c]
e_{tpb}	Storage to power block efficiency	99%[c]
e_{pb}	Power block thermal to electrical efficiency at design point	41.2%[c]
$r_{parasitic}$	Electrical parasitic losses	10%[d]
$capcdown$	Average off line percentage of collector array and storage	10%[e]
$temp_{cold}$	Cooled storage medium temperature	290 °C[e]
$temp_{hot}$	Heated storage medium temperature	565 °C[e]
r_{leak}	Thermal storage medium heat leakage rate	0.031% per hour[f]
$f_{hot,shutdown}$	Threshold heated fraction of thermal storage medium for shut down	0.05/storage time in hours[c]
C_v	Volumetric heat capacity	2.785 MJ/m^{3}/°C[g]
f_{outmin}	Minimum operational electrical output as a fraction of P_{rated}	0.25[c]
α_{deploy}	Solar altitude angle at which heliostats deploy and stow	8°[c]
$f_{rstartup}$	Minimum receiver incident power as a fraction of receiver rated power	0.25[c]
$maxramp$	Maximum ramp rate	6% of rated capacity/min[h]

[a]Spencer (1976). [b]Gives solar capacity factor ~0.21. [c]Calibration with System Advisor Model (Wagner 2008).[d]Avila et al. (2013). [e]Singer et al. (2010). [f]Madaeni et al. (2012). [g]Bayon and Rojas (2013). [h]Denholm et al. (2013).

The solar field efficiency e_{sr} Root Mean Square Error (RMSE) between SAM and the model developed here was less than 4% over one year of simulation. The power output RMSE compared to SAM was less than 25%, and the stored energy RMSE was less than 10%. The overall solar to electric efficiency for a power tower with 15 hours storage was around 14.5%, slightly below the value of 15.8% predicted by Tyner and Wasyluk (2013) for a power tower with 13

hours of storage, but close to the value of 14.6% modelled by Hinckley et al. (2011) for a power tower with 6 hours of storage using SAM. It can be expected that efficiency will rise with increasing storage capacity, as more of the solar energy input can be captured and less is lost. Therefore these results indicated that the solar thermal model used in this thesis generates realistic but slightly conservative operational performance.

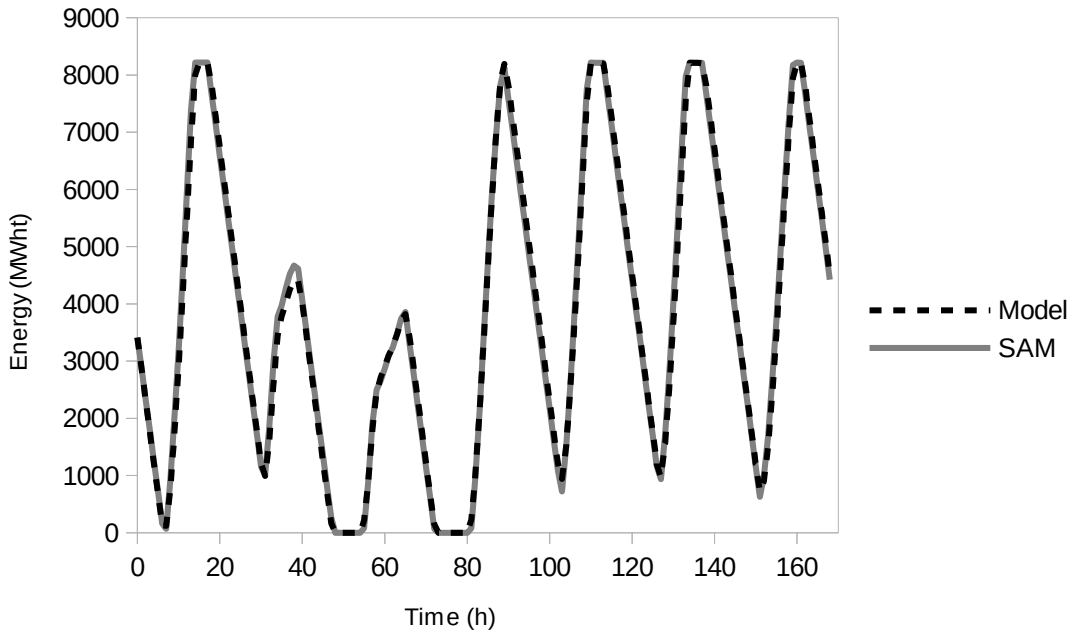

Figure 6.4. Stored thermal energy over one week for 200 MW solar power tower with 15 hours storage. Comparison between solar thermal model and System Advisor Model (SAM).

7 Wind power model

This chapter will detail the development of a regional wind power model for the SWWA. This model is needed to simulate power generation from existing wind farms connected to the SWIS and future hypothetical wind farms. First of all some background information about winds in the SWWA and the statistical modelling of wind power will be presented. Then the model development methodology and results will be detailed in the following sections. This chapter is based on the journal article "A Simple Hourly Wind Power Simulation for the South-West Region of Western Australia Using MERRA Data." (Laslett et al. 2016).

7.1 Background

The SWWA is characterised by a Mediterranean climate (Tan 2004), which is dominated by the eastward passage of high pressure sub tropical anti cyclonic cells. Mainly in winter, low pressure systems from the south cross the state every seven to ten days. Hence there are distinct differences in the seasonal wind speed variation at different places within the SWWA. Frequently, there is a strong diurnal sea/land breeze along the coastline (Pattiaratchi et al. 1997), more often in the summer months. This sea breeze can also penetrate as far inland as Kalgoorlie (Clarke 1989), which is about 350km from the nearest coast.

The wind speed at any site can be represented as the sum of several components operating at different temporal scales: seasonal, daily, diurnal, dependent and random. The seasonal component arises from the cyclical variation in the prevailing atmospheric systems as the earth orbits the sun. The

daily component arises from the passage of weather systems across a region with typical durations from 2 to 8 days (Burton et al. 2001). The diurnal component arises from the sea/land breeze system caused by temperature differences between the land and ocean. The dependent component arises because atmospheric phenomena can be persistent, resulting in a relationship between the wind speed at a particular time to the wind speed at previous times. Finally, most physical processes contain a random fluctuation component and wind speed is no different.

For a model to adequately represent the wind power generation potential at any one place in the SWWA, it is necessary to capture the variability at each temporal scale (Suomalainen et al. 2012). It will also be necessary to capture the spatial differences in these variabilities across the whole region of the SWWA. There have been several simple models that generate synthetic time series values of wind speed at one or more sites (eg. Billinton et al. (1996) and Karki et al. (2006)). These models attempt to mimic the observed statistical nature of the wind speed. There are also detailed models of wind speed at multiple sites or across a region that use meteorological physics, and tend to require much more computing power (Hill et al. 2012). This study will focus on the development of a statistical model designed to operate across the SWWA region.

The two parameter Weibull distribution has been the most widely used simple statistical representation of overall wind speed behaviour (Hill et al. 2012). The probability density function for this distribution is given by:

$$f(v)=\left(\frac{k}{\lambda}\right)\left(\frac{v}{\lambda}\right)^{k-1} e^{-\left(\frac{v}{\lambda}\right)^{k}} \quad v\geq 0 \tag{7.1}$$

$$f(v)=0 \qquad v<0$$

where v is the wind speed (m/s), *f(v)* is the probability density function, *k* is the shape parameter, and λ is the scale parameter. However, Carta et al. (2009) also reviewed other probability density functions used to represent wind speed frequencies, and concluded that although the Weibull distribution has some advantages over other distributions, it cannot adequately represent many of the wind speed probability density functions that might be encountered in the real world. Gunturu and Schlosser (2012) found that use of the Weibull distribution could lead to both over and under estimations of the wind power resource available.

Autoregressive Moving Average (ARMA) models (Box and Jenkins 1976) have also been widely applied to the statistical representation and prediction of many kinds of time series data (for example Fu (2011) and Soman et al. (2010)) as well as wind speeds. ARMA models are a combination of Autoregressive (AR) models, and Moving Average (MA) models, where the wind-speed value at time *t* is represented as the sum of a linear combination of wind speed values at previous times and the linear combination of a series of random values. Purely autoregressive models use only the random value at the present time:

$$y(t)=\sum_{k=1}^{p} \varphi_k \, y(t-k)+\rho \, r(t) \tag{7.2}$$

where $y(t)$ is the wind speed residual at time mark *t*, $y(t\text{-}k)$ is the wind speed residual at timemark *t-k*, and $r(t)$ is a series of uncorrelated white noise error values which is identically distributed with a normal frequency distribution, zero mean, and standard deviation of one. $y(t)$ is multiplied by the wind speed standard deviation and then added to the mean wind speed to get a wind speed value. φ_k are the AR parameters, and σ is the random noise parameter. The value of ρ is adjusted depending on the value of the AR parameters so that the

standard deviation of y(t) remains at one. The AR order p is the maximum value of k with a non-zero value of φ_k. This is commonly written as an AR(p) model. ARMA models can capture the temporal dependency inherent in wind speed time series, while using a simple Weibull distribution cannot. However, Papaefthymiou and Klockl (2008) asserted that the frequency distribution (equivalent to the probability density function or PDF) of ARMA models rarely match the measured data, which can lead to under or over estimation of wind power.

Wind speed behaviour can also vary over several temporal scales, such as seasonal, daily, diurnal, and hourly. Seasonal variation is commonly modelled using one or more sinusoidal cycles (eg Hill et al. (2012) and Ward and Boland (2007)). Daily average wind speeds vary from the seasonal average and can have a skewed distribution (Klink 2002). Weibull, log-normal, modified normal and modified exponential distributions have been used to represent these distributions (eg Klink (2002), Bogardi and Matyasovszky (1996) and Donatelli et al. (2009)). Carlin and Haslett (1982) proposed the use of a "squared normal" distribution to simply model Weibull-like distributions, based on Western Australian wind data. Daily wind speeds have also been found to have an autoregressive dependency (eg Mohandes et al. (1998), Tol (1997) and Suomalainen et al. (2012)).

A common way of modelling diurnal trends has been to calculate the average measured wind speed at every hour of the day for each month or season (e.g. Hill et al. (2012)). Fixed cyclic functions have also been used (e.g. Donatelli et al. (2009)). However these approaches don't explicitly catch the variation in peak daily wind speed magnitude and time that occurs throughout each month or season. ARMA models and high order AR models have also been developed that model diurnal variation (eg Billinton et al. (1996) and Haslett and Raftery

(1989)). Suomalainen et al. (2012) concluded that these approaches were not sufficiently realistic and developed a model that identified day types defined by the time of day that the peak wind speed occurs, and defining a diurnal pattern for each day type.

After the seasonal, daily, and diurnal components of wind speed have been removed, what is left is the de-trended hourly wind speed. Similarly to the daily wind speed, the value at a particular time has a dependency on the values at previous times, and ARMA models have been commonly used to model this effect.

However, the above form of ARMA equation has been found to be generally suitable for use only if the time series data and the error values are normally distributed. If the data is not normally distributed, then the choice of distribution for the random error values needed to produce the same distribution as the data is not clear (Lawrance and Lewis 1980). For example, Ward and Boland (2007) found that de-trended wind speeds at sites in South Australia had a double exponential distribution (also called a Laplace distribution). But Damsleth and El-Shaarawi (1989) found that even the simplest AR model (of order 1) would not necessarily generate a time series with a double exponential distribution, even if the random variable was given a double-exponential distribution. Lawrance and Lewis (1980) suggested an alternate form of autoregressive equation, but with impractical restrictions on the allowable values of the autoregressive coefficients.

A possible solution is to convert the de-trended wind speed time series values into a normal distribution using a data transformation function. Mach et al. (2006) tested a number of transformations on different types of data. If the data are found to have an exponential distribution, then the authors recommended a

power transformation to convert the data to a normal distribution. Although a double exponential distribution is symmetric about the mean, unlike a standard exponential distribution, this might point the way to a suitable transformation function. If the data are found to have a Weibull-like distribution (such as daily wind speeds), then Mach et al. (2006) recommended the use of a Box-Cox or power law transformation to convert to a normal distribution. Widger (1977) used the square-root normal distribution to model wind speeds, suggesting that taking the square-root of the data (power law 1/2) may effectively convert a Weibull-like distributed wind speed time series into a normal-like distributed series. Carlin and Haslett (1982) used a square-root transformation function on Western Australian wind data, and Brown et al. (1984) used a square-root transformation function on data from the Pacific Northwest region of North America.

For an interactive hourly wind speed simulation, limiting the numerical complexity is important. However the simple Weibull model will be insufficient, as it does not account for persistence at this time scale. An ARMA model or some other model that accounts for persistence must be used. If a site has a significant diurnal component, then this must also be accounted for. This study found wind speed residuals that were not normally distributed. It was shown that using a model with normally distributed residuals led to significantly different, and less representative, statistical behaviour of the resulting wind power time series.

Several wind farms, each using a different wind turbine, are now often present on large scale electrical power grids. Hence once a representative time series of wind speeds at a reference height above ground has been generated, two further steps must be taken: scaling the wind speed to the hub height of a

particular turbine, and then converting the scaled wind speed to an electrical power output.

Horizontal wind speeds at different heights above ground often have different values. This effect is commonly called wind shear. There have been two equations commonly used to characterise the wind shear. The first is the logarithmic relationship:

$$\frac{v_2}{v_1} = \frac{\ln\left(\frac{h_2}{z_o}\right)}{\ln\left(\frac{h_1}{z_o}\right)} \tag{7.3}$$

where v_1 is the wind speed at height h_1, v_2 is the wind speed at height h_2, and z_o is the roughness length. This relationship is based on the physical aspects of atmospheric meteorological behaviour (Kubik et al. 2011). The simpler power law approximation is given by:

$$\frac{v_2}{v_1} \approx \left(\frac{h_2}{h_1}\right)^{\alpha} \tag{7.4}$$

where v_1 is the wind speed at height h_1, v_2 is the wind speed at height h_2, and α is the wind shear exponent, often set to 1/7 (Haslett and Raftery 1989). The logarithmic relationship implies that the wind shear at any one site does not change with time, and is based on the assumption that the atmosphere is in a neutrally stable condition where vertical air movement is neither encouraged or resisted (Gunturu and Schlosser 2012). In wind power studies, this assumption is commonly justified by the idea that when horizontal wind speeds become high enough to start generating power, mixing will ensure the atmosphere becomes neutrally stable (Coppin et al. 2003). Thus inaccuracies due to the atmosphere being in a different state are more likely to occur at low wind

speeds which will have little impact on the prediction of generated power. However, both Smith et al. (2002) and Rareshide et al. (2009) found that this is not always the case, especially in inland areas, and there might be significant diurnal and seasonal variation in wind shear factor at high wind speeds. Smith et al. (2002) found that wind shear was generally higher at night and lower during the day, when it might even be negative.

The specific power per unit area, P (W/m^2), in wind flowing past a wind turbine is a function of air density σ_{air} and the cube of wind-speed v:

$$P=\frac{1}{2}\sigma_{air} v^3 \text{ W/m}^2 \tag{7.5}$$

In practice, there is an upper limit to the fraction of this power that can be harvested, and a common approach to transforming wind speed into power output is to use a wind turbine power curve (Hill et al. 2012), which is a non-linear transformation function (Figure 7.1). In part of the middle region of the curve, power output is proportional to the air density (Gunturu and Schlosser 2012), hence an implicit assumption when using wind power curves is that the air density vertical profile at the turbine operational site is similar to the profile where the turbine was tested.

Holttinen (2005) reported that the wind power factor curve for an individual turbine must be modified if the wind power output from a whole wind farm, constructed using the same turbines, is required. This is probably due to variations in wind speed hitting different turbines within the wind farm. Generally Holttinen (2005) used a gentler full power transition slope and shut down slope with a decreased shut-down wind speed (Figure 7.1).

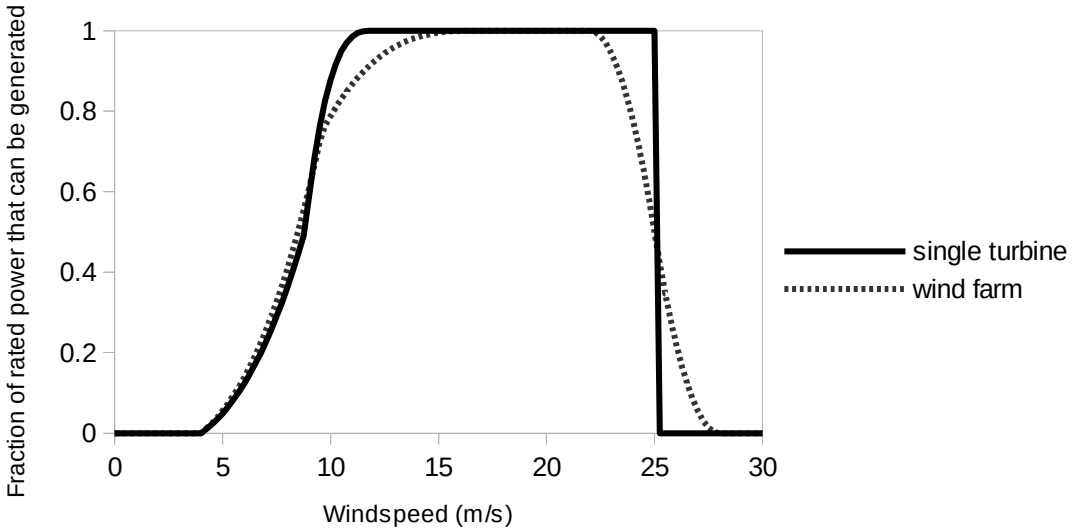

Figure 7.1. Typical wind turbine and wind farm power curve.

Because weather systems and hence wind patterns can extend over a wide area, wind farms sited close to each other are likely to have a significant correlation in wind speed and power output over time, but the correlation will decrease as the distance separating wind farms increases (Sinden 2007). Kavasseri and Nagarajan (2004) speculated that there would be less spatial correlation over shorter time scales because of local differences in topography and atmospheric behaviour, and more correlation over longer time scales due to global and regional weather system seasonal effects. Haslett and Raftery (1989) examined sites in Ireland and found a decaying exponential relationship for the correlation between hourly wind speeds at two sites and the distance between sites, with the exception that sites very close together but not coincident can have a correlation significantly less than one. Carlin and Haslett (1982) reported decreasing wind speed correlation with distance for sites in Western Australia.

A regional SWWA wind power simulation model should take this phenomenon into account. Correia and Ferreira de Jesus (2010) developed a first order vector AR model with user specified spatial correlation between several sites, and

Gibescu et al. (2006) used a decaying exponential relationship to model the spatial correlation between wind speeds at different sites.

7.2 Method

In this study, a model was developed for the purpose of simulating wind power generation for any site in the SWWA. Synthetic wind speeds were generated using square-root transformations of a normal distribution and AR models. Historical 50 metre wind speed data was used to calibrate the simulation at each temporal scale: seasonal, daily, diurnal, and hourly dependent, with a random fluctuation component also added. Spatial correlation was introduced by creating distance weighted semi-dependencies in the random numbers used to generate the daily and diurnal components of wind speed.

A spatially and temporally dependent wind shear conversion factor model was developed so that wind speed at different turbine hub-heights could be estimated from these 50m wind speeds. Measured wind data at two sites was used to calibrate the wind shear conversion factor model. Finally, synthetic wind farm power output data was generated from the hub-height wind speed using modified wind turbine power curves. The simulation wind power output was compared to measured Supervisory Control and Data Acquisition (SCADA) wind farm power output data at 6 existing wind farm sites. Grasmere and Albany were considered to be separate, though adjacent, wind farms because different wind turbines are used at each site. The fit of the seasonal averages, and the daily, diurnal and hourly frequency distributions (equivalent to the probability density function or PDF) of the simulation and two other simpler models was compared to the SCADA data, to see which was sufficient to represent the statistical behaviour of the measured wind power output. The

two other models were a Weibull model, and an autoregressive model with normally distributed residuals.

To obtain hourly wind speeds near the hub-heights commonly used in modern wind farms, the Modern Era Retrospective Analysis for Research and Applications (MERRA) database (Rienecker et al. 2011) was accessed. A grid of hourly wind speeds at 50 metres above the surface of South Western Australia was obtained from this database. The grid contains 330 nodes (15 x 22) with a spacing of 2/3° in longitude (approximately 62.5 km), and 1/2° in latitude (approximately 56 km). The South West corner of the grid is at 112° east, 36° south, and the North East corner is at 126° east, 29° south. 106 of these nodes which are over land or close to the coastline were used to develop the simulation, with most concentrated near the coast-line (Figure 7.2).

The wind speeds were divided into 4 components for analysis: seasonal, daily, diurnal, and hourly. For all components, the distance from the coast of the wind farm was an important parameter. In a process similar to Laslett et al. (2014), a shape map of the Western Australian coastline was constructed from the GEODATA COAST 100K 2004 data package published by Geoscience Australia (2004). This data set is based on a 1:100,000 scale map sheet. The shape map consists of a vector map of the coastline and state border in longitude and latitude coordinates. It does not include any of the islands off the coast of Western Australia that are included in the data package. A global simplification algorithm (Visvalingam and Whyatt 1993) was used to simplify the map down to a 500 vertex coastline map.

The yearly average MERRA 50m wind speed varies across the SWWA with an average of 6.7 m/s and standard deviation of 2.6 m/s. Two modes of seasonal variation were recognised in the monthly average MERRA wind speeds (for

examples, see Figure 7.3). The first mode has a maximum during the summer months and a minimum during winter, and is predominant at mid latitudes. The second mode is significant at southern latitudes. Both are attenuated at sites further inland.

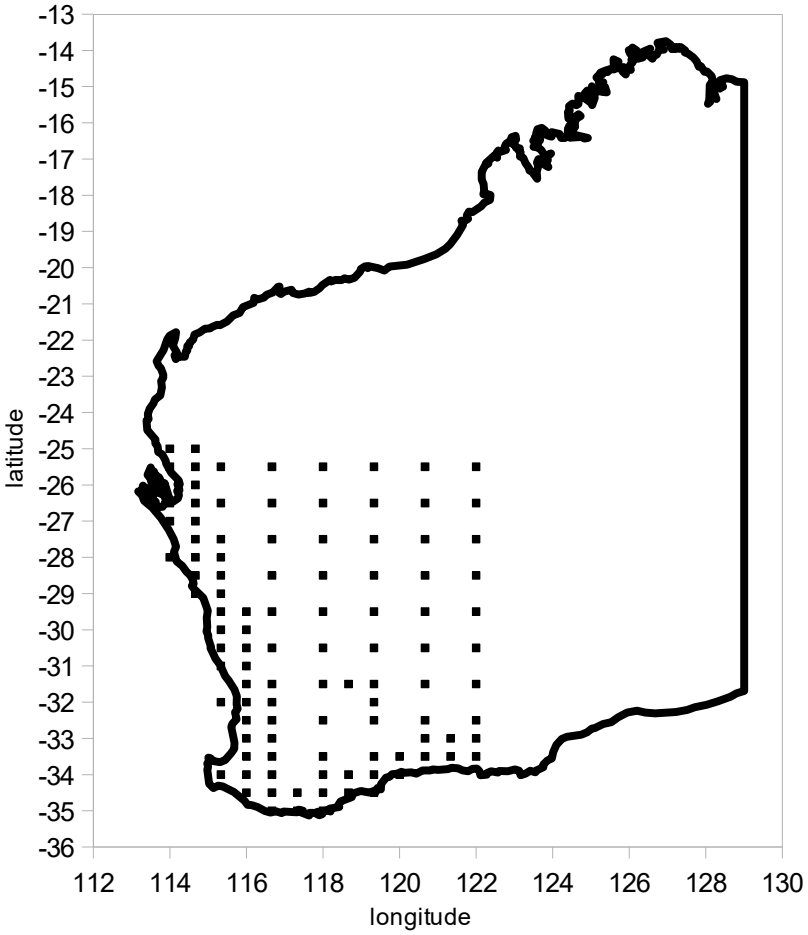

Figure 7.2. MERRA nodes used to simulate wind speed in the South-West region of Western Australia.

To simulate seasonal wind speed at a particular site, the yearly average wind speed V_{yav} was estimated to be the linear distance weighted average of the four yearly average wind speeds from the surrounding MERRA grid square. The seasonal wind speed at any particular day of the year was then calculated from V_{yav} using a weighted combination of each seasonal mode:

$$V_{season} = V_{yav}\left(1 + kslat_1 V_{mode1}(DOY) + kslat_2 V_{mode2}(DOY)\right) \quad (7.6)$$

where DOY is the day of the year, V_{season} is the seasonal wind speed at DOY, $kslat_1$ and $kslat_2$ are the weighting coefficients for each mode, and V_{mode1} and V_{mode2} are the magnitudes of each mode at DOY. $kslat_1$ and $kslat_2$ were found to have a dependency on latitude and distance from the coast. V_{mode1} and V_{mode2} were represented using piecewise linear functions. See Appendix B for the precise parameterisations.

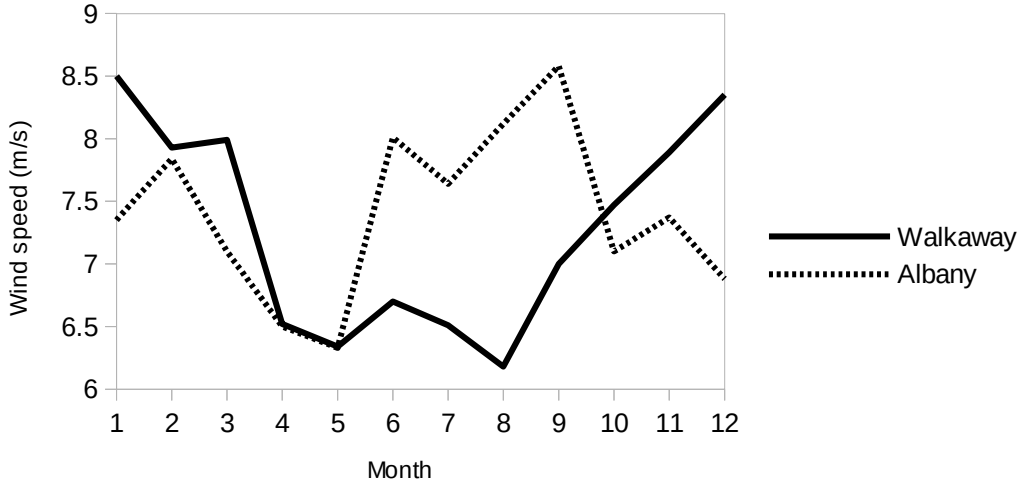

Figure 7.3. Seasonal MERRA wind speeds near Walkaway and Albany wind farms.

The distribution of MERRA daily average 50m wind speeds was found to have a similar shape to a translated Weibull distribution (Figure 7.4). Similarly to Carlin and Haslett (1982), the square-root residual of the MERRA daily average wind speed was found to have a normal-like distribution (Figure 7.5). The square-root residual was obtained by subtracting the mean of the square root wind speeds and then dividing by the standard deviation of the square root wind speeds. The standard deviation σ_d was found to have both a spatial and seasonal dependency. See Appendix B for parameterisations.

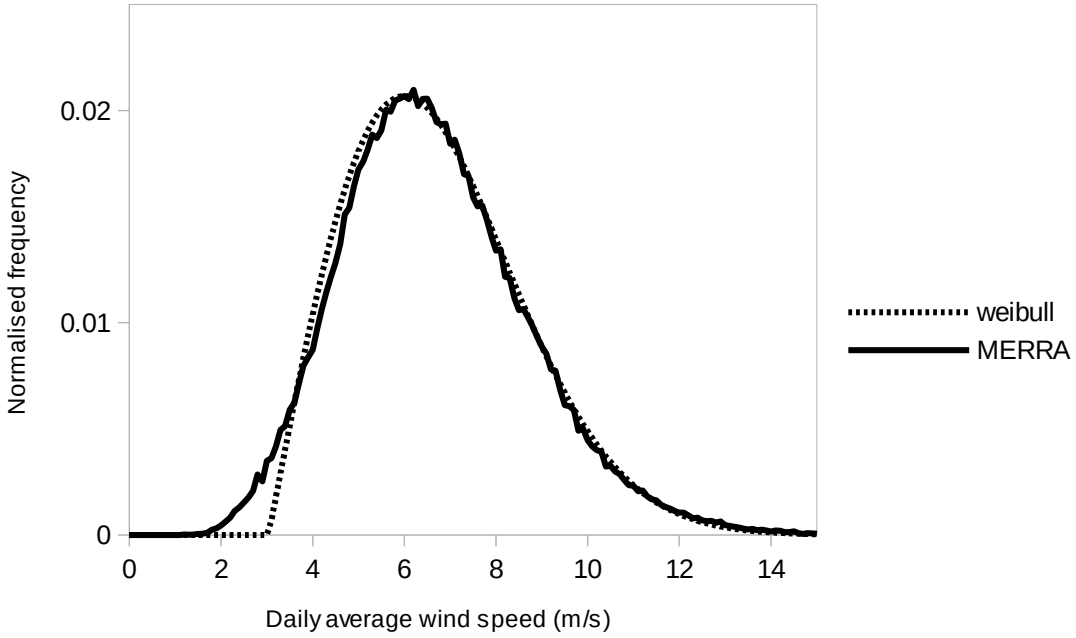

Figure 7.4. Normalised frequency distribution of MERRA daily average 50m wind speed compared to a translated Weibull distribution.

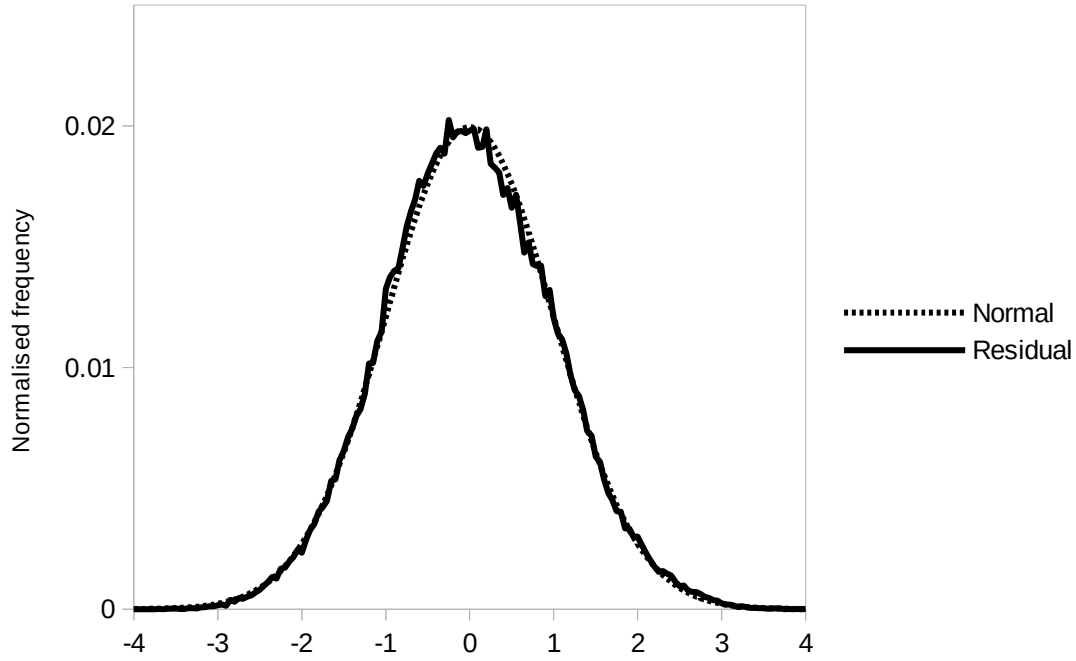

Figure 7.5. Normalised frequency distribution of MERRA daily average 50m wind speed square-root residual compared to normal distribution.

Examination of the auto-regression and partial auto-regression coefficients of the square-root residuals at each MERRA node (for example Figures 7.6 and 7.7) indicated a possible Autoregressive (AR) signature with dependency of order two. The dependency could also possibly be a second order Moving Average MA(2) or combined ARMA(1,1) model. For the residual at each node, the least squares method (Zheng 2003) and numerical maximum likelihood estimation was used to calculate the Root Mean Square Error (RMSE) for ARMA models with coefficients up to order (5,4) (for example Table 7.1). These indicated that the pure AR models gave sightly lower RMSE values. For increasing AR order, the RMSE initially decreased and then substantially levelled off after order 2. To confirm that an AR order of two was necessary and sufficient to capture most of the dependency within the time series, the Bayesian Information Criterion (BIC) (Schwarz 1978) was used in the following form:

$$BIC = n\log_e\left(RMSE^2\right) + \left(p+q+1\right)\log_e n \tag{7.7}$$

where n is the number of data points (1827), p is the AR order and q is the MA order. BIC was calculated and ranked in ascending order for each ARMA(p,q) model, $0 \le p \le 5$ and $0 \le q \le 4$, at each node (for example Table 7.2). The model with the lowest BIC was ARMA(2,0) or AR(2). The value of the AR(2) coefficients were found to be fairly consistent across all of the MERRA nodes, so the average coefficient values were used in the simulation.

To remove the seasonal and daily components, the 24 hour trend was found for each hourly MERRA wind speed value by calculating the average wind speed from 12 hours before to 11 hours after that hour. This trend was then subtracted to obtain a de-trended hourly MERRA wind speed dataset. Similarly to Skidmore and Tatarko (1990), the simulation used a single sinusoid to represent the diurnal wind speed:

$$v_{diurnal} = t_{mag} \cos\left(2\pi \frac{(t - t_{peak})}{t_{period}}\right) \quad t_{peak} - 0.75t_{period} < t < t_{peak} + 0.25t_{period} \tag{7.8}$$

where t is the time of day (hours), t_{peak} is the time of day (hours) when the peak wind speed occurs within the de-trended dataset, t_{period} is timespan between the beginning and the end of the sinusoid (hours), and t_{mag} is the magnitude of the sinusoid (ms^{-1}).

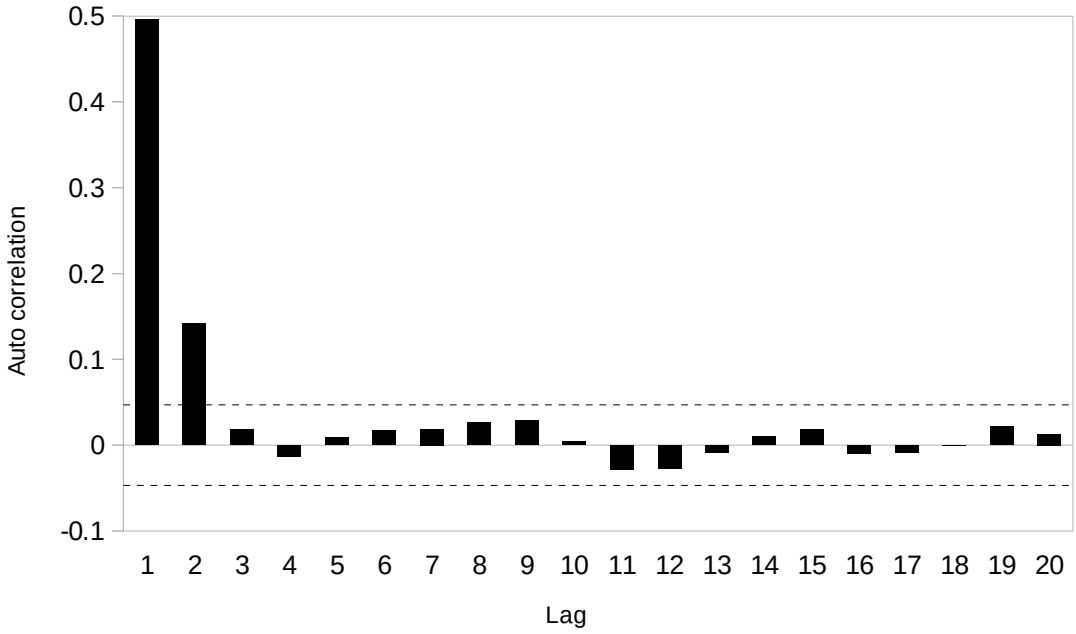

Figure 7.6. Example auto-correlation of the MERRA daily average wind speed square-root residual at a single node. Dashed lines indicate 95% significance levels for a population value of zero.

For each day, the difference between maximum and minimum wind speed values (in the de-trended MERRA dataset), and the hour when these occurred was used to formulate the magnitude, period, and peak hour of the sinusoid for the simulation. The average peak hour was found to occur later as distance from the coast increased (Figure 7.8). This indicated that the peak sea-breeze front travels inland initially at about 33 kmh^{-1} (9.17 ms^{-1}), which is consistent

with the average offshore land-breeze propagation speed of 32.4 ± 14.4 kmh^{-1} (9 ± 4 ms^{-1}) reported by Gille et al. (2005).

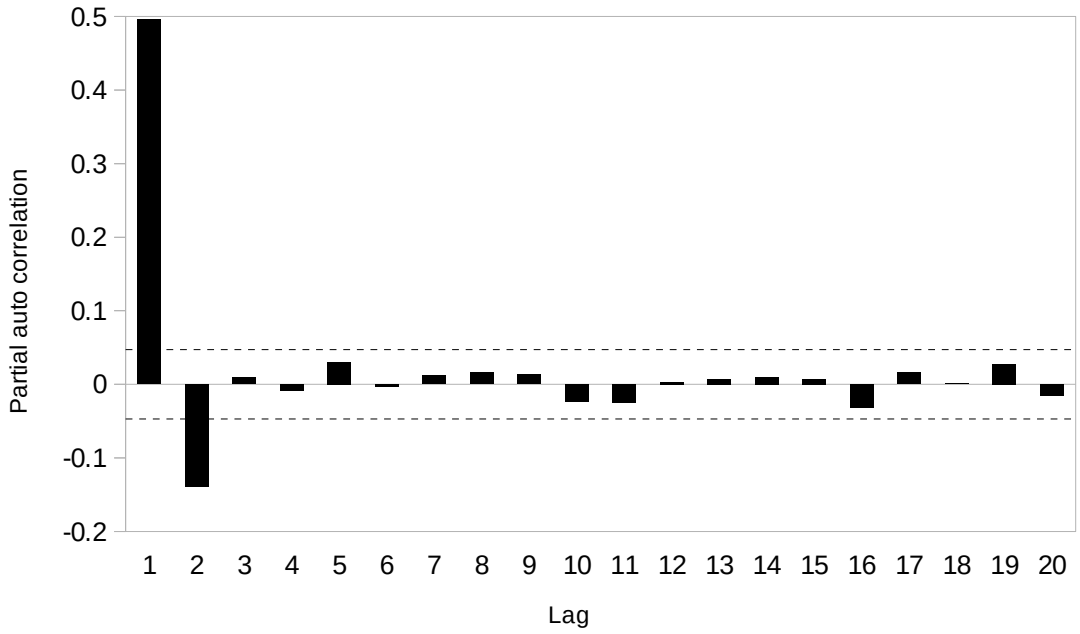

Figure 7.7. Example partial auto-correlation of the MERRA daily average wind speed square-root residual at a single node. Dashed lines indicate 95% significance levels for a population value of zero.

Table 7.1. Example Root Mean Square Error (RMSE) for different orders of Autoregressive Moving Average (ARMA) models of the MERRA daily average wind speed square root residual at a single MERRA node.

	MA order				
AR order	**0**	**1**	**2**	**3**	**4**
0	0.99993	0.87811	0.87811	0.87811	0.87811
1	0.87673	0.86891	0.86887	0.86887	0.86887
2	0.86863	0.86882	0.86870	0.86867	0.86864
3	0.86884	0.86887	0.86885	0.86884	0.86884
4	0.86829	0.86831	0.86830	0.86829	0.86829
5	0.86818	0.86819	0.86819	0.86819	0.86819

The Autoregressive (AR) order increases with each row downward, and the Moving Average (MA) order increases to the right.

Table 7.2. Example Bayesian Information Criterion (BIC) and ranking in ascending order for different orders of Autoregressive Moving Average (ARMA) models of the MERRA daily average wind speed square root residual at a single MERRA node.

	MA order				
AR order	**0**	**1**	**2**	**3**	**4**
0	7.25	-459.93	452.42	-444.91	-437.40
	30	20	24	27	29
1	-465.69	-490.90	-483.59	-476.07	-468.57
	15	2	5	8	14
2	-492.09	-483.78	-476.79	-469.39	-462.01
	1	3	7	12	18
3	-483.69	-476.06	-468.61	-461.17	-453.67
	4	9	13	19	23
4	-478.51	-470.89	-463.46	-455.96	-448.46
	6	11	17	22	26
5	-471.46	-463.90	-456.38	-448.86	-441.35
	10	16	21	25	28

The Autoregressive (AR) order increases with each row downward, and the Moving Average (MA) order increases to the right. The ARMA(2,0), or AR(2), model had the lowest BIC (rank 1).

The sea-breeze magnitude, period, and peak hour variabilities were also found to have a seasonal dependence as well as dependence on distance from the coast-line. The diurnal component was subtracted from the de-trended hourly wind speed to obtain the hourly MERRA wind speed residual y. y was then normalised by subtracting the overall mean and dividing by the overall standard deviation, σ. σ was found to have a spatial dependence. Hill et al. (2012) found the de-trended wind speed distribution for sites in the UK to follow a normal distribution. However in this study the normalised residual y was found to roughly follow a double exponential distribution with a slight skew, rather than a normal distribution (Figure 7.9). Ward and Boland (2007) also found a double exponential distribution for wind data in South Australia.

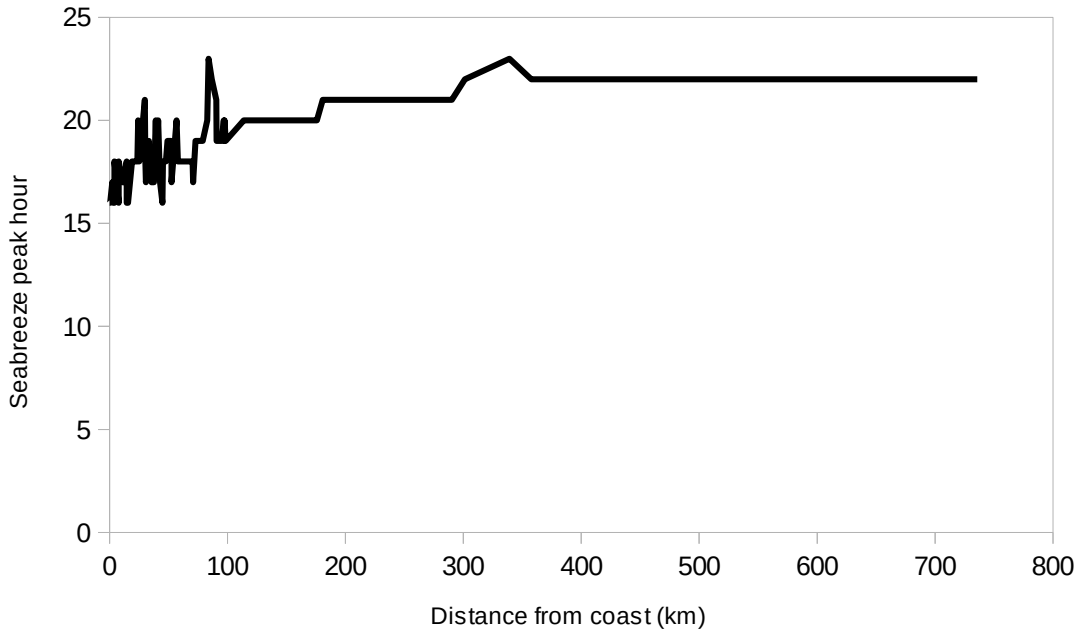

Figure 7.8. Variation in summer sea-breeze peak hour with distance from the coast-line.

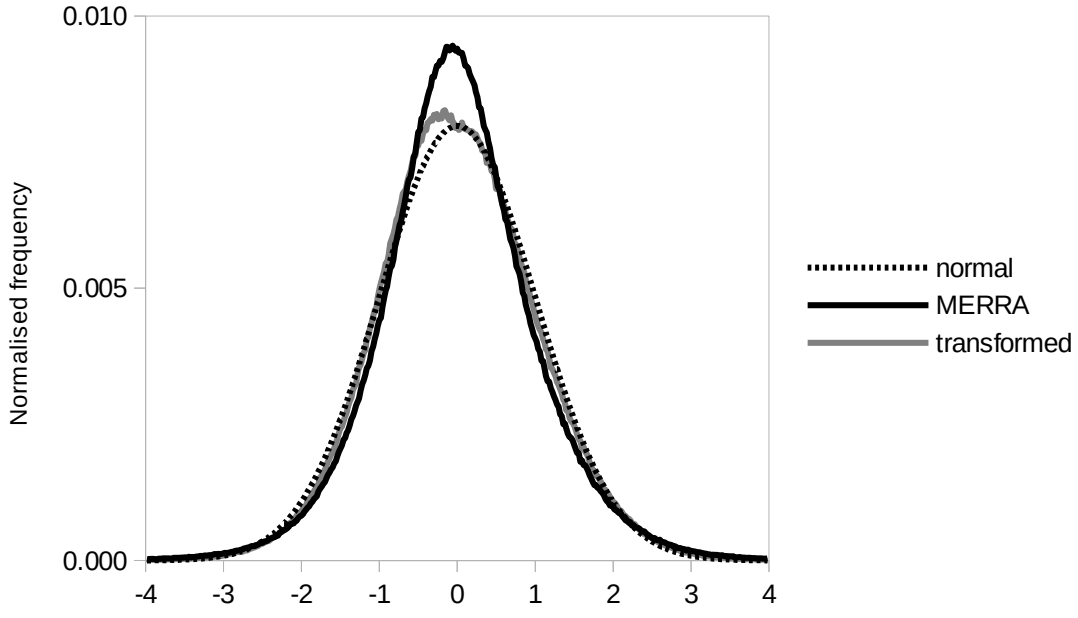

Figure 7.9. Normalised frequency distribution of MERRA 50m wind speed residual and transformed residual compared to normal distribution.

As pointed out by Lawrance and Lewis (1980) and Damsleth and El-Shaarawi (1989), there is a tendency for autoregressive equations to produce time series with normal distributions, even if the distribution of the random term is not normal. Hence a data transformation function was required to convert the distribution of y to a normal-like distribution. Because a double exponential distribution is symmetric about the mean, a simple symmetric form of square-root conversion was used on the data:

$$y_n(t)=\frac{\left(1.4-\sqrt{1.96-y(t)}\right)}{0.302} \quad y(t)<0$$
$$y_n(t)=\frac{\left(\sqrt{y(t)+1.96}-1.4\right)}{0.302} \quad y(t)\geq 0 \tag{7.9}$$

where $y_n(t)$ is the transformed hourly MERRA wind speed residual. The transformed distribution is more normal-like (Figure 7.9). The auto-correlation coefficients and partial auto-correlation coefficients of $y_n(t)$ for each node indicated that there was an Autoregressive (AR) dependency of order three within the $y_n(t)$ time series (For example Figures 7.10 and 7.11). However there remained possibly significant low levels of dependence at lags greater than three. In a similar procedure to the daily average wind speed square root residuals, the least squares method and numerical maximum likelihood estimation was used to calculate the Root Mean Square Error (RMSE) for models with coefficients up to order ARMA(5,4) for each residual (for example Table 7.3). These indicated that the pure AR models gave sightly lower RMSE values. For increasing AR order, the RMSE initially decreased and then substantially levelled off after order three. To confirm which AR order was necessary and sufficient to capture most of the dependency within the time series, the Bayesian Information Criterion (BIC) was calculated and ranked in

ascending order for each ARMA(p,q) model, $0 \le p \le 5$ and $0 \le q \le 4$, at each node (for example Table 7.4). For hourly data, n = 43824.

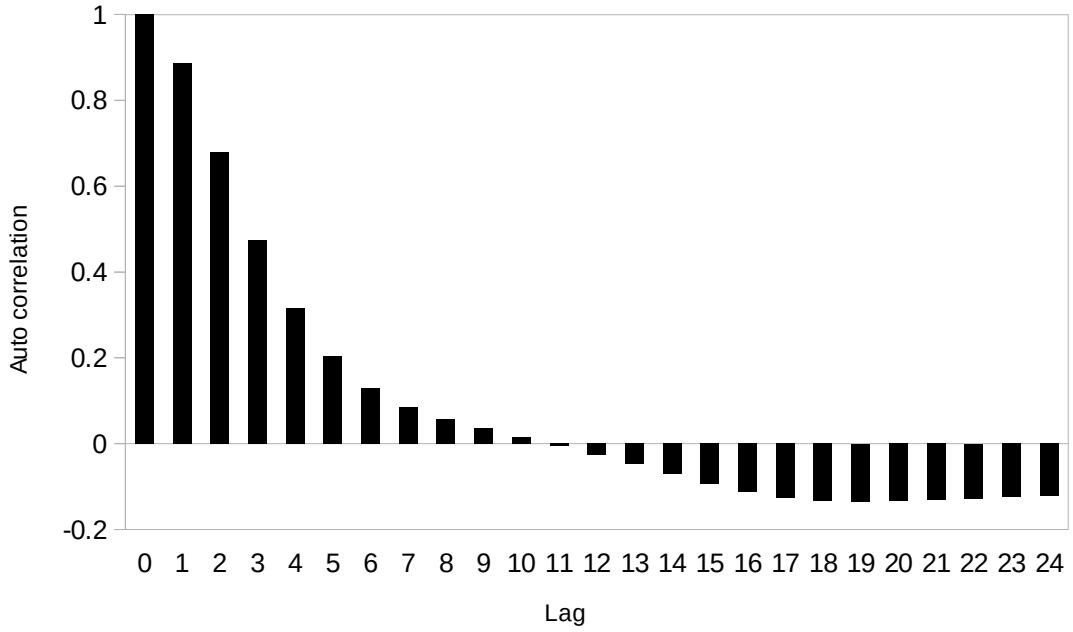

Figure 7.10. Example auto-correlation of the MERRA hourly wind speed transformed residual at a single node. 95% significance level for a population value of zero is ~0.01.

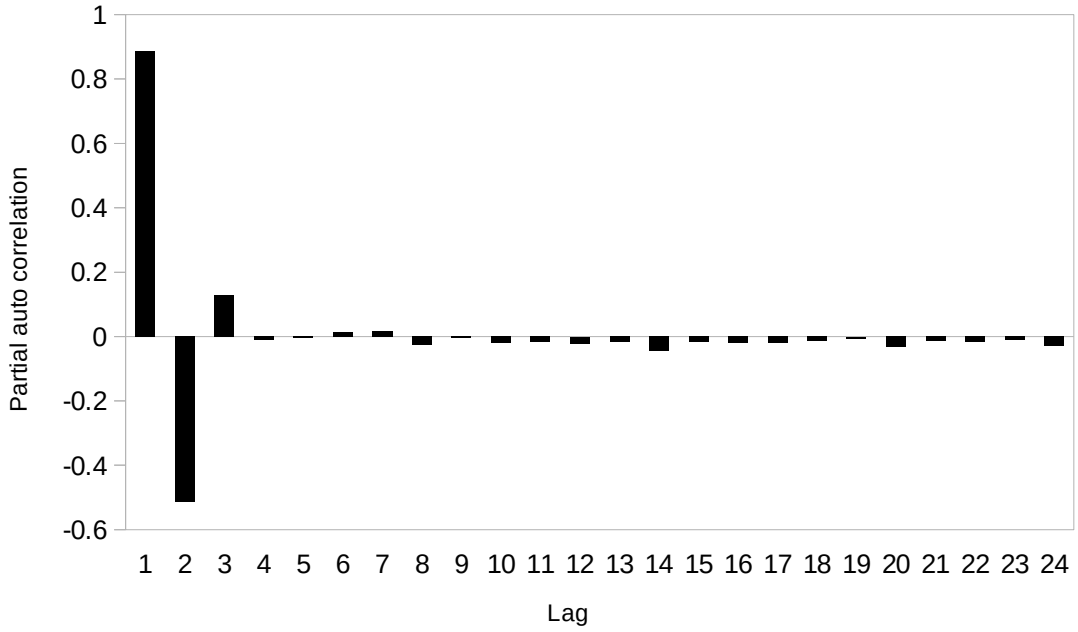

Figure 7.11. Example partial auto-correlation of the MERRA hourly wind speed transformed residual at a single node. 95% significance level for a population value of zero is ~0.01.

Table 7.3. Example Root Mean Square Error (RMSE) between different Autoregressive Moving Average (ARMA) models and the MERRA hourly wind speed transformed residual at a single node.

	MA order				
AR order	**0**	**1**	**2**	**3**	**4**
0	0.99501	0.59737	0.59737	0.59737	0.59737
1	0.45858	0.39830	0.39830	0.39830	0.39830
2	0.39308	0.39035	0.39018	0.39010	0.39010
3	0.38983	0.38982	0.38982	0.38982	0.38982
4	0.38981	0.38982	0.38987	0.38984	0.38983
5	0.38981	0.38983	0.38985	0.38983	0.38986

The Autoregressive (AR) order increases with each row downward, and the Moving Average (MA) order increases to the right.

The results were not definitive as models with the lowest BIC were a mixture of ARMA(3,0) and ARMA(4,0). ARMA(3,0), or AR(3), models were chosen as the difference in RMSE values between the two models was small (typically < 1%).

Table 7.4. Example Bayesian Information Criterion (BIC) and ranking in ascending order for different orders of Autoregressive Moving Average (ARMA) models of the MERRA hourly wind speed transformed residual at a single node.

	MA order				
AR order	**0**	**1**	**2**	**3**	**4**
0	-428.19	-45136.44	-45125.75	-45115.06	-45104.38
	30	26	27	28	29
1	-68311.50	-80651.62	-80640.93	-80630.25	-80619.34
	25	21	22	23	24
2	-81807.56	-82409.56	-82436.04	-82442.40	-82435.33
	20	19	17	16	18
3	-82524.81	-82517.95	-82507.11	-82496.83	-82485.26
	1	3	5	7	10
4	-82518.49	-82505.93	-82485.36	-82481.62	-82472.63
	2	6	9	11	13
5	-82507.70	-82494.41	-82477.41	-82471.13	-82453.59
	4	8	12	14	15

The Autoregressive (AR) order increases with each row downward, and the Moving Average (MA) order increases to the right. In this case, the ARMA(3,0), or AR(3), model had the lowest BIC (rank 1).

The AR(3) coefficient values were found to have a spatial dependency. See Appendix B for the full parameterisation of the spatial dependencies.

It was now possible to start generating synthetic hourly wind speed values. Firstly, the synthetic normally distributed hourly residual $y_{ns}(t)$ was generated using a standard AR(3) equation:

$$y_{ns}(t)=\varphi_1 y_{ns}(t-1)+\varphi_2 y_{ns}(t-2)+\varphi_3 y_{ns}(t-3)+\rho r(t) \tag{7.10}$$

where $r(t)$ is a normally distributed random variable and ρ is set so that the standard deviation of $y_{ns}(t)$ is one. φ_1, φ_2 and φ_3 are the AR(3) coefficients (see Appendix B). The initial values of $y_{ns}(t\text{-}1)$, $y_{ns}(t\text{-}2)$ and $y_{ns}(t\text{-}3)$ were set to standard normally distributed random values. The computational benefit of using the square-root data transformation in equation (7.9) is that generation of synthetic wind speed residuals requires a simple reverse transformation involving a calculation of the square:

$$\begin{aligned} y_s(t)&=1.96-(1.4-0.302\,y_{ns}(t))^2 \quad y_{ns}(t)<0 \\ y_s(t)&=(1.4+0.302\,y_{ns}(t))^2-1.96 \quad y_{ns}(t)\geq 0 \end{aligned} \tag{7.11}$$

where $y_s(t)$ is the synthetic hourly wind speed residual for wind farm w. The distribution of $y_s(t)$ was similar to the MERRA wind speed residual distribution, but without the slight skew (Figure 7.12).

The synthetic average daily wind speed residual $y_{ds}(t)$ was generated using a standard AR(2) equation:

$$y_{ds}(t)=\varphi_{d1} y_{ds}(t-1)+\varphi_{d2} y_{ds}(t-2)+\rho_d r_d(t) \tag{7.12}$$

where ρ_d was set to a value such that the standard deviation of $y_{ds}(t)$ is 1. $r_d(t)$ is a standard normally distributed random value. The initial values of $y_{ds}(t\text{-}1)$, and $y_{ds}(t\text{-}2)$ were set to standard normally distributed random values.

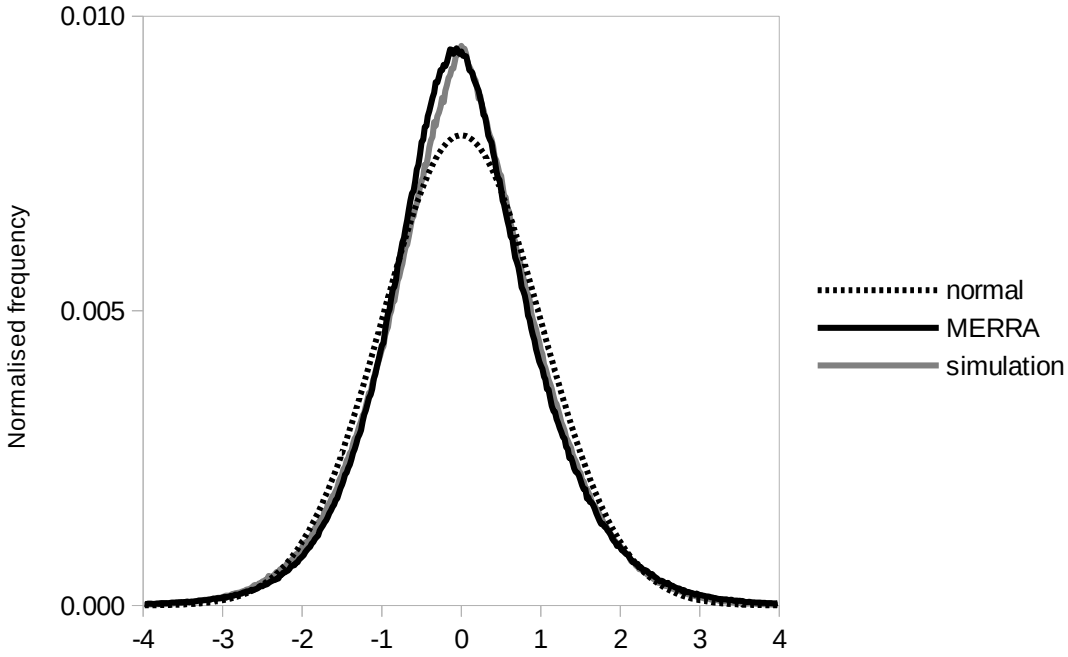

Figure 7.12. Normalised frequency distribution of MERRA and simulation hourly 50m wind-speed residual.

Synthetic daily average wind speeds $v_{ds}(t)$ were generated by squaring y_{ds} and using V_{season} as the average:

$$v_{ds}(t)=\left(\sqrt{V_{season}}+\sigma_d y_{ds}(t)\right)^2-\sigma_d^2 \tag{7.13}$$

The σ_d^2 term is present to make the mean of $v_{ds}(t)$ be V_{season}. The hourly synthetic wind speed v_s could now be assembled as the sum of the daily average component, the diurnal component, and the hourly dependent component:

$$v_s(t)=v_{ds}(t)+v_{diurnal}(t)+\sigma y_s(t) \tag{7.14}$$

See Appendix B for the full wind speed simulation algorithm. v_s is the wind speed 50 metres above the ground, but as the hub height of most modern wind turbines is higher than 50 metres, v_s must be scaled to the hub-height wind speed $v_{hh}(t)$.

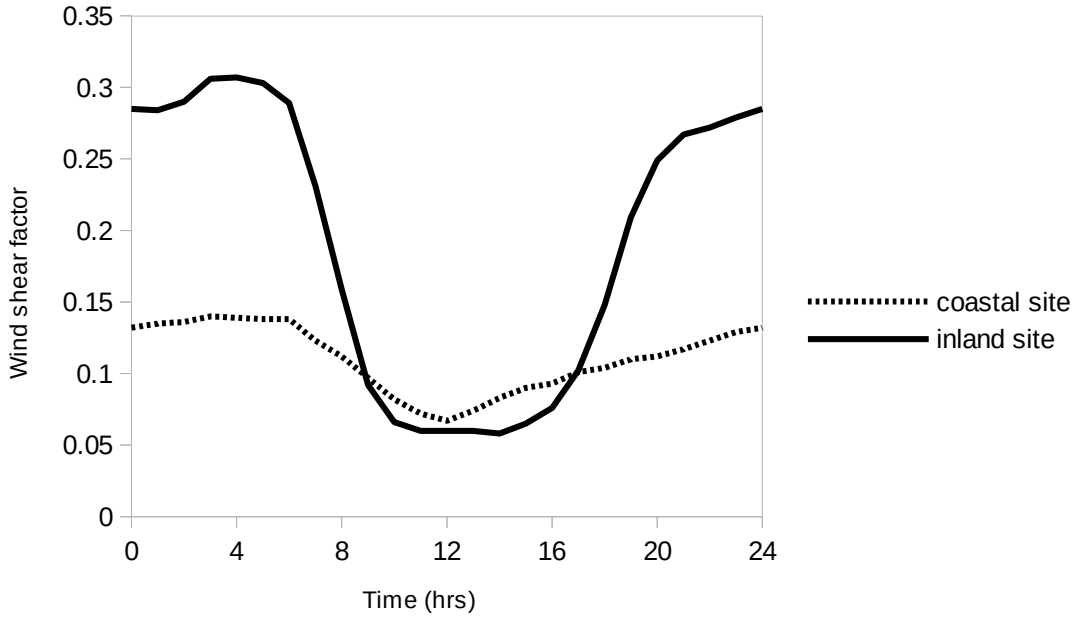

Figure 7.13. Change in average wind shear factor with time of day for a coastal site and an inland site.

The simpler power law estimation for wind shear (equation 7.4) was used because no extra information about surface friction is required. MERRA data was only available for one height, so measured data at different heights from two sites, one coastal and one inland, was used. This data indicated that the wind shear is more pronounced in inland areas, and varies with hour of the day, with wind shear exponent α being usually larger at night (Figure 7.13). There was also a seasonal variation superimposed on this, with α being even greater at night during the winter months.

Hourly wind farm power output was estimated from the hub height wind speed v_{hh} using wind turbine power curves modified according to the findings

of Holttinen (2005) (Figure 7.1). The parameters for wind turbines used in the SWWA are given in Table B.1 of Appendix B. Since the SWWA has a generally low elevation, it was assumed that there was no significant difference in air density between the sites used to measure the turbine technical specifications, and the actual air density encountered by the turbines used in Western Australia.

The model developed in this chapter, called here the 'transformed residual' model, was run for a period of 5 years, from 2009 to 2013. The simulation was started by calculating the spatial and seasonal parameters for a chosen day of the year, then generating power output values hour by hour. Daily and seasonal parameters were recalculated at the beginning of each day. The simulated wind farm power output was compared to actual wind farm power output data for the SWIS grid, measured using the Supervisory Control And Data Acquisition (SCADA) system. Six of the largest wind farms connected to the SWIS grid were chosen for comparison. All of these wind farms have capacities greater than 10MW.

The parameters used to generate the model synthetic seasonal wind speed V_{season} have a dependence on latitude and distance from the coast (see equation B.7), so there is already an implicit correlation in the seasonal wind speed between two nearby sites. Correlation between the daily and diurnal components of wind speed for different wind sites was introduced using a matrix of distance weighted combinations of the random numbers used to generate these values. The weighting factor between two sites was given an inverse relationship to distance apart (equations B.11 to B.15), so that distant sites would be less correlated than nearer sites. The hourly autoregressive and random components of wind speed at each site were assumed to be uncorrelated.

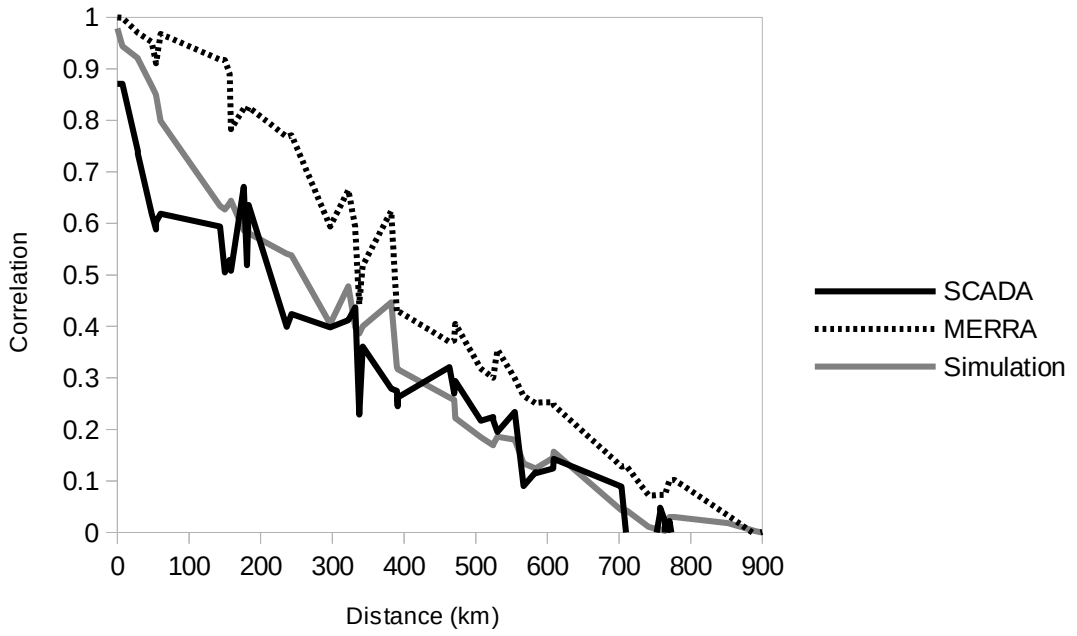

Figure 7.14. Average correlation with inter wind farm distance for wind farm power output for the SWWA.

The MERRA 50m wind speeds were also scaled to hub-height and converted to wind power values. It was found that the distance correlation between these MERRA wind power values was greater than the SCADA data distance correlation (Figure 7.14), suggesting that there is an extra source of spatial variability other than the wind speed. Therefore the model was instead calibrated to the distance correlation values reported in Carlin and Haslett (1982) for wind measurements at several sites in Western Australia, which correspond more closely to the SCADA correlation.

To assess the simulation, the results from two other models were also compared. The first model, called here the 'Weibull' model, used the Weibull distribution to generate hourly time series wind speed data with no dependency on previous values of wind speed. The seasonal wind speed V_{season} was used to calculate the scale parameter λ, and the shape parameter k was

estimated using the maximum likelihood method from the hourly wind speed data. The second model was the same as the transformed residual model, except that normally distributed residuals were used, with no data transformation. This model was called the 'normal residual' model. The average of 10 simulation runs of all three models were compared to the measured SCADA wind power output data. Two statistical measures used to compare the models with the measured data were the Root Mean Square Error (RMSE), and the Mean Bias Error (MBE). The RMSE is a measure of the magnitude of the difference between individual data points in each data set. The sign of the difference is ignored. The MBE is a measure of the average difference between individual data points in each data set, or whether the model generated data set is biased higher or lower compared to the measured data on the whole. Here the sign of the difference is not ignored. Generally, a model with a lower RMSE than another fits the data more closely. In this study a model with a negative MBE might be considered more favourably than a model with a similar but positive MBE because under predicting wind power generation on the whole is more desirable than over predicting. Representing RMSE and MBE as a percentage gives an idea of how significant the error is compared to the average value of the measured data. See Appendix C for definitions of these measures.

7.3 Results

The three simulation generated overall average Capacity Factor (CF) values for the six largest wind farms connected to the SWIS (Albany and Grasmere are considered separate wind farms) were generally comparable to the measured SCADA values (Table 7.5), with differences less than 12%, except for Walkaway wind farm, where the three models underestimated the yearly average CF by 9-16%. The normal residual model slightly overestimated the yearly average CF.

The Weibull and transformed residual models underestimated the overall average CF. These two models generated similar CF values for 4 out of the 6 wind farms. For Grasmere and Albany wind farms, the transformed residual model generated slightly lower values than the Weibull model. However the magnitude of the differences between these two models and the SCADA overall CF were similar, indicating that the models were similarly close.

The errors between the simulation and SCADA yearly average capacity factors (Table 7.6) indicated that the Weibull model was slightly closer to the measured SCADA data. The greatest RMSE error for the Weibull and transformed residual model occurred at the Walkaway wind farm, and for the normal residual model, the greatest error was at the Albany wind farm. These results indicated that actual power generation at the Walkaway wind farm is significantly greater than predicted by all the models, which are based on MERRA data. Local effects may be increasing wind speeds at this site. Comparing the SCADA and simulation monthly average capacity factors, the Weibull model achieved a lower RMSE than the other two models. However, the normalised frequency distribution of average daily capacity factors (Figure 7.15) indicated that the Weibull model generated a significantly different distribution to the measured SCADA data, with CF values concentrated on intermediate values between 0.2 and 0.5.

Although less pronounced, the normal residual model also generated a distribution more concentrated on intermediate values of CF. The transformed residual model generated a distribution closest to the SCADA distribution, with a slight skew towards lower CF values, reflecting the slight conservative bias of this model.

Table 7.5. SCADA and simulated overall average Capacity Factor (CF) for six wind farms within the SWWA using three simulation models: the Weibull model, the normal residual model, and the transformed residual model.

Name	Capacity (MW)	Distance from Coast (km)	SCADA CF	Weibull model CF	Normal residual model CF	Transformed residual CF
Grasmere	13.8	0.67	0.33	0.33	0.36	0.32
Albany	21.6	0.67	0.32	0.33	0.36	0.32
Mumbida	55	14.6	0.39	0.38	0.41	0.38
Emu Downs	79.2	23.6	0.35	0.33	0.36	0.33
Walkaway	89.1	15.8	0.43	0.36	0.39	0.36
Collgar	206	255	0.37	0.34	0.36	0.34

Model values are the average of 10 simulation runs.

These discrepancies were reflected in the error values (Table 7.6). The normal and transformed residual models achieved much lower RMSE values than the Weibull model. The transformed residual model achieved the lowest RMSE values overall, although the value for Mumbida wind farm was comparable to the normal residual model, and the value for Walkaway was significantly higher. The Weibull and normal residual models also generated a significantly different diurnal peak hour distribution (Figure 7.16). Peak hour is the hour of the day when CF (and hence wind power output) is at a maximum. The transformed residual model achieved lower RMSE values than the Weibull or normal residual models, except for Emu Downs wind farm, where the values were comparable. The hourly CF normalised frequency distribution (Figure 7.17) of the Weibull model fitted the SCADA distribution slightly better than the other two models. The transformed residual model again exhibited a slight skew towards lower CF values.

Table 7.6. Errors in the yearly and monthly average Capacity Factor (CF) estimation, daily average CF frequency distribution, diurnal peak hour distribution and hourly average CF frequency distribution of three simulation models compared to measured SCADA wind power data.

Time scale	Measure	Weibull model		Normal residual model		Transformed residual model	
Yearly	RMSE(%)	Grasmere	1.74	Grasmere	10.4	Grasmere	5.3
		Albany	9.77	Albany	19.2	Albany	9.6
		Mumbida	4.59	Mumbida	3.9	Mumbida	5.4
		Emu Downs	7.71	Emu Downs	8.4	Emu Downs	9.7
		Walkaway	15.11	Walkaway	9.6	Walkaway	16.1
		Collgar	9.0	Collgar	5.6	Collgar	10.4
		Average	**8.0**	**Average**	**9.5**	**Average**	**9.4**
	MBE(%)	Grasmere	1.2	Grasmere	9.8	Grasmere	-1.1
		Albany	8.6	Albany	18.2	Albany	6.1
		Mumbida	-4.6	Mumbida	3.9	Mumbida	-5.4
		Emu Downs	-4.1	Emu Downs	4.0	Emu Downs	-4.2
		Walkaway	-14.5	Walkaway	-7.6	Walkaway	-15.2
		Collgar	-8.1	Collgar	-1.3	Collgar	-8.2
		Average	**-3.6**	**Average**	**4.5**	**Average**	**-4.6**
Monthly	RMSE(%)	Grasmere	15.4	Grasmere	25.5	Grasmere	30.0
		Albany	20.4	Albany	30.4	Albany	30.3
		Mumbida	12.5	Mumbida	31.1	Mumbida	26.8
		Emu Downs	16.9	Emu Downs	22.1	Emu Downs	23.4
		Walkaway	18.9	Walkaway	21.2	Walkaway	24.0
		Collgar	17.3	Collgar	22.1	Collgar	24.1
		Average	**16.9**	**Average**	**25.4**	**Average**	**26.4**
	MBE(%)	Grasmere	1.3	Grasmere	9.5	Grasmere	-2.5
		Albany	8.1	Albany	16.6	Albany	5.0
		Mumbida	1.6	Mumbida	12.2	Mumbida	5.7
		Emu Downs	-4.1	Emu Downs	4.0	Emu Downs	-4.0
		Walkaway	-14.4	Walkaway	-8.0	Walkaway	-14.8
		Collgar	-5.2	Collgar	1.5	Collgar	-4.1
		Average	**-2.1**	**Average**	**6.0**	**Average**	**-2.4**
Daily frequency distribution	RMSE(%)	Grasmere	143	Grasmere	32.5	Grasmere	25.2
		Albany	147	Albany	40.7	Albany	17.0
		Mumbida	122	Mumbida	35.1	Mumbida	35.9
		Emu Downs	126	Emu Downs	25.5	Emu Downs	23.5
		Walkaway	129	Walkaway	28.8	Walkaway	37.8
		Collgar	136	Collgar	25.1	Collgar	22.3
		Average	**134**	**Average**	**31.3**	**Average**	**26.9**
Diurnal peak hour distribution	RMSE(%)	Grasmere	47.1	Grasmere	38.0	Grasmere	25.9
		Albany	47.0	Albany	39.9	Albany	18.5
		Mumbida	58.6	Mumbida	55.3	Mumbida	43.8
		Emu Downs	49.5	Emu Downs	48.5	Emu Downs	50.6
		Walkaway	58.0	Walkaway	52.0	Walkaway	42.0
		Collgar	107	Collgar	77.1	Collgar	20.5
		Average	**61.2**	**Average**	**51.8**	**Average**	**33.5**
Hourly frequency distribution	RMSE(%)	Grasmere	27.2	Grasmere	79.0	Grasmere	18.4
		Albany	15.6	Albany	65.1	Albany	18.9
		Mumbida	19.7	Mumbida	43.2	Mumbida	30.8
		Emu Downs	48.9	Emu Downs	26.6	Emu Downs	56.3
		Walkaway	27.8	Walkaway	48.1	Walkaway	36.6
		Collgar	35.2	Collgar	78.6	Collgar	27.2
		Average	**29.0**	**Average**	**56.8**	**Average**	**31.3**

RMSE and MBE values are given as a percentage of the average SCADA capacity factor or average SCADA CF frequency.

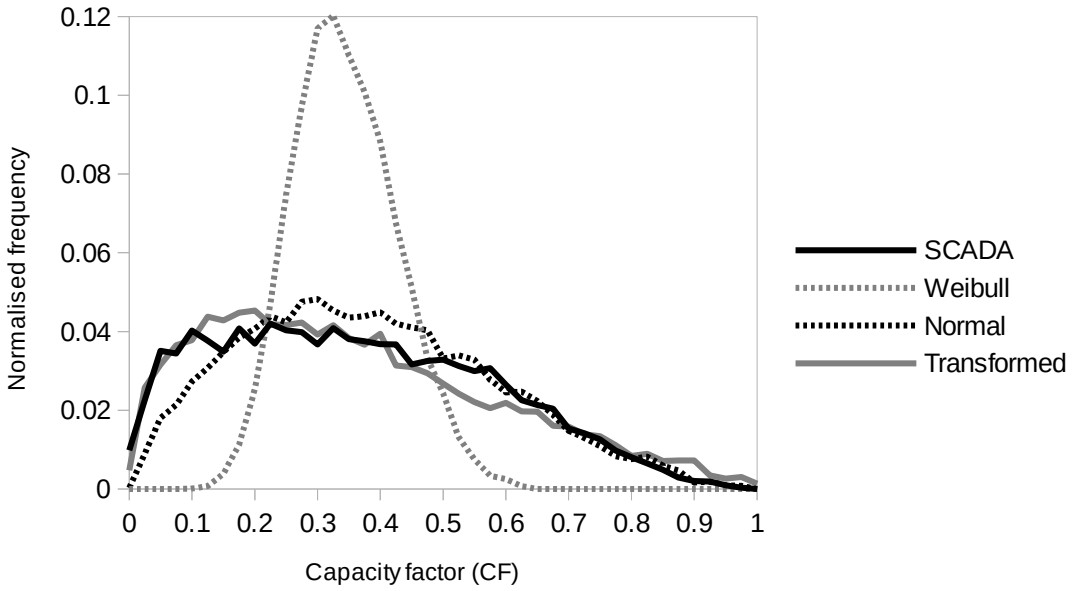

Figure 7.15. Normalised frequency distribution of average daily capacity factors. Three models (Weibull, normal residual, and transformed residual) are compared to measured SCADA wind power output data.

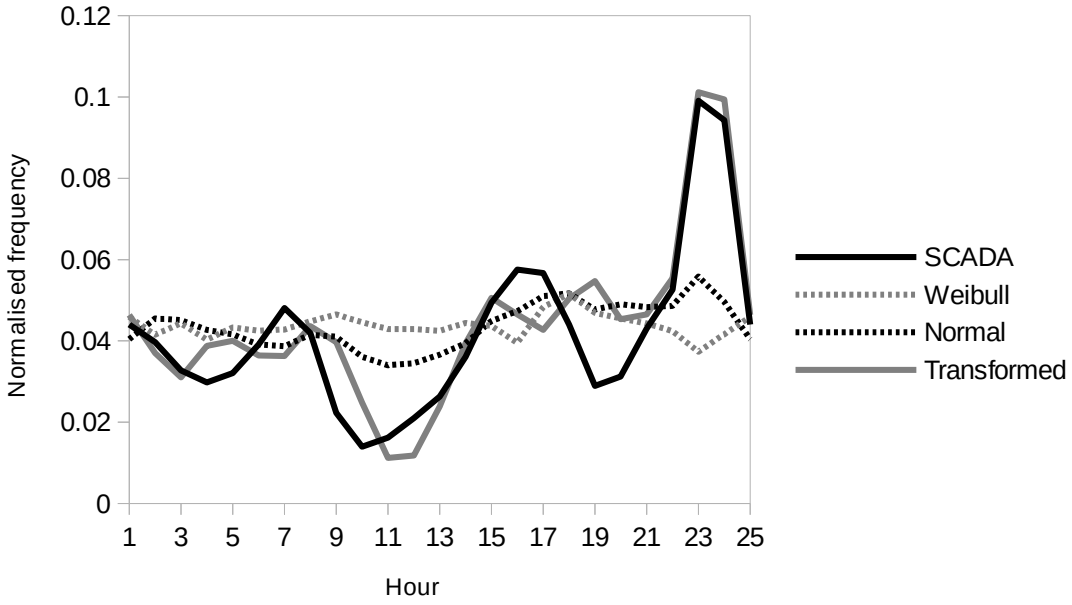

Figure 7.16. Diurnal Capacity Factor (CF) peak hour distribution. Peak hour is the hour of the day when CF (and hence wind power output) is at a maximum. Three models (Weibull, normal residual, and transformed residual) are compared to measured SCADA wind power output data. The 25th hour is the same data point as the 1st hour and is provided for continuity.

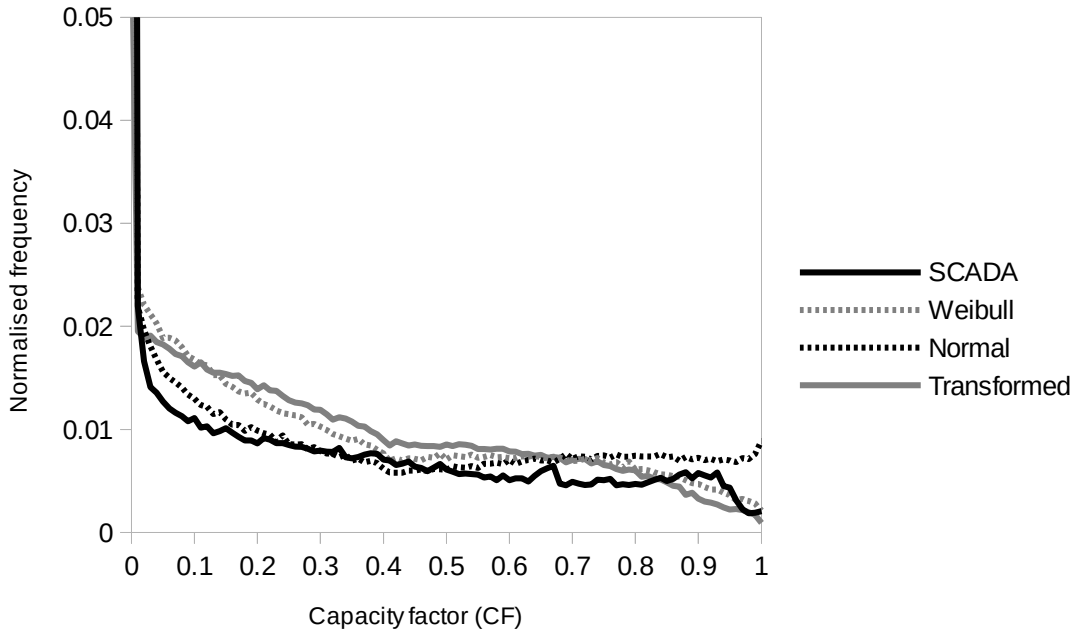

Figure 7.17. Normalised frequency distribution of average hourly capacity factors. Three models (Weibull, normal residual, and transformed residual) are compared to measured SCADA wind power output data.

7.4 Summary

Even though the Weibull model generated yearly capacity factors slightly closer to the measured SCADA data than the transformed residual model, both the Weibull and normal residual models generated significantly different daily average capacity factor and diurnal peak hour distributions to the measured SCADA data, and hence would generate unrealistic statistical behaviour if they were used to simulate existing or hypothetical wind power systems in the SWWA. The transformed residual model generated daily average capacity factors and diurnal peak hours with a much closer distribution to the measured data and demonstrated the necessity of characterising the wind speed residual properly, and not blindly assuming that it has a normal distribution.

Wind power is a distributed resource that is increasing in use world-wide. Therefore simulating the operation of large scale electrical grids with significant levels of wind power is becoming more important. To do this it is necessary to build regional scale wind power models that can account for spatial, seasonal and hour by hour variation. The results from this chapter indicated that using MERRA data as the basis of such a wide area simulation is a viable method. The MERRA dataset is freely available and covers the whole surface of the world, including many regions that would have no access to suitable hub-height wind speed data.

The wind farm capacity factors were found to have a greater distance correlation when estimated from MERRA data, than when calculated directly from the measured SCADA data. Hence there may be more variability in air density, wind shear factor, wind farm wide wind speed variability, or some other factor than accounted for here. It is important to confirm this finding in future studies over other regions, as wind variability can have a significant effect on the operation of a large scale electrical grid. Simulations based on MERRA data can be built for any site or region in the world, but they must incorporate a means for correctly setting the distance correlation between wind farm sites.

The simulation in this instance was conservative. Although measured data were used to calibrate the wind shear factor, similar simulations could be developed for regions with no available measured data. Setting the wind shear exponent to zero would generate even more conservative synthetic power output data, but still usable because the 50m height above ground level is within the range of most modern wind turbine hub heights.

The frequency distribution of the AR-based simulation capacity factor was similar to the measured data capacity factor, due to the use of the novel data transformation functions, which also have applicability to other sites that have an exponential wind speed residual distribution. Matching the measured and simulated wind power frequency distribution is important for detailed estimation of wind power potential.

Similarly to Ward and Boland (2007), it was found that wind sites closer to the coast tended to have diurnal output peaks in the afternoon, earlier than those wind sites further inland which peak later in the evening. This implies that a mix of coastal and inland wind farm sites is beneficial for avoiding large peaks and lulls in wind power generation and maintaining a supply of wind power that is consistent with the peak in electricity demand.

8 Integrated power system scenarios

Models for generating synthetic hourly solar irradiance, solar thermal power and wind power data over seasonal time scales for any location within the SWWA were developed in the previous chapters. These models do not reproduce average weather conditions, but reproduce typical conditions that capture variability on hourly, daily and seasonal time scales.

Using the solar irradiance model, a model for solar PV power generation will be developed in this chapter. Solar PV generation already has a significant presence on the SWIS grid. Simple models for home battery storage, power to gas storage and energy efficiency will also developed, as these could have a significant future presence within the SWIS.

The SWIS already has systems to maintain electrical supply stability on sub-hourly time scales. However, the operation of these systems could be impacted by changing the configuration and characteristics of power plants and storage. Hence before further model development could begin, a necessary first step will be to examine the current SWIS grid in more detail, before describing the methods used to build the models.

When all of these models are in place, it will be possible to create hypothetical systems of multiple solar and wind power plants, all in different locations, and estimate the combined hourly power output of the entire system on an hour by hour basis. The hourly SWIS load demand, mediated by energy efficiency measures and population increase, can be compared to this combined power output and the percentage of renewable energy generation estimated. If enough generation and storage capacity is added, then scenarios can be developed for

renewable energy systems that attempt to completely balance energy supply and demand in the SWIS on an hour by hour basis. Because the solar and wind resource varies both hourly and seasonally, the question remains whether these systems can balance supply and demand at every hour throughout the year. However, even if a scenario is developed that can do this, there is an additional requirement. Changing a large-scale fossil fuel dominated electricity system to run on renewable energy cannot happen overnight. While many global emission reduction studies set a target year of 2050 (Loftus et al. 2015), the urgency to reduce emissions means the transition should happen more quickly. Therefore a target year of 2030 will be set. For each scenario, the required installation rate of each technology to implement the system within this time frame will be estimated, while also taking into account population growth. To be a feasible option for rapidly reducing emissions and making the SWIS 100% renewable, the required capacity for each technology must be moderate enough such that it can be installed within this short time scale.

The potential of power to gas seasonal storage systems to reduce the required build, and scenarios with very high levels of wind generation (as these may have the lowest cost), will also be examined.

8.1 The SWIS in more detail

The SWIS is made up of a transmission network and a number of sub-transmission and distribution networks. The present configuration of energy generation systems connected to the SWIS is dominated by conventional fossil fuel power stations, with about 1600 MW of coal fired generation capacity, 1640 MW of gas fired generation capacity, and a further 1310 MW of mixed gas and liquid generation capacity (IMOWA, 2015). The main load centre is the city of Perth, which is connected to three main transmission line corridors (see Figure

8.1). The SWIS is isolated from all other grids and does not currently have access to large-scale hydroelectric resources. Hence it is particularly dependent on 'spinning reserve' being provided by fossil fuel generation to maintain stability (Mullan et al. 2011). Spinning reserve refers to reserved excess capacity of high inertial mass generators that spin in synchronisation with the grid. The reserved capacity is not used until required. Around 317 MW of spinning reserve was maintained on the SWIS grid in 2013 (Western Power 2013). Renewable power plants are also already present. As of 2015, there was about 460 MW of onshore wind capacity and almost 500 MW of roof top solar PV capacity connected to the SWIS.

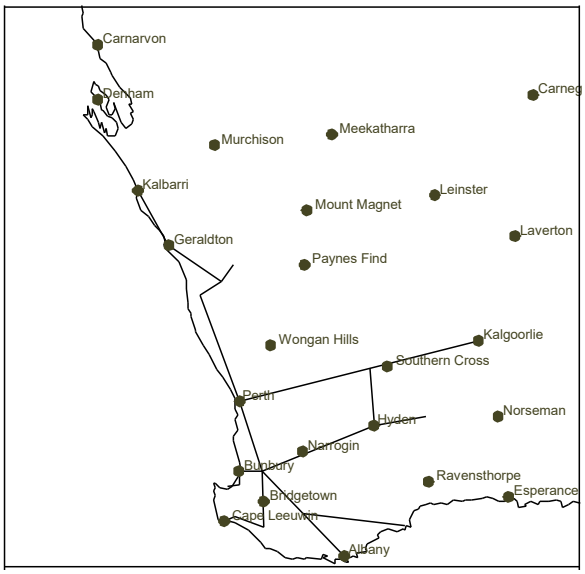

Figure 8.1. SWIS grid backbone links used by the model.

The word 'dispatchable' is commonly used to represent flexible generation systems which can adjust output according to demand, and 'non-dispatchable' to those that are variable and cannot adjust upwards to meet demand, such as wind and solar. Conventional coal fired power stations are considered to be dispatchable, but have a required minimum operational power output level. If output is below this level, they must either shut down completely or operate at

reduced efficiency. In reality, any generation system will have a degree of dispatchability (either more or less), that might differ over different time scales. Conventional power plants also often have a maximum sustainable ramp rate, which is a measure of how fast the power output can change (either rising or falling). Exceeding this rate could lead to higher maintenance costs or damage to the plant. In general, dispatchable generators are expected to respond to changes in the output of non-dispatchable generators and changes in demand to balance the system.

On sub-hourly time scales, there are systems to maintain a stable frequency and voltage amplitude. Conventional grids have traditionally relied on synchronous generators with a large rotational inertia for frequency stability control and fast voltage regulation for voltage stability and control. The inertia determines the initial rate of change of frequency in response to sudden changes in generator loading, before the primary and secondary stability control systems activate. The larger the inertia, the smaller the rate of change of frequency. The primary stability control systems attempt to arrest the frequency change, while the secondary control systems attempt to return the frequency to its reference value. Riesz et al. (2010) estimated that there was around 12.4 GWs of inertia on average in the SWIS grid, meaning that over 200 MW of power can be supplied or absorbed for a second with a frequency change of less than 1%. This inherent reserve gives active stability and safety systems more time to activate in response to a fault. The inertia is provided predominantly by conventional fossil fuel power plants. These power plants would be retired under a 100% renewable energy scenario, leading to a large reduction of inertia in the system. Therefore alternate means must found to maintain frequency and voltage stability. One possible option is to have some of the existing synchronous generators spinning but disconnected from their rotational energy source ('de-

clutched'), in effect acting as synchronous compensators with no fuel input. Power losses in these generators could be up to 2% of the rated power (Da Silva et al. 2001).

Batteries and photovoltaic systems can provide voltage control but have no intrinsic rotational inertia. However, there are ways in which they could provide fast responding active frequency stability control, to compensate for the reduced system inertia. Battery storage systems have a very rapid response rate and can provide frequency stability capability, if they are maintained in a partially charged state (Cha et al. 2012). They can also provide 'synthetic rotational inertia' or 'inertia mimicking' (Ulbig et al. 2013). The findings of Knap et al. (2014) suggested that the inertia constant of lithium ion batteries is at least 50 MWs per MW of output power. If the maximum battery charge and discharge rate was 0.2 MW per MWh of capacity (McCloskey 2015), then 1.24 GWh of battery storage could provide a synthetic inertia similar to the present inertia within the SWIS grid (1.24 GWh is equivalent to a 7 kWh battery system installed in almost 20% of suitable houses. See section 8.3 below for a discussion of possible storage capacities).

PV systems can already respond to increases in system frequency by decreasing generated power. They can also be deliberately operated at less than their maximum potential power at any one time, as determined by the solar irradiance. These 'de-loaded' PV systems can thus increase their generated power in response to decreasing system frequency (Rahmann and Castillo 2014). Thus standalone PV systems could provide extra synthetic inertia during times of peak demand, but not at night.

The rotating generators of solar thermal power stations can also provide inertia. However on the SWIS most solar thermal stations are likely to be far from the

main load centre (the greater Perth metropolitan area). If there is no central source of inertia, then the risk of these remote generators losing synchronism with one another increases. Wind turbines can be configured to provide synthetic inertia, and can more easily recover from faults or disturbances that could cause loss of synchronism. However, the risk of faults or disturbances in the grid isolating a wind farm (and its synthetic inertia) from the main load centre increases with longer transmission distances.

Vidal-Amaro et al. (2015) considered grid stability for high penetration (although not 100%) renewable energy scenarios. However, absent in many previous 100 percent renewable generation simulation studies is consideration of the potential threat to system stability from loss of inertia as conventional generators are replaced by renewable energy systems. As a consequence, possible increases in the required installed capacity of renewable energy and storage technologies, in order to deploy systems to mitigate the potential for instability, are not accounted for. For all the 100% renewable energy scenarios developed here, systems to maintain stability were implemented, and integrated into each scenario. The inertia for each scenario was estimated and compared to the 12.4 GWs of inertia in the current SWIS system.

8.2 Method

The scenarios are described in section 8.3. For each scenario developed, hourly values for solar radiation were generated at each location where a solar power station was placed, and hourly values for hub-height wind speed were generated at each location where a wind farm was placed. To translate these values into power generation, the behaviour of the energy collection and generation device at each location was modelled. The amount of non renewable energy generation required for each hour was calculated using:

$$nonre = Load_{y,h} - EE_h - P_{out,storage} - glf_{rtpv} P_{out,rtpv} - \sum_{n=1}^{n_{large}} glf_n P_{out,n} \quad (8.1)$$

where *nonre* is the non-renewable power generation (MW), $Load_{y,h}$ is the simulated hourly baseline SWIS load demand at hour h for year $y \geq 2009$ (MW). EE_h is the load demand reduction at hour h due to any energy efficiency measures, if implemented (MW). $P_{out,storage}$ is the output power from distributed storage, if present on the grid (MW). $P_{out,rtpv}$ is the total output from rooftop solar connected to the grid (MW). glf_{rtpv} is the grid loss factor for distributed rooftop PV generation. glf_n is the grid loss factor for large power station n. n_{large} is the number of large-scale renewable power stations on the system. $P_{out,n}$ is the output power for each station (MW). Each large power station could be modelled as a fixed PV array, a wind farm, or a solar thermal farm. If distributed storage is present in a scenario, then the simulation attempts to adjust $P_{out,storage}$ so that *nonre* is zero.

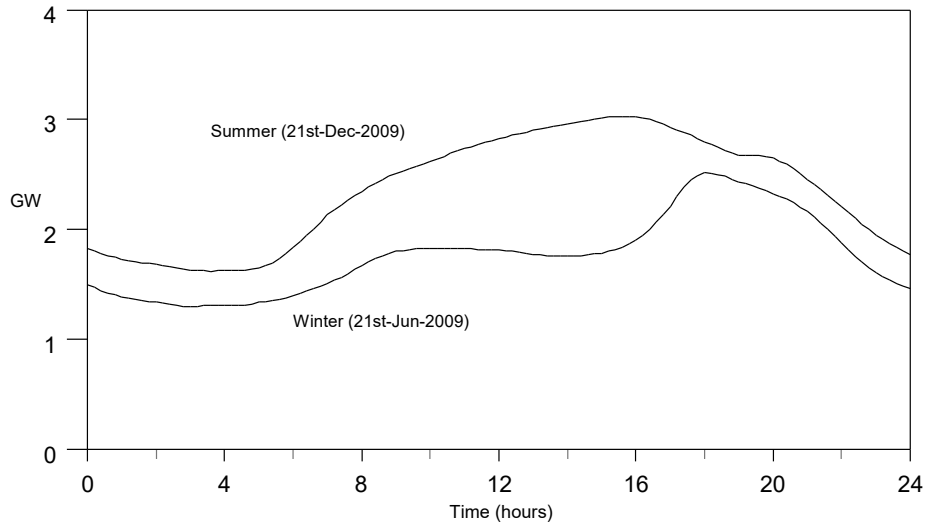

Figure 8.2. Typical summer and winter daily load profile on the SWIS grid for the year 2009.

Publicly available half hourly demand data for the SWIS over seasonal time scales were aggregated into average hourly values. The total SWIS load demand for every hour throughout the year of 2009 was used as a baseline for the load demand profile (for typical summer and winter daily profiles, see Figure 8.2). The year 2009 was chosen because after that time significant amounts of distributed roof top solar generation began to be connected to the grid, reducing daytime demand.

The effect of future population increase on baseline power demand was modelled by multiplying the 2009 load demand by a factor reflecting compounded yearly population growth:

$$Load_{y,h} = Load_{2009,h}\left(1+\frac{pop}{100}\right)^{(y-2009)} \quad (8.2)$$

where $Load_{y,h}$ is the load profile for year y at hour h (MW), $Load_{2009,h}$ is the 2009 profile at hour h (MW), and pop is the percentage yearly population increase. pop was set to a value of 2% per year, reflecting the average growth rate of Australian greater capital cities from 2013 to 2014 (ABS 2015). y was set to 2030 to establish the implementation target year.

To assess whether complete renewable energy generation had been achieved, 100 simulation runs under typical weather conditions were carried out for each scenario, and the maximum shortfall in renewable energy generation compared to the load was recorded. Two SWIS reliability standards were used to access the shortfall. The first reliability standard was taken to be a 0.05% loss of load probability (LOLP), estimated as the fraction of time that renewable energy generation fell short of the load demand (MR 2012). The second standard was a 0.002% shortfall in generated energy over one year. Renewable energy

generation capacity was added to each scenario until these standards were met for 95 runs out of 100.

8.2.1 Transmission losses

To model generation from regional power stations, transmission losses between the stations and the load were estimated. In the SWIS system, the city of Perth is the major load centre. To approximate the losses incurred when transporting power through the grid, it was assumed that all electricity generated by each power station travelled to Perth. Up-conversion losses from each power station to the grid, and down-conversion and distribution losses to the loads were each modelled as a set power percentage loss. The backbone of the SWIS grid was modelled as having several links (Figure 8.1). Any new power station added to the system attached a new grid link from the power station to the nearest backbone link. All new links were assumed to use High Voltage Alternating Current (HVAC) technology, to allow easy interconnection with the existing HVAC grid.

Although cross-conversion losses between one grid link and another are likely to be lower than the up-conversion losses, they were assumed to be similar for modelling simplicity. Transmission losses were represented as a power percentage loss per 1000 kilometres of transmission line. The electricity generated by a power station would typically travel over several grid links before reaching Perth. For a power station n, $1 \le n \le n_{large}$, the total grid loss was estimated using:

$$glf_n = (1 - 0.01\,ld)\left\{\prod_{i=0}^{nlink_n - 1}(1 - 0.01\,lup_i)\right\}\left\{\prod_{j=1}^{nlink_n} e^{\left(-\frac{tl_j d_j}{10^5}\right)}\right\} \tag{8.3}$$

where $nlink_n$ is the number of links travelled before reaching Perth, ld is the percentage down-conversion and distribution loss, lup_i is the percentage up-conversion loss from the power station when i=0 and the cross-conversion loss between grid link i and grid link i+1 when $i > 0$, tl_j is the percentage transmission loss per 1000 km for grid link j, d_j is the length of grid link j (km) and glf_n is the total grid transmission factor (the fraction of power that reaches the end users in Perth) for the power station. glf_n will be different for each power station, depending on its location, proximity to Perth, and which grid links the electricity travels through. The values used for each parameter are given in Table 8.1 below.

Table 8.1. Grid conversion and transmission loss parameters.

Parameter	Description	Value
lup	Up-conversion and cross-conversion loss (%)	0.62[a]
ld	Step-down and distribution loss (%)	9.5[b]
tl	Line loss (% per 1000 km)	6.93[c]

[a]Negra et al. (2006). [b]Dortalina and Nadira (2005) and Masoum et al. (2010). [c]Bahrman (2008).

Roof top solar PV was assumed to be scattered throughout the Perth distribution network and was subject to an 8% up-conversion and distribution loss on average (Koutroulis and Blaabjerg 2013), such that glf_{rtpv} = 0.92. 2034 MW of existing gas or mixed fuel gas turbines situated near Perth were also retrofitted or configured to operate in synchronous compensator mode, with the gas turbines de-clutched from the synchronous generators, which have some rotational inertia. This was to provide a stable frequency reference near the load centre for the more distant generators to synchronise with, and back-up generation capacity in case of generator failures or shortfalls during periods

of sustained low solar and wind availability. There is usually no fuel input to the turbines, and the extra continuous load required to keep the back-up generators spinning was estimated to be about 41 MW, assuming the power required was 0.2% of the rated capacity of the generators (Da Silva et al. 2001).

8.2.2 Solar PV model

The global solar irradiance, I_g, is the total solar power per unit area falling on a flat surface and can be divided into three components: beam (also called direct), diffuse, and reflected. The beam component has come directly from the sun, the diffuse component results from radiation that has been scattered in the atmosphere, and the reflected component results from radiation reflected off other surfaces. The diffuse and reflected components are indirect, and they have a complex relationship with the beam component, depending on clouds and atmospheric conditions.

The solar model developed in chapter 5 can generate hourly values of all three components, and PV systems can generally use them all. Fixed PV panels will not always be orientated perpendicular to the position of the sun as it moves through the sky, so the solar model recalculated irradiance each hour accounting for the changing angle of incidence between the sun and the panel.

An ideal solar cell has a power output that is linearly proportional to the global solar irradiance I_g. The performance ratio (PR) is a measure of how well a cell performs compared to an ideal cell (Carr and Pryor 2004):

$$PR = \left(\frac{P_{out}}{P_{rated}} \right) / \left(\frac{I_g}{1000} \right) \tag{8.4}$$

where P_{out} is the electrical output power (W), P_{rated} is the rated output (W) and I_g is measured in Wm^{-2}. Carr and Pryor (2004) tested a number of cells in the Perth

area and found *PR* values ranging from 0.79 to 0.93, with the highest values occurring during winter. The efficiency of solar cells has been found to decrease with lower global irradiance and higher temperatures. To model this behaviour for fixed axis PV power stations and rooftop PV arrays, cell efficiency drop off was approximated by using an empirical expression for P_{out}:

$$P_{out}(I_g, DOY, h) = \left\{\frac{16250 + I_g^2}{25000 + I_g^2}\right\} \frac{I_g}{1000} \left\{1 - \frac{0.17}{4}(1 + \cos(\frac{2\pi}{365}(DOY - 16)))(1 + \cos(\frac{2\pi}{24}(h - 14)))\right\} P_{rated} \qquad (8.5)$$

where *DOY* is the day of the year (1 to 365), *h* is the hour of the day and P_{out} will have the same units as P_{rated} (MW for a large power station). Using this approximation, when I_g decreases toward 0 Wm^{-2}, cell efficiency will drop to 65% of the ideal efficiency, comparable to the performance drop of a crystalline silicon PV cell (Huld et al. 2010). During summer in the middle of the afternoon, P_{out} decreases further by up to 17% to account for heating related efficiency loss (Huld et al. 2010). Both of these effects will decrease *PR*.

For rooftop PV systems, the tilt angle from horizontal was set to be 22.6° (Jones et al. 2012), and panels were assumed to be facing northward, although in reality there will be a spread of orientations around these values. The baseline installed capacity of rooftop PV arrays was taken to be 500 MW for the start of 2016, based on an installed capacity of 571 MW in early March 2016 (APVI 2016).

There were more than 726,000 private dwellings in the greater Perth area in 2011 (ABS 2011), of which under 10% are flats, units, apartments, or other types of dwelling that might be unsuitable for rooftop PV installation. The average floor area of houses in Australia is at least 150 m^2 (DIT 2012). Assuming that on average, a roof area equal to 25% of the floor area is suitable for north facing PV installation, then the total area per suitable house is 37.5 m^2. Assuming that the

current average size of a 250 W solar PV panel is 1.65 m^2 (Good et al. 2016), then 22 panels could fit onto an average house, to give a maximum system size of 5.5 kW per house. If it was assumed that a 2% per year population growth rate translated into the same percentage growth in housing number, then the 653,403 suitable houses (90% of 726,004) in 2011 would grow into about 951,885 houses in 2030. Because of the spread of roof orientations, the simulation assumed a conservative total potential home rooftop capacity of 3.42 GW, consisting of 3.6 kW of north facing 22.6° tilt panels installed on 950,000 homes in 2030. Another factor that might affect the capacity is that the proportion of the population living in high density housing less suitable for rooftop PV will probably increase by 2030. Conversely, solar PV energy conversion efficiencies are also likely to increase by 2030.

For those scenarios with 100% renewable generation, the total PV capacity was de-loaded by 10% to enable frequency control capability. In reality, rooftop PV systems with battery storage would not need to operate in de-loaded mode (unless the battery storage level is low). If the batteries are installed behind the solar inverter, the inverter's output would still need to be limited to 90% of rated capacity for these systems, so that the batteries can inject at least 10% (if storage level is adequate), but the PV panels can still operate up to full output when also charging the battery. Nevertheless, the total PV capacity was de-loaded, for model simplicity, and to avoid the assumption that all PV systems must be tied to a battery. For PV systems without storage, de-loading enables frequency control capability.

8.2.3 Existing and proposed wind farms

Wind is considered one of the cheapest forms of renewable energy, and renewable energy scenarios for Australia based on lowest cost have high

penetrations of wind generation capacity (Riesz et al. 2016). A number of wind farms are already connected to the SWIS, and the wind power model developed in chapter 7 generated conservative values of simulated wind power generation for the six largest wind farms (Table 8.2).

Table 8.2. Measured and simulated average yearly Capacity Factor (CF) for the six largest wind farms within the South West of Western Australia.

Name	Capacity (MW)	Measured CF	Simulation CF
Grasmere	13.8	0.33	0.32
Albany	21.6	0.32	0.32
Mumbida	55	0.39	0.38
Emu Downs	79.2	0.35	0.33
Walkaway	89.1	0.43	0.37
Collgar	206	0.37	0.33

A number of new wind farms in the SWWA have already been proposed, with a total capacity of 1482 MW (Table 8.3).

Table 8.3. Proposed wind farms in the SWWA region.

Name	Capacity (MW)
Dandaragan	513.4
Warradarge	250
Williams	210
Nilgen	132.5
Badgingarra	123
Coronation	104
Walkaway 2	94.05
Mileannup	55

Since the wind power model was developed to cover the SWWA region, rather than one location, the hypothetical generation from these proposed wind farms could be estimated, as well as any other site chosen for a wind farm. Addition of these proposed wind farms would bring the total wind capacity up to 1947

MW. However for scenarios with very high wind power generation, much more capacity would be needed.

8.2.4 Distributed battery storage model

Distributed energy storage for the simulation was loosely based on using batteries. Losses were incurred when energy is transferred from the grid to storage, and from storage to the grid. Additionally, limits were imposed on the maximum charging and discharging rates. For those scenarios with 100% renewable generation, the storage system was not allowed to become completely full or completely empty, so as to enable frequency stability control. For battery storage systems, the state of charge is often constrained between set limits to prolong battery life. In this study, storage capacity values refer to the capacity that is usable within these constraints rather than total capacity. The settings used are given in Table 8.4 below:

Table 8.4. Distributed storage simulation parameters.

Parameter	Value
Maximum allowed storage level	95% of rated capacity
Minimum allowed storage level	5% of rated capacity
Grid-to-storage conversion efficiency	89%[a]
Storage-to-grid conversion efficiency	89%[a]
Maximum charge rate to storage	0.2 MW per MWh of storage[b]
Maximum discharge rate from storage	0.2 MW per MWh of storage[b]
Self discharge rate	3% per month[c]
Synthetic inertia	10 MWs per MWh of storage[d]

[a]Based on 90% round trip efficiency for Li-ion batteries (Soloveichik 2011) and 94% average PV inverter efficiency (Koutroulis and Blaabjerg 2013). [b]McCloskey (2015). [c]Mishra et al. (2015). [d]0.2 MW/MWh x 50 MWs/MW (Knap et al. 2014).

8.2.5 Power to gas (P2G) storage model

Since the SWWA region already has a natural gas supply network, methane was chosen as the gas storage medium. Estimates of the efficiency of the P2G process for methane range from 49% to 80% (Jentsch et al. 2014). The overall round trip efficiency (electricity to gas and back to electricity) depends on the efficiency of the gas turbine or other electrical generation technology. Weitemeyer et al. (2015) used a round trip efficiency of 30%. This study assumed that a P2G plant would only operate when there was excess renewable electricity available, and so may operate at less than full capacity. The gas turbines were also assumed to operate at partial capacity in response to changes in demand. Therefore the round trip efficiency was set at a lower value of 20% to account for efficiency losses due to these variable operating conditions. This is equivalent to an 18% efficiency drop at both the electricity to gas and gas to electricity conversion stages, which seems a reasonable amount to account for partial capacity efficiency losses. Since electricity was converted into methane only when excess generation was available, rather than at a constant rate, the total load demand was not increased. If charge level in the distributed energy storage system became low, then the P2G system was used to recharge the distributed storage, so that the overall combined generation capacity of both distributed storage and P2G could be maintained. The P2G storage methane leakage rate was set at 0.2% per month (Alvarez et al. 2012). Preliminary estimation of the extra greenhouse emissions at this leakage rate was less than 3 gCO_2e/kWh.

8.2.6 Energy efficiency model

Improving the energy efficiency of the devices that use electricity is a type of demand-side management, where the demand is permanently decreased, rather than increasing generation capacity. Modelling the improvement in

instantaneous power consumption, throughout the day, for a single appliance, device or machine would be complex and dependent on individual usage patterns. However, the model assumed that in aggregate, these would level out, such that the saving in power demand through the day would be a constant fraction of the total load without efficiency improvements:

$$EE_h = \frac{eepc * Load_{y,h}}{100} \text{ MW} \tag{8.6}$$

where *eepc* is the percentage energy efficiency improvement.

Estimates of technically possible improvements in energy efficiency vary. Backlund et al. (2012) estimated 25%, while Nadel et al. (2004) estimated a median value of around 33%. Chua et. al. (2013) estimated a 33% improvement in air conditioning efficiency was readily achievable (air conditioning is a significant portion of the summer peak load), and Matheisen et al. (2011) assumed a 50% decrease in household electricity consumption was possible by 2050. However, there is also significant household use of gas, which is not counted as part of the SWIS electrical demand. Some energy efficiency improvements could result in a shift from gas use to electricity use, for example induction cook tops replacing gas cook tops and reverse cycle air conditioning replacing gas heating. Also other barriers may prevent full implementation, and the rebound effect, where efficiency improvements encourage greater use, may also reduce savings in energy use (Huntington 2011). Therefore a middle range improvement value of *eepc* = 30% was used as a reference in this thesis, with 40% probably achievable. The current global average yearly reduction rate in energy intensity is around 1.5% (REN21 2016, 21). If energy demand on the SWIS decreased at the same rate every year, then after 15 years the energy

efficiency improvement would be about 20%, which was used as a lower bound.

8.3 Results

For the purpose of this study, the results of five scenarios were presented (Figures 8.3 to 8.7 and Table 8.5), although many more combinations are possible. The first scenario considered (S1) was a "small is beautiful" approach, where there is addition of more household solar and distributed storage capacity, but no more large power stations are added to the grid. Every suitable home was provided with a 3.6 kW rooftop PV and 12 kWh battery storage system. Assuming there were about 950,000 suitable houses available by the time installation was complete, the total capacity was 3.42 GW of rooftop PV with 11.4 GWh of storage.

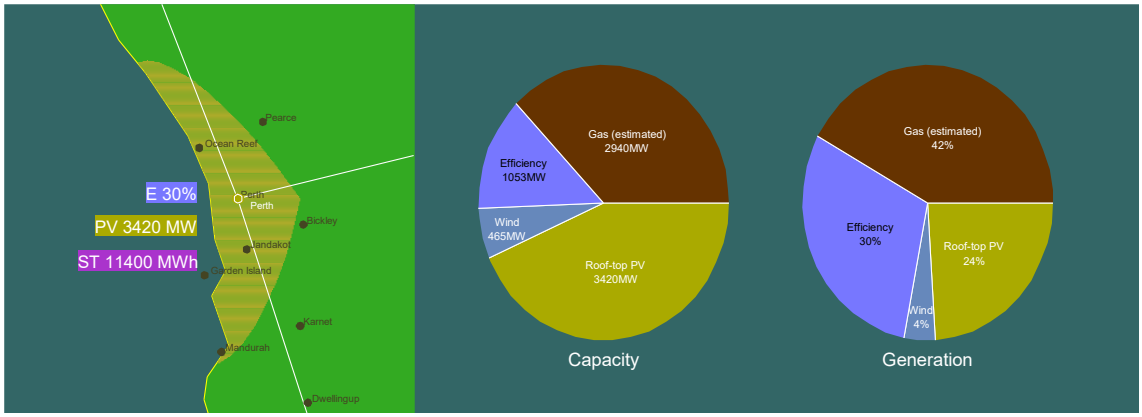

Figure 8.3. Scenario S1, "Small is beautiful": 3.42 GW Rooftop PV, 11.4 GWh of storage, 30% EE improvements. PV stands for photovoltaic, EE stands for energy efficiency.

The PR of the roof top PV arrays was found to vary between 0.79 and 0.93, with the highest values occurring during winter. This was consistent with the findings of Carr and Pryor (2004). The modelling of this scenario indicated that although it was not possible to generate all of the power required by the SWIS using renewable energy, on many days the demand peak was substantially

reduced, and shifted to later in the evening (for example Figure 8.8). The storage system also significantly reduced the maximum ramp rate required from dispatchable generation to balance supply and demand from over 20 MW per minute to under 8 MW per minute.

In this scenario, approximately 20 kWh per household per day on average was generated over a year. This is enough to supply the electricity use of every household on average, even without energy efficiency improvements, or moderate improvements counteracted by a shift from gas to electricity use.

To achieve 100% renewable energy generation, throughout the year, using only roof top PV arrays and storage required the addition of much more PV and storage capacity (Figures 8.4 and 8.9). This scenario (S2) required 19 GW of solar PV and 90.25 GWh of storage to achieve the SWIS reliability standards of a LOLP less than 0.05% and yearly energy shortfall less than 0.002% under typical weather conditions for 95 out of 100 years. This translates to about 20 kW of roof top PV and 95 kWh of storage per household.

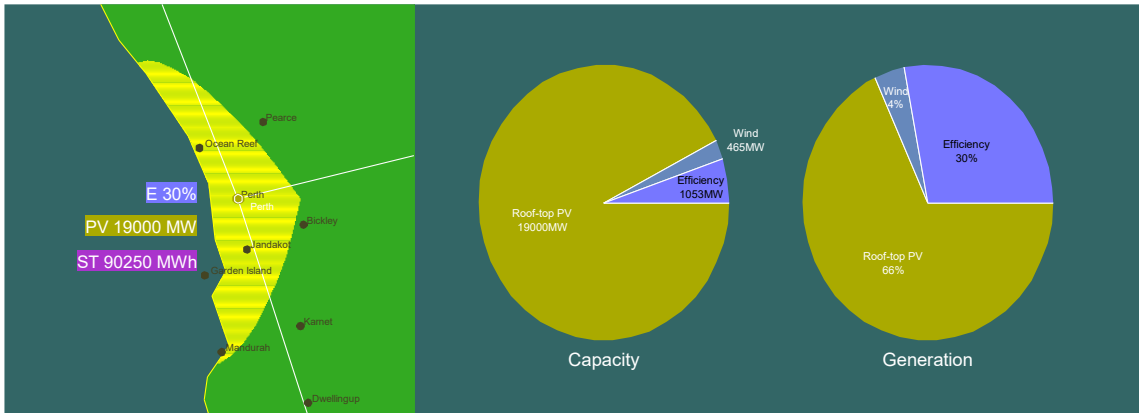

Figure 8.4. Scenario S2, "PV": 19 GW Rooftop PV, 90.25 GWh of storage, 30% EE improvements. PV stands for photovoltaic, EE stands for energy efficiency.

Winter was found to be the most challenging season to meet the energy demand due to the reduced availability of the solar resource and shorter day

lengths. The storage requirement is at the upper end of the range of current electric vehicle battery capacities, but 20 kW of roof top PV per household is not currently feasible, assuming there is little more rooftop area per house that could be utilised. However there is large untapped potential for commercial rooftop PV and the use of other surfaces. If a 250 W Solar PV panel has a surface area of 1.65 m^2, then 126 km^2 of solar PV arrays would be required, which is about 2.3% of the surface area of the Perth greater metropolitan area of 5386 km^2 (AWDC 2011). A technical difficulty for this scenario is that the current SWIS grid is designed for power to flow unidirectionally from the transmission networks to the distribution networks. Residential households are connected to one of the distribution networks and may be supplied via roof top PV and home battery storage from other homes on the same network, but there may be imbalances in the supply and demand within each individual network. Also, some commercial or industrial loads may be connected to the higher voltage sub-transmission network and be inaccessible. Modification would be needed to enable bidirectional power flow between different distribution networks and the sub-transmission network. The maximum power shortfall encountered in 100 years of simulation was 2450 MW, which is greater than the modelled back-up generation capacity of 2034 MW, indicating this scenario could be vulnerable to sustained periods of low solar insolation in the Perth area. The reserve capacity would have to be increased, or an alternative seasonal energy storage or generation system would be needed to replenish the battery storage system. It would not be necessary to keep extra reserve capacity spinning as weather forecasting and the battery storage capacity would allow enough lead time for powering up.

An alternative (scenario S3) was to use solar thermal power stations with storage (Figure 8.5). In this scenario, a reference level of grid distributed

generation and storage was set, where overall household capacity reaches 3.42 GW of PV and 11.4 GWh of battery storage, or 3.6 kW PV and 12 kWh per home as before. The same again is added to commercial properties, to bring the total rooftop PV capacity to 6.84 GW and storage capacity to 22.8 GWh.

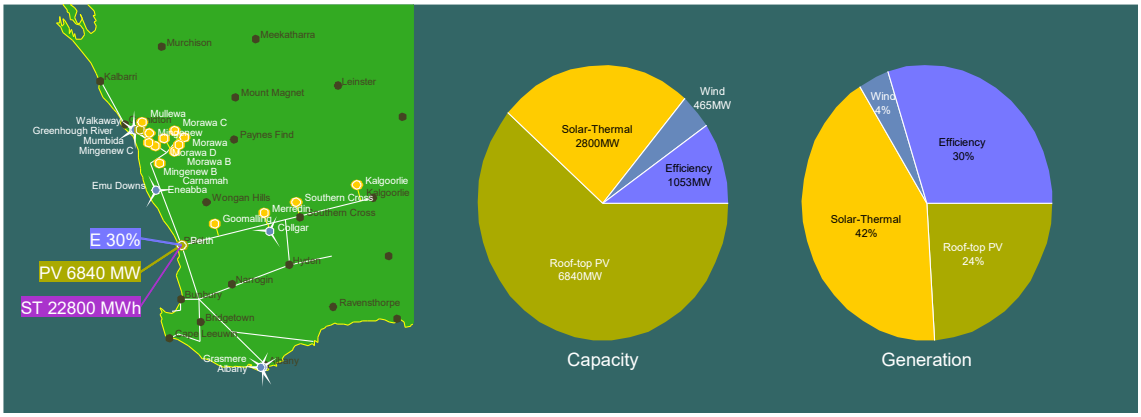

Figure 8.5. Scenario S3, "Solar thermal": 2.8 GW solar thermal (15h thermal storage), 6.84 GW Rooftop PV, 22.8 GWh of storage, 30% EE improvements. PV stands for photovoltaic, EE stands for energy efficiency.

All further demand was met using a network of 14 solar thermal power stations, each with a capacity of 200 MW and molten salt thermal storage capacity of 15 hours. Four solar thermal stations were located to the east of Perth, to help stabilise the grid and take advantage of the solar resource in this low rainfall region. One of the stations was located fairly close to Perth to help provide high inertia centrally located generation, which provides a stable frequency reference for synchronous stability of remote generation. The largest cluster of solar thermal stations was located north of Perth to take advantage of the better solar resource at more northerly latitudes. Transmission line capacity from both of these clusters would need to be upgraded.

For this scenario, winter was again found to be the most challenging season to meet the energy demand, and there was usually excess capacity over the summer months. The maximum power shortfall encountered in 100 years of

simulation was 1163 MW, which is lower than the backup generation capacity of 2034 MW.

A high wind power scenario (S4) was considered next (Figure 8.6). With 2% per year population increase and 30% energy efficiency improvements, the yearly average SWIS power demand by the year 2030 would be about 2.1 GW. Hence if the currently proposed wind farms were built the total wind power capacity would rise to 1947 MW, which could supply around 30% of grid electrical demand assuming the overall capacity factor remains between 0.3 and 0.45, similar to the existing wind farms (see Table 8.2). To meet the whole demand, it was found that increasing the wind power capacity to nearly 8 GW was required, along with enough storage capacity to balance the peaks and troughs in wind power output.

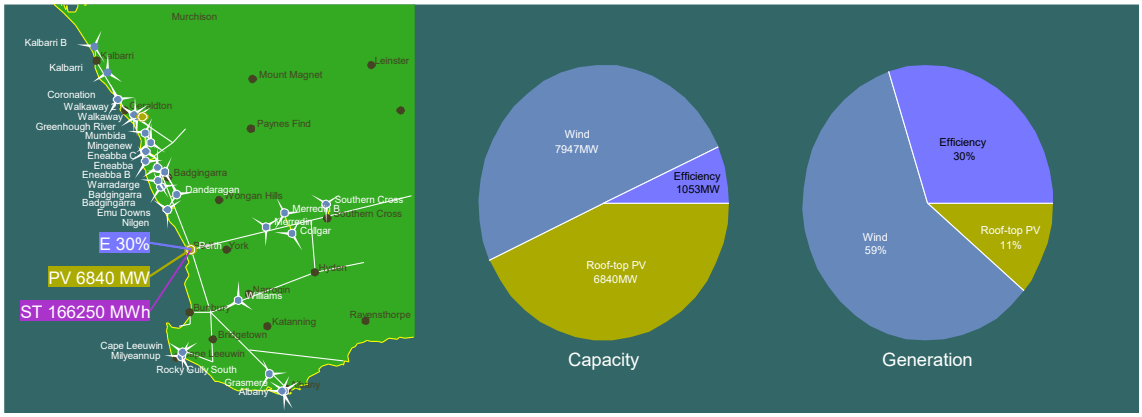

Figure 8.6. Scenario S4, "Wind": 7.947 GW wind, 6.84 GW Rooftop PV, 166.25 GWh of storage, 30% EE improvements. PV stands for photovoltaic, EE stands for energy efficiency.

Assuming that the total rooftop PV capacity reaches 6.84 GW as in scenario S3 before, it was found that a very large storage capacity of 166.25 GWh was needed to meet the SWIS reliability criteria 95% of the time over 100 simulation runs. This equates to 175 kWh of storage per home for 950,000 homes. If the storage capacity is the same as for scenario S3 above (22.8 GWh), then the

energy supply shortfall is about 3%. However, the reliability standards could be met if a P2G plant capable of converting electricity to fuel at a rate of 450 MW was installed on the grid. In this scenario, about 80% of the energy generated was from wind.

Alternatively, if the currently proposed wind farms were built along with solar thermal stations (scenario S5), then only 2.5 GW of solar thermal capacity needed to be built instead of 2.8 GW (Figures 8.7 and 8.10). If less distributed storage was installed, then the required solar thermal capacity increased (Figure 8.11).

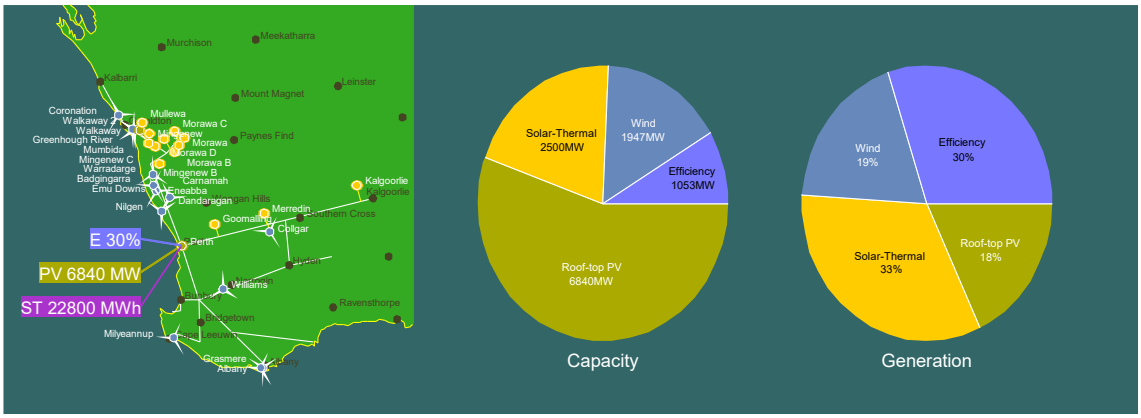

Figure 8.7. Scenario S5, "Mixed Solar thermal and wind": 2.5 GW solar thermal (15h thermal storage), 1.947 GW wind, 6.84 GW Rooftop PV, 22.8 GWh of storage, 30% EE improvements. PV stands for photovoltaic, EE stands for energy efficiency.

The sensitivity of the solar thermal capacity to the level of distributed storage reduced in magnitude as storage capacity decreased to very low levels or increased to very high levels. At low levels, storage was the constraining factor, and was provided by the thermal storage of the power plants. At high levels, storage had saturated and generation capacity was the constraining factor, also provided by the solar thermal power plants.

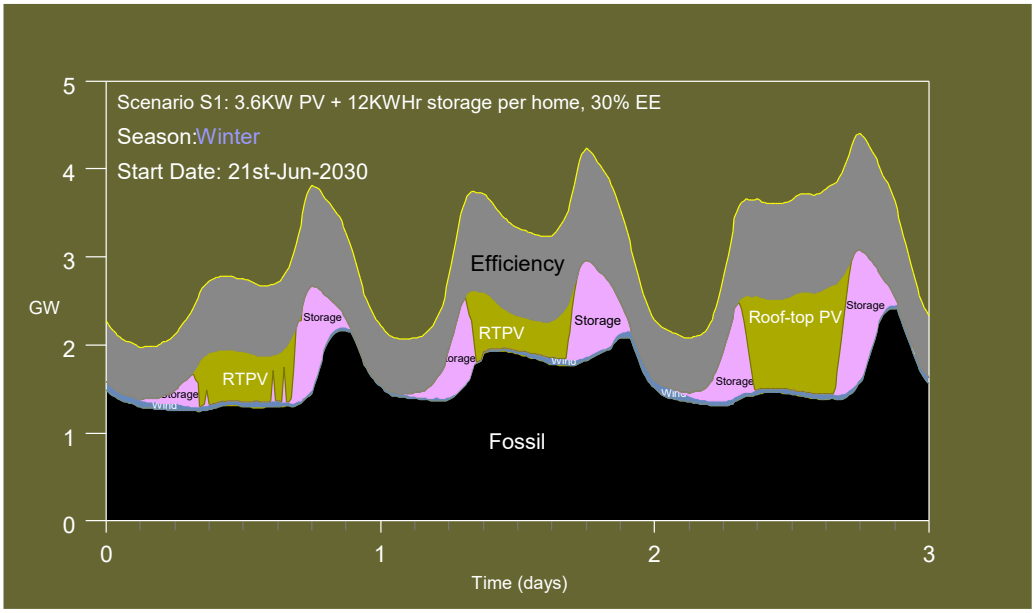

Figure 8.8. Scenario S1 example three day load profile of winter demand peak reduction using household 3.6 kW rooftop solar systems with 12 kWh storage and 30% energy efficiency improvements. Winter was chosen for this example for comparison with other scenarios. RTPV = rooftop photovoltaic arrays.

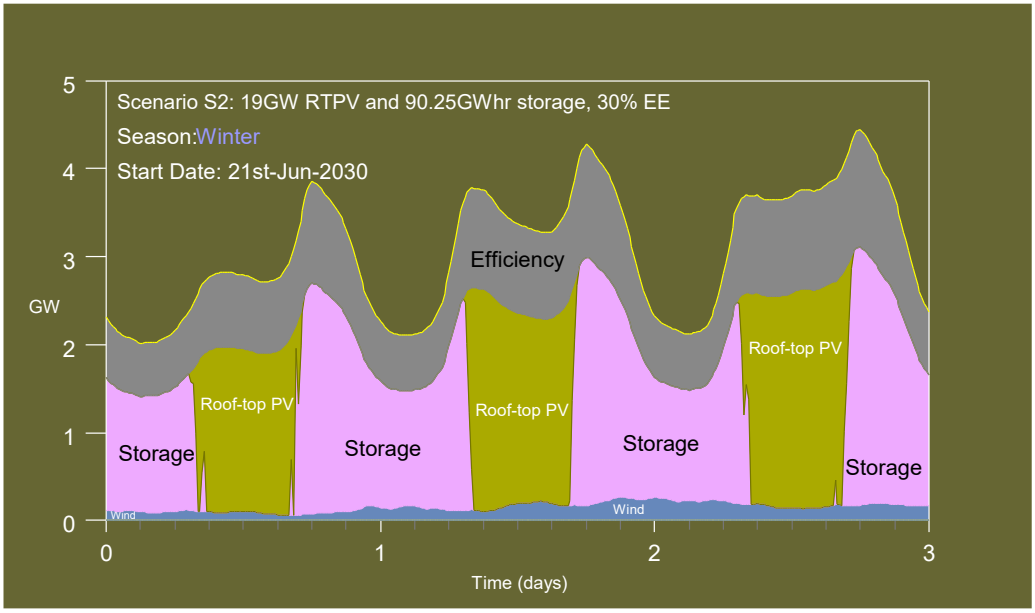

Figure 8.9. Scenario S2 example winter three day load profile of complete renewable energy generation using 19 GW of solar PV systems with 90.25 GWh of storage and 30% energy efficiency improvements. Winter was chosen for this example because this season was found to be the most challenging to meet the energy demand due to the reduced availability of the solar resource and shorter day lengths.

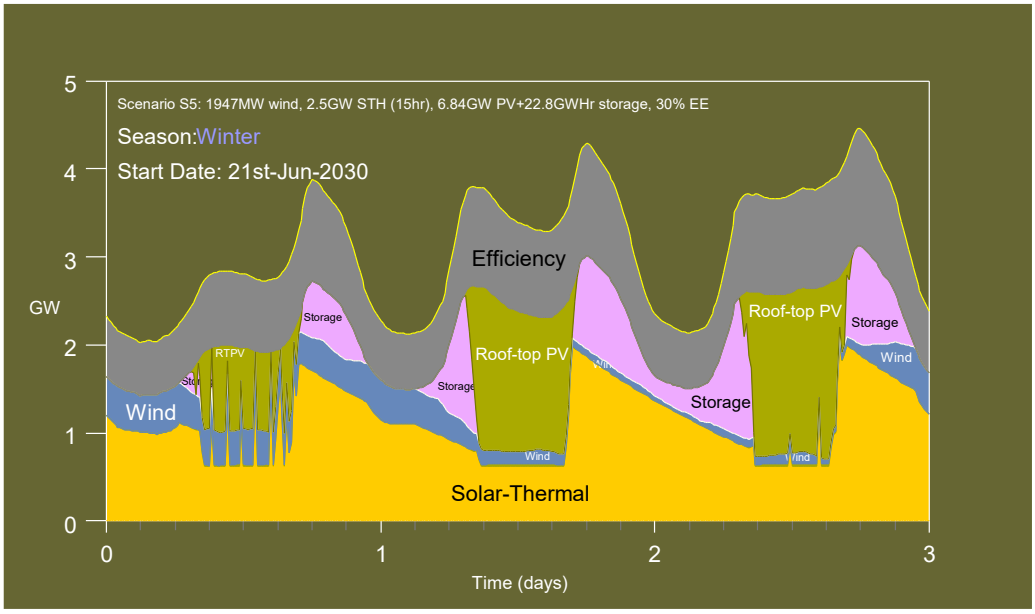

Figure 8.10. Scenario S5 example winter three day load profile of complete renewable energy generation using 2.5 GW of solar thermal stations (with 15h thermal storage), 1947 MW wind power, 6.84 GW rooftop solar PV systems with 22.8 GWh of storage and 30% energy efficiency improvements. Winter was chosen for this example because this season was found to be the most challenging to meet the energy demand due to the reduced availability of the solar resource and shorter day lengths. RTPV = rooftop photovoltaic arrays.

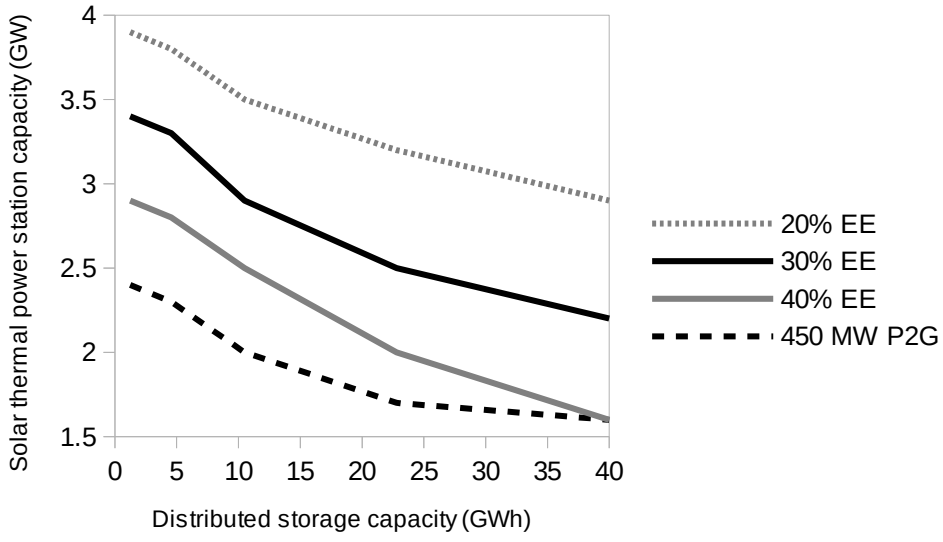

Figure 8.11. Solar thermal power plant capacity required for different levels of distributed storage capacity for variations of scenario S5. The input power capacity of the Power to Gas (P2G) system was 450 MW with round trip efficiency of 0.2. EE stands for energy efficiency improvements.

If a 450 MW P2G system was installed with round trip efficiency of 20%, similar to the high wind scenario S4, then required solar thermal capacity was decreased significantly at all storage levels (Figure 8.11), and to 1.7 GW at the reference 22.8 GWh distributed storage level. Alternatively, if no P2G system was used but energy efficiency measures were increased from 30% to 40%, then another 500 MW of solar thermal capacity could be avoided at the reference 22.8 GWh storage level, reducing the total to 2 GW. At high storage levels this 10% increase in efficiency was almost as effective as the P2G system at reducing the required solar thermal capacity. However, if energy efficiency improvements only reached 20%, then the amount of required solar thermal capacity increased by 700 MW at the reference 22.8 GWh distributed storage level.

Table 8.5. Installed capacity for each 100% renewable scenario for the SWIS electrical grid.

Scenario	Energy efficiency	Solar PV	Distributed storage	Power to gas	Solar thermal	Wind
Current SWIS capacity	-	500 MW*	120 MWh*	-	-	465 MW
S2 PV	30%	19 GW	90.25 GWh	-	-	465 MW
S3 Solar thermal	30%	6.84 GW	22.8 GWh	-	2.8 GW	465 MW
S4 Wind	30%	6.84 GW	166.25 GWh	-	-	7.947 GW
S4 + P2G	30%	6.84 GW	22.8 GWh	450 MW	-	7.947 GW
S5 Mixed solar thermal and wind	30%	6.84 GW	22.8 GWh	-	2.5 GW	1.947 GW
S5 + P2G	30%	6.84 GW	22.8 GWh	450 MW	1.7 GW	1.947 GW
S5 + less EE	20%	6.84 GW	22.8 GWh	-	3.2 GW	1.947 GW
S5 + more EE	40%	6.84 GW	22.8 GWh	-	2 GW	1.947 GW

*Estimated

The required capacities for each technology in each scenario were now finalised (Table 8.5), and the required installation schedules for each scenario could be estimated (Table 8.6).

Table 8.6. Yearly constant installation rates required for each 100% scenario to be completed by the year 2030.

Scenario	Energy Efficiency*	Solar PV	Distributed storage	Power to gas	Solar thermal	Wind
S2 PV	2%	1267 MW	6017 MWh	-	-	-
S3 Solar thermal	2%	187 MW	1520 MWh	-	187MW (or one 200MW plant per year for 14 years)	-
S4 Wind	2%	187 MW	11083 MWh	-	-	433 MW
S4 + P2G	2%	187 MW	1520 MWh	30 MW	-	433 MW
S5 Mixed solar thermal and wind	2%	187 MW	1520 MWh	-	167 MW (or one 200 MW plant per year for 12 years and then one 100 MW plant)	99 MW
S5 + P2G	2%	187 MW	1520 MWh	30 MW	113 MW (or one 150 MW plant per year for 11 years and then one 50 MW plant)	99 MW
S5 + less EE	1.33%	187 MW	1520 MWh	-	213 MW	99 MW
S5 + more EE	2.67%	187 MW	1520 MWh	-	133 MW (or one 200MW plant per year for 10 years)	99 MW

PV = photovoltaic arrays, EE = energy efficiency improvement. *% reduction of load demand with no efficiency improvements.

Solar PV, wind, and battery storage have exhibited the potential for exponential growth in installed capacity, and energy efficiency improvements could be represented as a percentage reduction in energy demand. When compared to current global growth rates (Table 8.7), the required growth rates for these

technologies were either less or similar in most cases, except for the high PV and wind scenarios S2, S4 and S4+P2G, which would require accelerated roll out of distributed storage, and wind capacity for the high wind scenarios.

In all scenarios except the low efficiency scenario (S5 + less EE), to reach 30% energy efficiency improvements in 15 years would require an accelerated reduction in demand compared to the current global improvement rate. However the 2.35 to 3.35% rate of demand reduction per year seemed feasible, especially since the amount of reduction actually decreases as demand reduces.

Table 8.7. Yearly exponential installation rates for each 100% scenario to be completed by the year 2030.

Scenario	Energy efficiency	Solar PV	Battery storage	Wind
Current SWIS capacity	-	500 MW*	120 MWh*	465 MW
Global growth rate 2015	1.5%[a]	28%[b]	50%[c]	17%[b]
S2 PV	2.35%	27.5%	55.5%	-
S3 Solar thermal	2.35%	19%	41.9%	-
S4 Wind	2.35%	19%	62%	20.8%
S4 + P2G	2.35%	19%	41.9%	20.8%
S5 Mixed solar thermal and wind	2.35%	19%	41.9%	10%
S5 + P2G	2.35%	19%	41.9%	10%
S5 + less EE	1.48%	19%	41.9%	10%
S5 + more EE	3.35%	19%	41.9%	10%

*Estimate. [a]% reduction in energy intensity per year (REN21 2016). [b]REN21 (2016). [c]IRENA (2015).

There is currently no installed capacity of solar thermal power tower and power to gas plants on the SWIS, so an exponential growth rate for these technologies could not be quantified. These are the least mature technologies. Required installed capacity for both was reduced by high installation rates of energy efficiency improvements and distributed storage.

For all of the 100% renewable energy scenarios (S2 to S5), it was found that winter was the most challenging time for the power systems, because of the

lower availability of solar and wind resources, and shorter day length. Therefore significant extra capacity had to be installed, resulting in generation overcapacity during the summer months.

For all of these scenarios, the reference storage capacity was 22.8 GWh. Reserving the upper and lower 5% of storage capacity to provide synthetic inertia meant that the storage system could provide at least 228 GWs of inertia, much greater than the 12.4 GWs of inertia on the present SWIS grid (Table 8.8), and also absorb or supply more than 4 GW of power for 15 minutes in response to a sudden load change or generation fault. 15 minutes is enough time for the spinning reserve generators to start generating power and provide spinning reserve if required. Hence the storage system could provide frequency stability control services as well. To provide these services a portion of the storage capacity would have to be connected directly to the transmission and sub-transmission networks, rather than the distribution networks that connect most homes. The lowest storage level considered in Figure 8.11 was 1.24 GWh, enough to provide the same inertia as the present SWIS grid.

Table 8.8. Synthetic inertia from reserving the upper and lower 5% of storage capacity for each 100% renewable energy scenario.

Scenario	Storage (GWh)	Inertia (GWs)	Current SWIS inertia (GWs)
S2	90.25	902.5	12.4
S3	22.8	228	12.4
S4	166.25	1662.5	12.4
S4 + P2G	22.8	228	12.4
S5	22.8 (1.24 to 40)	228 (12.4 to 400)	12.4
S5 + P2G	22.8 (1.24 to 40)	228 (12.4 to 400)	12.4
S5 + less EE	22.8 (1.24 to 40)	228 (12.4 to 400)	12.4
S5 + more EE	22.8 (1.24 to 40)	228 (12.4 to 400)	12.4

For scenarios S3 to S5, most of the large generators are far from the main load centre (the Perth area). Therefore the spinning synchronous compensator reserve close to Perth may aid the synchronous stability of the large remote generators. In these scenarios, the maximum power shortfall encountered in 100 years of simulation was lower than the back-up generation capacity of 2034 MW. This indicated that for those rare times of sustained and widespread low solar and wind generation, the reserve could most probably compensate for shortfalls without any load shedding.

Table 8.9. Potential peak power flow running through the three main transmission corridors to Perth for each 100% renewable energy scenario.

Scenario	Generation type	Southern corridor (MW)	Eastern corridor (MW)	Northern corridor (MW)
S2	Solar	0	0	10
	Wind	35	206	223
	Total	35	206	233
S3	Solar	0	800	2010
	Wind	35	206	223
	Total	35	1006	2233
S4	Solar	0	0	40
	Wind	1300	1706	4940
	Total	1300	1706	4980
S4 + P2G	Solar	0	0	40
	Wind	1300	1706	4940
	Total	1300	1706	4980
S5	Solar	0	600	1940
	Wind	300	206	1440
	Total	300	806	3380
S5 + P2G	Solar	0	600	1140
	Wind	300	206	1440
	Total	300	806	2580
S5 + less EE	Solar	0	600	2640
	Wind	300	206	1440
	Total	300	806	4080
S5 + more EE	Solar	0	600	1440
	Wind	300	206	1440
	Total	300	806	2880

Also in these scenarios, generation capacity tends to move from fossil fuel based generation in the south to solar and wind generation in the north and east, hence transmission capacity would need to be expanded along the northern and eastern corridors. With a back-up generation capacity of 2034 MW, scenarios S3 to S5 were found to be potentially vulnerable to a simultaneous interruption of all transmission capacity along the northern corridor (Table 8.9). The distributed storage system could compensate for a short time, however transmission line expansion should use multiple lines to reduce the probability of complete failure, or else reserve capacity should be increased.

9 Discussion

The results of this simulation indicated that for typical weather conditions it is feasible to supply 100% of the energy demand of the SWIS system, projected out to the year 2030, on an hour by hour basis using a combination of energy efficiency measures, residential and commercial roof top photovoltaic systems, solar thermal power stations with heat storage, wind power and distributed battery storage systems. All of these technologies are currently available, with energy efficiency, wind, solar PV, in large scale commercial operation and battery storage approaching large scale production. Although costs are not explicitly considered, the costs of wind power and solar PV have fallen rapidly over the past decade, to the point where new build wind power in particular can compete with new build fossil fuel power stations. However, the costs of solar thermal stations are currently higher, as they are not as far along the development curve. For 100% renewables, the over-generation required to cover winter loads will increase the capital costs. The use of battery storage enabled buffering of the variable output of solar PV and wind farms, meaning that the maximum ramping rates required of the dispatchable generators could be limited, which has the potential to reduce costs during transition periods when both renewable power generators and conventional fossil based generators are connected to the grid. The level of storage needed in the 100% renewable energy storage scenarios meant that, as well as providing synthetic inertia, participation in primary and secondary frequency stability control services was possible. This would reduce the need to keep existing synchronous generators spinning to provide these services, however they are needed to provide a backup in the case of generation shortfall or transmission line fault.

The estimated synthetic inertia for these scenarios (S2 to S5) was greater than the inertia currently on the SWIS grid, confirming that the amount of distributed battery storage is compatible with grid stability.

The solar thermal scenario S3 and mixed scenario S5 used 22.8 GWh of storage, which is equivalent to 0.95 gigawatt days. This is consistent with the claim by Pickard et al. (2009) that storage levels in the order of gigawatt days would be needed to maintain grid stability. However this level of storage came about from a 'bottom-up' approach. It was a tally of the storage capacity if 90% of homes installed a small 12 kWh storage system, and commercial buildings matched them. The PV scenario S2 required 90.25 GWh of storage (3.76 gigawatt days), and the predominant wind scenario S4 with no P2G storage required a much higher 166.25 GWh (6.93 gigawatt days). These were determined by a 'top-down' approach of meeting the SWIS reliability standards. Thus the claim by Pickard et al. (2009) was supported in these two scenarios.

The simulation assumed typical weather conditions in which the solar and wind resources are strongest in the summer season and weakest in the winter season, when day length is short. Similar to the findings of Elliston et al. (2012), the winter evening peak period was the most difficult to supply, and there was usually large overcapacity in the summer months. If winter weather conditions are encountered that cause a shortfall in generation from solar and wind, then a reserve source of energy could be used to maintain storage levels and required generation.

The results of the scenarios with a P2G system indicated that this kind of system could act as a reserve and significantly reduce either the required solar thermal and storage capacity, or both, and may be necessary for a high wind power scenario to meet SWIS reliability standards without a very large amount

of storage. However this technology is still in the development stage. The balance between using more distributed storage or more P2G capacity would be an economic decision as well as a technical one. Improving the flexibility and efficiency of P2G systems should be a priority. Improving energy efficiency reduced the capacity of solar thermal power, distributed storage or P2G needed to supply the demand.

Alternatively to P2G, a renewable energy resource that is strong during the winter months, such as wave power (Hughes and Heap 2010), could be utilised. Wave power technology is advancing into commercial operation and it is worthwhile modelling the potential contribution to the SWIS grid. Another possible option is the use of biomass, which can be stored on seasonal time scales until it is needed, but attracts controversy over the use of native forest wood for fuel and the substitution of food production for energy production. Oil mallee biomass (Wu et al. 2008), from land in the wheat belt that cannot be used for food, may avoid both problems. However the capacity for sustainable large-scale production must be modelled, and also biomass cannot utilise any excess summer electrical generation from solar and wind. There have been proposals for ocean water pumped hydro storage systems that utilise the height of coastal cliffs (Hearps et al. 2014), as an alternative to only having battery storage. These could also store excess energy on seasonal time scales, and could utilise excess summer generation, although the main use is likely to be on daily time scales.

The installation rates required to implement each of the scenarios differed significantly, particularly with the yearly addition of storage capacity required. The predominant wind scenario S4 required the highest uptake at almost 11.1 GWh per year, or almost 64,000 homes per year with 175 kWh of storage each, which seems unrealistic. However if a more realistic storage level was reached,

and there was some other form of renewable energy available to cover the shortfall, then this scenario might be more viable. The mixed solar thermal and wind scenario S5 had the most balanced uptake rates, with reduced uptake rate for solar thermal power stations compared to the predominant solar thermal scenario S3. Solar thermal power station technology is perhaps the least commercially mature but the requirement to build one 200 MW plant per year seems feasible. Wind power is the most commercially mature technology, however uptake rates are limited by transmission line capacity limitations and necessary approval processes even though much of the land used by wind farms can still be used for other purposes. Use of the currently proposed new wind farm projects could be expected to reduce the lead times required. Energy efficiency, roof top PV, and distributed storage can perhaps be implemented the fastest, as they require no or little extra land. The value of implementing energy efficiency measures in reducing the required generation was demonstrated in scenario S5 and should be considered one of the most effective components of a large scale renewable energy electricity system. However, further improvements in energy efficiency become more difficult as efficiency improves. Use of the currently proposed new wind farm projects in the mixed solar thermal scenario S5 meant that 300 MW of solar thermal capacity was avoided compared to scenario S3, or about 15% of the installed wind power. This was within the 5-40% range of capacity credit (or effective load carrying capacity) for wind power found by DOE (2008) and similar to the Irish and Norwegian findings of around 14% at higher penetrations of wind power (Holttinen et al. 2007).

The development of this accessible interactive simulation tool that can be run in a web browser allowed different scenarios to be easily considered and modified. However this tool cannot be used to decide precise locations for

renewable energy power stations, as the solar and wind models are designed for simplicity and quick computation. However its greatest strength is as a first approximation tool to gain an idea of the scale of renewable energy capacity required for the SWIS to move to a 100% renewable energy system. Much more detailed solar and wind resource modelling, land use mapping and transmission system planning would be required to decide the actual sites.

This study modelled a snapshot of the possible SWIS hourly demand profile in the year 2030. Faster population increase, large-scale adoption of electric vehicles or a large-scale switch from using gas to using electricity could all significantly increase the demand for electricity from the SWIS grid, and hence the need to build more renewable energy capacity and improve energy efficiency. Improvements in energy efficiency could compensate for population growth in the short to medium term. Reductions in transportation energy use would require significant uptake of public transport and reorganisation of economic activity and housing densities. The rooftop area available for PV could be affected by changes in the housing mix as population grows. Conversely, improvements in PV cell efficiency will increase the capacity available for a given rooftop area. The urgency of reducing emissions is balanced by renewable energy technologies that are expanding rapidly on a global scale, which makes the task realistic. This simulation demonstrates the feasibility of a 100% renewable energy system for the SWIS. Although the costs will be higher for a rapid build, the urgency of reducing greenhouse emissions and the far higher economic, social, environmental and health costs of failing to prevent dangerous climate change, as well as the increase in human mortality, mean there is every justification to pursue this option.

10 Conclusions

This chapter addresses the original research questions and provides a wrap up of the main findings and implications of this research.

10.1 Research questions revisited

The principal objective of this research has been to answer the following questions:

1. *Do existing solar and wind renewable energy systems currently offer the best path for achieving a rapid transition to a sustainable, low emission, electricity system for the South West of Western Australia?* The principal criterion is the ability to rapidly expand generation and reduce greenhouse gas emissions. There are also ancillary criteria that should be considered, such as reliability, water use, and environmental impact. Cost is also an important factor. However, given the urgency of the climate situation, rapid reduction in greenhouse emissions must outweigh near term cost, or the long term cost is likely to be much greater.

2. *As a corollary to the first question, just how far can the renewable energy path be taken?* Can solar and wind renewable energy systems, aided by storage and energy efficiency improvements, completely replace the existing conventional generation systems? Is a 100% renewable energy system a technically feasible option for the SWIS?

These questions were answered in two parts. Firstly, an extensive literature search was conducted and three different options for reducing emissions

quickly were examined and compared. These options were nuclear power, Carbon Capture and Storage (CCS), and renewable energy. Secondly, models for solar power (both PV and solar thermal), wind power, storage (both battery and molten salt) and energy efficiency were developed. By comparing the total generation for a fleet of solar and wind stations with total load demand, on an hour by hour basis, several different scenarios for 100 percent renewable electricity supply for the SWIS grid were developed. The reliability and construction schedules for these scenarios were examined.

10.2 Summary of key findings

10.2.1 Literature search

The literature search compared renewable energy to two other major options, nuclear power and carbon capture and storage. The relative merits of each option were summarised in Table 3.6 and repeated here in Table 10.1.

The growth rates of solar and wind energy systems were found to be currently much greater than either nuclear or CCS systems, and the ability to expand nuclear and CCS systems fast enough to avoid dangerous climate change was found to be questionable. Further investment in deploying these technologies would be a dead end unless alternatives such as renewables cannot be deployed quickly enough to avoid dangerous climate change, or cheaply enough to avoid the economic attractiveness of interim measures. The use of renewable energy and energy efficiency was found to be the most viable option, but many questions remain about the large-scale deployment of these technologies. On a global scale, there are more than enough renewable energy sources to meet world energy demand, though some countries have more resources available than others.

Table 10.1. Advantages and disadvantages of alternative technologies for reducing emissions from electrical power generation.

Technology	Advantages	Disadvantages
Nuclear power	Current large installed base	Can't provide peaking power efficiently, safety concerns, weapons proliferation, waste disposal, cost, poor scalability, slow pace of emission reductions, resource limitations, high water use, threat to civil liberties
Renewable energy	Modularity, good scalability, rapid pace of emissions reductions, wide distribution of resources	Variability, diffuse resource, need for storage or reserve generation, possible material constraints, possible constraint on battery deployment, high water use for solar thermal with water cooled systems
Carbon Capture and Storage (CCS)	Can be applied to existing power plants	Poor scalability, unknown pace of emission reductions, leakage concerns, cost, health concerns, resource limitations, high water use

Embodied energy and life-cycle emissions of any of the technological choices, coupled with the risk of reaching a climate tipping point, mean there is an upper bound to their growth rate if they are to play an effective role in reducing greenhouse emissions. Renewable energy breeding and improvements in energy efficiency are potential ways to achieve a rapid transition to a low emission energy system, and also improvement in global living standards without increasing overall energy use. To restrain net manufacturing energy requirements and environmental impacts, recycling of batteries and improving their cycle lives will be high priorities if the current battery technologies are to be used for grid electrical energy storage on a large scale.

The short-term spatial and temporal variability of solar and wind energy systems is a challenge that must be met for these technologies to have a significant impact. Storage and the use of sustainable bioenergy as reserve generation were identified as ways to balance the supply and demand variability. Conversely, the modularity, scalability, and short lead times of solar and wind technologies mean there is lower long-term financial uncertainty than in large fossil or nuclear plants. Small fossil fuel cell or gas turbine technologies may also reduce long-term financial uncertainty. The distributed nature of many renewable energy forms and their localised sources of energy confers energy security advantages compared to fossil and nuclear power in many countries (though not in the case of Australia which has its own coal and uranium reserves). The lower levels of air pollution and waste disposal problems are also advantages.

10.2.2 Model development

The second part of this research involved simulation of hypothetical 100 percent renewable energy (including energy efficiency) scenarios for electrical supply of the SWIS grid. Models, which were simple and fast enough to allow for interactive operation, were built to simulate solar and wind resources on an hourly time scale for any location in the South West region of Western Australia. Simple models for solar PV power generation and battery storage were also developed. A generic solar power tower model with molten salt heat storage was developed and calibrated to the power tower model used by the System Advisor Model (SAM). With the integration of all these models, it was possible to simulate hour by hour energy generation and electricity demand for the overall SWIS grid, and develop scenarios for energy supply under different configurations of renewable energy systems. It was found that:

1. For the solar model, if a single metric of 'cloudiness' was simulated, then the beam, diffuse and reflected components of irradiance could be efficiently obtained from the same components estimated for clear sky conditions. Hence the model could be used in simulations of both flat surface devices (such as PV) and concentrating solar power devices (such as solar thermal), and the flat surface devices could be angled at different tilt angles to horizontal. Since rainfall and cloudiness tend to decrease further inland from the coast of Western Australia, position along the coast and distance inland were used as alternative position metrics to latitude and longitude, to simplify the required calculations. Data from weather stations concentrated in the South West region of Western Australia were used to calibrate and test the simulation. The model generated synthetic horizontal radiation data on hourly, daily and seasonal time scales with accuracies in the range of other models developed for wide areas or several locations, and also generated hourly cloudiness data with reasonably similar statistical characteristics to the measured data. Therefore in other parts of the world with a pattern of declining rainfall inland from the coast, there is potential for using position along the coast and distance inland as alternative position metrics to latitude and longitude, to simplify the required calculations.

2. Measurements of wind speed near the ground do not give a good representation of wind speeds at the hub height of modern wind turbines, so wind speed data at 50m above the ground from the MERRA global atmospheric database were used to calibrate the wind power generation model, along with hub-height measured data at two sites to characterise the wind shear. Simulated wind power output on hourly, daily and seasonal time scales was compared to measured SCADA data

from wind farms already operating on the SWIS grid. Analysis of the MERRA data indicated that wind sites closer to the coast tended to have diurnal output peaks in the afternoon, earlier than those wind sites further inland which peak later in the evening. Also, the normalised residual of hourly wind speed had a double exponential distribution rather than a normal distribution. A translated square-root transformation function $y_n=(\sqrt{(1.96+y_e)}-1.4)/0.302$ was used to convert this to a normal-like distribution so that autoregressive time series analysis could be used to develop the model. Wind farm capacity factors were found to have a greater correlation to other wind farms (as a function of distance) when estimated from MERRA data than when calculated directly from the measured SCADA data. Hence there may be more variability in air density, wind shear factor, wind farm wide wind speed variability, or some other factor than accounted for using solely MERRA data. Therefore the model used historical measured distance correlation data to calibrate distance correlation between wind farms, rather than MERRA data. Simulated wind power output was compared to measured wind power output at the six largest wind farms in Western Australia. The simulation tended to generate slightly conservative wind power output values compared to the measured values. Since the MERRA database has global coverage, using it in other parts of the world to simulate hourly wind power generation from multiple wind farms is a viable option if hub height wind speed data is not available. However, possible discrepancies in distance correlation must be accounted for.

3. The year 2009 was the last year before significant amounts of rooftop solar PV systems were connected to the SWIS grid, so this year was used

as a base year for the hour by hour electricity demand profile. Starting with the level of renewable energy generation present in 2015, a target year of 2030 for complete renewable energy generation was set, and electricity demand was increased with population growth and then also potentially decreased if energy efficiency measures were deployed. The number of homes suitable for roof top PV and storage installation was projected to increase from around 653 000 in 2011 to around 950,000 by 2030. It was found that if energy efficiency measures reduced demand by 30%, and the 950,000 suitable homes each had a 3.6 kW rooftop solar array and 12 kWh of battery storage, then current residential electricity demand of 17 kWh per home per day could be supplied, and the demand peak would be reduced and shifted to later in the evening on many days. However the total SWIS demand could not be met.

4. The current SWIS reliability standards are a loss of load probability of no more 0.05%, and no more than a 0.002% shortfall in generated energy over one year. If energy efficiency was improved by 30%, commercial roof tops and other surfaces were utilised such that 126 km^2, or about 2.3% of the surface area of the Perth greater metropolitan area of 5386 km^2, was covered in solar panels to bring capacity up to 19 GW, and 90.25 GWh of storage (95 kWh per household on average) was added, then the SWIS grid could be completely powered from the sun, meeting the current reliability standards at least 95 times out of 100 under typical weather conditions. Even though summer peak demand is greater, winter was found to be the most challenging season to meet the energy demand due to the reduced availability of the solar resource and shorter day lengths. Because of the geographic concentration of most solar

power generation in one area, this scenario is more likely to be vulnerable to prolonged periods of low solar insolation around Perth.

5. A reference level for grid distributed generation and storage was set at 6.84 GW of residential and commercial rooftop solar PV arrays, and 22.8 GWh of battery storage. This was equivalent to 3.6 kW PV and 12 kWh storage per home for the 950,000 homes, with the same again added to commercial properties. With these systems in place, a combination of 30% improvement in energy efficiency and 2.8 GW of solar thermal power stations (with 15 hours storage) could supply the total SWIS demand, meeting the current reliability standards. The winter months were again the most challenging time for meeting the demand.

6. Although onshore wind power is now one the cheapest forms of energy generation, a scenario relying mainly on wind power required nearly 8 GW of wind power capacity, 6.84 GW solar PV and very large amounts of distributed storage (166.25 GWh), to meet the current reliability level of the SWIS grid. This high storage requirement might reflect the smaller geographic distribution of energy generation, in that solar is not generated from locations outside Perth city. If 22.8 GWh storage was used instead (similar to the previous scenarios), then the energy shortfall was about 3%, leaving open the possibility of using biomass or some other renewable energy source as a backup. Alternatively a Power to Gas (P2G) system with a capacity to convert up to 450 MW of excess electricity from the grid into methane, and a round trip efficiency (electricity to gas to electricity) of 20% could provide seasonal storage and enable the high wind system to meet the reliability standards with 22.8 GWh of distributed storage.

7. Wind power could be used to reduce the required capacity of the solar thermal scenario. A combination of 30% improvement in energy efficiency, 1947 MW of currently proposed wind farms, 2.5 GW of solar thermal power stations (with 15 hours storage), with the reference 6.84 GW of residential and commercial rooftop solar arrays, and 22.8 GWh of distributed storage could supply the total SWIS demand. 300 MW of solar thermal capacity was avoided, or about 15% of the installed wind power. This was within the 5-40% range for capacity credit found by DOE (2008) and similar to the Irish and Norwegian findings (Holttinen et al. 2007).

8. The sensitivity of the required solar thermal capacity to the level of distributed storage reduced in magnitude as storage capacity decreased to very low levels or increased to very high levels. At low levels, storage was the constraining factor, and was provided by the thermal storage of the power plants. At high levels, storage had saturated and generation capacity was the constraining factor, also provided by the solar thermal power plants.

9. If energy efficiency improvements could be increased to 40%, then a further 500 MW of solar thermal capacity was able to be avoided at the 22.8 GWh distributed storage level, indicating that improving energy efficiency should be a priority for any renewable system roll out. Alternatively, around 10 GWh of distributed storage (see Figure 8.11) could be avoided at the 2.5 GW solar thermal capacity level, again emphasising the importance of energy efficiency improvements, given the possible embodied energy and environmental constraints to large scale battery production.

10. A 450 MW P2G system with a 20% round trip efficiency significantly reduced the required solar thermal capacity at all levels of distributed storage. At very high levels of distributed storage, increasing energy efficiency became almost as effective as P2G at reducing the required solar thermal capacity.

11. The 100% renewable energy scenarios all had distributed storage on the grid. This storage was kept in a partially charged state so that synthetic inertia could be provided. The lowest level of storage considered was 1.24 GWh, estimated to provide around 12.4 GWs of inertia, similar to the inertia presently on the SWIS grid. At the reference 22.8 GWh storage level, the synthetic inertia was estimated to be at least 228 GWs, far more than presently on the SWIS grid.

12. The solar thermal scenarios used 22.8 GWh of storage as a reference, which is equivalent to 0.95 gigawatt days. This is consistent with the claim by Pickard et al. (2009) that storage levels in the order of gigawatt days would be needed to maintain grid stability. However this level of storage came about from a 'bottom-up' approach. It was a tally of the storage capacity if 90% of homes installed a small 12 kWh storage system, and commercial buildings matched them. The PV scenario required 90.25 GWh of storage (3.76 gigawatt days), and the predominant wind scenario required a much higher 166.25 GWh (6.93 gigawatt days). These were determined by a 'top-down' approach of meeting the SWIS reliability standards. Thus the claim by Pickard et al. (2009) was supported by these scenarios.

13. For all of these 100% renewable energy scenarios, it was found that winter was the most challenging time for the power systems, because of

the lower availability of solar and wind resources, and shorter day length. Therefore significant extra capacity had to be installed, resulting in generation overcapacity during the summer months.

14. The installation rates required to implement each of the scenarios differed significantly, particularly with the yearly addition of storage capacity required. The predominant wind scenario required the highest uptake at almost 11.1 GWh per year, or almost 64,000 homes per year with 175 kWh of storage each. The mixed solar thermal and wind scenarios had the most balanced uptake rates, with reduced uptake rates for solar thermal power stations compared to the predominant solar thermal scenario. The required average yearly uptakes were a 2% improvement in energy efficiency per year, 187 MW of rooftop PV per year, 1520 MWh of distributed storage per year, 167 MW of solar thermal capacity per year, and 99 MW of wind power per year. If the uptake of energy efficiency measures were increased to 2.67% per year, then the rate of solar thermal capacity uptake could be reduced to 133 MW per year. Compared to current exponential global growth rates of solar PV, wind, storage, and energy efficiency, only efficiency improvements needed to be implemented at a faster rate (2.35% per year exponential reduction in energy use compared to 1.5%).

The overall finding was that the answer to the second research question is yes. Solar and wind renewable energy systems, aided by storage and energy efficiency improvements, could completely replace the existing conventional generation systems. A 100% renewable energy system is a technically feasible option for the SWIS, and the required installation rates for many of the scenarios considered here are reasonable, given a short time frame of completion by 2030. Although the costs will be higher for a rapid build, the

urgency of reducing greenhouse emissions and the far higher economic, social, environmental and health costs of failing to prevent dangerous climate change, as well as the increase in human mortality, mean the overall cost will still be far less. Care must be taken to minimise direct environmental impacts by siting wind farms and solar power stations on previously cleared land (such as farms) if possible, away from bird migration corridors, and close to existing transmission line corridors.

Some preliminary cost estimates have been made for the 100% renewable energy scenarios (Laslett 2017). These estimates indicate that the S4+P2G scenario, with high wind capacity and utilising power to gas storage, is the cheapest at current prices, but there is great uncertainty over the costs of the nascent P2G technology. The cost of the mixed scenario S5 was reduced by increasing energy efficiency measures, which might be achieved using more mature technologies. Also the costs of many renewable energy technologies are falling at a rapid rate, so it is difficult to predict what balance of generation, storage and energy efficiency will be the most cost effective. The high wind scenario S4 (with no P2G) was the most expensive at current prices, because of the very high distributed storage levels required, followed by the high solar PV scenario S2, again because of the high levels of storage.

10.3 Limitations and further research

As with all models, there are limitations. A perfect model would need to be as complex as reality, and therefore useless. In particular, the following limitations were noted, with scope for future model expansion and research:

1. Each scenario was simulated over 100 years, which would cover typical variations in weather conditions, but there was no simulation of atypical

weather conditions, particularly the frequency and duration of long periods of low solar and wind availability, and how this may be affected by climate change.

2. The network of weather stations used to calibrate the solar model is limited in number, and the MERRA grid used to calibrate the wind model is limited to a north-south resolution of approximately 56 km and an east-west resolution of approximately 62.5 km. So these models are limited in their spatial precision and do not account for the local meteorological effects needed to predict exactly the sun and wind conditions for a particular site. Also no account is taken of land use, which may prohibit the use of a particular site for a renewable energy power plant. Much more detailed solar and wind resource modelling, land use mapping and transmission system planning would be required to decide actual sites for solar power stations or wind farms.

3. The simulation did not model correlations of demand with weather conditions, meaning that the required generation capacity or storage capacity for each scenario might be an overestimation. For example, days with a high peak demand may be correlated with strong solar irradiance and high temperatures, but the simulation may have generated low solar irradiance and/or wind speeds for that day, putting a greater burden on storage reserves to meet the demand, or requiring an increase in generation capacity to compensate for the low resource and meet the reliability conditions.

4. The electrical demand on the SWIS system would increase if there is a significant switch from gas to electrical appliances, or a significant

uptake of plug in hybrid or electric vehicles. In these cases, more generation and storage capacity would need to be added.

5. The number of options available for scenario building could be increased if biomass and wave power modelling were incorporated, and might reduce the storage capacity required. It would be advantageous to model as many different renewable energy resources and storage technologies as possible, as this will increase the options to provide a more balanced and diverse energy supply, which may also mitigate any material bottlenecks which may arise.

6. Since most of the distribution network is concentrated on Perth city, the potential for siting large scale power stations within the major part of the distribution network is limited, other than for small scale solar and storage. These are already assumed to be located within the distribution network and can reduce capacity constraints. However there are areas outside of the Perth metropolitan area that might also suffer from network capacity constraints, such as Mandurah (Western Power 2016b) and the Geraldton area (Western Power 2016a). One possible solution is the deployment of concentrating solar thermal power stations with storage at strategic locations (Rutovitz et al. 2013). Capturing the value of avoided network upgrades could improve the cost competitiveness of solar thermal.

7. Since there is high transmission capacity between the Collie area and Perth, it is worth examining options to continue generation from this area after coal is phased out. A solar thermal/biomass hybrid plant (Peterseim et al. 2014) is worth considering as there is potential biomass resource from oil mallee crops and waste streams that could be

transferred to Collie for power generation. However uneven topography may increase the cost of a solar thermal plant in the Collie region.

8. If hourly temperature data were available, a model that uses the synthetically generated hourly cloudiness to generate ambient temperature data could be developed. This model could be used to more accurately characterise the effect of temperature on solar PV power generation, and also on load demand, which is partially correlated with temperature.

9. The energy used and greenhouse gases emitted from manufacturing, construction and installation of energy efficiency measures are difficult to characterise in a generic fashion. Also the overall reduction in power demand on an hourly time scale from energy efficiency measures is probably more complex than characterised in this research. There is much scope for research in this area.

10. Explicit forms of demand management such as load curtailment and load shifting were not considered in this research. The ability to adjust the load to match the available generation has the potential to reduce the requirement for storage, and is worth modelling. Time of use pricing is one method of signalling to a flexible load when there is high demand and curtailment may be favourable. Pricing based both on generation availability and demand level could potentially reduce the needed storage capacity even more. Martinot (2016) introduces the paradigm of flexible demand to complement the requirement for flexible supply in a grid with high levels of variable renewable energy generation. Charging of electric vehicles has the potential to be a type of flexible demand. Charging schedules could respond to dynamic pricing or control signals

to shift charging into periods of high generation availability. How well this could fit in with driver travel requirements needs to be characterised. Conversion of the transport fleet to electric propulsion represents a convergence between transport energy use and stationary electrical energy use, and will significantly increase grid demand unless charging comes mainly from rooftop PV, in which case extra PV capacity will be required. Since not every home is suitable for rooftop PV, it is likely that grid power flows will increase at the distribution level at least.

11. Even if global greenhouse emissions were stopped tomorrow, further warming is inescapable due to inertia in the Earth's climate system. Therefore it is important to take into account any effects of climate change on the solar and wind resources.

12. This research along with Elliston et al. (2012) mean that 100% renewable energy simulations now cover the main Australian electrical grids. Electrical generation in the north west of Western Australia and the Northern Territory remain to be simulated. Both these regions have a strong solar resource. Wright and Hearps (2010) laid out a vision for a fully connected Australia-wide electrical grid system. Under this plan the SWIS is connected both to the national electric grid (NEM) and the north west interconnected system (NWIS) in the north of Western Australia. Although it may not be necessary to connect these grids, this option is also worth modelling in more detail.

These multiple avenues for further research demonstrate that in many ways this thesis is just the beginning. However, it is way past the time for action, not just research.

10.4 Final words

It has been demonstrated that the SWIS grid can rapidly transition to the use of solar energy, wind energy and energy efficiency, whilst maintaining current levels of reliability. Because the SWIS is one of the more difficult cases, this result can be extended to a global scale. This thesis demonstrates that the required technology is already available, rapidly scaling, and decreasing in cost. Although resource bottlenecks may become apparent at very high levels of global use of renewable energy, that is no impediment to rapidly moving at this point in time.

Stern (2013) outlined some of the potentially catastrophic consequences of climate change and the horrific cost in human suffering that may occur. On a global scale, these include drought, desertification, flooding, heat stress, erosion, loss of tree cover, deforestation, cyclones, storm surges, salination, sea level rise, and bush fires. These would be accompanied by biodiversity loss, agricultural collapse, and human migration on scales never before seen in the period of human civilisation. Recent simulations have suggested that Antarctic ice sheet melting might cause global sea levels to rise more than expected and take thousands of years to reverse (DeConto and Pollard 2016), but most sea level rise might be avoided if global temperature rise is kept under 1.5°C. Thus the urgency is greater than ever.

If it does turn out that these warnings are overblown, then the downsides of our rapid mitigation action are few. We will still end up with a clean, diversified, resilient, energy system. The question is no longer "can we change to a renewable energy system?". The question is now "why aren't we changing to a 100% renewable energy system as fast as possible?"

Glossary

α	Solar altitude angle (radians) or wind shear exponent
α_{deploy}	Solar altitude angle at which heliostats deploy and stow
Δf_{hot}	Change in solar thermal storage heated fraction for one time step (°c)
κ_w	Translated Weibull distribution shape coefficient
λ	Weibull scale parameter
λ_w	Translated Weibull distribution scale coefficient
φ	Autocorrelation coefficient constant
φ_{d1}	Synthetic daily wind speed residual first order auto-regression coefficient
φ_{d2}	Synthetic daily wind speed residual second order auto-regression coefficient
φ_k	Generic *k*-th order auto-regression parameter
$\varphi_{w,1}$	Synthetic hourly wind speed residual first order auto-regression coefficient for wind farm w
$\varphi_{w,2}$	Synthetic hourly wind speed residual second order auto-regression coefficient for wind farm w
$\varphi_{w,3}$	Synthetic hourly wind speed residual third order auto-regression coefficient for wind farm w
ρ	Generic hourly wind speed residual random noise component standard deviation
ρ_d	Synthetic daily average wind speed residual random noise component standard deviation
ρ_w	Hourly wind speed residual random noise component standard deviation for wind farm w
σ	Synthetic average hourly cloudiness standard deviation or generic hourly wind speed standard deviation coefficient
σ_{air}	Air density (kg/m^3)
σ_d	Random component standard deviation
σ_{dbw}	Base daily wind speed standard deviation coefficient for wind farm w (m$^{1/2}$s$^{-1/2}$)
σ_{dw}	Seasonally adjusted daily wind speed standard deviation coefficient for wind farm w (m$^{1/2}$s$^{-1/2}$)
σ_{month}	Monthly mean standard deviation of daily average cloudiness
σ_w	Hourly wind speed standard deviation coefficient for wind farm w (ms^{-1})
θ_w	Translated Weibull distribution location coefficient
AC	Alternating current
af_w	Diurnal peak time coefficient for wind farm w
asb_w	Diurnal peak time coefficient for wind farm w
a_{wt}	Wind farm wide power curve parameter for turbine type wt (m^{-2}s^2)
$afterdawn_{w,m}$	Time of day at 4 hours after dawn for wind farm w during month m (h)
am	Diurnal wind magnitude constant component coefficient
AR	Autoregressive model
ARMA	Autoregressive moving average model
$awsf_{w,m}$	Wind shear factor coefficient for wind farm w
$azimuth$	Horizontal angle between a line perpendicular to the surface and a line running due north, with

	angles east of north being positive and west of north being negative (degrees)
b	Day of year angle for equation of time (radians)
b_{wt}	Wind farm wide power curve parameter for turbine type wt ($m^{-3}s^3$)
$beforedusk_{w,m}$	Time of day at 1 hour before dusk for wind farm w during month m (h)
bf_w	Diurnal peak time coefficient for wind farm w
BIC	Bayesian information criterion
BIG-GT	Biomass gasification gas turbine
bm	Diurnal wind magnitude daily wind speed component coefficient
bsb_w	Diurnal peak time coefficient for wind farm w
$bwsf_w$	Wind shear factor coefficient for wind farm w
c	Cloudiness
ca	Collector area (m^2)
cae	Total effective collector area (m^2)
CAES	Compressed air energy storage
can	No-storage collector area (m^2)
$capacity_w$	Full power capacity for wind farm w (MW)
$capcdown$	Average off line percentage of solar thermal collector array and storage
car	Reference collector area (m^2)
cas	Collector area required for storage (m^2)
CCS	Carbon capture and storage
c_d	Daily average cloudiness
c_{davmon}	Monthly mean of daily average cloudiness
$cdist$	Distance inland from the nearest part of the coastline (km)
$cdist_w$	Distance inland of wind farm w from the nearest part of the coastline (km)
c_{dsdmon}	Monthly standard deviation in mean daily cloudiness
CF	Capacity factor
cf^{-1}	Inverse cumulative frequency distribution function
cf_w	Diurnal peak time coefficient for wind farm w
CH_4	Methane
c_{hm}	Synthetic average hourly cloudiness
CHP	Combined heat and power
cic	Tilted surface sun angle calculation coefficient
$cicc$	Tilted surface sun angle calculation coefficient
$cics$	Tilted surface sun angle calculation coefficient
CIGS	Copper indium gallium selenide
cik	Tilted surface sun angle calculation coefficient
$cikc$	Tilted surface sun angle calculation coefficient
$ciks$	Tilted surface sun angle calculation coefficient
cis	Tilted surface sun angle calculation coefficient
$ciss$	Tilted surface sun angle calculation coefficient
$clca$	Tilted surface sun angle calculation coefficient

cline	Cumulative distance along coastline (km)
cm	Diurnal wind magnitude peak component coefficient
CO_2	Carbon dioxide
cosazr	Cosine of the azimuth
coslat	Cosine of the latitude
costilt	Cosine of the tilt angle
cpos	Distance along the coastline from the Northern Territory border (km)
csm	Wind shear seasonal coefficient for month *m*
C_v	Storage medium volumetric heat capacity (joules $m^{-3}{}^{o}c^{-1}$)
CWD	Coarse woody debris
$cwsf_w$	Wind shear factor coefficient for wind farm *w*
c_{wt}	Wind farm wide power curve parameter for turbine type *wt* ($m^{-3}s^3$)
d	Square of distance along one line segment of coastline map (km^2) or square of distance between wind farm *w* and coast-line segment *i* (km^2)
d_1	Square of distance from a location to beginning vertex of coastline line segment (km^2) or distance factor 1 between two wind farms (km)
d_2	Square of distance from a location to end vertex of coastline line segment (km^2) or distance factor 2 between two wind farms (km^8)
dawn	Sunrise local time (h)
DC	Direct current
df_w	Diurnal peak time coefficient for wind farm *w*
$dist_{w1w2}$	Distance estimate between wind farm *w1* and wind farm *w2* (km)
d_j	Length of grid link *j* (km)
dm	Square of distance along coastline line segment to point nearest a location (km^2) or diurnal wind magnitude variation coefficient
d_{min}	Square of current minimum distance from coastline to a location ($degrees^2$) or square of distance inland from the nearest part of the coastline (km^2)
dmm	Mid-month cumulative day of year array
dom	End of month cumulative day of year array
DOY	Day of year, 1 = 1st January, 365 = 31st December (366 during leap years)
d_s	Declination angle of the earth's spin axis with respect to the sun (radians)
ds	Solar declination angle (radians)
dt	Diurnal wind magnitude peak hour factor
dusk	Sunset local time (h)
dx	Horizontal distance estimate between two wind farms (km)
dy	Vertical distance estimate between two wind farms (km)
dv	Diurnal wind magnitude daily wind speed factor
$dwsf_w$	Wind shear factor coefficient for wind farm *w*
ECBM	Enhanced coal bed methane recovery
EE_h	Load demand reduction at hour *h* due to any energy efficiency measures if implemented (MW)
ELCC	Effective load carrying capacity

EOR	Enhanced oil and gas recovery
EOT	Equation of time (h)
e_{pb}	Power block thermal to electrical efficiency at design point
EPBT	Energy pay back time (y)
e_{rs}	Receiver-to-storage efficiency at design point
e_{sr}	Solar field efficiency at design point
e_{st}	Solar thermal solar-to-storage efficiency
E_{sv}	Maximum energy stored per unit volume (joules/m^3)
e_{te}	Solar thermal storage-to-electrical efficiency
e_{tpb}	Storage to power block efficiency
E_{ts}	Storage energy required to maintain rated output power over rated design storage time (joules)
f	Length fraction along coastline line segment to point nearest a location or probability density function (also frequency distribution) for wind as a function of wind speed
f0c	Coastal first seasonal mode maximum amplitude
f0mc	Coastal first seasonal mode maximum amplitude by month array
f0w	First seasonal mode maximum amplitude for wind farm *w*
f0i	Inland first seasonal mode maximum amplitude
f0mi	Inland first seasonal mode maximum amplitude by month array
f1	Second seasonal mode maximum amplitude
f1m	Second seasonal mode maximum amplitude by month array
fardist	Ar parameter distance factor
farlat	Ar parameter latitude factor
$fdc_{w1,w2}$	Distance correlation factor between wind farm *w1* and wind farm *w2*
fdctot	Sum of raw distance correlation factors between wind farm *w* and all other wind farms
fdctotsq	Reciprocal of the sum of squares of the fractional distance correlation factors between wind farm *w* and all other wind farms
$fdist_w$	Diurnal distance coefficient
f_{hot}	Fraction of storage medium heated to $temp_{hot}$
$f_{hot,shutdown}$	Threshold heated fraction of thermal storage medium for shut down
fi_{lat}	Latitude interpolation factor
fi_{lon}	Longitude interpolation factor
$flat_w$	Diurnal latitude coefficient
fmm	Seasonal mode maximum amplitude linear interpolation coefficient
f_{out}	Solar thermal power station electrical output as a fraction of p_{rated}
f_{outmin}	Minimum operational electrical output as a fraction of p_{rated}
f_{pk}	Diurnal wind sinusoid peak hour distribution factor 1
f_{pk2}	Diurnal wind sinusoid peak hour distribution factor 2
$f_{rstartup}$	Minimum receiver incident power as a fraction of receiver rated power
fseason	Seasonal coefficient
$fshear_w$	Wind shear distance coefficient
fsm	Seasonal coefficient by month array

ft	Wind shear factor time coefficient
Ga	Gallium
g CO_2e/kWh	Grams of carbon dioxide equivalent per kilowatt hour
GDP	Gross domestic product
Ge	Germanium
glf	Grid power loss factor between power plant and load centre (Perth), or in the case of rooftop PV, the distribution loss factor
H	Global daily radiation falling a horizontal surface (MJ/m^2)
h_1	Height above ground (m)
h_2	Height above ground (m)
h_d	Measured data value
h_{dav}	Average of the measured hourly values of h_d
H_{ex}	Global daily radiation falling a horizontal surface at the top of the atmosphere (MJ/m^2)
hh_{wt}	Hub height for wind turbine wt (m)
h_m	Model generated synthetic data value
hr	Hour of day
h_s	Hour angle (radians)
hsd	Time between sunrise and noon, or noon and sunset (h)
HVAC	High voltage alternating current
HVDC	High voltage direct current
I_b	Beam irradiance (W/m^2)
I_{bn}	Beam normal solar irradiance (W/m^2)
I_{bnref}	Reference solar beam normal irradiance
I_d	Diffuse irradiance (W/m^2)
I_g	Global solar irradiance (W/m^2)
I_h	Horizontal global irradiance (W/m^2)
I_{hb}	Horizontal beam irradiance (W/m^2)
I_{hcs}	Clear sky horizontal global irradiance (W/m^2)
I_{hd}	Horizontal diffuse irradiance (W/m^2)
I_{hex}	Extraterrestrial solar irradiance onto a plane parallel with a horizontal plane on the surface (W/m^2)
I_{hm}	Measured horizontal irradiance (W/m^2)
I_o	Extraterrestrial solar irradiance falling on a surface perpendicular to the direction of the sun (W/m^2)
I_r	Reflection irradiance on a tilted surface (W/m^2)
$justafterdawn_{w,m}$	Time of day of 2 hours after dawn for wind farm w during month m (h)
k	Weibull shape parameter
$k0_w$	Seasonal variation mode 0 coefficient
$k1_w$	Seasonal variation mode 1 coefficient
K_{b1}	Clear sky beam transmittance magnitude constant
K_{b2}	Clear sky beam transmittance absorption constant
K_{cd}	Coastal inland distance coefficient

K_{cf}	Daily average cloudiness cumulative frequency distribution coefficient
k_{cloud}	Diffuse radiation cloudiness transmission factor
K_{cp}	Coastal position setpoint coefficient
k_d	Diffuse fraction
k_{dcs}	Clear sky diffuse fraction
K_{dr}	Diffuse fraction cloud slope coefficient
K_{dv}	Hourly cloudiness standard deviation estimation coefficient
K_h	Average hourly cloudiness estimation coefficient
K_m	Coastal setpoint constant
K_{sac}	Solar altitude angle coefficient
K_{sas}	Solar altitude angle coefficient
$kslat_1$	Weighting coefficient for seasonal mode 1
$kslat_2$	Weighting coefficient for seasonal mode 2
k_t	Irradiance clearness index
K_t	Daily or monthly radiation clearness index
K_{yac}	Autocorrelation coefficient constant
lat	Latitude (degrees north of equator)
lat_i	Latitude of coast-line map vertex i (degrees)
$latmerra_i$	Latitude of MERRA grid nodes i,j, $j = 1$ to n_{lon} (degrees)
$latmerra_{in}$	Latitude of nearest MERRA node with latitude greater than lat_w (degrees)
lat_w	Latitude of wind farm w (degrees)
LCOE	Levelised cost of energy
ld	Grid step-down and distribution loss (%)
len	Distance along one line segment of coastline (km)
LED	Light emitting diode
$Load_{y,h}$	Swis load demand for year y at hour h (MW)
LOLP	Loss of load probability
lon	Longitude (degrees east of Greenwich)
lon_i	Longitude of coast-line map vertex i (degrees)
$lonmerra_j$	Longitude of MERRA grid nodes i,j, $i = 1$ to n_{lat} (degrees)
$lonmerra_{jn}$	Longitude of the nearest MERRA node with longitude greater than lon_w (deg)
lon_w	Longitude of wind farm w (degrees)
$lossfact$	Thermal storage loss factor (sec^{-1})
$loss_{max}$	Maximum loss factor (W/m^3)
lr	Latitude of wind farm w in radians (radians)
lup	Grid up-conversion and cross-conversion loss (%)
M	Optical air mass ratio
MA	Moving average model
MAPE	Mean absolute percent error
$maxramp$	Maximum solar thermal station ramp rate (% rated capacity/min)
MBE	Mean bias error

mdoy	Mid-month day of year array
MERRA	Modern era retrospective analysis for research and applications
MSW	Municipal solid waste
$night_{w,m}$	Time of day at 3 hours after dusk for wind farm w during month m (h)
N	Number of data points
NEM	National electricity market (covering the eastern states of Australia)
NIMBY	Not in my back yard
n_{large}	Number of large-scale renewable power stations
N_{lat}	Number of horizontal MERRA grid lines (22)
nlink	Number of grid links travelled by power between power station and load centre (Perth)
N_{lon}	Number of vertical MERRA grid lines (15)
NO_2	Nitrous oxide
noon	Local time at which solar altitude is maximum (h)
nonre	Non-renewable power generation (MW)
NREL	National renewable energy laboratory
N_{wf}	Number of wind farms
OECD	Organisation for economic cooperation and development
OF	Orbital factor
olf	Online fraction
p	Autoregressive model order
P	Specific power per unit area (W/m^2)
P2G	Power to gas
P_{in}	Available power input from sun (W)
pop	Percentage yearly population increase (% per year)
P_{out}	Power plant actual output power (MW)
$power_w$	Power output for wind farm w (MW)
PR	Performance ratio
P_{rated}	Power plant rated output power (MW)
P_{recin}	Solar power incident on the central receiver (MW)
P_{recr}	Design-point receiver input power (MW)
P_{recmax}	Maximum receiver input power (MW)
P_{req}	Power plant output power requested by the grid (MW)
$P_{storein}$	Power input to thermal storage
Pu-239	Plutonium 239 isotope
$P_{storeout}$	Power output from thermal storage
PV	Photovoltaic
q	Moving average model order
r	Generic normally distributed random variable or random number with uniform frequency distribution between 0 and 1, often used as a cumulative frequency value.
r_d	Generic normally distributed random variable for daily synthetic wind speed residual generation
$rdc_{w,i}$	Distance weighted combination random variables for wind farm w, i = 1 to 4

r_g	Ground reflectance coefficient
r_h	Standard normally distributed random variable for hourly synthetic wind speed residual generation
r_{leak}	Thermal storage medium heat leakage rate
RMSE	Root mean square error
$r_{parasitic}$	Solar thermal electrical parasitic losses
r_w	Random number with translated Weibull frequency distribution of mean 0 and standard deviation 1
$r_{w,i}$	Normally distributed random variables for wind farm w, i = 1 to 4
SAM	System advisor model
$sin\alpha$	Sine of solar altitude angle
sinazr	Sine of the azimuth
sinlat	Sine of the latitude
sintilt	Sine of the tilt angle
sm	Solar multiple
S_o	Solar constant (1367 W/m^2)
sv	Final storage volume (m^3)
svi	Effective required storage volume (m^3)
SWIS	South west interconnected system
SWWA	South west of Western Australia
t	Time of day (h)
t_b	Beam(or direct) radiation atmospheric transmittance
t_{bcs}	Clear sky beam radiation atmospheric transmittance
t_c	Cloudiness transmission factor
t_d	Diffuse radiation atmospheric transmittance
t_{dcs}	Clear sky diffuse radiation atmospheric transmittance
TDR	Total daily radiation (j/m^2)
$temp_{cold}$	Cooled thermal storage medium temperature (°c)
$temp_{hot}$	Heated thermal storage medium temperature (°c)
$tfreq_{w,0}$	Frequency of yesterday's diurnal wind sinusoid for wind farm w (radians per h)
$tfreq_{w,1}$	Frequency of today's diurnal wind sinusoid for wind farm w (radians per h)
t_{gh}	Global horizontal radiation transmittance
Th-231	Thorium 231 isotope
Th-232	Thorium 232 isotope
t_{ghm}	Measured global horizontal radiation transmittance
tilt	Vertical angle between a surface and the horizontal plane (degrees)
tl	Line power loss over one grid link (%/1000km)
t_{mag}	Generic magnitude of diurnal wind sinusoid (ms^{-1})
$tmag_{w,0}$	Magnitude of yesterday's diurnal wind sinusoid for wind farm w (ms^{-1})
$tmag_{w,1}$	Magnitude of today's diurnal wind sinusoid for wind farm w (ms^{-1})
TNT	Trinitrotoluene explosive

tod	Time of day in local time (h)
tod_{noon}	Time of day when solar noon occurs (sun is midway between sunrise and sunset) (h)
t_{peak}	Generic time of day when peak wind speed occurs in de-trended dataset (h)
$tpeak_{w,0}$	Peak hour of yesterday's diurnal wind sinusoid for wind farm w (h)
$tpeak_{w,1}$	Peak hour of today's diurnal wind sinusoid for wind farm w (h)
t_{period}	Generic timespan of diurnal wind sinusoid (h)
$tperiod_{w,0}$	Period of yesterday's diurnal wind sinusoid for wind farm w (h)
$tperiod_{w,1}$	Period of today's diurnal wind sinusoid for wind farm w (h)
t_r	Reflected radiation atmospheric transmittance
t_{rcs}	Clear sky reflected radiation atmospheric transmittance
ts	Design storage time (h)
tsb_w	Sea breeze peak time of day base value for wind farm w (h)
$tstart_{w,0}$	Start time of day of yesterday's diurnal wind sinusoid for wind farm w (h)
$tstart_{w,1}$	Start time of day of today's diurnal wind sinusoid for wind farm w (h)
$tstep$	Simulation time step (h)
$tstop_{w,0}$	Stop time of day of yesterday's diurnal wind sinusoid for wind farm w (h)
$tstop_{w,1}$	Stop time of day of today's diurnal wind sinusoid for wind farm w (h)
t_z	Time zone (+8 hours for Western Australia) (h)
U_3O_8	Yellow-cake
U-233	Uranium 233 isotope
U-235	Uranium 235 isotope
U-238	Uranium 238 isotope
UF_6	Uranium hexafluoride
UK	United Kingdom
UO_2	Uranium oxide
US	United States
v	Wind speed (m/s)
v_1,v_2	Wind speed at heights h_1,h_2 (m/s)
$vc_{w,t}$	Wind farm wide cut-in wind speed for turbine type wt (ms^{-1})
$vco_{w,t}$	Single turbine cut-in wind speed for turbine type wt (ms^{-1})
$Vdav_w$	Daily average wind speed base value (ms^{-1})
$Vdavl_w$	Daily average wind speed base value from yesterday (ms^{-1})
$V_{diurnal}$	Generic diurnal wind speed (ms^{-1})
$Vdiurnal_w$	Diurnal wind speed for wind farm w (ms^{-1})
$vds(t)$	Synthetic daily average wind speed (ms^{-1})
$vf_{w,t}$	Wind farm wide power curve level-off threshold wind speed for turbine type wt (ms^{-1})
vhh_w	Hub height wind speed for wind farm w (ms^{-1})
vhm_w	Daily average wind speed trend (ms^{-1})
vi_1	Interpolated wind speed 1 (ms^{-1})
vi_2	Interpolated wind speed 2 (ms^{-1})
V_{mode1}	Magnitude of seasonal mode 1

V_{modee2}	Magnitude of seasonal mode 2
$vr_{w,t}$	Wind farm wide reference wind speed for turbine type wt (ms^{-1})
$vro_{w,t}$	Single turbine reference wind speed for turbine type wt (ms^{-1})
$vs_{w,t}$	Wind farm wide shut down wind speed for turbine type wt (ms^{-1})
$v_s(t)$	Synthetic hourly wind speed (ms^{-1})
$Vseason$	Generic seasonal wind speed (ms^{-1})
$Vseasonw$	Seasonal wind speed for wind farm w (ms^{-1})
$vso_{w,t}$	Single turbine shut down wind speed for turbine type wt (ms^{-1})
$Vyav$	Yearly average wind speed (ms^{-1})
$Vyavij$	Yearly average wind speed at MERRA node i,j $i = 1$ to n_{lat}, $j = 1$ to n_{lon} (ms^{-1})
$Vyavw$	Estimate of yearly average wind speed at wind farm w (ms^{-1})
wsf	Wind shear factor
$wsfbase_{w,m}$	Base wind shear factor for wind farm w during month m
xi	Horizontal position coordinate for coast-line map line segment i (km)
xw	Horizontal position coordinate for wind farm w (km)
y	Year or hourly wind speed residual
y_d	Daily cloudiness residual
y_{ds}	Synthetic daily average wind speed residual
$yd_{w,0}$	Daily average wind speed residual for wind farm w
$yd_{w,1}$	Daily average wind speed residual for wind farm w from yesterday
$yd_{w,2}$	Daily average wind speed residual for wind farm w from two days ago
y_h	Hourly cloudiness residual
y_i	Vertical position coordinate for coast-line map line segment i (km)
y_n	Transformed hourly MERRA wind speed residual
y_{ns}	Generic synthetic normally distributed hourly wind speed residual
$yns_{w,0}$	Synthetic normally distributed hourly wind speed residual for wind farm w for present hour
$yns_{w,1}$	Synthetic normally distributed hourly wind speed residual for wind farm w for previous hour
$yns_{w,2}$	Synthetic normally distributed hourly wind speed residual for wind farm w for two hours before present
y_s	Generic synthetic hourly wind speed residual
ys_w	Present hour synthetic wind speed residual for wind farm w
y_w	Vertical position coordinate for wind farm w (km)
z	Random variable uniformly distributed between 0 and 1
z_o	Roughness length (m)

Appendices

A Solar simulation model

The following algorithm for generating synthetic hourly cloudiness at any location was used. Cloudiness mean and variance change throughout the day as a function of average daily cloudiness and solar altitude angle. This algorithm is split into 4 sections. The first section must be computed once per location:

(1.1) From the latitude and longitude of the location (*lon*, *lat*), use Euclidean geometry and the coastline shape map coordinate data to calculate the coast position *cpos* and distance from the coast *cdist* (both in km). The coastline shape map consists of 500 vertices in longitude and latitude coordinates (lon_i, lat_i), i = 1 to 500. The first vertex is the start of the coastline and is where the coast crosses the Northern Territory border. The coastline is approximated by a set of line segments, each defined by a pair of adjacent vertices (lon_i,lat_i) (lon_{i+1},lat_{i+1}), i = 1 to 499.

(i) Calculate:

$$x = 111.195\left(lon - 129\right)\cos\left(\frac{\pi}{180}lat\right)$$
$$y = 111.195\,lat \qquad \text{(A.1)}$$

(ii) Set *cline* = 0 and $d_{min} = 10^8$. Starting at $i = 0$, perform the following iteration steps (iii) to (vi) for each line segment in turn:

(iii) Calculate:

$$x_i = 111.195\left(lon_i - 129\right)\cos\left(\frac{\pi}{180} lat_i\right)$$

$$y_i = 111.195\, lat_i \tag{A.2}$$

$$x_{i+1} = 111.195\left(lon_{i+1} - 129\right)\cos\left(\frac{\pi}{180} lat_{i+1}\right)$$

$$y_{i+1} = 111.195\, lat_{i+1} \tag{A.3}$$

$$d = \left(x_{i+1} - x_i\right)^2 + \left(y_{i+1} - y_i\right)^2$$

$$d_1 = \left(x - x_i\right)^2 + \left(y - y_i\right)^2$$

$$d_2 = \left(x - x_{i+1}\right)^2 + \left(y - y_{i+1}\right)^2 \tag{A.4}$$

$$f = \frac{1}{2}\left(1 + \frac{\left(d_1 - d_2\right)}{d}\right)$$

(iv)

$$\text{if } f < 0,\ d_m = d_1 \text{ and } f = 0$$

$$\text{else if } f > 1,\ d_m = d_2 \text{ and } f = 1 \tag{A.5}$$

$$\text{else } d_m = d_1 - f^2 d$$

(v)

$$If\ d_m < d_{min},\ d_{min} = d_m \text{ and } cpos = cline + f \times len \tag{A.6}$$

(vi) Update *cline*, then go back to (iii) and repeat the calculations for the next line segment, until all are done:

$$cline = cline + len \tag{A.7}$$

(vii) Calculate:

$$cdist = \sqrt{\left(d_{min}\right)} \text{ km} \tag{A.8}$$

After the calculation has been performed on all line segments, *cpos* will be the distance from the start to the point along the coastline (in km) that is closest to the location. *cdist* will be the distance (in km) from this point to the location.

(1.2) Using the coastal setpoints, piecewise straight-line interpolation, and exponential function, calculate the coefficients K_{cdi} i = 1 to 18. For each K_{cdi}, there is a set of N_{kmi} coastal setpoints ($cpos_{i,j}$,$K_{mi,j}$) j = 1 to N_{kmi} (see Table A.1 for the values of these coefficients). Find the two adjacent coastal positions $cpos_{i,j}$ and $cpos_{i,j+1}$ such that *cpos* lies between the two. Using straight-line interpolation, calculate K_{cpi}:

$$K_{cpi} = K_{mi,j} + \left(K_{mi,j+1} - K_{mij}\right)\frac{\left(cpos - cpos_{i,j}\right)}{\left(cpos_{i,j+1} - cpos_{i,j}\right)} \tag{A.9}$$

Calculate K_{cdi} using the distance from the coast *cdist* and two additional distance parameters $K_{mi,Nkmi+1}$ and $K_{mi,Nkmi+2}$:

$$K_{cdi} = K_{cpi}\left(1 + K_{mi,Nkmi+1}\,cdist\right)e^{-K_{mi,Nkmi+2}\,cdist} \tag{A.10}$$

(1.3) Calculate the cosine and sine of the latitude:

$$coslat = \cos(lat)$$
$$sinlat = \sin(lat) \tag{A.11}$$

where *lat* is the latitude.

(1.4) For surfaces tilted at angles other than horizontal, calculate the following parameters:

$$cosazr = \cos(azimuth)$$
$$sinazr = \sin(azimuth)$$
$$clca = coslat\ \ cosazr \tag{A.12}$$
$$cics = sinlat\ \ cosazr$$

where *azimuth* is the horizontal angle between a line perpendicular to the surface and a line running due north, with angles east of north being positive and west of north being negative. For surfaces with dual axis sun tracking, it is not necessary to calculate these parameters. For fixed surfaces, the following two parameters can be calculated here instead of hourly:

$$costilt = \cos(tilt)$$
$$sintilt = \sin(tilt) \tag{A.13}$$

where *tilt* is the vertical angle of the surface from the horizontal.

The second section must be computed at the beginning of each month:

(2.1) Calculate the monthly mean average daily cloudiness and monthly standard deviation of the average daily cloudiness using:

$$c_{davmonth} = K_{cd1} + K_{cd2} \sin\left(\frac{\pi}{6}\left(month + K_{cd3}\right)\right)$$

$$\sigma_{month} = K_{cd4} + K_{cd5} \sin\left(\frac{\pi}{6}\left(month + K_{cd6}\right)\right) \quad \text{(A.14)}$$

(2.2) Calculate the four cumulative frequency distribution coefficients using:

$$K_{cfj} = K_{cd(4+3j)} + K_{cd(5+3j)} \sin\left(\frac{\pi}{6}\left(month + K_{cd(6+3j)}\right)\right) \; for\; j = 1,4 \quad \text{(A.15)}$$

The third section must be calculated at the beginning of each day:

(3.1) Generate a random number *r*, with a uniform distribution between 0 and 1.

(3.2) Calculate the average daily cloudiness normalised residual value *y* using

$$y = K_{cf1} + K_{cf2}\, r + K_{cf3}\, r^2 + K_{cf4}\, r^8 \quad \text{(A.16)}$$

(3.3) Calculate the average daily cloudiness using:

$$c_d = c_{davmonth} + \sigma_{month}\, y \quad \text{(A.17)}$$

(3.4) Calculate the autocorrelation coefficient ϕ using:

$$\varphi = K_{yac}\left(1-8\left(c_d-0.5\right)^3\right) \tag{A.18}$$

See Table A.2 for the value of K_{yac}.

(3.5) Calculate the random component standard deviation σ_d using:

$$\sigma_d = \sqrt{\left(1-\varphi^2\right)} \tag{A.19}$$

(3.6) Calculate the equation of time value, *EOT* (h), and the time of day at solar noon, tod_{noon} (h):

$$B = \frac{2\pi}{365}\left(DOY-81\right)\ radians$$

$$EOT = \frac{9.87\sin\left(2\mathrm{B}\right)-7.53\cos\left(B\right)-1.5\sin\left(B\right)}{60}\ hours \tag{A.20}$$

$$tod_{noon} = 12-\left(\frac{longitude}{15}-tz\right)-EOT\ \text{hours}$$

where *DOY* is the day of the year and *tz* is the time zone (+8 hours for Western Australia).

(3.7) Calculate the declination angle d_s and the solar altitude angle constants K_{sas} and K_{sac}:

$$d_s = 0.40928 \sin\left(\frac{2\pi}{365}(284 + DOY)\right) \; radians$$

$$K_{sas} = \sin(d_s)\, sinlat \tag{A.21}$$

$$K_{sac} = \cos(d_s)\, coslat$$

(3.8) Calculate the orbital factor *OF*:

$$OF = 1 + 0.0344 \cos(0.0172142\, DOY) \tag{A.22}$$

(3.9) For surfaces that are not horizontal, and are fixed or have vertical axis sun tracking, calculate the following parameters. If the surface has dual axis sun tracking, it is not necessary to calculate these parameters.

$$cikc = \sin(d_s)\, sinlat$$

$$ciks = \sin(d_s)\, clca$$

$$ciss = \cos(d_s)\, sinazr \tag{A.23}$$

$$cicc = \cos(d_s)\, coslat$$

If the surface is fixed, the following parameters can be calculated here instead of hourly:

$$cik = cikc\ costilt - ciks\ sintilt$$

$$cis = ciss\ sintilt \tag{A.24}$$

$$cic = cicc\ costilt + cics\ sintilt$$

The fourth section must be calculated for each hour, h, from 1 to 24.

(4.1) Calculate the hour angle h_s:

$$h_s = \frac{\pi}{12}\left(tod_{noon} - h + 0.5\right) \; radians \tag{A.25}$$

(4.2) Calculate the sine of the solar altitude angle, sinα:

$$\sin\alpha = K_{sas} + K_{sac}\cos\left(h_s\right) \tag{A.26}$$

If sinα is greater than zero, then the sun is above the horizon. Otherwise, set all solar irradiances to zero and go to the next hour.

(4.3) Calculate the hourly average cloudiness c_{hm} using:

$$c_{hm} = c_d\left(1 + K_{h0}\frac{\left(1 - c_d\right)}{\left(1 + K_{h1}c_d^2\right)}\left(\sin\alpha + K_{h2}\sin^2\alpha + K_{h3}\sin^3\alpha\right)\right) \tag{A.27}$$

See Table A.2 for the values of K_{hi}, for i = 0 to 3.

(4.4) Calculate the hourly average standard deviation using:

$$\sigma = c_d\left(1 - c_d\right)\left(\frac{K_{dv0}}{\left(1 + K_{dv1}c_d\right)} + \frac{K_{dv2}}{\left(1 + K_{dv3}c_d\right)}\sin\alpha + \frac{K_{dv4}}{\left(1 + K_{dv5}c_d\right)}\sin^2\alpha\right) \tag{A.28}$$

See Table A.2 for the values of K_{dvi}, for i = 0 to 5.

(4.5) Generate a random number r, with a uniform distribution between 0 and 1.

(4.6) Map r to a translated Weibull distribution using:

$$r_w = \theta_w + \lambda_w \left(-\ln\left(1-r\right)\right)^{\left(\frac{1}{\kappa_w}\right)} \tag{A.29}$$

See Table A.2 for the values of θ_w, λ_w and κ_w.

(4.7) Generate a cloudiness residual y_h using:

$$y_h = \varphi y_{h-1} + \sigma_d r_w \tag{A.30}$$

y_{h-1} is the residual for the previous hour. If h is the first hour on or after sunrise to be calculated then use $y_{h-1} = 0$.

(4.8) Generate the synthetic hourly cloudiness c using:

$$c = c_{hm} + \sigma y_h \tag{A.31}$$

(4.9) Calculate the air mass ratio M, and the clear sky beam and diffuse transmissivities t_{bcs} and t_{dcs}:

$$M = \frac{1.002432\sin^2\alpha + 0.148386\sin\alpha + 0.0096467}{\sin^3\alpha + 0.149864\sin^2\alpha + 0.0102963\sin\alpha + 0.000303978}$$

$$t_{bcs} = K_{b1} e^{K_{b2} M} \tag{A.32}$$

$$t_{dcs} = 0.271 - 0.294\, t_{bcs}$$

See Table A.2 for the values of K_{b1} and K_{b2}.

(4.10) Calculate the diffuse transmittance cloudiness coefficient $k_{cloud}(c)$:

$$k_{cloud}(c)=\frac{(1-c)(1+K_{dr}c)}{1-K_{dr}c\dfrac{t_{dcs}}{t_{bcs}}} \tag{A.33}$$

where K_{dr} is set to 0.5.

(4.11) For horizontal surfaces (assuming diffuse radiation can be utilised), calculate the beam and diffuse transmittances t_b, t_d, the global horizontal transmittance t_{gh}, the horizontal beam and diffuse irradiance components I_{hb} and I_{hd}, and the global horizontal irradiance I_h:

$$t_b=(1-c)\,t_{bcs}$$

$$t_d=k_{cloud}(c)\,t_{dcs}$$

$$t_{gh}=t_b+t_d=(1-c)\,t_{bcs}+k_{cloud}(c)\,t_{dcs}$$

$$I_{hex}=1367\ OF\ \sin\alpha \tag{A.34}$$

$$I_{hb}=t_b\,I_{hex}$$

$$I_{hd}=t_d\,I_{hex}$$

$$I_h=t_{gh}\,I_{hex}$$

(4.12) For surfaces at angles other than horizontal, calculate the beam irradiance I_b. Firstly, calculate the extraterrestrial irradiance I_o (W/m^2):

$$I_o=1367\,OF \tag{A.35}$$

For vertical axis sun tracking surfaces, calculate the following parameters:

$$costilt = \sin\alpha$$

$$sintilt = \sqrt{\left(1-\sin^2\alpha\right)}$$

$$cik = cikc\ costilt\ -\ ciks\ sintilt \tag{A.36}$$

$$cis = ciss\ sintilt$$

$$cic = cicc\ costilt + cics\ sintilt$$

For fixed and vertical axis sun tracking surfaces, calculate the beam irradiance I_b:

$$I_b = I_o t_b\left(cik + cis\ \sin\left(h_s\right) + cic\ \cos\left(h_s\right)\right) \tag{A.37}$$

For dual axis sun tracking surfaces, calculate the beam irradiance I_b:

$$I_b = I_o t_b \tag{A.38}$$

(4.13) For photovoltaic surfaces, calculate the diffuse and reflection components of the irradiance, I_d and I_r. For fixed photovoltaic surfaces:

$$I_d = 0.5\, I_o t_d \sin\alpha\left(1 + costilt\right)$$

$$t_r = t_b + t_d \tag{A.39}$$

$$I_r = 0.5 r_g\, I_o t_r \sin\alpha\left(1 - costilt\right)$$

where r_g is the ground reflectance coefficient. See Table A.2 for the value of r_g.

For vertical axis and dual axis sun tracking photovoltaic surfaces, *costilt* = sinα, so:

$$I_d = 0.5\, I_o\, t_d \sin\alpha \left(1 + \sin\alpha\right)$$

$$t_r = t_b + t_d \qquad \text{(A.40)}$$

$$I_r = 0.5\, r_g\, I_o\, t_r\, sin\alpha \left(1 - sin\alpha\right)$$

(4.13) The global irradiance falling on the surface can now be calculated. For photovoltaic surfaces,

$$I_g = I_b + I_d + I_r \qquad \text{(A.41)}$$

For concentrating mirror surfaces,

$$I_g = I_b \qquad \text{(A.42)}$$

The 334 coefficients were generated using all the measured data from every station as calibration data:

Table A.1. Coastal set points and distance parameters.

i	N_{kmi}	Coastal setpoints	Distance parameters
1	7	(0.000121233,0.181881)(4358.68,0.118325)(5855,0.196657) (6107.18,0.308299)(6382.57,0.361306)(7578.43,0.241622) (7704.56,0.112202)	-4.74725e-05,0.00129837
2	9	(0.00211302,0.149049)(5295.77,0.00929281)(6062.87,0.0743396) (6170.42,0.0544799)(6817.07,0.0385803)(6919.46,0.0462027) (7019.46,0.00995161)(7324.11,0.0279123)(7424.38,0.0251248)	0.0126305,0.00709556
3	6	(3557.6,13.8123)(5548.36,8.12282)(6936.52,6.38246)(7133.08,2.9477) (7263.64,14.263)(7626.37,2.83333)	-4.62672e-15,-9.41605e-16
4	5	(183.127,0.140565)(5548.28,0.163597)(6177.15,0.181829) (7276.71,0.194041)(8058.94,0.15176)	8.20061e-05,0.000200941
5	9	(4.82931e-05,0.0619347)(5548.36,0.0382522)(5648.53,0.0125194) (5951.32,0.0278242)(6414,0.00509126)(6544.79,0.0112567) (6644.79,0.021321)(7238.27,0.00511463)(7939.27,0.0704454)	0.0146506,0.00801621
6	8	(1.03457e-05,13.243)(5948.94,8.23257)(6438.31,12.9464) (7155.63,4.14219)(7263.64,13.999)(7377.2,7.63296)(7718.7,1.97949) (9614.86,2.64167)	8.16237e-14,-1.96663e-14
7	8	(759.862,-1.15271)(4450.09,-0.888514)(5855,-1.04833)(6095.42,-1.43222)(6382.57,-1.70468)(7096.81,-1.37403)(7297.2,-1.49405) (7645.29,-0.922309)	-0.000668503,4.28529e-06
8	9	(2804.47,0.374811)(5655.77,0.0806366)(6339.57,0.353919) (6439.57,0.109719)(6680.68,0.182641)(7096.81,0.0446732) (7634.3,0.0769718)(8069.9,0.414361)(9195.84,0.0299513)	0.0266459,0.00849817
9	8	(278.366,8.43906)(4434.12,8.01394)(6059.16,14.3246) (6897.37,12.0145)(7142.72,19.6262)(7333.4,14.2362) (7783.43,16.4985)(8659.08,9.26487)	4.22435e-16,-4.45298e-16
10	8	(1.67366,1.75907)(2590.43,0.168708)(5782.19,0.90459) (5969.6,1.43466)(6069.64,2.28332)(6433.7,2.91901)(7353.76,2.06326) (7821.81,0.298694)	-0.0004577,0.00125533
11	8	(1.85017e-07,1.34352)(5823.34,0.289987)(5923.36,0.778804) (6049.55,0.886153)(6177.76,1.40718)(6721.28,0.682705) (7101.11,0.220369)(7338.59,0.501468)	0.0162485,0.0083404
12	6	(1.56914e-12,2.53601)(5753.42,2.17944)(5934.42,21.3562) (6177.72,19.5243)(7169.75,18.1674)(7269.75,21.8962)	4.9505e-15,7.50947e-15
13	7	(196.582,0.251853)(4694.57,0.613485)(5782.25,1.08065) (6107.18,0.355968)(6463.88,0.397888)(6565.85,0.252028) (6936.44,0.411005)	0.0133546,0.00437936
14	6	(3586.43,0.14879)(5541.96,1.21734)(5641.96,0.779202) (6107.96,0.592607)(7215.47,0.346493)(7429.46,0.540601)	0.00817635,0.00410551
15	7	(3.78325e-05,16.7796)(3556.04,21.1344)(5927.72,20.0101) (6165.06,13.6784)(6863.41,12.7892)(6963.41,21.9553) (7316.56,26.1913)	-2.25303e-10,-5.96227e-12
16	9	(0.00116518,2.29642)(4383.42,2.99919)(6081.62,1.63957) (6186.12,1.45255)(6294.7,1.08039)(6891.98,1.22188) (6991.98,1.83623)(7232.26,1.11177)(7455.14,2.80992)	0.0010551,0.0001511
17	7	(1.92816e-12,1.21493)(5782.25,0.966054)(6058.36,0.763544) (6315.79,0.174561)(6936.45,0.298013)(7364.85,0.143312) (7732.08,0.690034)	0.0172375,0.00741007
18	9	(1096.22,20.1305)(3940.9,19.6107)(6637.71,10.9754) (6761.42,6.77296)(6897.98,15.706)(6997.98,5.88923)(7396.6,9.65186) (7603.63,8.74399)(8422.38,8.22955)	5.81999e-14,2.03159e-15

Table A.2. Model cloudiness generation coefficients

Coefficients	Values
Kh_i, i = 0,3	3.53164,6.58553,-2.65914,1.53216
K_{dvi}, i = 0,5	2.9409,3.05052,-4.08909,4.88456,1.14796,1.03685
k_{yac}	0.342923
θ_w	-1.82568
λ_w	2.05741
κ_w	1.89893
K_{b1}	0.85295
K_{b2}	-0.114757
r_g	0.2

B Wind simulation model

The following algorithm for generating synthetic hourly wind farm output power at any location within the SWWA was used. This algorithm is split into 4 sections depending on how often computation is required. Latitude and longitude values are in degrees, but all sine and cosine terms assume the argument is in radians, and the $\cos^{-1}$ term produces a value in radians. The simulation can be started on any day of the year, and at any hour of the day, by setting the day of the year variable *DOY* and hour of the day variable *hr* to the desired values. *DOY* can range from 1 to 365 (or 1 to 366 for modelling leap years), and *hr* from 0 to 23. The initial values of daily and hourly residuals $yd_{w,0}$, $yd_{w,1}$, $yns_{w,0}$, $yns_{w,1}$ and $yns_{w,2}$ are set to standard normally distributed random values. For a simulation of N_{wf} wind farms, to enable distance correlation to be set, at each hour the wind power for each wind farm $w = 1, N_{wf}$ is calculated together.

The first section must be computed once before the simulation begins:

(1.1) Calculate wind shear seasonal coefficients. For month m, $m = 1$ to 12, calculate:

$$cs_m = \cos\left(\frac{\pi}{6}(m-6)\right) \tag{B.1}$$

(1.2) Set daily auto-regression coefficients

$$\varphi_{d1} = 0.523237$$

$$\varphi_{d2} = -0.160552 \tag{B.2}$$

$$\rho_d = 0.88102$$

The second section must be computed once per wind farm w, w = 1,N_{wf}, before the simulation begins:

(2.1) From the latitude and longitude of the location of wind farm w (lon_w, lat_w), use Euclidean geometry and the coastline shape map coordinate data to calculate the distance from the coast $cdist_w$ (in km). The coastline shape map consists of 500 vertices in longitude and latitude coordinates (lon_i,lat_i), i = 1 to 500. The first vertex is the start of the coastline and is where the coast crosses the Northern Territory border. The coastline is approximated by a set of line segments, each defined by a pair of adjacent vertices (lon_i,lat_i) (lon_{i+1},lat_{i+1}), i = 1 to 499. First calculate the horizontal and vertical position coordinates for wind farm w.

$$x_w = 111.195(lon_w - 129)\cos\left(\frac{\pi}{180} lat_w\right)$$
$$y_w = 111.195\, lat_w \qquad \text{(B.3)}$$

Set $d_{min} = 10^8$. For each line segment i = 1 to 499, calculate

$$x_i = 111.195\left(\frac{(lon_i + lon_{i+1})}{2} - 129\right)\cos\left(\frac{\pi}{180}\frac{(lat_i + lat_{i+1})}{2}\right)$$
$$y_i = 111.195\frac{(lat_i + lat_{i+1})}{2}$$
$$d = (x_w - x_i)^2 + (y_w - y_i)^2 \qquad \text{(B.4)}$$
$$if\,(d < d_{min})\, d_{min} = d$$

Calculate

$$cdist_w = \sqrt{(d_{min})}\ \text{km} \qquad \text{(B.5)}$$

(2.2) If the grid of MERRA yearly average wind speeds have locations [$latmerra_i$,$lonmerra_j$], where $latmerra_i$ is the latitude (degrees) and $lonmerra_j$ is the longitude (degrees) of node i,j, $i = 1$ to N_{lat}, $j = 1$ to N_{lon}, then let the matrix of MERRA year average wind speeds be denoted by $Vyav_{ij}$. For wind farm w, if lat_w is the latitude, and lon_w is the longitude, then find $latmerra_{in}$, the latitude of the nearest MERRA node with latitude greater than lat_w, and find $lonmerra_{jn}$, the longitude of the nearest MERRA node with longitude greater than lon_w, then calculate the average yearly wind speed $vyav_w$:

$$fi_{lat} = \frac{(lat_w - latmerra_{\text{in}})}{(latmerra_{\text{in}} - latmerra_{\text{in-1}})}$$

$$fi_{lon} = \frac{(lon_w - lonmerra_{\text{jn}})}{(lonmerra_{\text{jn}} - lonmerra_{\text{jn-1}})}$$

$$vi_1 = (1 - fi_{lat})\, vyav_{\text{in-1,jn-1}} + fi_{lat}\, vyav_{\text{in,jn-1}} \qquad \text{(B.6)}$$

$$vi_2 = (1 - fi_{lat})\, vyav_{\text{in-1,jn}} + fi_{lat}\, vyav_{\text{in,jn}}$$

$$vyav_w = (1 - fi_{lon})\, vi_1 + fi_{lon}\, vi_2$$

(2.3) For each wind farm w, calculate the seasonal variation coefficients, the diurnal and wind shear distance coefficients, and the diurnal latitude and peak time coefficients:

$$
\begin{aligned}
k0_w &= \frac{0.0395956(lat_w+34)}{1+0.00794402(lat_w+34)^3} + \frac{lat_w+34}{2(50+cdist_w)} \\
k1_w &= \frac{0.0804696}{(1+0.741463(lat_w+35.1))(1+\frac{cdist_w}{200})} \\
fc_w &= \frac{1}{1+(\frac{cdist_w}{75})^2} \\
fdist_w &= \frac{(100+cdist_w)}{(200+cdist_w)} \\
fshear_w &= \frac{cdist_w}{(50+cdist_w)} \\
awsf_{w,m} &= 0.005(1-cs_m)(1-fshear_w)\ \ m=1,12 \\
bwsf_w &= 0.056+0.0625\,fshear_w \\
cwsf_w &= 0.01+0.1\,fshear_w \\
dwsf_w &= 0.005+0.08125\,fshear_w \\
flat_w &= \frac{1}{36+lat_w} \\
asb_w &= 16.5+\frac{32.5\,cdist_w}{(700+3\,cdist_w)} \\
bsb_w &= 1.75-\frac{6.25\,cdist_w}{(125+5\,cdist_w)} \\
af_w &= 0.72+0.21\,fdist_w \\
bf_w &= 0.394\,fdist_w-0.08\,flat_w-0.572 \\
cf_w &= 1.75+0.13\,fdist_w-0.5\,flat_w \\
df_w &= 0.261-1.16\,fdist_w
\end{aligned}
\qquad \text{(B.7)}
$$

(2.4) For each wind farm w, calculate the hourly and daily auto-regression coefficients:

$$farlat = 0.05 + 0.4\frac{(36 + lat_w)}{(37 + lat_w)}$$

$$fardist = \frac{1}{1 + \frac{cdist_w}{100}}$$

$$\varphi_{w,1} = farlat\,(1.28 + 0.17\,fardist)$$

$$\varphi_{w,2} = farlat\,(-0.55 - 0.27\,fardist)$$

$$\varphi_{w,3} = farlat\,(0.095 + 0.07\,fardist) \qquad \text{(B.8)}$$

$$\rho_w = 0.45 - \frac{0.051}{(1 + \frac{cdist_w}{50})}$$

$$\sigma_w = (1 - \frac{0.15}{(1 + 0.01\,cdist_w)})(1 - \frac{0.15}{(36 + lat_w)})$$

$$\sigma_{dbw} = 0.43\,(0.91 + \frac{0.09}{(1 + 0.01\,cdist_w)})(0.67 + \frac{1.32}{(39 + lat_w)})$$

(2.5) For each wind farm w, and month m, m = 1 to 12, calculate dawn and dusk times. Let $mdoy$ = [15,44,75,105,136,166,197,228,258,289,319,350]

$$
\begin{aligned}
&DOY = mdoy[m] \\
&b = 0.017453(DOY - 81) \\
&eot = \frac{(9.87\sin(2b) - 7.53\cos(b) - 1.5\sin(b))}{60} \\
&ds = -0.40928\sin(0.0172142(284 + DOY)) \\
&noon = 12.275 - eot - \frac{(lon_w - 115.87)}{15} \\
&lr = 0.017453\, lat_w \\
&hsd = 3.8197186\cos^{-1}\left(\frac{-\sin(lr)\sin(ds)}{\cos(lr)\cos(ds)}\right) \\
&if(hsd < 0)\, hsd = -hsd \\
&dawn = noon - hsd \\
&dusk = noon + hsd \\
&justafterdawn_{w,m} = dawn + 2 \\
&afterdawn_{w,m} = dawn + 4 \\
&beforedusk_{w,m} = dusk - 1 \\
&night_{w,m} = dusk + 3 \\
&wsfbase_{w,m} = 0.11 + 0.0625\, fshear_w + 0.02\, cs_m
\end{aligned}
\tag{B.9}
$$

(2.6) For each wind farm w, that uses wind turbine type wt, modify reference velocities for the individual turbine to represent overall wind farm operation. If another wind farm uses the same type of turbine, this step does not have to be repeated.

$$
\begin{aligned}
vc_{wt} &= vco_{wt} - 0.5 \\
vr_{wt} &= vro_{wt} + 5 \\
vf_{wt} &= 0.4\,vc_{wt} + 0.6\,vro_{wt} \\
vs_{wt} &= vso_{wt} - 3 \\
c_{wt} &= \frac{0.5}{(vr_{wt} - vf_{wt})^3} \\
b_{wt} &= \frac{0.5}{(vf_{wt}^3 - vc_{wt}^3)} \\
a_{wt} &= -b_{wt}\,vc_{wt}
\end{aligned}
\qquad \text{(B.10)}
$$

where parameters with suffix o refer to the original individual wind turbine parameters. vco_{wt} is the cut-in wind speed, vro_{wt} is the reference wind speed (the speed at which the turbine reaches full power output), and vso_{wt} is the shut-down wind speed. These parameters can be obtained from the wind turbine technical specifications. Values for some turbines which are used in the simulation are given below in Table B.1. a_{wt}, b_{wt}, and c_{wt} are constants associated with the partial power section of the turbine power curve.

Table B.1. Wind turbine power curve parameters.

Turbine	Capacity (MW)	*vco* (m/s)	*vro* (m/s)	*vso* (m/s)	Hub-height (m)
ENERCON-E40	0.6	2.5	12	28	46
ENERCON-E48	0.8	2.5	14	28	50
ENERCON-E53	0.8	2.5	14	28	73
ENERCON-E66	1.8	2.5	15	28	65
ENERCON-E70	2.3	2.5	15	28	64
ENERCON-E126	7.5	2.5	17	28	135
VESTAS-V82	1.65	3.5	12.5	20	78
VESTAS-V90	1.856	4	12	25	80
VESTAS-V112	3	3	12	25	119
GE 2.5-100	2.5	3	12.5	25	75
REPOWER 3.4M104	3.4	3.5	13.5	25	78

(2.7) For each wind farm w, calculate distance correlation weighting coefficients f_{dc}. Estimate $dist_{w1w2}$, the distance between wind farm w_1 and wind farm w_2 (km), and fdc_{w1w2}, the distance weighting factor between wind farm w_1 and wind farm w_2 for every possible pair of wind farms w_1 and w_2. For wind farms $w_1 = 1$ to N_{wf} - 1, and for wind farms $w_2 = w_1+1$ to N_{wf}:

$$
\begin{aligned}
dx &= 111.195\left(\left(lon_{w1}-129\right)\cos\left(\frac{\pi}{180}lat_{w1}\right)-\left(lon_{w2}-129\right)\cos\left(\frac{\pi}{180}lat_{w2}\right)\right)\\
dy &= 111.195\left(lat_{w1}-lat_{w2}\right)\\
dist_{w1w2} &= \sqrt{dx^2+dy^2}\\
d_1 &= \frac{dist_{w1w2}}{60}\\
d_2 &= \left(\frac{dist_{w1w2}}{500}\right)^8\\
fdc_{w1,w2} &= \frac{1}{\left(1+d_1\right)\left(1+d_2\right)}\\
fdc_{w2,w1} &= fdc_{w1,w2}\\
fdc_{w1,w1} &= 1
\end{aligned}
\qquad \text{(B.11)}
$$

For wind farms $w = 1$ to N_{wf}

$$fdctot = \sum_{w_1=1,N_{wf}} fdc_{w,w1} \tag{B.12}$$

$$fdc_{w,w1} = \frac{fdc_{w,w1}}{fdctot} \text{ for } w_1 = 1 \text{ to } N_{wf} \tag{B.13}$$

$$fdctotsq = \frac{1}{\sum_{w_1=1,N_{wf}} fdc^2_{w,w1}} \text{ for } w_1 = 1 \text{ to } N_{wf} \tag{B.14}$$

$$fdc_{w,w1} = fdc_{w,w1} fdctotsq \text{ for } w_1 = 1 \text{ to } N_{wf} \tag{B.15}$$

$$fdc_{w,N_{wf}+1} = fdctotsq \tag{B.16}$$

The third section must be calculated at the beginning of each day (*hr* = 0), and at the beginning of the simulation if *hr* does not start at 0.

(3.1) Calculate the seasonal variation coefficient *fseason*, first seasonal mode maximum amplitude coastal and inland components *f0c* and *f0i*, and the second seasonal mode maximum amplitude f_1 (all same for every wind farm). Let:

dom[13] = {0,31,59,90,120,151,181,212,243,273,304,334,366},

dmm[14] = {-15,15,44,75,105,136,166,197,228,258,289,319,350,380},

fsm[13] = { -1,-1,-1,-0.5,0,0.5,1,1,1,0.5,0,-0.5,-1 },

f0mi[14] = { 0.75,1.8,0.75,0.6,-1.0,-0.4,-0.5,-1.7,-1.7,0.4,0.5,1.4,0.75,1.8 },

f0mc[14] = { 1.2,1.5,0.5,0.7,-0.6,-0.7,-0.6,-0.7,-1.25,-0.3,0,0.6,1.2,1.5 }, and

f1m[14] = { -0.3,0,0.3,-0.25,-0.6,-0.75,0.5,0.12,0.25,1,-0.25,0.1,-0.3,0 }

Unless the simulation is just beginning, increment day of year *DOY* by 1. From *DOY*, find the month m (m = 1..12) such that $dom[m\text{-}1] < DOY \le dom[m]$, and the mid-month number mm (mm = 1..13) such that $dmm[mm\text{-}1] < DOY \le dmm[mm]$.

$$
\begin{aligned}
&fseason = 1 + fsm[m] \\
&f_{mm} = \frac{(doy - dmm[mm-1])}{(dmm[mm] - dmm[mm-1])} \\
&f0c = f0mc[mm-1] + f_{mm}(f0mc[mm] - f0mc[mm-1]) \\
&f0i = f0mi[mm-1] + f_{mm}(f0mi[mm] - f0mi[mm-1]) \\
&f1 = f1m[mm-1] + f_{mm}(f1m[mm] - f1m[mm-1])
\end{aligned}
\tag{B.17}
$$

(3.2) For each wind farm w, calculate the first seasonal mode maximum amplitude:

$$f0_w = fc_w f0c + (1 - fc_w) f0i \tag{B.18}$$

(3.3) For each wind farm w, calculate the seasonal wind speed:

$$Vseason_w = Vyav_w(1 + k0_w f0_w + k1_w f1) \tag{B.19}$$

At the beginning of the simulation only, set $vdav_w$ to $Vseason_w$.

(3.4) For each wind farm w, calculate the sea breeze peak time:

$$
\begin{aligned}
&tsb_w = asb_w + bsb_w\, fseason \\
&\text{if } (tsb_w < 0)\ tsb_w = 0 \\
&\text{if } (tsb_w > 23)\ tsb_w = 23
\end{aligned}
\tag{B.20}
$$

(3.5) For each wind farm w, generate four normally distributed random numbers, $r_{w,i}$, $i = 1..4$. For each $r_{w,i}$, z is a random number uniformly distributed on (0,1):

$$r_{w,i} = \frac{\left(z^{0.135} - (1-z)^{0.135}\right)}{0.1975} \tag{B.21}$$

(3.6) For each wind farm w, distance weight the random variables $rdc_{w,i}$, $i = 1$ to 4:

$$rdc_{w,i} = \sum_{q=1,N_{wf}} fdc_{w,q} r_{q,i} \tag{B.22}$$

(3.7) For each wind farm w, calculate the average daily velocity. The previous daily autoregressive residual calculations are moved one day back and today's daily residual $yd_{w,0}$ is calculated.

$$\begin{aligned} yd_{w,2} &= yd_{w,1} \\ yd_{w,1} &= yd_{w,0} \\ yd_{w,0} &= \varphi_{d1} yd_{w,1} + \varphi_{d2} yd_{w,2} + \rho_d rdc_{w,1} \end{aligned} \tag{B.23}$$

Move previous daily average wind speed one day back, and apply reverse square root transformation to $yd_{w,0}$.

$$\begin{aligned} vdavl_w &= vdav_w \\ \sigma_{dw} &= (1 + 0.225 fseason)\sigma_{dbw} \\ vdav_w &= \left(\sqrt{Vseason_w} + \sigma_{dw}\ yd_{w,0}\right)^2 - {\sigma_{dw}}^2 \\ if\left(vdav_w > 16.5\right) vdav_w &= 16.5 \\ if\left(vdav_w < 1\right) vdav_w &= 1 \end{aligned} \tag{B.24}$$

(3.8) For each wind farm w, calculate the diurnal component coefficients. The previous day's calculations are moved one day back (a late peaking diurnal component from the previous day may still remain active into the present day).

$$
\begin{aligned}
&tpeak_{w,0} = tpeak_{w,1} - 24 \\
&tperiod_{w,0} = tperiod_{w,1} \\
&tfreq_{w,0} = tfreq_{w,1} \\
&tstart_{w,0} = tstart_{w,1} - 24 \\
&tstop_{w,0} = tstop_{w,1} - 24 \\
&tmag_{w,0} = tmag_{w,1}
\end{aligned}
\tag{B.25}
$$

(3.9) Calculate today's diurnal component peak time of day, $tpeak_{w,1}$

$$
\begin{aligned}
&f_{pk} = af_w + bf_w fseason \\
&f_{pk2} = cf_w + df_w fseason \\
&tpeak_{w,1} = 15 - 0.5(f_{pk2} - rdc_{w,2}) \quad rdc_{w,2} < -f_{pk2} \\
&tpeak_{w,1} = 7.5 + 0.5\, fseason - 3(f_{pk} - rdc_{w,2}) \quad -f_{pk2} < rdc_{w,2} < -f_{pk} \\
&\quad \text{if } -f_{pk} < rdc_{w,2} < f_{pk} \\
&\qquad \{ tsb_w = asb_w + bsb_w fseason \\
&\qquad\quad \text{if } (tsb_w < 0)\ tsb_w = 0 \\
&\qquad\quad \text{if } (tsb_w > 23)\ tsb_w = 23 \\
&\qquad\quad tpeak_{w,1} = tsb_w + 3\, rdc_{w,2} \} \\
&tpeak_{w,1} = 7.5 + 0.5\, fseason + 3(rdc_{w,2} - f_{pk}) \quad f_{pk} < rdc_{w,2} < f_{pk2} \\
&tpeak_{w,1} = 15 + 0.5(rdc_{w,2} - f_{pk2}) \quad rdc_{w,2} > f_{pk2}
\end{aligned}
\tag{B.26}
$$

while $tpeak_{w,1} < 0$ add 24 hours to $tpeak_{w,1}$

while $tpeak_{w,1} \geq 36$ subtract 24 hours from $tpeak_{w,1}$

(3.10) Calculate this days diurnal component period $tperiod_{w,1}$

$$
\begin{aligned}
&tperiod_{w,1} = 24 + 2\,rdc_{w,3} \quad tpeak_{w,1} < 6 \\
&tperiod_{w,1} = 16 - fseason + (3 - 0.75\,fseason)\,rdc_{w,3} \quad 6 \le tpeak_{w,1} \\
&\text{if } tperiod_{w,1} < 6 \quad tperiod_{w,1} = 6 \\
&\text{if } tperiod_{w,1} > 36 \quad tperiod_{w,1} = 36
\end{aligned}
\tag{B.27}
$$

(3.11) Calculate this days diurnal component magnitude $tmag_{w,1}$

$$
\begin{aligned}
&dt = tpeak_{w,1} - 8.5 \\
&dv = vdav_w - 5 + 0.25\,fseason \\
&am = -0.825 - 0.66\,fseason \\
&bm = 0.1485 + 0.033\,fseason \\
&cm = 3.2959 - 0.21327\,fseason - 0.7755 / (1 + 0.5\,dt^2) \\
&dm = 0.275 - 0.1155\,fseason + 0.11\,vdav_w \\
&tmag_{w,1} = (1 - 0.15\,flat_w\,(2 - fseason))(am + bm\ vdav_w + cm/(1 + 0.15\ dv^2)) + dm\ rdc_{w,4} \\
&\text{if } (tmag_{w,1} < 0)\ tmag_{w,1} = 0 \\
&\text{if } (tmag_{w,1} > vdav_w)\ tmag_{w,1} = vdav_w \\
&\text{if } (tmag_{w,1} > 7)\ tmag_{w,1} = 7
\end{aligned}
\tag{B.28}
$$

(3.12) Calculate $tstart_{w,1}$, $tstop_{w,1}$, and $tfreq_{w,1}$. Make sure today's diurnal component doesn't start before midnight ($hr = 0$).

$$
if\,(tpeak_{w,1} < 12) \quad \{ tmag_{w,1} = -tmag_{w,1},\ tpeak_{w,1} = tpeak_{w,1} + \frac{tperiod_{w,1}}{2} \}
\tag{B.29}
$$

$$
\begin{aligned}
&tstart_{w,1} = tpeak_{w,1} - \frac{3\,tperiod_{w,1}}{4} \\
&if\,(tstart_{w,1} < 0) \quad \{ tperiod_{w,1} = 1.333\,tpeak_{w,1},\ tstart_{w,1} = 0 \}
\end{aligned}
\tag{B.30}
$$

$$tstop_{w,1} = tpeak_{w,1} + \frac{tperiod_{w,1}}{4}$$
$$tfreq_{w,1} = \frac{2\pi}{tperiod_{w,1}} \tag{B.31}$$

The fourth section must be calculated each hour for each wind farm:

(4.1) For each wind farm w, calculate total hourly wind speed, where hr is the hour of the day. First generate a normally distributed random number, then move the previous hourly autoregressive calculations one hour back and calculate this hour's synthetic normally distributed residual $yns_{w,0}$. z is a random number uniformly distributed on (0,1):

$$r_h = \frac{\left(z^{0.135} - (1-z)^{0.135}\right)}{0.1975}$$
$$yns_{w,3} = yns_{w,2}$$
$$yns_{w,2} = yns_{w,1} \tag{B.32}$$
$$yns_{w,1} = yns_{w,0}$$
$$yns_{w,0} = \varphi_{w,1}\, yns_{w,1} + \varphi_{w,2}\, yns_{w,2} + \varphi_{w,3}\, yns_{w,3} + \rho_w r_h$$

Apply reverse data transformation to calculate this hour's synthetic wind speed residual ys_w:

$$ys_w = 1.96 - \left(1.4 - 0.302\, yns_{w,0}\right)^2 \quad yns_{w,0} < 0$$
$$ys_w = \left(1.4 + 0.302\, yns_{w,0}\right)^2 - 1.96 \quad yns_{w,0} \geq 0 \tag{B.33}$$

Calculate diurnal wind speed:

$$
\begin{aligned}
&vdiurnal_w = 0 \\
&vdiurnal_w = vdiurnal_w + tmag_{w,0} \cos\left(tfreq_{w,0}\left(hr - tpeak_{w,0}\right)\right) \;\; tstart_{w,0} < hr < tstop_{w,0} \\
&vdiurnal_w = vdiurnal_w + tmag_{w,1} \cos\left(tfreq_{w,1}\left(hr - tpeak_{w,1}\right)\right) \;\; tstart_{w,1} < hr < tstop_{w,1}
\end{aligned}
\tag{B.34}
$$

Calculate daily average wind speed trend:

$$
vhm_w = vdavl_w + \frac{hr\left(vdav_w - vdavl_w\right)}{24} \tag{B.35}
$$

Calculate total hourly wind speed:

$$
\begin{aligned}
&v_w = vhm_w + vdiurnal_w + \sigma_w \, ys_w \\
&if\left(v_w < 0\right) v_w = 0
\end{aligned}
\tag{B.36}
$$

(4.2) For each wind farm w, calculate wind shear factor and hub height wind speed. m is the number of the current month.

$$
\begin{aligned}
&if\left(hr < justafterdawn_{w,m}\right)\ hr = hr + 24\\
&if\left(hr < beforedusk_{w,m}\right)\\
&\{\ if\left(hr < afterdawn_{w,m}\right)\\
&\quad wsf = wsfbase_{w,m} + 0.5\left(hr - justafterdawn_{w,m}\right)\left(awsf_{w,m}\left(v_w - 5\right) - bwsf_w\right)\\
&\ else\\
&\quad wsf = wsfbase_{w,m} + awsf_{w,m}\left(v_w - 5\right) - bwsf_w\ \ \}\\
&else\\
&\{ if\left(hr < night_{w,m}\right)\\
&\quad wsf = wsfbase_{w,m} + 0.25\left(hr - beforedusk_{w,m}\right)\left(cwsf_w + dwsf_w\left(8 - v_w\right)\right)\\
&\ \ else\\
&\quad wsf = wsfbase_{w,m} + cwsf_w + dwsf_w\left(8 - v_w\right)\ \}\\
&if\left(wsf < 0\right) wsf = 0\\
&if\left(wsf > 0.7\right) wsf = 0.7\\
&vhh_w = v_w\left(\frac{hh_{wt}}{50}\right)^{wsf}
\end{aligned}
\qquad \text{(B.37)}
$$

where hh_{wt} is the hub height of turbine wt used by wind farm w, and vhh_w is the hub-height wind speed of wind farm w.

(4.3) Calculate wind farm power output for each wind farm w, using wind turbine wt:

$$
\begin{aligned}
&if\left(vhh_w \le vc_{wt}\right) CF = 0\\
&else\\
&\{ if\left(vhh_w \ge vr_{wt}\right)\\
&\quad \{ if\left(vhh_w > vs_{wt}\right)\\
&\quad\quad \{ vd = vhh_w - vs_{wt}\\
&\quad\quad\quad if\left(vd \ge 6\right) CF = 0\\
&\quad\quad\quad else\\
&\quad\quad\quad if\left(vd \ge 3\right)\\
&\quad\quad\quad\quad CF = \frac{\left(vd-6\right)^2}{18}\\
&\quad\quad\quad else\\
&\quad\quad\quad\quad CF = 1 - \frac{vd^2}{18} \ \}\\
&\quad\quad else \ \ CF = 1 \ \}\\
&\quad else\\
&\quad\quad if\left(vhh_w \le vf_{wt}\right) \ CF = a_{wt} + b_{wt} vhh_w^3\\
&\quad\quad else\\
&\quad\quad \{ \ vd = vr_{wt} - vhh_w\\
&\quad\quad\quad CF = 1 - c_{wt} vd^3 \ \}\}\\
&power_w = CF * capacity_w
\end{aligned}
\tag{B.38}
$$

where $capacity_w$ is the full power capacity of wind farm w.

(4.4) Advance the hour of the day variable hr by 1. If $hr \ge 24$, advance the day of year variable DOY by 1 and set $hr = 0$. If $DOY > 365$ (or $DOY > 366$ if a leap year is being modelled), set $DOY = 1$.

C Formulation of statistical measures

The Root Mean Square Error (RMSE) is calculated using:

$$\mathrm{RMSE}=\frac{1}{N}\sqrt{\sum_{i=1}^{N}\left(h_m-h_d\right)^2}$$

where h_d is the measured data value, h_m is the model generated synthetic data value, and N is the number of data points. RMSE can be represented as a percentage value by dividing by the mean value of h_d and multiplying by 100.

The Mean Bias Error (MBE) is calculated using:

$$\mathrm{MBE}=\frac{1}{N}\sum_{i=1}^{N}\left(h_m-h_d\right)$$

MBE can be represented as a percentage value by dividing by the mean value of h_d and multiplying by 100. The RMSE is a measure of the magnitude of the difference between individual data points in each data set. The sign of the difference is ignored. The MBE is a measure of the average difference between individual data points in each data set, or whether the model generated data set is biased higher or lower compared to the measured data on the whole. Here the sign of the difference is not ignored. Generally, a model with a lower RMSE than another fits the data more closely. In this study a model with a negative MBE might be considered more favourably than a model with a similar but positive MBE because under predicting power generation on the whole is more desirable than over predicting. Representing RMSE and MBE as a percentage gives an idea of how significant the error is compared to the average value of the measured data.

The Mean Absolute Percentage Error (MAPE) is calculated using:

$$\mathrm{MAPE}=\frac{1}{N}\sum_{i=1}^{N}\frac{\left|h_m-h_d\right|}{h_d}$$

To be represented as a percentage value, the MAPE can be multiplied by 100. The Mean Relative Variance (MRV) is calculated using:

$$\mathrm{MRV}=\frac{\sum_{i=1}^{N}\left(h_m-h_d\right)^2}{\sum_{i=1}^{N}\left(h_d-h_{\mathrm{dav}}(h)\right)^2}$$

where $h_{dav}(h)$ is the average of the measured hourly values h_d for hour h. Standard error for monthly average of daily values is calculated using:

$$\mathrm{SE}=\frac{1}{12}\sqrt{\sum_{m=1}^{12}\left((h_{mdav}(m)-h_{dav}(m))dim(m)\right)^2}$$

where $h_{dav}(m)$ is the monthly average of the measured daily values, $h_{mdav}(m)$ is the monthly average of the model generated synthetic daily values, and dim(m) is the number of days in each month.

References

ABS. 2011. "2011 Census QuickStats Greater Perth." Perth: Australian Bureau of Statistics. http://www.censusdata.abs.gov.au/census_services/getproduct/census/2011/quickstat/5GPER?opendocument&navpos=220.

———. 2015. "3218.0 - Regional Population Growth, Australia, 2013-14." Canberra: Australian Bureau of Statistics. http://www.abs.gov.au/AUSSTATS/abs@.nsf/Lookup/3218.0Main+Features12013-14?OpenDocument.

ACT Government. 2016. "100% Renewable Energy by 2020." *Environment and Planning Directorate - Environment*. March 5. http://www.environment.act.gov.au/home/latest_news/100-renewable-energy-by-2020.

Aguiar, R., and M. Collares-Pereira. 1992. "TAG: A Time-Dependent, Autoregressive, Gaussian Model for Generating Synthetic Hourly Radiation." *Solar Energy* 49 (3): 167–74. doi:10.1016/0038-092X(92)90068-L.

Ahlstrom, M., L. Jones, R. Zavadil, and W. Grant. 2005. "The Future of Wind Forecasting and Utility Operations." *Power and Energy Magazine, IEEE* 3 (6): 57–64.

Ahmad, M. J., and G. N. Tiwari. 2008. "Study of Models for Predicting the Mean Hourly Global Radiation from Daily Summations." *Open Environmental Journal* 2: 6–14.

Ahmadi, L., S. B. Young, M. Fowler, R. A. Fraser, and M. A. Achachlouei. 2015. "A Cascaded Life Cycle: Reuse of Electric Vehicle Lithium-Ion Battery Packs in Energy Storage Systems." *The International Journal of Life Cycle Assessment* 22 (1): 111–24. doi:10.1007/s11367-015-0959-7.

Allinson, G., Y. Cinar, W. Hou, and P. R. Neal. 2009. "The Costs of CO2 Transport and Injection in Australia." *School of Petroleum Engineering, the University of New South Wales, Sydney, Australia. CO2TECH Report Number RPT09-1536*. https://www.researchgate.net/profile/Peter_Neal/publication/254532325_Costs_Of_CO2_Transport_And_Injection_In_Australia/links/53f7372f0cf22be01c454d93.pdf.

Alvarez, R. A., S. W. Pacala, J. J. Winebrake, W. L. Chameides, and S. P. Hamburg. 2012. "Greater Focus Needed on Methane Leakage from Natural Gas Infrastructure." *Proceedings of the National Academy of Sciences* 109 (17): 6435–6440.

Anderson, K., and A. Bows. 2008. "Reframing the Climate Change Challenge in Light of Post-2000 Emission Trends." *Philosophical Transactions of the Royal Society A: Mathematical, Physical and Engineering Sciences* 366 (1882): 3863–82. doi:10.1098/rsta.2008.0138.

Aoki, M., and G. Rothwell. 2013. "A Comparative Institutional Analysis of the Fukushima Nuclear Disaster: Lessons and Policy Implications." *Energy Policy* 53 (February): 240–47. doi:10.1016/j.enpol.2012.10.058.

APVI. 2016. "Australian PV Institute (APVI) Solar Map, Funded by the Australian Renewable Energy Agency." Australian PV Institute. pv-map.apvi.org.au.

Archer, C. L., and M. Z. Jacobson. 2003. "Spatial and Temporal Distributions of US Winds and Wind Power at 80 M Derived from Measurements." *Journal of Geophysical Research: Atmospheres* 108 (D9). http://onlinelibrary.wiley.com/doi/10.1029/2002JD002076/full.

———. 2007. "Supplying Baseload Power and Reducing Transmission Requirements by Interconnecting Wind Farms." *Journal of Applied Meteorology and Climatology* 46 (11): 1701–17. doi:10.1175/2007JAMC1538.1.

Asadullah, M. 2014. “Barriers of Commercial Power Generation Using Biomass Gasification Gas: A Review.” *Renewable and Sustainable Energy Reviews* 29 (January): 201–15. doi:10.1016/j.rser.2013.08.074.

Asdrubali, F., G. Baldinelli, F. D’Alessandro, and F. Scrucca. 2015. “Life Cycle Assessment of Electricity Production from Renewable Energies: Review and Results Harmonization.” *Renewable and Sustainable Energy Reviews* 42 (February): 1113–22. doi:10.1016/j.rser.2014.10.082.

Ashley, S. F., G. T. Parks, W. J. Nuttall, C. Boxall, and R. W. Grimes. 2012. “Nuclear Energy: Thorium Fuel Has Risks.” *Nature* 492 (7427): 31–33.

Avila-Marin, A. L., J. Fernandez-Reche, and F. M. Tellez. 2013. “Evaluation of the Potential of Central Receiver Solar Power Plants: Configuration, Optimization and Trends.” *Applied Energy* 112 (December): 274–88. doi:10.1016/j.apenergy.2013.05.049.

AWDC. 2011. “Perth Snapshot 2011.” Perth: Aboriginal workforce development centre. Government of Western Australia department of training and workforce development. http://www.dtwd.wa.gov.au/employeesandstudents/aboriginalworkforcedevelopmentcentre/resources/regional-snapshots/Documents/Final%20Perth%20Snapshot%202011%20V1%202.pdf.

Backlund, S., P. Thollander, J. Palm, and M. Ottosson. 2012. “Extending the Energy Efficiency Gap.” *Energy Policy* 51: 392–396.

Baharoon, D. A., H. A. Rahman, W. Z. W. Omar, and S. O. Fadhl. 2015. “Historical Development of Concentrating Solar Power Technologies to Generate Clean Electricity Efficiently – A Review.” *Renewable and Sustainable Energy Reviews* 41 (January): 996–1027. doi:10.1016/j.rser.2014.09.008.

Bahrman, M. P. 2008. “HVDC Transmission Overview.” In *Transmission and Distribution Conference and Exposition, 2008. T&# x00026; D. IEEE/PES*, 1–7. IEEE. http://ieeexplore.ieee.org/xpls/abs_all.jsp?arnumber=4517304.

Barbour, E., D. Mignard, Y. Ding, and Y. Li. 2015. “Adiabatic Compressed Air Energy Storage with Packed Bed Thermal Energy Storage.” *Applied Energy* 155 (October): 804–15. doi:10.1016/j.apenergy.2015.06.019.

Barnham, K. W. J., M. Mazzer, and B. Clive. 2006. “Resolving the Energy Crisis: Nuclear or Photovoltaics?” *Nature Materials* 5 (3): 161–164.

Barnhart, C. J., and S. M. Benson. 2013. “On the Importance of Reducing the Energetic and Material Demands of Electrical Energy Storage.” *Energy & Environmental Science* 6 (4): 1083. doi:10.1039/c3ee24040a.

Barrett, M. 2006. “A Renewable Electricity System for the UK. A Response to the 2006 Energy Review.” Complex Built Environment Systems Group, Bartlett School of Graduate Studies, University College London.

Bartle, J., and A. Abadi. 2010. “Toward Sustainable Production of Second Generation Bioenergy Feedstocks †.” *Energy & Fuels* 24 (1): 2–9. doi:10.1021/ef9006438.

Bartle, J., G. Olsen, D. Cooper, and T. Hobbs. 2007. “Scale of Biomass Production from New Woody Crops for Salinity Control in Dryland Agriculture in Australia.” *International Journal of Global Energy Issues* 27 (2): 115–137.

Bayless, C. E. 2010. “The Case for Baseload.” *Electric Perspectives*, September.

Bayón, R., and E. Rojas. 2013. “Simulation of Thermocline Storage for Solar Thermal Power Plants: From Dimensionless Results to Prototypes and Real-Size Tanks.” *International Journal of Heat and Mass Transfer* 60 (May): 713–21. doi:10.1016/j.ijheatmasstransfer.2013.01.047.

Bilgili, M., A. Ozbek, B. Sahin, and A. Kahraman. 2015. “An Overview of Renewable Electric Power Capacity and Progress in New Technologies in the World.” *Renewable and Sustainable Energy Reviews* 49 (September): 323–34. doi:10.1016/j.rser.2015.04.148.

Billinton, R., H. Chen, and R. Ghajar. 1996. "Time-Series Models for Reliability Evaluation of Power Systems Including Wind Energy." *Microelectronics Reliability* 36 (9): 1253–61.

Blackburn, J. 2010. "Matching Utility Loads with Solar and Wind Power in North Carolina Dealing with Intermittent Electricity Sources." Takoma Park, USA: Institute for Energy and Environmental Research. http://www.geni.org/globalenergy/library/technical-articles/generation/policy/eere/groundbreaking-study-finds/NC-Wind-Solar.pdf.

Bogardi, I., and I. Matyasovzky. 1996. "Estimating Daily Wind Speed under Climate Change." *Solar Energy* 57 (3): 239–248.

Boland, J. 1995. "Time-Series Analysis of Climatic Variables." *Solar Energy* 55 (5): 377–388.

BOM. 2012. "Mean Monthly, Season and Annual Solar Exposure Data." Bureau Of Meteorology. http://www.bom.gov.au/jsp/ncc/climate_averages/solar-exposure/index.jsp.

Boudghene Stambouli, A., Z. Khiat, S. Flazi, H. Tanemoto, M. Nakajima, H. Isoda, F. Yokoyama, et al. 2014. "Trends and Challenges of Sustainable Energy and Water Research in North Africa: Sahara Solar Breeder Concerns at the Intersection of Energy/Water." *Renewable and Sustainable Energy Reviews* 30 (February): 912–22. doi:10.1016/j.rser.2013.11.042.

Bouman, E. A., A. Ramirez, and E. G. Hertwich. 2015. "Multiregional Environmental Comparison of Fossil Fuel Power generation—Assessment of the Contribution of Fugitive Emissions from Conventional and Unconventional Fossil Resources." *International Journal of Greenhouse Gas Control* 33 (February): 1–9. doi:10.1016/j.ijggc.2014.11.015.

Box, G. E. P., and G. M. Jenkins. 1976. *Time Series Analysis: Forecasting and Control*. Rev. ed. Holden-Day Series in Time Series Analysis and Digital Processing. San Francisco: Holden-Day.

Bradshaw, J., B. Bradshaw, G. Allinson, A. Rigg, V. Nguyen, and L. Spencer. 2002. "The Potential for Geological Sequestration of CO2 in Australia: Preliminary Findings and Implications for New Gas Field Development." *APPEA Journal*.

Brown, B. G., R. W. Katz, and A. H. Murphy. 1984. "Time Series Models to Simulate and Forecast Wind Speed and Wind Power." *Journal of Climate and Applied Meteorology* 23 (8): 1184–95. doi:10.1175/1520-0450(1984)023<1184:TSMTSA>2.0.CO;2.

Budischak, C., D. Sewell, H. Thomson, L. Mach, D. E. Veron, and W. Kempton. 2013. "Cost-Minimized Combinations of Wind Power, Solar Power and Electrochemical Storage, Powering the Grid up to 99.9% of the Time." *Journal of Power Sources* 225 (March): 60–74. doi:10.1016/j.jpowsour.2012.09.054.

Burton, T., D. Sharpe, N. Jenkins, and E. Bossanyi. 2001. *Wind Energy Handbook*. 2nd ed. John Wiley & Sons.

Butt, N., M. New, Y. Malhi, A. C. L. da Costa, P. Oliveira, and J. E. Silva-Espejo. 2010. "Diffuse Radiation and Cloud Fraction Relationships in Two Contrasting Amazonian Rainforest Sites." *Agricultural and Forest Meteorology* 150 (3): 361–68. doi:10.1016/j.agrformet.2009.12.004.

Carlin, J., and J. Haslett. 1982. "The Probability Distribution of Wind Power from a Dispersed Array of Wind Turbine Generators." *Journal of Applied Meteorology* 21 (3): 303–313.

Carr, A. ., and T. . Pryor. 2004. "A Comparison of the Performance of Different PV Module Types in Temperate Climates." *Solar Energy* 76 (1–3): 285–94. doi:10.1016/j.solener.2003.07.026.

Carta, J. A., P. Ramírez, and S. Velázquez. 2009. "A Review of Wind Speed Probability Distributions Used in Wind Energy Analysis." *Renewable and Sustainable Energy Reviews* 13 (5): 933–55. doi:10.1016/j.rser.2008.05.005.

Cavallo, A. J. 1995. "High-Capacity Factor Wind Energy Systems." *TRANSACTIONS-AMERICAN SOCIETY OF MECHANICAL ENGINEERS JOURNAL OF SOLAR ENERGY ENGINEERING* 117: 137–137.

Celik, A. N. 2002. "The System Performance of Autonomous Photovoltaic–wind Hybrid Energy Systems Using Synthetically Generated Weather Data." *Renewable Energy* 27 (1): 107–121.

Cha, S. T., H. Zhao, Q. Wu, A. Saleem, and J. Østergaard. 2012. "Coordinated Control Scheme of Battery Energy Storage System (BESS) and Distributed Generations (DGs) for Electric Distribution Grid Operation." In *IECON 2012-38th Annual Conference on IEEE Industrial Electronics Society*, 4758–4764. IEEE. http://ieeexplore.ieee.org/xpls/abs_all.jsp?arnumber=6389587.

Charles, W., R. Cord-Ruwisch, G. Ho, M. Costa, and P. Spencer. 2006. "Solutions to a Combined Problem of Excessive Hydrogen Sulfide in Biogas and Struvite Scaling." *Water Science and Technology* 53 (6): 203–211.

Chen, Z., and F. Blaabjerg. 2009. "Wind farm–A Power Source in Future Power Systems." *Renewable and Sustainable Energy Reviews* 13 (6–7): 1288–1300.

Cheng, S., D. Xing, D. F. Call, and B. E. Logan. 2009. "Direct Biological Conversion of Electrical Current into Methane by Electromethanogenesis." *Environmental Science & Technology* 43 (10): 3953–58. doi:10.1021/es803531g.

Cherubini, F., N. D. Bird, A. Cowie, G. Jungmeier, B. Schlamadinger, and S. Woess-Gallasch. 2009. "Energy- and Greenhouse Gas-Based LCA of Biofuel and Bioenergy Systems: Key Issues, Ranges and Recommendations." *Resources, Conservation and Recycling* 53 (8): 434–47. doi:10.1016/j.resconrec.2009.03.013.

Chua, K. J., S. K. Chou, W. M. Yang, and J. Yan. 2013. "Achieving Better Energy-Efficient Air Conditioning – A Review of Technologies and Strategies." *Applied Energy* 104 (April): 87–104. doi:10.1016/j.apenergy.2012.10.037.

Clarke, R. 1989. "Sea-Breezes and Waves: The Kalgoorlie Sea-Breeze and the Goondiwindi Breeze." *Aust. Met. Mag* 37: 99–107.

Cochran, T. B. 2010. *Fast Breeder Reactor Programs: History and Status*.

Connolly, D., H. Lund, B. V. Mathiesen, and M. Leahy. 2011. "The First Step towards a 100% Renewable Energy-System for Ireland." *Applied Energy* 88 (2): 502–7. doi:10.1016/j.apenergy.2010.03.006.

Coops, N. C., R. H. Waring, and J. B. Moncrieff. 2000. "Estimating Mean Monthly Incident Solar Radiation on Horizontal and Inclined Slopes from Mean Monthly Temperatures Extremes." *International Journal of Biometeorology* 44 (4): 204–11.

Coppin, P., K. Ayotte, and N. Steggel. 2003. *Wind Resource Assessment in Australia: A Planners Guide*. CSIRO Wind Energy Research Unit.

Correia, P. F., and J. M. Ferreira de Jesus. 2010. "Simulation of Correlated Wind Speed and Power Variates in Wind Parks." *Electric Power Systems Research* 80 (5): 592–98. doi:10.1016/j.epsr.2009.10.031.

Da Silva, E. L., J. J. Hedgecock, J. C. O. Mello, and J. C. F. Da Luz. 2001. "Practical Cost-Based Approach for the Voltage Ancillary Service." *Power Systems, IEEE Transactions on* 16 (4): 806–812.

Damen, K., M. van Troost, A. Faaij, and W. Turkenburg. 2006. "A Comparison of Electricity and Hydrogen Production Systems with CO2 Capture and Storage. Part A: Review and Selection of Promising Conversion and Capture Technologies." *Progress in Energy and Combustion Science* 32 (2): 215–46. doi:10.1016/j.pecs.2005.11.005.

Damsleth, E., and A. H. El-Shaarawi. 1989. "ARMA Models with Double-Exponentially Distributed Noise." *Journal of the Royal Statistical Society. Series B (Methodological)* 51 (1): 61–69.

Darling, S. B., F. You, T. Veselka, and A. Velosa. 2011. "Assumptions and the Levelized Cost of Energy for Photovoltaics." *Energy & Environmental Science* 4 (9): 3133. doi:10.1039/c0ee00698j.

Davies, J. A., M. Abdel-Wahab, and J. E. Howard. 1985. “Cloud Transmissivities for Canada.” *Monthly Weather Review* 113 (3): 338–48. doi:10.1175/1520-0493(1985)113<0338:CTFC>2.0.CO;2.

Davis, W., and M. Martín. 2014. “Optimal Year-Round Operation for Methane Production from CO2 and Water Using Wind Energy.” *Energy* 69 (May): 497–505. doi:10.1016/j.energy.2014.03.043.

DeConto, R. M., and D. Pollard. 2016. “Contribution of Antarctica to Past and Future Sea-Level Rise.” *Nature* 531 (7596): 591–97. doi:10.1038/nature17145.

Delucchi, M. A., and M. Z. Jacobson. 2011. “Providing All Global Energy with Wind, Water, and Solar Power, Part II: Reliability, System and Transmission Costs, and Policies.” *Energy Policy* 39 (3): 1170–90. doi:10.1016/j.enpol.2010.11.045.

Denholm, P., and M. Hand. 2011. “Grid Flexibility and Storage Required to Achieve Very High Penetration of Variable Renewable Electricity.” *Energy Policy* 39 (3): 1817–30. doi:10.1016/j.enpol.2011.01.019.

Denholm, P., and R. Margolis. 2006. “Very Large-Scale Deployment of Grid-Connected Solar Photovoltaics in the United States: Challenges and Opportunities.” In , 9–13. Denver: U.S. Department of Energy Office of Scientific and Technical Information.

Denholm, P., and M. Mehos. 2011. “Enabling Greater Penetration of Solar Power via the Use of CSP with Thermal Energy Storage.” National Renewable Energy Laboratory.

Denholm, P., Y.-H. Wan, M. Hummon, and M. Mehos. 2013. “An Analysis of Concentrating Solar Power with Thermal Energy Storage in a California 33% Renewable Scenario.” *Contract* 303: 275–3000.

Diesendorf, M. 2005. “Can Nuclear Energy Reduce CO2 Emissions?” *Australasian Science*, July.

———. 2006a. “Can Geosequestration Save the Coal Industry?” *Transforming Power: Energy, Environment, and Society in Conflict* 9: 221.

———. 2006b. “Wind Power in Australia.” *International Journal of Environmental Studies* 63 (6): 765–76. doi:10.1080/00207230601047099.

Digman, B., H. S. Joo, and D.-S. Kim. 2009. “Recent Progress in Gasification/Pyrolysis Technologies for Biomass Conversion to Energy.” *Environmental Progress & Sustainable Energy* 28 (1): 47–51. doi:10.1002/ep.10336.

DIT. 2012. *State of Australian Cities 2012.* Canberra, ACT: Infrastructure Australia, Department of Infrastructure and Transport Major Cities Unit.

DOE. 2008. “20% Wind Energy by 2030 Increasing Wind Energy’s Contribution to U.S. Electricity Supply.” U.S. Department of Energy.

Donatelli, M., G. Bellocchi, E. Habyarimana, R. Confalonieri, and F. Micale. 2009. “An Extensible Model Library for Generating Wind Speed Data.” *Computers and Electronics in Agriculture* 69 (2): 165–70. doi:10.1016/j.compag.2009.07.022.

Dortolina, C. A., and R. Nadira. 2005. “The Loss That Is Unknown Is No Loss At All: A Top-Down/Bottom-Up Approach for Estimating Distribution Losses.” *IEEE Transactions on Power Systems* 20 (2): 1119–25. doi:10.1109/TPWRS.2005.846104.

Droege, P. 2012. *100% Renewable: Energy Autonomy in Action*. Routledge.

Ela, E., and B. Kirby. 2008. *ERCOT Event on February 26, 2008: Lessons Learned*. National Renewable Energy Laboratory. http://consultkirby.com/files/NREL-TP-500-43373_ERCOT_Event_on_February_26_2008_Lessons_Learned.pdf.

Elliston, B., M. Diesendorf, and I. MacGill. 2012. “Simulations of Scenarios with 100% Renewable Electricity in the Australian National Electricity Market.” *Energy Policy* 45 (June): 606–13. doi:10.1016/j.enpol.2012.03.011.

Elliston, B., I. MacGill, and M. Diesendorf. 2014. “Comparing Least Cost Scenarios for 100% Renewable Electricity with Low Emission Fossil Fuel Scenarios in the Australian National Electricity Market.” *Renewable Energy* 66 (June): 196–204. doi:10.1016/j.renene.2013.12.010.

Eltawil, M. A., and Z. Zhao. 2010. "Grid-Connected Photovoltaic Power Systems: Technical and Potential problems—A Review." *Renewable and Sustainable Energy Reviews* 14 (1): 112–29. doi:10.1016/j.rser.2009.07.015.

EPRI. 2015. "The Australian Power Generation Technology Report." Australia: Electric Power Research Institute.

ESIEP. 2011. "Tasmania's Energy Sector–an Overview." Discussion Paper. Tasmania: Electricity Supply Industry Expert Panel. http://webarchive.linc.tas.gov.au/20120306075025/http://www.electricity.tas.gov.au/__data/assets/pdf_file/0017/141803/Tasmania_s_Energy_Sector_-_an_Overview.PDF.

Evans, A., V. Strezov, and T. J. Evans. 2010. "Sustainability Considerations for Electricity Generation from Biomass." *Renewable and Sustainable Energy Reviews* 14 (5): 1419–27. doi:10.1016/j.rser.2010.01.010.

Ferreira, H. L., R. Garde, G. Fulli, W. Kling, and J. P. Lopes. 2013. "Characterisation of Electrical Energy Storage Technologies." *Energy* 53 (May): 288–98. doi:10.1016/j.energy.2013.02.037.

Foley, A. M., P. G. Leahy, A. Marvuglia, and E. J. McKeogh. 2012. "Current Methods and Advances in Forecasting of Wind Power Generation." *Renewable Energy* 37 (1): 1–8. doi:10.1016/j.renene.2011.05.033.

Fortin, J. G., F. Anctil, L. É. Parent, and M. A. Bolinder. 2008. "Comparison of Empirical Daily Surface Incoming Solar Radiation Models." *Agricultural and Forest Meteorology* 148 (8): 1332–1340.

Fthenakis, V. M., H. C. Kim, and E. Alsema. 2008. "Emissions from Photovoltaic Life Cycles." *Environmental Science & Technology* 42 (6): 2168–2174.

Fu, T. 2011. "A Review on Time Series Data Mining." *Engineering Applications of Artificial Intelligence* 24 (1): 164–81. doi:10.1016/j.engappai.2010.09.007.

Gadonneix, P., F. B. de Castro, N. F. de Medeiros, R. Drouin, C. P. Jain, Y. D. Kim, J. Ferioli, et al. 2010. "2010 Survey of Energy Resources." London: World Energy Council. http://citeseerx.ist.psu.edu/viewdoc/download?doi=10.1.1.366.3256&rep=rep1&type=pdf.

Gardiner, W. D. 2013. "Analysis of the Technical Feasibility of Powering the South-West Interconnected System (SWIS) on 100% Renewable Energy." Masters Dissertation, Murdoch.

Gates, D. M. 2003. *Biophysical Ecology*. Courier Dover Publications.

Gauché, P., S. Pfenninger, A. J. Meyer, T. W. von Backström, and A. C. Brent. 2012. "Modeling Dispatchability Potential of CSP in South Africa." *SASEC 2012*. http://concentrating.sun.ac.za/wp-content/uploads/2012/07/PL-03.pdf.

Gazela, M., and E. Mathioulakis. 2001. "A New Method for Typical Weather Data Selection to Evaluate Long-Term Performance of Solar Energy Systems." *Solar Energy* 70 (4): 339–48. doi:10.1016/S0038-092X(00)00151-1.

Georgilakis, P. S. 2008. "Technical Challenges Associated with the Integration of Wind Power into Power Systems." *Renewable and Sustainable Energy Reviews* 12 (3): 852–863.

Geoscience Australia. 2004. "GEODATA COAST 100K 2004." http://www.ga.gov.au/meta/ANZCW0703006621.html.

Geoscience Australia, and ABARE. 2010. *Australian energy resource assessment*. Canberra, A.C.T.: Dept. of Resources, Energy and Tourism, Geoscience Australia, Australian Bureau of Agricultural and Resource Economics.

Gesthuizen, J. 2011. "Water, Air or Both?" *Sun & Wind Energy*, February.

Gibescu, M., B. C. Ummels, and W. L. Kling. 2006. "Statistical Wind Speed Interpolation for Simulating Aggregated Wind Energy Production under System Studies." In *Probabilistic Methods Applied to Power Systems, 2006. PMAPS 2006. International Conference on*, 1–7. IEEE. http://ieeexplore.ieee.org/xpls/abs_all.jsp?arnumber=4202376.

Giebel, G. 2000. “The Capacity Credit of Wind Energy in Europe, Estimated from Reanalysis Data.” In *Shaping the Future (CD-ROM)*, edited by B. Bretschneider, H. Ehrenfeld, H. Hettche, S. Oetzmann, W. Ternes, and G. F. Walter. EXPO 2000.

Gille, S. T., S. G. Llewellyn Smith, and N. M. Statom. 2005. “Global Observations of the Land Breeze.” *Geophysical Research Letters* 32 (5).

Good, C., T. Kristjansdottír, A. Houlihan Wiberg, L. Georges, and A. G. Hestnes. 2016. “Influence of PV Technology and System Design on the Emission Balance of a Net Zero Emission Building Concept.” *Solar Energy* 130 (June): 89–100. doi:10.1016/j.solener.2016.01.038.

Gordon, J. M., and T. A. Reddy. 1988. “Time Series Analysis of Daily Horizontal Solar Radiation.” *Solar Energy* 41 (3): 215–26. doi:10.1016/0038-092X(88)90139-9.

Götz, M., J. Lefebvre, F. Mörs, A. McDaniel Koch, F. Graf, S. Bajohr, R. Reimert, and T. Kolb. 2016. “Renewable Power-to-Gas: A Technological and Economic Review.” *Renewable Energy* 85 (January): 1371–90. doi:10.1016/j.renene.2015.07.066.

Graham, V. A., and K. G. T. Hollands. 1990. “A Method to Generate Synthetic Hourly Solar Radiation Globally.” *Solar Energy* 44 (6): 333–41. doi:10.1016/0038-092X(90)90137-2.

Graham, V. A., K. G. T. Hollands, and T. E. Unny. 1988. “A Time Series Model for Kt with Application to Global Synthetic Weather Generation.” *Solar Energy* 40 (2): 83–92. doi:10.1016/0038-092X(88)90075-8.

Green, D. G. 2015. “Initial Fuel Possibilities for the Thorium Molten Salt Reactor.” http://scholarsmine.mst.edu/masters_theses/7398/.

Green, M. A., K. Emery, Y. Hishikawa, W. Warta, and E. D. Dunlop. 2015. “Solar Cell Efficiency Tables (Version 45): Solar Cell Efficiency Tables.” *Progress in Photovoltaics: Research and Applications* 23 (1): 1–9. doi:10.1002/pip.2573.

Guandalini, G., S. Campanari, and M. C. Romano. 2015. “Power-to-Gas Plants and Gas Turbines for Improved Wind Energy Dispatchability: Energy and Economic Assessment.” *Applied Energy* 147 (June): 117–30. doi:10.1016/j.apenergy.2015.02.055.

Gueymard, C. A. 2004. “The Sun’s Total and Spectral Irradiance for Solar Energy Applications and Solar Radiation Models.” *Solar Energy* 76 (4): 423–53. doi:10.1016/j.solener.2003.08.039.

Gunturu, U. B., and C. A. Schlosser. 2012. “Characterization of Wind Power Resource in the United States.” *Atmospheric Chemistry and Physics* 12 (20): 9687–9702. doi:10.5194/acp-12-9687-2012.

Gutierrez, M. J. F. 2005. “Nitrous Oxide (N2O) Emissions from Waste and Biomass to Energy Plants.” *Waste Management & Research* 23 (2): 133–47. doi:10.1177/0734242X05052803.

Hadjipaschalis, I., A. Poullikkas, and V. Efthimiou. 2009. “Overview of Current and Future Energy Storage Technologies for Electric Power Applications.” *Renewable and Sustainable Energy Reviews* 13 (6–7): 1513–1522.

Haslett, J., and A. E. Raftery. 1989. “Space-Time Modelling with Long-Memory Dependence: Assessing Ireland’s Wind Power Resource.” *Applied Statistics* 38 (1): 1. doi:10.2307/2347679.

Hay, J. E. 1979. “Calculation of Monthly Mean Solar Radiation for Horizontal and Inclined Surfaces.” *Solar Energy* 23 (4): 301–7. doi:10.1016/0038-092X(79)90123-3.

Hearps, P., R. Dargaville, D. McConnell, M. Sandiford, and P. Seligman. 2014. “Opportunities for Pumped Hydro Energy Storage in Australia.” Melbourne: Melbourne Energy Institute.

Herbergs, S., H. Lehmann, and S. Peter. 2009. “The Computer-Modelled Simulation Of Renewable Electricity Networks.” Aachen: ISUSI, Institute for Sustainable Solutions and Innovations.

Hernandez, R. R., S. B. Easter, M. L. Murphy-Mariscal, F. T. Maestre, M. Tavassoli, E. B. Allen, C. W. Barrows, et al. 2014. “Environmental Impacts of Utility-Scale Solar Energy.”

Renewable and Sustainable Energy Reviews 29 (January): 766–79. doi:10.1016/j.rser.2013.08.041.

Herring, H. 2006. "Energy Efficiency–a Critical View." *Energy* 31 (1): 10–20.

Hertwich, E. G., T. Gibon, E. A. Bouman, A. Arvesen, S. Suh, G. A. Heath, J. D. Bergesen, A. Ramirez, M. I. Vega, and L. Shi. 2015. "Integrated Life-Cycle Assessment of Electricity-Supply Scenarios Confirms Global Environmental Benefit of Low-Carbon Technologies." *Proceedings of the National Academy of Sciences* 112 (20): 6277–6282.

Hill, D. C., D. McMillan, K. R. W. Bell, and D. Infield. 2012. "Application of Auto-Regressive Models to U.K. Wind Speed Data for Power System Impact Studies." *IEEE Transactions on Sustainable Energy* 3 (1): 134–41. doi:10.1109/TSTE.2011.2163324.

Hinkley, J., B. Curtin, J. Hayward, A. Wonhas, R. Boyd, C. Grima, A. Tadros, R. Hall, K. Naicker, and A. Mikhail. 2011. "Concentrating Solar Power–drivers and Opportunities for Cost-Competitive Electricity." *Clayton South: CSIRO*. https://publications.csiro.au/rpr/download?pid=csiro:EP111647&dsid=DS3.

Ho, D. P., H. H. Ngo, and W. Guo. 2014. "A Mini Review on Renewable Sources for Biofuel." *Bioresource Technology* 169 (October): 742–49. doi:10.1016/j.biortech.2014.07.022.

Hohmeyer, O., and T. Trittin. 2008. "IPCC Scoping Meeting on Renewable Energy Sources Ii – Proceedings." Intergovernmental Panel on Climate Change.

Hollands, K. G. T., and R. G. Huget. 1983. "A Probability Density Function for the Clearness Index, with Applications." *Solar Energy* 30 (3): 195–209. doi:10.1016/0038-092X(83)90149-4.

Holttinen, H. 2005. "Hourly Wind Power Variations in the Nordic Countries." *Wind Energy* 8 (2): 173–195.

Holttinen, H., V. T. T. Bettina Lemstr\öm, F. P. Meibom, H. Bindner, and others. 2007. "Design and Operation of Power Systems with Large Amounts of Wind Power." *Final Report, IEA WIND Task* 25 (October): 2006–2008.

Holttinen, H., M. Milligan, E. Ela, N. Menemenlis, J. Dobschinski, B. Rawn, R. J. Bessa, D. Flynn, E. Gomez Lazaro, and N. Detlefsen. 2013. "Methodologies to Determine Operating Reserves due to Increased Wind Power." In *Power and Energy Society General Meeting (PES), 2013 IEEE*, 1–10. IEEE. http://ieeexplore.ieee.org/xpls/abs_all.jsp?arnumber=6673067.

Hontoria, L., J. Aguilera, and P. Zufiria. 2002. "Generation of Hourly Irradiation Synthetic Series Using the Neural Network Multilayer Perceptron." *Solar Energy* 72 (5): 441–46. doi:10.1016/S0038-092X(02)00010-5.

Hontoria, L., J. Aguilera, and P. Zufiria. 2005. "An Application of the Multilayer Perceptron: Solar Radiation Maps in Spain." *Solar Energy* 79 (5): 523–530.

Hosenuzzaman, M., N. A. Rahim, J. Selvaraj, M. Hasanuzzaman, A. B. M. A. Malek, and A. Nahar. 2015. "Global Prospects, Progress, Policies, and Environmental Impact of Solar Photovoltaic Power Generation." *Renewable and Sustainable Energy Reviews* 41 (January): 284–97. doi:10.1016/j.rser.2014.08.046.

Hoste, G., M. Dvorak, and M. Z. Jacobson. 2009. *Matching Hourly and Peak Demand by Combining Different Renewable Energy Sources*. VPUE Final Report, Stanford University, Palo Alto, California.

Hughes, M. G., and A. D. Heap. 2010. "National-Scale Wave Energy Resource Assessment for Australia." *Renewable Energy* 35 (8): 1783–91. doi:10.1016/j.renene.2009.11.001.

Huld, T., R. Gottschalg, H. G. Beyer, and M. Topič. 2010. "Mapping the Performance of PV Modules, Effects of Module Type and Data Averaging." *Solar Energy* 84 (2): 324–38. doi:10.1016/j.solener.2009.12.002.

Huntington, H. G. 2011. "The Policy Implications of Energy-Efficiency Cost Curves." *The Energy Journal* 32 (SI1): 7–22.

Hutchinson, M. F., T. H. Booth, J. P. McMahon, and H. A. Nix. 1984. "Estimating Monthly Mean Valuesof Daily Total Solar Radiation for Australia." *Solar Energy* 32 (2): 277–290.

IEA. 2007. "Biomass for Power Generation and CHP." Brief. International Energy Agency.

———. 2014. "Renewable Energy Medium-Term Market Report 2014." https://www.iea.org/Textbase/npsum/MTrenew2014sum.pdf.

IPCC. 2005. *IPCC Special Report on Carbon Dioxide Capture and Storage. Prepared by Working Group III of the Intergovernmental Panel on Climate Change [Metz, B., O. Davidson, H. C. de Coninck, M. Loos, and L. A. Meyer (Eds.)].* Cambridge: Cambridge University Press, for the Intergovernmental Panel on Climate Change.

———. 2013. "Climate Change 2013: The Physical Science Basis: Working Group I Contribution to the Fifth Assessment Report of the Intergovernmental Panel on Climate Change." New York: Cambridge University Press.

IRENA. 2015. "Battery Storage For Renewables: Market Status And Technology Outlook."

Islam, M. R., S. Mekhilef, and R. Saidur. 2013. "Progress and Recent Trends of Wind Energy Technology." *Renewable and Sustainable Energy Reviews* 21 (May): 456–68. doi:10.1016/j.rser.2013.01.007.

Itard, L. 2007. "Environmental Impacts of Renovation Activities." In *ENHR International Conference Sustainable Urban Areas W15-Housing and Urban Sustainability*.

Jacobson, M. Z. 2009. "Review of Solutions to Global Warming, Air Pollution, and Energy Security." *Energy & Environmental Science* 2 (2): 148. doi:10.1039/b809990c.

Jacobson, M. Z., M. A. Delucchi, G. Bazouin, Z. A. F. Bauer, C. C. Heavey, E. Fisher, S. B. Morris, D. J. Y. Piekutowski, T. A. Vencill, and T. W. Yeskoo. 2015. "100% Clean and Renewable Wind, Water, and Sunlight (WWS) All-Sector Energy Roadmaps for the 50 United States." *Energy Environ. Sci.* 8 (7): 2093–2117. doi:10.1039/C5EE01283J.

Jean, J., P. R. Brown, R. L. Jaffe, T. Buonassisi, and V. Bulović. 2015. "Pathways for Solar Photovoltaics." *Energy Environ. Sci.* 8 (4): 1200–1219. doi:10.1039/C4EE04073B.

Jentsch, M., T. Trost, and M. Sterner. 2014. "Optimal Use of Power-to-Gas Energy Storage Systems in an 85% Renewable Energy Scenario." *Energy Procedia* 46: 254–61. doi:10.1016/j.egypro.2014.01.180.

Jones, B., N. Wilmot, and A. Lark. 2012. "Study on the Impact of Photovoltaic (PV) Generation on Peak Demand." *Network*. http://pdc-cmsdgp02.westernpower.com.au/documents/Photovoltaic_Forecast_Public_Version_2012.pdf.

Kaldellis, J. K., D. Zafirakis, and K. Kavadias. 2009. "Techno-Economic Comparison of Energy Storage Systems for Island Autonomous Electrical Networks." *Renewable and Sustainable Energy Reviews* 13 (2): 378–392.

Kambezidis, H. D., A. D. Adamopoulos, N. K. Sakellariou, H. G. Pavlopoulos, R. Aguiar, J. Bilbao, A. de Miguel, and E. Negro. 1998. "The 'Meteorological Radiation Model.'" *Bull. Hell. Assoc. Chart. Mech.-Electr. Engineers* 3 (2): 38–42.

Karki, R., P. Hu, and R. Billinton. 2006. "A Simplified Wind Power Generation Model for Reliability Evaluation." *IEEE Transactions on Energy Conversion* 21 (2): 533–40. doi:10.1109/TEC.2006.874233.

Kavasseri, R. G., and R. Nagarajan. 2004. "Evidence of Crossover Phenomena in Wind-Speed Data." *IEEE Transactions on Circuits and Systems I: Regular Papers* 51 (11): 2255–62. doi:10.1109/TCSI.2004.836846.

Kazimi, M. S. 2003. "Thorium Fuel for Nuclear Energy: An Unconventional Tactic Might One Day Ease Concerns That Spent Fuel Could Be Used to Make a Bomb." *American Scientist* 91 (5): 408–15.

Kleijn, R., E. van der Voet, G. J. Kramer, L. van Oers, and C. van der Giesen. 2011. "Metal Requirements of Low-Carbon Power Generation." *Energy* 36 (9): 5640–48. doi:10.1016/j.energy.2011.07.003.

Klein, S. J. W., and E. S. Rubin. 2013. "Life Cycle Assessment of Greenhouse Gas Emissions, Water and Land Use for Concentrated Solar Power Plants with Different Energy Backup Systems." *Energy Policy* 63 (December): 935–50. doi:10.1016/j.enpol.2013.08.057.

Klink, K. 2002. "Trends and Interannual Variability of Wind Speed Distributions in Minnesota." *Journal of Climate* 15 (22): 3311–3317.

Knap, V., R. Sinha, M. Swierczynski, D.-I. Stroe, and S. Chaudhary. 2014. "Grid Inertial Response with Lithium-Ion Battery Energy Storage Systems." In *Industrial Electronics (ISIE), 2014 IEEE 23rd International Symposium on*, 1817–22. doi:10.1109/ISIE.2014.6864891.

Köberle, A. C., D. E. H. J. Gernaat, and D. P. van Vuuren. 2015. "Assessing Current and Future Techno-Economic Potential of Concentrated Solar Power and Photovoltaic Electricity Generation." *Energy* 89 (September): 739–56. doi:10.1016/j.energy.2015.05.145.

Koutroulis, E., and F. Blaabjerg. 2013. "Design Optimization of Transformerless Grid-Connected PV Inverters Including Reliability." *IEEE Transactions on Power Electronics* 28 (1): 325–35. doi:10.1109/TPEL.2012.2198670.

Kreith, F., and J. F. Kreider. 1978. *Principles of Solar Engineering*. Hemisphere Pub. Corp.

Kubik, M., P. J. Coker, and C. Hunt. 2011. "Using Meteorological Wind Data to Estimate Turbine Generation Output: A Sensitivity Analysis." In *World Renewable Energy Congress, Sweden*, 4074–4081.

Kumar, L., A. K. Skidmore, and E. Knowles. 1997. "Modelling Topographic Variation in Solar Radiation in a GIS Environment." *International Journal of Geographical Information Science* 11 (5): 475–497.

Lanini, F. 2010. "Division of Global Radiation into Direct Radiation and Diffuse Radiation." Disserta\ccão não. http://www.climatestudies.unibe.ch/students/theses/msc/34.pdf.

Larcher, D., and J.-M. Tarascon. 2014. "Towards Greener and More Sustainable Batteries for Electrical Energy Storage." *Nature Chemistry* 7 (1): 19–29. doi:10.1038/nchem.2085.

Laslett, D. 2017. "Greenhouse Emissions and Provisional Costs for 100% Renewable Scenarios for the South West Interconnected System (SWIS) in Western Australia, Based on Solar, Wind, Energy Efficiency, and Battery Storage." In *World Renewable Energy Congress XVI Proceedings*. Perth.

Laslett, D., C. Carter, C. Creagh, and P. Jennings. 2017. "A Large-Scale Renewable Electricity Supply System by 2030: Solar, Wind, Energy Efficiency, Storage and Inertia for the South West Interconnected System (SWIS) in Western Australia." *Renewable Energy* (Submitted).

Laslett, D., C. Creagh, and P. Jennings. 2014. "A Method for Generating Synthetic Hourly Solar Radiation Data for Any Location in the South West of Western Australia, in a World Wide Web Page." *Renewable Energy* 68 (August): 87–102. doi:10.1016/j.renene.2014.01.015.

———. 2016. "A Simple Hourly Wind Power Simulation for the South-West Region of Western Australia Using MERRA Data." *Renewable Energy* 96 (October): 1003–14. doi:10.1016/j.renene.2016.05.024.

Lawrance, A. J., and P. A. W. Lewis. 1980. "The Exponential Autoregressive-Moving Average EARMA (P,q) Process." *Journal of the Royal Statistical Society. Series B (Methodological)* 42 (2): 150–61.

Lazard. 2015. "Lazard's Levelized Cost of Energy Analysis—version 9.0." Lazard.

Lehmann, H. 2003. "Energy Rich Japan." Institute for Sustainable Solutions and Innovations (ISUSI).

Lei, M., L. Shiyan, J. Chuanwen, L. Hongling, and Z. Yan. 2009. "A Review on the Forecasting of Wind Speed and Generated Power." *Renewable and Sustainable Energy Reviews* 13 (4): 915–920.

Lenzen, M. 2008. "Life Cycle Energy and Greenhouse Gas Emissions of Nuclear Energy: A Review." *Energy Conversion and Management* 49 (8): 2178–99. doi:10.1016/j.enconman.2008.01.033.

Leung, D. Y. C., G. Caramanna, and M. M. Maroto-Valer. 2014. "An Overview of Current Status of Carbon Dioxide Capture and Storage Technologies." *Renewable and Sustainable Energy Reviews* 39 (November): 426–43. doi:10.1016/j.rser.2014.07.093.

Liu, B. Y. H., and R. C. Jordan. 1960. "The Interrelationship and Characteristic Distribution of Direct, Diffuse and Total Solar Radiation." *Solar Energy* 4 (3): 1–19. doi:10.1016/0038-092X(60)90062-1.

Liu, D. L., and B. J. Scott. 2001. "Estimation of Solar Radiation in Australia from Rainfall and Temperature Observations." *Agricultural and Forest Meteorology* 106 (1): 41–59.

Liu, X., X. Mei, Y. Li, Q. Wang, J. R. Jensen, Y. Zhang, and J. R. Porter. 2009. "Evaluation of Temperature-Based Global Solar Radiation Models in China." *Agricultural and Forest Meteorology* 149 (9): 1433–1446.

Loftus, P. J., A. M. Cohen, J. C. S. Long, and J. D. Jenkins. 2015. "A Critical Review of Global Decarbonization Scenarios: What Do They Tell Us about Feasibility?" *Wiley Interdisciplinary Reviews: Climate Change* 6 (1): 93–112. doi:10.1002/wcc.324.

Lontzek, T. S., Y. Cai, K. L. Judd, and T. M. Lenton. 2015. "Stochastic Integrated Assessment of Climate Tipping Points Indicates the Need for Strict Climate Policy." *Nature Climate Change* 5 (5): 441–44. doi:10.1038/nclimate2570.

Lovins, A. B. 2007. "Energy Myth Nine–Energy Efficiency Improvements Have Already Reached Their Potential 1." In *Energy and American society–Thirteen Myths*, 239–263. Springer. http://link.springer.com/content/pdf/10.1007/1-4020-5564-1_10.pdf.

———. 2009. "Four Nuclear Myths." Review. Rocky Mountain Institute.

Lu, X., M. B. McElroy, and J. Kiviluoma. 2009. "Global Potential for Wind-Generated Electricity." *Proceedings of the National Academy of Sciences* 106 (27): 10933.

Lund, H., A. N. Andersen, P. A. Østergaard, B. V. Mathiesen, and D. Connolly. 2012. "From Electricity Smart Grids to Smart Energy Systems – A Market Operation Based Approach and Understanding." *Energy* 42 (1): 96–102. doi:10.1016/j.energy.2012.04.003.

Luo, X., J. Wang, M. Dooner, and J. Clarke. 2015. "Overview of Current Development in Electrical Energy Storage Technologies and the Application Potential in Power System Operation." *Applied Energy* 137 (January): 511–36. doi:10.1016/j.apenergy.2014.09.081.

Lyons, T. J., and P. R. Edwards. 1982. "Estimating Global Solar Irradiance for Western Australia, Part I." *Archives for Meteorology, Geophysics, and Bioclimatology Series B* 30 (4): 357–69. doi:10.1007/BF02324676.

Mach, P., J. Thuring, and D. Samal. 2006. "Transformation of Data for Statistical Processing." In *29th International Spring Seminar on Electronics Technology, 2006. ISSE '06*, 278–82. doi:10.1109/ISSE.2006.365112.

Macintosh, A., and C. Downie. 2006. "Wind Farms, the Facts and the Fallacies." http://www.mrsgonline.org.au/wp-content/uploads/2011/07/Wind-Farms-Facts-and-Fallacies.pdf.

MacKay, D. 2010. *Sustainable Energy - without the Hot Air*. Reprinted. Cambridge: UIT Cambridge.

Madaeni, S. H., R. Sioshansi, and P. Denholm. 2012. "How Thermal Energy Storage Enhances the Economic Viability of Concentrating Solar Power." *Proceedings of the IEEE* 100 (2): 335–47. doi:10.1109/JPROC.2011.2144950.

Martin, B. 2015. "Nuclear Power and Civil Liberties." http://ro.uow.edu.au/lhapapers/2126/.

Martinot, E. 2016. "Grid Integration of Renewable Energy: Flexibility, Innovation, and Experience." *Annual Review of Environment and Resources* 41 (1): 223–51. doi:10.1146/annurev-environ-110615-085725.

Masoum, A. S., S. Deilami, P. S. Moses, and A. Abu-Siada. 2010. "Impacts of Battery Charging Rates of Plug-in Electric Vehicle on Smart Grid Distribution Systems." In *Innovative Smart Grid Technologies Conference Europe (ISGT Europe), 2010 IEEE PES*, 1–6. IEEE. http://ieeexplore.ieee.org/xpls/abs_all.jsp?arnumber=5638981.

Mathiesen, B. V., H. Lund, D. Connolly, H. Wenzel, P. A. Østergaard, B. Möller, S. Nielsen, et al. 2015. "Smart Energy Systems for Coherent 100% Renewable Energy and Transport Solutions." *Applied Energy* 145 (May): 139–54. doi:10.1016/j.apenergy.2015.01.075.

Mathiesen, B. V., H. Lund, and K. Karlsson. 2011. "100% Renewable Energy Systems, Climate Mitigation and Economic Growth." *Applied Energy* 88 (2): 488–501. doi:10.1016/j.apenergy.2010.03.001.

McCloskey, B. D. 2015. "Expanding the Ragone Plot: Pushing the Limits of Energy Storage." *J. Phys. Chem. Lett* 6 (18): 3592–3593.

Meehl, G. A., T. F. Stocker, W. D. Collins, P. Friedlingstein, A. T. Gaye, J. M. Gregory, A. Kitoh, et al. 2007. "Global Climate Projections." *Climate Change* 3495: 747–845.

Meinshausen, M., N. Meinshausen, W. Hare, S. C. B. Raper, K. Frieler, R. Knutti, D. J. Frame, and M. R. Allen. 2009. "Greenhouse-Gas Emission Targets for Limiting Global Warming to 2 °C." *Nature* 458 (7242): 1158–62. doi:10.1038/nature08017.

Mellit, A., M. Benghanem, A. H. Arab, and A. Guessoum. 2005. "A Simplified Model for Generating Sequences of Global Solar Radiation Data for Isolated Sites: Using Artificial Neural Network and a Library of Markov Transition Matrices Approach." *Solar Energy* 79 (5): 469–482.

Mendez, S., A. Martinez, W. Millan, C. E. Montano, and F. Perez-Cebolla. 2014. "Design, Characterization, and Validation of a 1-kW AC Self-Excited Switched Reluctance Generator." *IEEE Transactions on Industrial Electronics* 61 (2): 846–55. doi:10.1109/TIE.2013.2254098.

Meneguzzo, F., R. Ciriminna, L. Albanese, and M. Pagliaro. 2015. "The Great Solar Boom: A Global Perspective into the Far Reaching Impact of an Unexpected Energy Revolution." *Energy Science & Engineering*, October, n/a-n/a. doi:10.1002/ese3.98.

Milligan, M., B. Frew, B. Kirby, M. Schuerger, K. Clark, D. Lew, P. Denholm, B. Zavadil, M. O'Malley, and B. Tsuchida. 2015. "Alternatives No More: Wind and Solar Power Are Mainstays of a Clean, Reliable, Affordable Grid." *IEEE Power and Energy Magazine* 13 (6): 78–87. doi:10.1109/MPE.2015.2462311.

Mills, D., and R. Morgan. 2007. "Solar Thermal Power As The Plausible Basis Of Grid Supply." Palo Alto (CA): AUSRA.

Mishra, A., R. Sitaraman, D. Irwin, T. Zhu, P. Shenoy, B. Dalvi, and S. Lee. 2015. "Integrating Energy Storage in Electricity Distribution Networks." In , 37–46. ACM Press. doi:10.1145/2768510.2768543.

MIT. 2003. *The Future of Nuclear Power: An Interdisciplinary MIT Study.* [Boston MA]: Massachusetts Institute of Technology.

Mitchell, K., M. Nagrial, and J. Rizk. 2009. "Network Benefits of Embedded Solar Systems: A Case Study from Western Sydney." *Renewable Energy* 34 (12): 2592–2596.

Mohandes, M. A., S. Rehman, and T. O. Halawani. 1998. "A Neural Networks Approach for Wind Speed Prediction." *Renewable Energy* 13 (3): 345–54. doi:10.1016/S0960-1481(98)00001-9.

Mohandes, M., A. Balghonaim, M. Kassas, S. Rehman, and T. O. Halawani. 2000. "Use of Radial Basis Functions for Estimating Monthly Mean Daily Solar Radiation." *Solar Energy* 68 (2): 161–68. doi:10.1016/S0038-092X(99)00071-7.

Monteith, J. L., and M. H. Unsworth. 1990. *Principles of Environmental Physics*. Butterworth-Heinemann.

Mora-Lopez, L. L., and M. Sidrach-de-Cardona. 1998. "Multiplicative ARMA Models to Generate Hourly Series of Global Irradiation." *Solar Energy* 63 (5): 283–291.

MR. 2012. “Review of SWIS Planning Criterion.” Market Research.
Mudd, G. M. 2014. “The Future of Yellowcake: A Global Assessment of Uranium Resources and Mining.” *Science of The Total Environment* 472 (February): 590–607. doi:10.1016/j.scitotenv.2013.11.070.
Mudd, G. M., and M. Diesendorf. 2008. “Sustainability of Uranium Mining and Milling: Toward Quantifying Resources and Eco-Efficiency.” *Environmental Science & Technology* 42 (7): 2624–2630.
Mullan, J., D. Harries, T. Bräunl, and S. Whitely. 2011. “Modelling the Impacts of Electric Vehicle Recharging on the Western Australian Electricity Supply System.” *Energy Policy* 39 (7): 4349–59. doi:10.1016/j.enpol.2011.04.052.
Muneer, T., and S. Younes. 2006. “The All-Sky Meteorological Radiation Model: Proposed Improvements.” *Applied Energy* 83 (5): 436–450.
Muneer, T., S. Younes, and S. Munawwar. 2007. “Discourses on Solar Radiation Modeling.” *Renewable and Sustainable Energy Reviews* 11 (4): 551–602. doi:10.1016/j.rser.2005.05.006.
Murphy, J. D., and E. McKeogh. 2004. “Technical, Economic and Environmental Analysis of Energy Production from Municipal Solid Waste.” *Renewable Energy* 29 (7): 1043–57. doi:10.1016/j.renene.2003.12.002.
Nadel, S., A. Shipley, and R. N. Elliott. 2004. “The Technical, Economic and Achievable Potential for Energy-Efficiency in the US–A Meta-Analysis of Recent Studies.” In *Proceedings of the 2004 ACEEE Summer Study on Energy Efficiency in Buildings*, 8–215.
Negra, N. B., J. Todorovic, and T. Ackermann. 2006. “Loss Evaluation of HVAC and HVDC Transmission Solutions for Large Offshore Wind Farms.” *Electric Power Systems Research* 76 (11): 916–27. doi:10.1016/j.epsr.2005.11.004.
NFEE. 2003. “Preliminary Assessment of Demand-Side Energy Efficiency Improvement Potential and Costs.” Melbourne: National Framework for Energy Efficiency.
Norgate, T., N. Haque, and P. Koltun. 2014. “The Impact of Uranium Ore Grade on the Greenhouse Gas Footprint of Nuclear Power.” *Journal of Cleaner Production* 84 (December): 360–67. doi:10.1016/j.jclepro.2013.11.034.
NREL. 2016. “Concentrating Solar Power Projects - Crescent Dunes Solar Energy Project | Concentrating Solar Power Research | NREL.” http://www.nrel.gov/csp/solarpaces/project_detail.cfm/projectID=60.
Nugent, D., and B. K. Sovacool. 2014. “Assessing the Lifecycle Greenhouse Gas Emissions from Solar PV and Wind Energy: A Critical Meta-Survey.” *Energy Policy* 65 (February): 229–44. doi:10.1016/j.enpol.2013.10.048.
Oliveira, L., M. Messagie, J. Mertens, H. Laget, T. Coosemans, and J. Van Mierlo. 2015. “Environmental Performance of Electricity Storage Systems for Grid Applications, a Life Cycle Approach.” *Energy Conversion and Management* 101 (September): 326–35. doi:10.1016/j.enconman.2015.05.063.
Ong, S., C. Campbell, P. Denholm, R. Margolis, and G. Heath. 2013. “Land-Use Requirements for Solar Power Plants in the United States.” *Golden, CO: National Renewable Energy Laboratory* 140. http://www.nrel.gov/docs/fy13osti/56290.pdf.
Ou, Y., H. Zhai, and E. S. Rubin. 2016. “Life Cycle Water Use of Coal- and Natural-Gas-Fired Power Plants with and without Carbon Capture and Storage.” *International Journal of Greenhouse Gas Control* 44 (January): 249–61. doi:10.1016/j.ijggc.2015.11.029.
Outhred, H. 2003. “National Wind Power Study: An Estimate of Readily Accepted Wind Energy in the National Electricity Market, 2003.” Canberra, ACT: Australian Greenhouse Office.
Owano, N. 2015. “High Efficiency Rating Shines on Panasonic Solar Panel.” Techxplore. http://techxplore.com/news/2015-10-high-efficiency-panasonic-solar-panel.html.
Pachauri, R. K., L. Mayer, and Intergovernmental Panel on Climate Change, eds. 2015. *Climate Change 2014: Synthesis Report*. Geneva, Switzerland: Intergovernmental Panel on

Climate Change. http://www.ipcc.ch/pdf/assessment-report/ar5/syr/SYR_AR5_FINAL_full.pdf.
Papaefthymiou, G., and B. Klockl. 2008. "MCMC for Wind Power Simulation." *IEEE Transactions on Energy Conversion* 23 (1): 234–40. doi:10.1109/TEC.2007.914174.
Patterson, W. C. 1983. *Nuclear Power*. Penguin Books.
Pattiaratchi, C., B. Hegge, J. Gould, and I. Eliot. 1997. "Impact of Sea-Breeze Activity on Nearshore and Foreshore Processes in South Western Australia." *Continental Shelf Research* 17 (13): 1539–1560.
Pearce, J. M. 2008. "Thermodynamic Limitations to Nuclear Energy Deployment as a Greenhouse Gas Mitigation Technology." *International Journal of Nuclear Governance, Economy and Ecology* 2 (1): 113–130.
Peixoto, J. P., and A. H. Oort. 1992. *Physics of Climate*. American Institute of Physics.
Perez, R., P. Ineichen, R. Seals, and A. Zelenka. 1990. "Making Full Use of the Clearness Index for Parameterizing Hourly Insolation Conditions." *Solar Energy* 45 (2): 111–14. doi:10.1016/0038-092X(90)90036-C.
Perez, R., M. Taylor, T. Hoff, and J. P. Ross. 2009. "Redefining PV Capacity." *Public Utilities Fortnightly* 147 (2). http://asrc.albany.edu/people/faculty/perez/2009/peak%20shaving/02012009_TechCorridor_redefining_PV_capacity.pdf.
Peter, S., A. Doleschek, H. Lehmann, and J. Mirales. 2007. "Solar Catalonia. A Pathway to a 100% Renewable Energy System for Catalonia." Fundació Terra, iSuSI, Ecoserveis.
Peters, J. F., M. Baumann, B. Zimmermann, J. Braun, and M. Weil. 2017. "The Environmental Impact of Li-Ion Batteries and the Role of Key Parameters – A Review." *Renewable and Sustainable Energy Reviews* 67 (January): 491–506. doi:10.1016/j.rser.2016.08.039.
Peterseim, J. H., A. Herr, S. Miller, S. White, and D. A. O'Connell. 2014. "Concentrating Solar Power/Alternative Fuel Hybrid Plants: Annual Electricity Potential and Ideal Areas in Australia." *Energy* 68 (April): 698–711. doi:10.1016/j.energy.2014.02.068.
Pickard, W. F., A. Q. Shen, and N. J. Hansing. 2009. "Parking the Power: Strategies and Physical Limitations for Bulk Energy Storage in Supply-Demand Matching on a Grid Whose Input Power Is Provided by Intermittent Sources." *Renewable and Sustainable Energy Reviews* 13 (8): 1934–1945.
Press, W. H., S. A. Teukolsky, W. T. Vetterling, and B. P. Flannery. 1992. *Numerical Recipes in C: The Art of Scientific Computing. Second Edition*.
Pryor, S. C., and R. J. Barthelmie. 2010. "Climate Change Impacts on Wind Energy: A Review." *Renewable and Sustainable Energy Reviews* 14 (1): 430–437.
Psomopoulos, C. S., A. Bourka, and N. J. Themelis. 2009. "Waste-to-Energy: A Review of the Status and Benefits in USA." *Waste Management* 29 (5): 1718–24. doi:10.1016/j.wasman.2008.11.020.
Punyawardena, B. V. R., and D. Kulasiri. 1996. "Stochastic Simulation of Solar Radiation from Sunshine Duration in Sri Lanka." Canterbury, N.Z: Lincoln University Centre for Computing and Biometrics.
Rahmann, C., and A. Castillo. 2014. "Fast Frequency Response Capability of Photovoltaic Power Plants: The Necessity of New Grid Requirements and Definitions." *Energies* 7 (10): 6306–22. doi:10.3390/en7106306.
Rareshide, E., A. Tindal, C. Johnson, A. Graves, E. Simpson, J. Bleeg, T. Harris, and D. Schoborg. 2009. "Effects of Complex Wind Regimes on Turbine Performance." In *Scientific Proceedings. American Wind Energy Association WINDPOWER Conference*. http://www.germanlloyd.org/assets/technical/Effects_of_complex_wind_regimes_on_turbine_performance_14May09_final.pdf.
Rasi, S., J. Läntelä, and J. Rintala. 2011. "Trace Compounds Affecting Biogas Energy Utilisation – A Review." *Energy Conversion and Management* 52 (12): 3369–75. doi:10.1016/j.enconman.2011.07.005.

Reddy, K. ., and M. Ranjan. 2003. “Solar Resource Estimation Using Artificial Neural Networks and Comparison with Other Correlation Models.” *Energy Conversion and Management* 44 (15): 2519–30. doi:10.1016/S0196-8904(03)00009-8.

Reikard, G. 2009. “Predicting Solar Radiation at High Resolutions: A Comparison of Time Series Forecasts.” *Solar Energy* 83 (3): 342–49. doi:10.1016/j.solener.2008.08.007.

Remund, J., E. Salvisberg, and S. Kunz. 1998. “On the Generation of Hourly Shortwave Radiation Data on Tilted Surfaces.” *Solar Energy* 62 (5): 331–344.

REN21. 2010. “Renewables 2010 Global Status Report.” Paris: REN21 Secretariat.

———. 2015. “Renewables 2015 Global Status Report.” Paris: REN21 Secretariat.

———. 2016. “Renewables 2016 Global Status Report.” Paris: REN21 Secretariat.

Revesz, R. L., P. H. Howard, K. Arrow, L. H. Goulder, R. E. Kopp, M. A. Livermore, M. Oppenheimer, and T. Sterner. 2014. “Global Warming: Improve Economic Models of Climate Change.” *Nature* 508 (7495): 173–75. doi:10.1038/508173a.

Rienecker, M. M., M. J. Suarez, R. Gelaro, R. Todling, J. Bacmeister, E. Liu, M. G. Bosilovich, et al. 2011. “MERRA: NASA’s Modern-Era Retrospective Analysis for Research and Applications.” *Journal of Climate* 24 (14): 3624–3648.

Riesz, J., B. Elliston, Vithayasrichareon, Peerapat, and MacGill, Ian. 2016. “100% Renewables for Australia?” Sydney: Centre for Energy and Environmental Markets, University of NSW. http://ceem.unsw.edu.au/sites/default/files/documents/100pc%20RE%20-%20Research%20Summary-2016-03-02a.pdf.

Riesz, J., S. Shiao, and A. Turley. 2010. “Assessment of FCS and Technical Rules.” Brisbane: Roam Consulting.

RIRDC. 2001. *Integrated Tree Processing of Mallee Eucalypts: A Report for the RIRDC/Land & Water Australia/FWPRDC Joint Venture Agroforestry Program*. Barton, A.C.T.: Rural Industries Research and Development Corp.

Rubin, J. 2007. “The Efficiency Paradox.” *CIBC World Markets, Toronto, Canada*.

Rudy, M. 1997. “Sun and Climate Modeling for Thermal Simulation.” In *Proceedings: Building Simulation’97, International Conference of IBPSA, Prague*. http://www.inive.org/members_area/medias/pdf/Inive/IBPSA/UFSC605.pdf.

Rutovitz, J., J. Peterseim, B. Elliston, S. Harris, S. Mohr, K. Lovegrove, A. Want, E. Langham, and I. MacGill. 2013. “Breaking the Solar Gridlock. Potential Benefits of Installing Concentrating Solar Thermal Power at Constrained Locations in the NEM.” *Prepared for the Australian Solar Thermal Energy Association (AUSTELA) by the Institute for Sustainable Futures, UTS*. http://citeseerx.ist.psu.edu/viewdoc/download?doi=10.1.1.667.1140&rep=rep1&type=pdf.

Saddler, H., M. Diesendorf, R. Denniss, Energy Strategies (Australia), and World Wildlife Fund Australia. 2004. *A Clean Energy Future for Australia a Study by Energy Strategies for the Clean Energy Future Group*. Ultimo, N.S.W.: WWF Australia.

Schaffer, M. B. 2013. “Abundant Thorium as an Alternative Nuclear Fuel.” *Energy Policy* 60 (September): 4–12. doi:10.1016/j.enpol.2013.04.062.

Schneider, M., and A. Froggatt. 2015. “The World Nuclear Industry Status Report 2015.” Mycle Schneider Consulting.

Schneider, M., S. Thomas, A. Froggatt, and D. Koplow. 2009. “The World Nuclear Industry Status Report 2009.” Mycle Schneider Consulting. http://www.worldnuclearreport.org/IMG/pdf/2009MSC-WorldNuclearReport-EN-V2.pdf.

Schwarz, G. 1978. “Estimating the Dimension of a Model.” *The Annals of Statistics* 6 (2): 461–464. doi:10.1214/aos/1176344136.

Scott, V., R. S. Haszeldine, S. F. B. Tett, and A. Oschlies. 2015. “Fossil Fuels in a Trillion Tonne World.” *Nature Climate Change* 5 (5): 419–23. doi:10.1038/nclimate2578.

Semenov, M. A., R. J. Brooks, E. M. Barrow, and C. W. Richardson. 1998. "Comparison of the WGEN and LARS-WG Stochastic Weather Generators for Diverse Climates." *Climate Research* 10: 95–107.

SEN. 2013. "SEN W.A. 100% Renewable Energy on the SWIS 2029." Perth: Sustainable Energy Now. www.sen.asn.au.

Seo, D., J. Huang, and M. Krarti. 2008. "Development of Models for Hourly Solar Radiation Prediction." *ASHRAE Transactions* 114: 392.

Shafiee, S., and E. Topal. 2009. "When Will Fossil Fuel Reserves Be Diminished?" *Energy Policy* 37 (1): 181–89. doi:10.1016/j.enpol.2008.08.016.

Shlyakhter, A., and R. Wilson. 1992. "Chernobyl: The Inevitable Results of Secrecy." *Public Understanding of Science* 1 (3): 251.

Sims, R., B. Barton, P. Bennett, N. Isaacs, S. Kerr, J. Leaver, A. Reisinger, J. Higham, and E. Mason. 2016. "Transition to a Low-Carbon Economy for New Zealand." New Zealand: The Royal Society of New Zealand.

Sinden, G. 2007. "Characteristics of the UK Wind Resource: Long-Term Patterns and Relationship to Electricity Demand." *Energy Policy* 35 (1): 112–27. doi:10.1016/j.enpol.2005.10.003.

Singer, C., R. Buck, R. Pitz-Paal, and H. Müller-Steinhagen. 2010. "Assessment of Solar Power Tower Driven Ultrasupercritical Steam Cycles Applying Tubular Central Receivers with Varied Heat Transfer Media." *Journal of Solar Energy Engineering* 132 (4): 041010.

Skartveit, A., Olseth J.A., and Tuft M.E. 1998. "An Hourly Diffuse Fraction Model with Correction for Variability and Surface Albedo." *Solar Energy* 63 (3): 173–83. doi:10.1016/S0038-092X(98)00067-X.

Skidmore, E., and I. Tatarko. 1990. "STOCHASTIC WIND SIMULATION FOR EROSION NIODELING." *SMR* 705: 16.

Smith, J. C., M. R. Milligan, E. A. DeMeo, and B. Parsons. 2007. "Utility Wind Integration and Operating Impact State of the Art." *IEEE Transactions on Power Systems* 22 (3): 900–908. doi:10.1109/TPWRS.2007.901598.

Smith, K., G. Randall, D. Malcolm, N. Kelley, and B. Smith. 2002. "Evaluation of Wind Shear Patterns at Midwest Wind Energy Facilities." In *American Wind Energy Association (AWEA) WINDPOWER 2002 Conference*. http://www.nrel.gov/docs/fy02osti/32492.pdf.

Smith Stegen, K. 2015. "Heavy Rare Earths, Permanent Magnets, and Renewable Energies: An Imminent Crisis." *Energy Policy* 79 (April): 1–8. doi:10.1016/j.enpol.2014.12.015.

Soloveichik, G. L. 2011. "Battery Technologies for Large-Scale Stationary Energy Storage." *Annual Review of Chemical and Biomolecular Engineering* 2 (1): 503–27. doi:10.1146/annurev-chembioeng-061010-114116.

Soman, S. S., H. Zareipour, O. Malik, and P. Mandal. 2010. "A Review of Wind Power and Wind Speed Forecasting Methods with Different Time Horizons." In *North American Power Symposium (NAPS), 2010*, 1–8. IEEE. http://ieeexplore.ieee.org/xpls/abs_all.jsp?arnumber=5619586.

Sorrell, S. 2009. "Jevons' Paradox Revisited: The Evidence for Backfire from Improved Energy Efficiency." *Energy Policy* 37 (4): 1456–1469.

Sovacool, B. K. 2008. "Valuing the Greenhouse Gas Emissions from Nuclear Power: A Critical Survey." *Energy Policy* 36 (8): 2950–2963.

———. 2009. "The Intermittency of Wind, Solar, and Renewable Electricity Generators: Technical Barrier or Rhetorical Excuse?" *Utilities Policy* 17 (3–4): 288–296.

Sözen, A., E. Arcaklıoğlu, M. Özalp, and N. Çağlar. 2005. "Forecasting Based on Neural Network Approach of Solar Potential in Turkey." *Renewable Energy* 30 (7): 1075–90. doi:10.1016/j.renene.2004.09.020.

Spencer, J. W. 1976. *Perth Solar Tables: Tables for Solar Position and Radiation for Perth (Latitude 32.0° S.) in SI Units*. Division of Building Research Technical Paper, 2. Ser., 10. Melbourne: Commonwealth Scient. and Industrial Research Org.

Spokas, K., and F. Forcella. 2009. "Estimating Hourly Incoming Solar Radiation from Limited Meteorological Data." http://www.wssajournals.org/perlserv/?request=get-abstract&issn=0043-1745&volume=054&issue=01&page=0182.

Steffen, W. 2007. "Climate Change: Science, Impacts and Policy Challenges." POLICY BRIEFS Climate Change and Public Policy. Canberra: Australian National University.

Steffen, W., L. Hughes, and A. Pearce. 2015. "Climate Change 2015: Growing Risks, Critical Choices." Climate Council of Australia.

Stern, N. 2013. "The Structure of Economic Modeling of the Potential Impacts of Climate Change: Grafting Gross Underestimation of Risk onto Already Narrow Science Models." *Journal of Economic Literature* 51 (3): 838–59. doi:10.1257/jel.51.3.838.

Suckling, P. W., and J. E. Hay. 1977. "A Cloud Layer-Sunshine Model for Estimating Direct, Diffuse and Total Solar Radiation." *Atmosphere* 15 (4): 194–207.

Suomalainen, K., C. A. Silva, P. Ferrão, and S. Connors. 2012. "Synthetic Wind Speed Scenarios Including Diurnal Effects: Implications for Wind Power Dimensioning." *Energy* 37 (1): 41–50. doi:10.1016/j.energy.2011.08.001.

Syed, A., and ABARE. 2007. *Australian Energy: National and State Projections to 2029-30*. Canberra, A.C.T.: Australian Bureau of Agricultural and Resource Economics.

Tabassum-Abbasi, M. Premalatha, T. Abbasi, and S. A. Abbasi. 2014. "Wind Energy: Increasing Deployment, Rising Environmental Concerns." *Renewable and Sustainable Energy Reviews* 31 (March): 270–88. doi:10.1016/j.rser.2013.11.019.

Tan, H. J. 2004. "Directional Waves in the Nearshore Coastal Region of Perth, Western Australia." University of Western Australia. http://www2.sese.uwa.edu.au/~pattiara/theses/TAN_Jean_2004.pdf.

Thomas, S. 2012. "What Will the Fukushima Disaster Change?" *Energy Policy* 45 (June): 12–17. doi:10.1016/j.enpol.2012.02.010.

Tian, Y., and C. Y. Zhao. 2013. "A Review of Solar Collectors and Thermal Energy Storage in Solar Thermal Applications." *Applied Energy* 104 (April): 538–53. doi:10.1016/j.apenergy.2012.11.051.

Tol, R. S. J. 1997. "Autoregressive Conditional Heteroscedasticity in Daily Wind Speed Measurements." *Theoretical and Applied Climatology* 56 (1–2): 113–122.

Tsoutsos, T., N. Frantzeskaki, and V. Gekas. 2005. "Environmental Impacts from the Solar Energy Technologies." *Energy Policy* 33 (3): 289–296.

Turchi, C., M. Mehos, C. K. Ho, and G. J. Kolb. 2010. "Current and Future Costs for Parabolic Trough and Power Tower Systems in the US Market." *SolarPACES 2010*. http://www.nrel.gov/docs/fy11osti/49303.pdf.

Turnbull, D., A. Glaser, and R. J. Goldston. 2015. "Investigating the Value of Fusion Energy Using the Global Change Assessment Model." *Energy Economics* 51 (September): 346–53. doi:10.1016/j.eneco.2015.08.001.

Tyner, C. E., and D. Wasyluk. 2013. "eSolar's Modular, Scalable Molten Salt Power Tower Reference Plant Design." In *19th Annual SolarPACES Symposium*. http://www.esolar.com/wp-content/uploads/2013/10/SolarPACES-2013.pdf.

Ulbig, A., T. S. Borsche, and G. Andersson. 2013. "Impact of Low Rotational Inertia on Power System Stability and Operation." *arXiv Preprint arXiv:1312.6435*. http://arxiv.org/abs/1312.6435.

Vidal-Amaro, J. J., P. A. Østergaard, and C. Sheinbaum-Pardo. 2015. "Optimal Energy Mix for Transitioning from Fossil Fuels to Renewable Energy Sources – The Case of the Mexican Electricity System." *Applied Energy* 150 (July): 80–96. doi:10.1016/j.apenergy.2015.03.133.

Viebahn, P., J. Nitsch, M. Fischedick, A. Esken, D. Sch\üwer, N. Supersberger, U. Zuberb\ühler, and O. Edenhofer. 2007. "Comparison of Carbon Capture and Storage with Renewable Energy Technologies Regarding Structural, Economic, and Ecological Aspects in Germany." *International Journal of Greenhouse Gas Control* 1 (1): 121–133.

Vignarooban, K., X. Xu, A. Arvay, K. Hsu, and A. M. Kannan. 2015. "Heat Transfer Fluids for Concentrating Solar Power Systems – A Review." *Applied Energy* 146 (May): 383–96. doi:10.1016/j.apenergy.2015.01.125.

Visvalingam, M., and J. D. Whyatt. 1993. "Line Generalisation by Repeated Elimination of Points." *Cartographic Journal, The* 30 (1): 46–51. doi:10.1179/000870493786962263.

Von Hippel, F., and M. Bunn. 2010. *The Uncertain Future of Nuclear Energy*.

Wagner, M. J. 2008. "Simulation and Predictive Performance Modeling of Utility-Scale Central Receiver System Power Plants." University of Wisconsin–Madison.

Wagner, M. J., and G. Zhu. 2011. "A Generic CSP Performance Model for NREL's System Advisor Model." In *Proceedings of 17th SolarPACES Symposium, Granada, Spain*. http://www.nrel.gov/docs/fy11osti/52473.pdf.

Wallner, A., and A. Wenisch. 2011. "Energy Balance of Nuclear Power Generation." Vienna: Austrian Energy Agency. http://ipx-fluid.onlinedienste.at/fileadmin/dam/pdf/publikationen/berichteBroschueren/Endbericht_LCA_Nuklearindustrie-engl.pdf.

Wang, C., L. Zhang, Y. Chang, and M. Pang. 2015. "Biomass Direct-Fired Power Generation System in China: An Integrated Energy, GHG Emissions, and Economic Evaluation for Salix." *Energy Policy* 84 (September): 155–65. doi:10.1016/j.enpol.2015.04.025.

Ward, K., and J. Boland. 2007. "Modelling the Volatility in Wind Farm Output." Modelling and Simulation Society of Australia and New Zealand. http://mssanz.org.au/MODSIM07/papers/30_s38/ModellingTheVolatility_s38_Ward_.pdf.

WAWA. 2012. "Western Australian Waste Strategy:'Creating the Right Environment.'" Perth: Waste Authority of Western Australia.

WEC. 2008. *Energy Efficiency Policies around the World: Review and Evaluation*. London: World Energy Council.

Weitemeyer, S., D. Kleinhans, T. Vogt, and C. Agert. 2015. "Integration of Renewable Energy Sources in Future Power Systems: The Role of Storage." *Renewable Energy* 75 (March): 14–20. doi:10.1016/j.renene.2014.09.028.

Western Power. 2013. "Ancillary Service Report 2013 Prepared under Clause 3.11.11 of the Market Rules by System Management." Perth: Western Power.

———. 2016a. "Annual Planning Report 2015/16." Perth: Western Power.

———. 2016b. "Mandurah Load Area Non-Network Options Report." Perth: Western Power.

Whitaker, M. B., G. A. Heath, J. J. Burkhardt, and C. S. Turchi. 2013. "Life Cycle Assessment of a Power Tower Concentrating Solar Plant and the Impacts of Key Design Alternatives." *Environmental Science & Technology* 47 (11): 5896–5903. doi:10.1021/es400821x.

Widén, J., N. Carpman, V. Castellucci, D. Lingfors, J. Olauson, F. Remouit, M. Bergkvist, M. Grabbe, and R. Waters. 2015. "Variability Assessment and Forecasting of Renewables: A Review for Solar, Wind, Wave and Tidal Resources." *Renewable and Sustainable Energy Reviews* 44 (April): 356–75. doi:10.1016/j.rser.2014.12.019.

Widger, W. K. 1977. "Estimations of Wind Speed Frequency Distributions Using Only the Monthly Average and Fastest Mile Data." *Journal of Applied Meteorology* 16 (3): 244–47. doi:10.1175/1520-0450(1977)016<0244:EOWSFD>2.0.CO;2.

WMAA. 2007. "Potential for Greenhouse Gas Abatement from Waste Management and Resource Recovery Activities in Australia." NSW: Waste Management Association of Australia.

WNA. 2009. "Military Warheads as a Source of Nuclear Fuel." World Nuclear Association. http://www.australianuranium.com.au/warheads-to-fuel.html.

Woldendorp, G., R. J. Keenan, and M. F. Ryan. 2002. "Coarse Woody Debris in Australian Forest Ecosystems." *A Report for the National Greenhouse Strategy, Module* 6. https://www.researchgate.net/profile/Rodney_Keenan/publication/227765571_Coarse_woody_debris_in_Australian_forest_ecosystems_A_review/links/00b4952c4e9944d752000000.pdf.

Wright, M., and P. Hearps. 2010. "Zero Carbon Australia: Stationary Energy Plan." Melbourne: Beyond Zero Emissions, Melbourne Energy Institute, University of Melbourne.

Wu, H., Q. Fu, R. Giles, and J. Bartle. 2008. "Production of Mallee Biomass in Western Australia: Energy Balance Analysis †." *Energy & Fuels* 22 (1): 190–98. doi:10.1021/ef7002969.

Yang, K., and T. Koike. 2002. "Estimating Surface Solar Radiation from Upper-Air Humidity." *Solar Energy* 72 (2): 177–186.

Yang, K., T. Koike, and B. Ye. 2006. "Improving Estimation of Hourly, Daily, and Monthly Solar Radiation by Importing Global Data Sets." *Agricultural and Forest Meteorology* 137 (1–2): 43–55. doi:10.1016/j.agrformet.2006.02.001.

Young, A. T. 1994. "Air Mass and Refraction." *Applied Optics* 33 (6): 1108–10. doi:10.1364/AO.33.001108.

Zakeri, B., and S. Syri. 2015. "Electrical Energy Storage Systems: A Comparative Life Cycle Cost Analysis." *Renewable and Sustainable Energy Reviews* 42 (February): 569–96. doi:10.1016/j.rser.2014.10.011.

Zhang, N., C. Kang, D. Kirschen, and Q. Xia. 2013. "Rigorous Model for Evaluating Wind Power Capacity Credit." *IET Renewable Power Generation* 7 (5): 504–13. doi:10.1049/iet-rpg.2012.0037.

Zheng, W. X. 2003. "Study of a Least-Squares-Based Algorithm for Autoregressive Signals Subject to White Noise." *Mathematical Problems in Engineering* 2003 (3): 93–101. doi:10.1155/S1024123X03210012.